DISSERTATION

BULKING COEFFICIENTS OF AERATED FLOW DURING WAVE OVERTOPPING SIMULATION ON PROTECTED LAND-SIDE SLOPES

Submitted by

Bryan N. Scholl

Department of Civil and Environmental Engineering

In partial fulfillment of the requirements

For the Degree of Doctor of Philosophy

Colorado State University

Fort Collins, Colorado

Summer 2016

Doctoral Committee:

Advisor: Christopher I. Thornton
Co-Advisor: Steven R. Abt

Steven A. Hughes
Subhas K. Venayagamoorthy
Stephanie K. Kampf

ABSTRACT

BULKING COEFFICIENTS OF AERATED FLOW DURING WAVE OVERTOPPING SIMULATION ON PROTECTED-SIDE SLOPES

Post hurricane Katrina there has been more interest in erosion on the landward side of levees resulting from wave overtopping during storm events. The development of wave overtopping simulators has enabled more rigorous evaluation of levee armoring alternatives under controlled conditions similar to those on levees. Steady state overtopping studies have demonstrated a reduction in shear stress due to air entrainment in the flow. There has not been an evaluation of air entrainment during wave overtopping simulation. For this reason, a study was conducted to quantify flow bulking occurring during wave overtopping simulation.

Testing was conducted at the Hydraulics Laboratory at Colorado State University at the Engineering Research Center using a wave overtopping simulator. The simulated levee was 6 ft wide. Levee geometry in the direction of flow was a 13.2 ft. horizontal crest, 30.5 ft levee face with 3:1 (horizontal:vertical) slope and 12.2 ft berm with 25:1 slope. Un-bulked flow thickness was measured with "surfboards" which hydroplane along the surface of flow. Bulked flow thicknesses were measured using visual observations of maximum flow thickness on eight staff gages along the wall of the simulated levee. Wave volumes ranged from 20 ft^3/ft to 175 ft^3/ft. Conservation of mass and testing repeatability is demonstrated.

Bulking values range from zero for the smallest wave volumes to over 100% for the largest wave volumes. An empirical model is developed to estimate bulking on the 3:1 levee slope. A

comparison is made to steady state flows with similar air entrainment. The effect of bulking on shear stress is a potential decrease in shear stress over 50% relative to un-bulked flow thickness. A method to incorporate wave overtopping bulking into design is proposed using a cumulative work approach.

ACKNOWLEDGEMENTS

It must be recognized this has been a group effort with multiple players providing long term support in many various ways. Dr. Chris Thornton was kind enough to provide Hydraulics Laboratory resources, financial support and general guidance and encouragement. Dr. Steve Abt has graciously given time out of his busy schedule, good advice that money could not buy and a welcome knack for gently "nudging" when needed. Dr. Steve Hughes has been invaluable as the "ace in the hole" and technical guru for all things to do with testing and wave overtopping, especially when the waves were getting high and the water was getting deep (metaphorically speaking, of course). Dr. Steve Hughes is also, most importantly, the progenitor of the study for recognizing the knowledge gap and generously suggesting it could be a dissertation topic. Thank you to my committee members Dr. Karan Venayagamoorthy and Dr. Stephanie K. Kampf for being so available, supportive and not forsaking that the end would ever come.

An acknowledgment would be incomplete without recognizing my family and their part: my mom for always being encouraging, my wife, Andrea, for having so much more patience than I have and Isabella for putting up with a "Papá" who has not always been as present as he would wish. My good friend, Jim Shreve, has also been a great moral support and his humor and help during a tough time was more appreciated than he will ever know.

TABLE OF CONTENTS

LIST OF TABLES

LIST OF FIGURES

LIST OF VARIABLES

Symbol	Description	Units
a	scale factor in the Weibull distribution $a = 0.84\frac{qT_m}{P_{ow}}$	[-]
b	empirical coefficient	[-]
β_W	grouping of terms, $\frac{1}{8}\rho f_D$	[kg/m^3]
B_C	crest width (outer to inner point)	[m]
c	empirical coefficient	[-]
c	wave celerity at the structure toe $c = \sqrt{g\ H_{m0}}$	[m/s]
C_e	mean aeration percent	[-]
c_h'	empirical coefficient for wave overtopping flow depth at the outer slope/crest transition	[-]
$c'_{h2\%}$	empirical coefficient for wave overtopping flow depth at the outer slope/crest transition exceeded by 2% of the incoming waves	[-]
c_q'	empirical coefficient for wave overtopping flow discharge at the outer slope/crest transition	[-]
c_u'	empirical coefficient for wave overtopping flow velocity at the outer slope/crest transition	[-]
$c'_{u2\%}$	empirical coefficient for wave overtopping velocity at the outer slope/crest transition exceeded by 2% of incoming waves	[-]
c_V'	empirical coefficient for wave overtopping flow volume per wave at the outer slope/crest transition	[-]
$c_h^{"}$	empirical coefficient for wave overtopping flow depth at the crest/inner slope transition	[-]
$c_q^{"}$	empirical coefficient for wave overtopping flow discharge at the crest/inner slope transition	[-]
$c_u^{"}$	empirical coefficient for wave overtopping flow velocity at the crest/inner slope transition	[-]
c_0	dimensionless coefficient	[-]
c_1	dimensionless coefficient	[-]
c_2	dimensionless coefficient $c_2 = 0.25\ \frac{c_1^2}{c_0}$	[-]

Symbol	Description	Units
c_2	dimensionless coefficient as a function of dike slope n ($c_2^* = c_2\ n = constant$)	[-]
c_2	dimensionless coefficient at point x_C on the crest	[-]
c_3	dimensionless coefficient	[-]
$c^*_{Ah2\%}$	empirical coefficient for wave runup flow depth on the outer slope exceeded by 2% of incoming waves	[-]
$c^*_{Au2\%}$	empirical coefficient for wave runup flow velocities on the outer slope exceeded by 2% of incoming waves	[-]
$c^*_{Ch2\%}$	empirical coefficient for wave overtopping flow depth on the crest exceeded by 2% of incoming waves	[-]
$c^*_{Cu2\%}$	empirical coefficient for maximum wave overtopping flow velocity on the crest exceeded by 2% of incoming waves	[-]
c'_h	empirical coefficient for wave overtopping flow depth on the outer slope	[-]
c'_q	empirical coefficient for wave overtopping flow discharge on the outer slope	[-]
c'_u	empirical coefficient for wave overtopping flow velocity on the outer slope	[-]
$c'_{u2\%}$	empirical coefficient for wave overtopping flow velocity on the outer slope exceeded by 2% of incoming waves	[-]
c'_V	empirical coefficient for wave overtopping flow volume on the outer slope	[-]
c''_q	empirical coefficient for wave overtopping flow discharge on the crest	[-]
c''_u	empirical coefficient for wave overtopping flow velocity on the crest	[-]
$c''_{h2\%}$	empirical coefficient for wave overtopping flow depth on the crest exceeded by 2% of incoming waves	[-]
$c''_{u2\%}$	empirical coefficient for wave overtopping flow velocity on the crest exceeded by 2% of incoming waves	[-]
c_{Ah}	empirical coefficient for flow depth at the outer slope/crest transition	[-]
c_{Au}	empirical coefficient for flow velocity at the outer slope/crest transition	[-]
c_s	empirical coefficient	[-]

Symbol	Description	Units
c_{transh}	empirical coefficient for wave overtopping flow depth at the outer slope/crest transition	[-]
C_z	Chezy coefficient	[-]
E_W	erosion due to excess work	[-]
E_ρ	erosion due to excess work and decreased water density	[-]
f	friction factor for surface roughness	[-]
f_D	Darcy's friction factor for surface roughness	[-]
f_F	Fanning surface friction factor for surface roughness	[-]
f_L	friction factor for inner slope roughness	[-]
g	acceleration due to gravity	[m/s^2]
H	wave height as the vertical distance between a wave crest and the preceding wave trough	[m]
h	wave runup flow depth	[m]
$h_{2\%}$	maximum wave overtopping flow depth at the crest outer point exceeded by 2% of the incoming waves	[m]
h_{B0}	maximum wave overtopping flow depth at the crest/inner slope transition	[m]
$h_{B02\%}$	maximum wave overtopping flow depth at the crest/inner slope transition exceeded by 2% of incoming waves	[m]
h_C	maximum wave overtopping flow depth at point x_c on the crest	[m]
$h_{C2\%}$	maximum wave overtopping flow depth at point x_C on the crest exceeded by 2% of incoming waves [m]	[m]
$h_{C02\%}$	maximum wave overtopping flow depth at the outer slope/crest transition exceeded by 2% of incoming waves	[m]
H_{m0}	spectral mean wave height $\left(H_{m0} = 4\sqrt{m_0}\right)$	[m]
H_s	significant wave height (average height of 1/3 highest waves at structure toe)	[m]
h_{SB}	maximum wave overtopping flow depth at point s_B on the inner slope	[m]
$h_{SB2\%}$	maximum wave overtopping flow depth at point s_B on the inner slope exceeded by 2% of incoming waves	[m]
h_{XC}	maximum wave overtopping flow depth at point x_C on the crest	[m]

Symbol	Description	Units
$h_{XC2\%}$	maximum wave overtopping flow depth at point x_c on the crest exceeded by 2% of incoming waves	[m]
$h_{ZA2\%}$	maximum wave runup flow depth at point z_A on the outer slope exceeded by 2% of incoming waves	[m]
k*	empirical coefficient	[-]
k_1	coefficient $k_1 = \sqrt{\frac{2\,f\,g\,\sin\beta}{h_B}}$	[-]
K_2	coefficient $K_2 = \sqrt[3]{g\ \sin\beta}$	[-]
K_3	coefficient $K_3 = \sqrt[3]{\frac{1}{2}\frac{f}{(h_{B02\%})(u_{B02\%})}}$	[-]
K_4	coefficient $K_4 = u_{B02\%} - \frac{K_2}{K_3}$	[-]
K_W	coefficient of erosion due to excess work	[-]
L_{0p}	peak deepwater wavelength $L_{0p} = \frac{g\,T_p^2}{2\,\pi}$	[m]
$L_{m-1,0}$	spectral mean deepwater wavelength $L_{m-1,0} = \frac{g\,T_{m-1,0}^2}{2\,\pi}$	[m]
m_0	zero moment of the energy spectrum	[m^2]
m_{-1}	first negative moment of the energy spectrum	[m^2 s]
m_n	n^{th} order moment of the energy spectrum	[?]
n	outer slope gradient (n:1 = h:v)	[-]
N_{ow}	number of overtopping waves for the storm duration $N_{ow} = N_w\,P_{ow}$	[-]
N_w	number of incoming waves for the storm duration	[-]
ρ	density of fluid	[kg/m^3]
p	dimensionless coefficient $p = 0.5\,\frac{c_1}{c_0}$	[-]
P_{ow}	probability of overtopping per wave $P_{ow} = N_{ow} / N_w$	[-]
P_V	probability of a wave overtopping volume per wave per unit width V being less than or equal to a specified wave overtopping volume per wave per unit width V_W	[-]
P_{VE}	probability of a wave overtopping volume per wave per unit width V being greater than or equal to a specified wave overtopping volume per wave per unit width	[-]
q	average wave overtopping discharge per unit width	[$m^3/s/m$]

Symbol	Description	Units
$q_{2\%}$	average wave overtopping flow discharge per unit width exceeded by 2% of incoming waves	[m^3/s/m]
q_{all}	allowable wave overtopping discharge per unit width	[m^3/s/m]
$q_{B02\%}$	maximum wave overtopping flow discharge per unit width at crest/inner slope transition exceeded by 2% of incoming waves	[m^3/s/m]
q_{TAW}	total average overtopping discharge per unit width determined by TAW empirical methods	[m^3/s/m]
R_C	crest freeboard above the SWL	[m]
R_u	wave runup above the SWL	[m]
$R_{u2\%}$	average wave runup flow height above the SWL exceeded by 2% of incoming waves	[m]
s_B	coordinate along the inner slope, with s_B = 0 at the crest/inner slope transition	[m]
$\sin\alpha$	sine of outer slope gradient (vertical distance/slope distance)	[m/m]
$\sin\beta$	sine of inner slope gradient (vertical distance/slope distance)	[m/m]
SWL	still water line	[m]
τ_0	shear stress	[N/m^2]
t	time variable	[s]
$\tan\alpha$	tangent of outer slope gradient (vertical distance/horizontal distance)	[m/m]
$\tanh\left(\frac{k_1\, t}{2}\right)$	tangent	[?]
t_E	duration of test or storm	[s]
T_m	average wave period T_m = storm duration/ N_w	[s]
T_m	average wave period (N_w T_m), the storm duration, or time interval considered	[s]
$T_{m-1,0}$	spectral mean wave period $T_{m-1,0} = \frac{m_{-1}}{m_0}$	[s]
$T_{ovt2\%}$	maximum wave overtopping time exceeded by 2% of incoming waves	[s]
T_p	peak period of the wave spectrum	[s]
$u_{2\%}$	maximum wave overtopping velocity at the crest outer point exceeded by 2% of incoming waves	[m/s]

Symbol	Description	Units
u_{B0}	maximum wave overtopping flow velocity at the crest/inner slope transition	[m/s]
$u_{B02\%}$	maximum wave overtopping flow velocity at the crest/inner slope transition exceeded by 2% of incoming waves	[m/s]
u_{C0}	maximum wave overtopping flow velocity at the outer slope/crest transition	[m/s]
$u_{C02\%}$	maximum wave overtopping flow velocity at the outer slope/crest transition exceeded by 2% of incoming waves	[m/s]
u_{SB}	maximum wave overtopping flow velocity at point s_B on the inner slope	[m/s]
$u_{SB2\%}$	maximum wave overtopping flow velocity at point s_B on the inner slope exceeded by 2% of incoming waves	[m/s]
u_{XC}	maximum wave overtopping flow velocity at point x_C on the on the crest	[m/s]
$u_{XC2\%}$	maximum wave overtopping flow velocity at point x_C on the crest exceeded by 2% of incoming waves	[m/s]
u_{ZA}	maximum wave runup flow velocity at point z_A on the outer slope	[m/s]
$u_{ZA2\%}$	maximum wave runup flow velocity at point z_A on the outer slope exceeded by 2% of incoming waves	[m/s]
v	measured velocity during wave overtopping	[m/s]
V	wave overtopping volume per wave per unit width	[m^3/m]
$V_{2\%}$	maximum wave overtopping volume per wave exceeded by 2% of incoming waves	[m^3/m]
$V_{B2\%}$	maximum wave overtopping volume per wave per unit dike crest lateral width at the crest/inner slope transition exceeded by 2% of incoming wave	[$m^{3/}$m]
V_{max}	maximum overtopping volume per wave per unit dike crest lateral width	[m^3/m]
V_W	wave overtopping volume per wave per unit width for a certain exceedance probability $(1 - P_V)$	[m^3/m]
V_W	specified wave overtopping volume per wave per unit width	[m^3/m]
x_*	remaining wave runup length $x_* = (x_z - x_A)$	[m]
x_A	horizontal coordinate on the outer slope with x_A = 0 at the SWL	[m]

Symbol	Description	Units
x_C	horizontal coordinate on the crest with x_C = 0 at the outer slope/crest transition	[m]
x_z	horizontal projection of the wave runup height R_u on the outer slope relative to the SWL $x_z = R_u/\tan\alpha$	[m]
z_A	vertical coordinate on the outer slope with z_A = 0 at the SWL	[m]
z_c	levee freeboard relative to the peak storm surge	[m]
γ	reduction factor $\gamma = \gamma_f\,\gamma_\beta$	[-]
$\gamma_\mathcal{B}$	reduction factor for oblique wave attack	[-]
γ_b	reduction factor for a berm	[-]
γ_f	reduction factor for surface roughness	[-]
γ_{fA}	reduction factor for surface roughness on the outer slope	[-]
γ_{fC}	reduction factor for surface roughness on the crest	[-]
γ_h	reduction factor for a shallow foreshore	[-]
γ_v	reduction factor for a vertical or very steep wall on a slope	[-]
π	relationship of a circle circumference to the circle diameter	[-]
ξ_{eq}	equivalent Iribarren number for a slope with a berm $\xi_{eq} = \gamma_b\,\xi_{op}$	[-]
ξ_{gr}	transition point between breaking waves and nonbreaking waves = 2	[-]
$\xi_{m-1,0}$	Iribarren number $= \tan\alpha/\sqrt{H_{m0}/L_{m-1,0}} = \tan\alpha/\sqrt{2\,\pi\,H_{m0}/g\,T_{m-1,0}^2}$	[-]
ξ_{op}	Iribarren number $= \tan\alpha/\sqrt{H_s/L_{0p}} = \tan\alpha/\sqrt{2\,\pi\,H_s/g\,T_p^2}$	[-]
$\xi_{S,-1}$	Iribarren number $= \tan\alpha/\sqrt{H_s/L_{0m}} = \tan\alpha/\sqrt{2\,\pi\,H_s/g\,T_{m-1,0}^2}$	[-]

1. Introduction

In 2005, Hurricane Katrina caused destruction in New Orleans, Louisiana, to an extent not experienced by previous hurricanes. Approximately 80% of the city was flooded and 986 deaths in Louisiana (Brunkard et al. 2008) are attributed to the event. In an effort to objectively understand how this had occurred, multiple review panels comprised of experts in their fields were formed. Three notable panels were the American Society of Civil Engineers External Review Panel (Andersen 2007), The Interagency Performance Evaluation Task Force (IPET (Link et al. 2009), and the Independent Levee Investigation Team (Seed et al. 2006). All aspects of the disaster were evaluated and a common thread of their findings was that the failure of levees was not from the water side, but *from the landward side*.

Water that overtops levees or dikes during storms exerts hydraulic loads on the landward-side slope protection. Grass and soil can be eroded by the resulting flow shear stresses and turbulence, and even robust armoring alternatives can be damaged at higher overtopping rates. In the absence of wind-generated waves, water will not overflow the levee until the water elevation exceeds the levee crown elevation. However, wave overtopping can occur before the water elevation reaches the levee crown elevation because the incident waves run up the flood-side (seaward-side) slope and flow across the levee crest before cascading down the landward-side slope. Large waves typical of hurricanes or tropical storms can cause significant overtopping even when the levee has several feet of freeboard (crown elevation minus still water elevation).

There are two means of levee crest overflow: steady overflow and wave overtopping. The main difference between steady overflow and wave overtopping is the variation of flow magnitudes in

space and time. Assuming the levee crown elevation is constant over a reach of levee, steady overflow has nearly constant discharge per unit length. On the landward-side slope the supercritical flow rapidly accelerates until terminal velocity is reached, and the flow momentum is balanced by the shear resistance of the slope.

Conversely, flow associated with overtopping of an individual wave is highly unsteady in both space and time. The largest flow thickness and velocity occur at the leading edge of the wave as it crosses the levee crest and accelerates down the landward-side slope. The unsteady flow is supercritical with both temporal and spatial accelerations. While achievement of terminal velocity is assumed, the flow remains unsteady in time due to the variation of discharge over individual waves and unsteady in space because of the variation in irregular wave overtopping volumes. The peak overtopping discharge of a wave can be between 100 and 1000 times the average overtopping discharge resulting from the storm event (Pullen et al. 2007). Thus, the overtopping wave exerts higher instantaneous shear stresses on the slope than steady overflow, but the duration of the highest loading is short relative to steady overflow. This difference may be important for levee slope protection that fails due to high intermittent loading rather than cumulative loading of small magnitude over longer durations.

1.1. Objectives

The terms “aeration” and “bulking” are at times used interchangeably in literature. For the purpose of outlining and fulfilling the objectives of this study, “aeration” is defined as the volume of air in a sample divided by the total sample volume (Wood 1983). “Bulking” is the increase in flow thickness resulting from aeration. Additional terminology to clarify is flow “depth” versus flow “thickness”. In steady state flow hydraulics, “depth” is depth of flow normal to the direction of flow, towards the free surface (Chow 1959). In coastal hydraulics, the

term flow thickness is frequently used in place of depth to describe the same parameter, as in Schüttrumpf and Oumeraci (2005).

Objectives for the current investigation are as follows:

1) Summarize previous wave overtopping investigations and their outcomes in addition to relevant steady state aeration studies predicting aeration percentage, which leads to flow bulking;
2) Identify the relevant physical parameters of aeration-induced bulking during wave overtopping flow on the landward side of levees;
3) Quantify flow bulking occurring on the crest and landward side of levees during wave overtopping simulation;
4) Perform analyses to develop a mathematical model for bulking prediction during wave overtopping simulation and determine statistical significance;
5) Provide a comprehensive summary of procedures, results, limitations and recommendations for bulking during wave overtopping flows.

Completion of the study objectives will improve the fundamental understanding of wave overtopping simulation processes, provide a model for predicting bulking on the landward side of levees during wave overtopping and provide a foundation for estimating flow bulking to improve quantification of shear stress values experienced by the levee surface during wave overtopping for levee armoring design.

1.2. Methodology

A systematic approach was taken to address the objectives. A comprehensive literature review of previous laboratory and field studies was conducted pertaining to wave overtopping of levees. Additionally, studies related to steady state overtopping aeration were reviewed. Input parameters and equations developed from wave overtopping studies are summarized and deficiencies in quantifying wave overtopping simulation processes are identified.

A series of experiments was conducted in a wave overtopping simulator located at the Engineering Research Center of Colorado State University. Data were collected from a wave overtopping simulator and adjacent, prototype scale levee section at Colorado State University (CSU). Subsequently, flow bulking predictive equations based on wave volume and distance down-slope from the wave overtopping simulator were developed and evaluated for goodness of fit to collected data. Recommended application of the equations for design purposes, limitations of the data, recommendations for further research and conclusions are presented.

2. Literature review

Extensive research has been conducted to characterize wave overtopping flows through field studies, laboratory experiments, mathematical deduction and empirical curve fitting. Methods for calculating overtopping flow thicknesses have been presented, but these methods fail to account for entrained air that increases the measured flow depth at prototype (full) scale. The purpose of this investigation is to provide a method for predicting the bulking occurring during wave overtopping flow simulation on the landward side (inner slope) of levees having a 3:1 (Horizontal: Vertical) slope. Thus the end user in the engineering design community has a better understanding of the flow forces involved.

Bulking is an indicator of the percent aeration, and aeration quantification is necessary for estimating slope surface shear stresses during wave overtopping events. For completeness, the more commonly applied wave runup and wave overtopping equations will be summarized. The summary literature review is presented to document the complexity of wave overtopping in levee design. A comprehensive table listing wave runup and overtopping equations, their application and their source is presented in Appendix A. In addition, this thorough examination of wave overtopping flow studies provides a cursory review of bulking in steady state overtopping flows.

The knowledge that flow aeration or bulking affects flow properties has been recognized for nearly a century as demonstrated by the pioneering Ehrenberger study (1926) to define and obtain the distribution of air in self-aerated flows. Though the results were marginal, the study laid the foundation for Lamb and Killen (1950) to develop a more robust method for measuring air entrainment. The new, electrical method allowed relatively rapid measurements (approximately 30 seconds each) when compared to mechanical methods and provided

acceptable aeration measurement values up to over 90 percent aeration. Technology for aeration measurement remained virtually unchanged until Boes and Hager (1998) developed a fiber-optical probe method with a faster signal response time, higher sampling frequency and less flow disturbance due to smaller size probe. Similar to the electrical method, a local average aeration is measured so the flow must be steady during the acquisition time. Unlike the electrical method which measures a change in electrical resistance, the fiber-optical method measures void fraction of bubbles contained in the flow.

An electrical method was used in multiple steady state studies summarized and analyzed by Wood (1983). It was shown that for uniform flow, self-aeration can be predicted and there is a mean air concentration and concentration distribution that is unique to each slope. In addition, Darcy's friction factor varies with air concentration and can be predicted based on the un-aerated friction factor and mean air concentration between the bed and depth where aeration is equal to 90% (Wood 1983). In addition, Wood (1983) presented a method for calculating aeration concentration as a function of location in the water column. Measurement methods produce inconsistent results at flow depths where aeration is greater than 90%. As a result, all reviewed steady state literature focuses on the flow region where aeration is 90% or less.

Chanson (2004a) provided a summary of air-water flows and measurement methods. It was also suggested that steady flow measurement techniques may be applied to unsteady flow conditions such as dam break wave propagation by calculating local void fractions over a short time interval. Importantly noted was that previous studies of air entrainment using seawater suggest a very different process than those observed with fresh water.

Dam break wave propagation may be considered similar to wave overtopping of levees, and aeration during wave propagation following a dam break was the subject of Chanson (2004b). Consistently strong aeration in the surge front leads to the conclusion that increased buoyancy reduction in "white water" will increase the relative density of particles (leading to increased bed load transport, in this case.) In addition, a different void fraction distribution shape, relative to steady state overtopping, was proposed. Possible explanations included a non-hydrostatic pressure field, a change in rheological fluid properties causing some change in the air-water structure between the leading edge and the main flow, a two-phase flow regime change from some slug flow at the leading edge to homogeneous bubbly flow after or a change in boundary friction between the wave front and the main flow.

In general, free surface aeration is a common occurrence in steady state flows and hydraulic structures. Chanson (2009) discussed potential issues with small-scale model studies into aeration versus prototype scale. His conclusions were that model studies drastically underestimate dimensionless turbulence, air-water interfacial areas and mass transfer rates leading to critical issues with model result extrapolation to prototype conditions. In addition, instrumentation type is rarely addressed, yet instrument type, probe sensor size and sampling rate affect the bubble size detectable which, in turn, affects final results. A final finding was turbulent air-water flows are poorly understood, and, due to the ubiquitousness of "white water" flows, numerical or hybrid numerical/scale modeling was proposed as a future research direction.

Hughes (2007) evaluates permissible wave overtopping criteria for earthen levees without protection and with protective systems for overtopping flow that have been in existence for many years. A few examples of such protections are vegetation, vegetation combined with synthetics in turf reinforcement mats, articulating concrete blocks, hydromulch and shotcrete. Design

guidance for levee protective systems intended for use under steady overtopping conditions is available from sources such as River Engineering for Highway Encroachments (Richardson et al. 2001). The limitations of steady overtopping design knowledge when combined with wave overtopping are succinctly summarized by Hughes (2008b).

In recent years, advances have been made into characterizing many of the hydrodynamic parameters associated with wave-only overtopping at trapezoidal levee and dike structures. Equations and methodologies are available for estimating wave run-up and average wave overtopping discharge (Van der Meer and Janssen 1995, Van der Meer 2002), distribution of overtopping wave volumes (Franco and van der Meer. 1994, Van der Meer and Janssen 1995), and leading edge flow thickness and velocity (Schüttrumpf et al. 2002, van Gent 2002b, Schüttrumpf and van Gent 2003, Schüttrumpf and Oumeraci 2005). These relationships are summarized in Pullen et al. (2007). Small-scale laboratory experiments of combined wave overtopping and steady overflow have provided empirical equations for average overtopping rates, distribution of overtopping volumes, and preliminary estimates of flow parameters on the landward-side slope (Hughes and Nadal 2009). In addition, prototype-scale testing of levee armoring performance on landward slopes has been conducted by Thornton et al. (2011 , 2012).

An outcome of wave runup and overtopping research has been proposed methods for evaluating the landward side of levees for erosional resistance to overtopping flows. The goal of proposed methods is the ability to incorporate steady flow knowledge and experience into an application addressing wave overtopping erosion challenges. Van der Meer et al. (2010) proposed a shear stress based, cumulative hydraulic loading approach reliant on peak overtopping wave velocities and a critical, threshold velocity that is a function of the levee protective cover. Dean et al. (2010b) evaluated three approaches: velocity, shear stress and a work basis approach. Each of

Dean's possible three approaches also incorporates a threshold concept above which erosion of the levee will occur. The conclusion was that the cumulative excess work basis approach is the most reasonable of the three evaluated and provides the best results. Hughes (2011a) evaluated Dean et al.'s erosional equivalence method and expanded it to "evaluate the strength and resiliency of earthen levee protection against wave overtopping during severe hurricanes" to create a more robust erosional equivalence method for evaluating land-side levee armoring to resist overtopping waves.

Van der Meer et al.'s (2010) cumulative hydraulic loading concept was not only the product of many years of accumulated research, but a result of wave over-topping simulation. The empirical equations for wave-only overtopping were incorporated into the theory used in creating modern-day *wave overtopping simulators* (Van der Meer et al. 2006, Van der Meer 2007a, Van der Meer et al. 2008b, Van der Meer et al. 2011). A mobile wave overtopping simulator is a large container temporarily installed on the crown of a levee or dike that simulates the wave overtopping hydraulics by releasing volumes of water in a manner that duplicates the correct leading edge thicknesses and velocities for a distribution of wave volumes associated with a specific storm condition.

Design and construction of the wave overtopping simulator was based on the velocity overtopping thickness prediction studies of Schüttrumpf and Van Gent (2003) (Van der Meer 2006). Schüttrumpf and Van Gent's (2003) predictive equations of wave overtopping velocity produced similar results to each other, however flow thicknesses did not agree. This discrepancy was investigated by Bosman (2007). Bosman (2007) hypothesized the difference in flow thickness could potentially be explained by differences in experimental setup, in particular the different seaward slopes, 1:4 and 1:6, used by the investigators. The hypothesis suffered a

setback when the Flowdike project data, a European Union Programme (Lorke et al. 2009, 2010), which had a slope of 1:3, fell between the data of Schüttrumpf and Van Gent (2003). When evaluating wave overtopping simulator results, van der Meer (2010) discussed these issues and demonstrated that existing velocity and flow depth predictions, when combined, violate the conservation of mass principle. Within the document, Van der Meer (2010) concluded further research is needed in this area.

In spite of advances in characterization of steady state aerated flow, little is known about aeration and bulking in wave overtopping flows, which vary in time and volume. The closest analogous work is presented in a few studies on dam break waves. Wave overtopping studies have largely minimized aeration as an issue as demonstrated in the EurOtop wave overtopping manual (Pullen et al. 2007) where the concept is mentioned.

Numerous studies on wave runup and overtopping have been conducted yielding many predictive equations. Overtopping and runup investigations relevant to this study are those providing the foundation for crest and landside flow thickness prediction. Studies of particular interest include prediction of maximum wave overtopping flow depth exceeded at the outer crest by two percent of incoming waves by Bosman (2007), van der Meer (2007a) and Valk (2009). Similar relationships are developed for the inner crest by van Gent (2002b) and Bosman (2007). Bosman (2007) reviews the work of Schüttrumpf et al. (2001) and van Gent (2002c) and finds a discrepancy in the coefficients for flow depth. Schüttrumpf's full scale model tests yielded a coefficient 2.2 times that of van Gent's (2002c) small scale tests. In addition, Schüttrumpf's velocity measurements failed to properly register when velocities exceeded 8.5 ft/s. Bosman's (2007) conclusion was turbulent, fast-moving aerated flow is difficult to quantify.

Van der Meer et al. (2006) used the work of Schüttrumpf and van Gent (2003) as the basis for a wave overtopping simulator. As there existed a discrepancy in predicted flow thicknesses, van der Meer (2006) used velocity as the basis of design. Hughes (2008a) provides an excellent summary of the equations for velocity, flow thickness and friction factor calculation for overtopping waves on the crest and landward side of levees. The literature does not address aeration effects on wave overtopping parameters. In light of known effects of flow aeration during steady state overtopping, such as changing friction factors and decreased buoyancy from decreased density (Wood 1983, Chanson 1994b), similar changes to friction factors and buoyancy are likely occurring during wave overtopping. Without incorporating improved knowledge of aeration and bulking in wave overtopping, erosion models such as those presented (Dean et al. 2010b, Hughes 2011a, van der Meer et al. 2010) will inaccurately portray erosion potential of irregular wave overtopping on the landward side of levees.

The key studies, Wood (1983), Chanson (1994b, 2004a, 2009), van der Meer et. al (2006, 2010), Bosman (2007), Pullen et. al (2007), Dean et. al (2010b), Hughes (2007, 2008a, 2008b, 2011a) and Thornton et. al (2011, 2012) have been referenced, but there are many more equations associated with wave overtopping and its prediction. A summary of basic predictive equations and their source is presented in Appendix A The table addresses common variables and defines key concepts from a selected body of research papers, reports, and manuals applicable to the field of designing and evaluating coastal structures to withstand wave runup and wave overtopping. Fundamental relationships commonly presented for designing and evaluating coastal structures to withstand wave runup and wave overtopping are identified, and similar equations presented in multiple sources are compared for consistency and differences in variable notation names are noted.

Investigations pertaining to aeration or bulking are notably lacking or altogether absent. For this reason, a testing program was devised and implemented with the objective of providing some quantification of the aeration and bulking occurring on landward side levee slopes during wave overtopping as presented in Section 1.1.

3. Test Facility, Instrumentation and Program

Wave overtopping events in the field are usually unpredictable. Environmental conditions related to overtopping are often dangerous and uncontrollable. For these reasons, a wave overtopping simulator (WOS) was designed and constructed at the Colorado State University (CSU) Hydraulics Laboratory. The CSU WOS is based on the work of van der Meer (2006, 2007a) and was constructed with funding from the United States Army Corps of Engineers, New Orleans District under Project Hope and the assistance of van der Meer Consulting B.V. Design and construction of the WOS are detailed in Thornton et al. (2010).

3.1. Facility

The Facility was funded by the United States Army Corps of Engineers, New Orleans District to investigate potential levee armoring materials. Anticipated wave overtopping conditions in the New Orleans area dictated the WOS capacity. The CSU WOS facility is capable of simulating full-scale wave overtopping having maximum average overtopping discharges up to 4.0 ft^3/s per ft (4.0 cfs/ft) and higher depending on the incident wave conditions. The Facility simulates intermittent wave overtopping by controlled periodic releases of specified volumes of water held in a large vertical container.

The WOS was constructed as a fixed-in-place simulator (versus a mobile simulator as in van der Meer (2006, 2007a, 2007b, 2008a, 2008b, 2010)) because of the size needed to generate large wave overtopping rates. Thus, for performance testing, instead of transporting a mobile simulator to an actual levee, it is necessary to construct a simulated levee surface at the simulator. Grass-covered and armored levee slopes are replicated by special planter trays that

contain appropriate soil and vegetation to simulate specific soil/grass characteristics. Slope armoring is installed in the test trays according to product specifications.

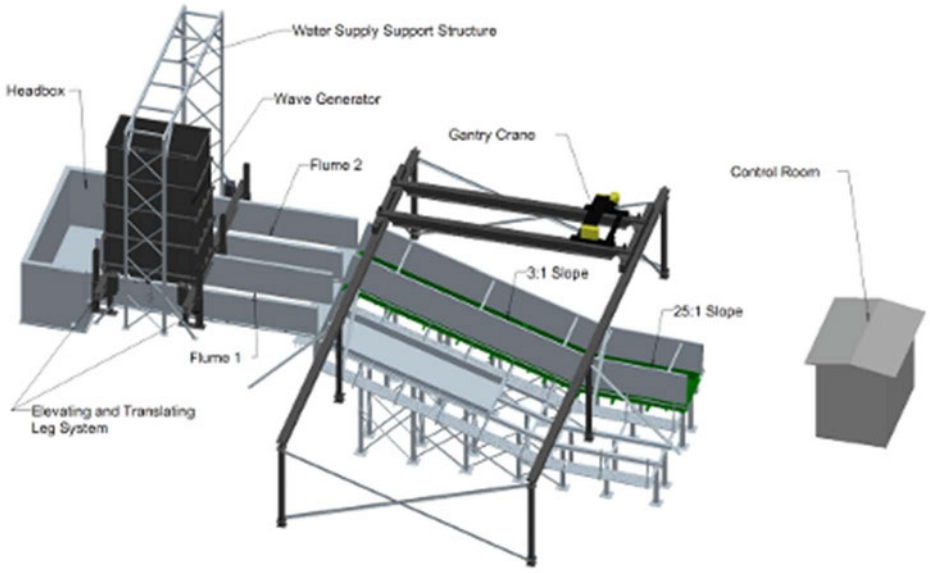

Figure 3-1. Schematic of wave overtopping test facility.

The facility design (Figure 3-1) features two side-by-side 6-ft-wide test channels with steel framework to support the levee trays. The wave overtopping simulator machine (large green vertical container shown positioned on the left-side channel in the Figure 3-2) was designed to be moved to either test channel. This feature expedites testing by permitting preparation of a test specimen in one channel while testing is in progress in the other channel. An overhead gantry crane facilitates placement and removal of the test planter trays.

Figure 3-2. CSU wave overtopping test facility.

The upper photograph of Figure 3-2 shows the Test Facility with the Overtopping Simulator container (large green box) and the support framework on which the test trays are mounted. The three sequential images on the lower portion of Figure 3-2 demonstrate the release of a large overtopping wave volume onto a set of test trays populated with Bermuda grass in this case.

For research purposes, a specially constructed set of steel trays was fabricated and installed to insure surface uniformity and eliminate the potential of varying test conditions resulting from erosion of soil and vegetation. Modifications were made to the typical flume configuration to allow for installation of instruments. Holes were placed in the test surface bed from the crest to

the berm with mounts for installation of flush mount pressure transducers as presented in Figure 3-3. The result was a full-scale, rigid bed, physical model of the crest, landward slope, and berm of a typical levee with the capability of data collection along the entire length as presented in Figure 3-3. Additional instruments visible in Figure 3-3 are surfboards for flow thickness measurement and paddle wheel flow sensors for velocity measurement.

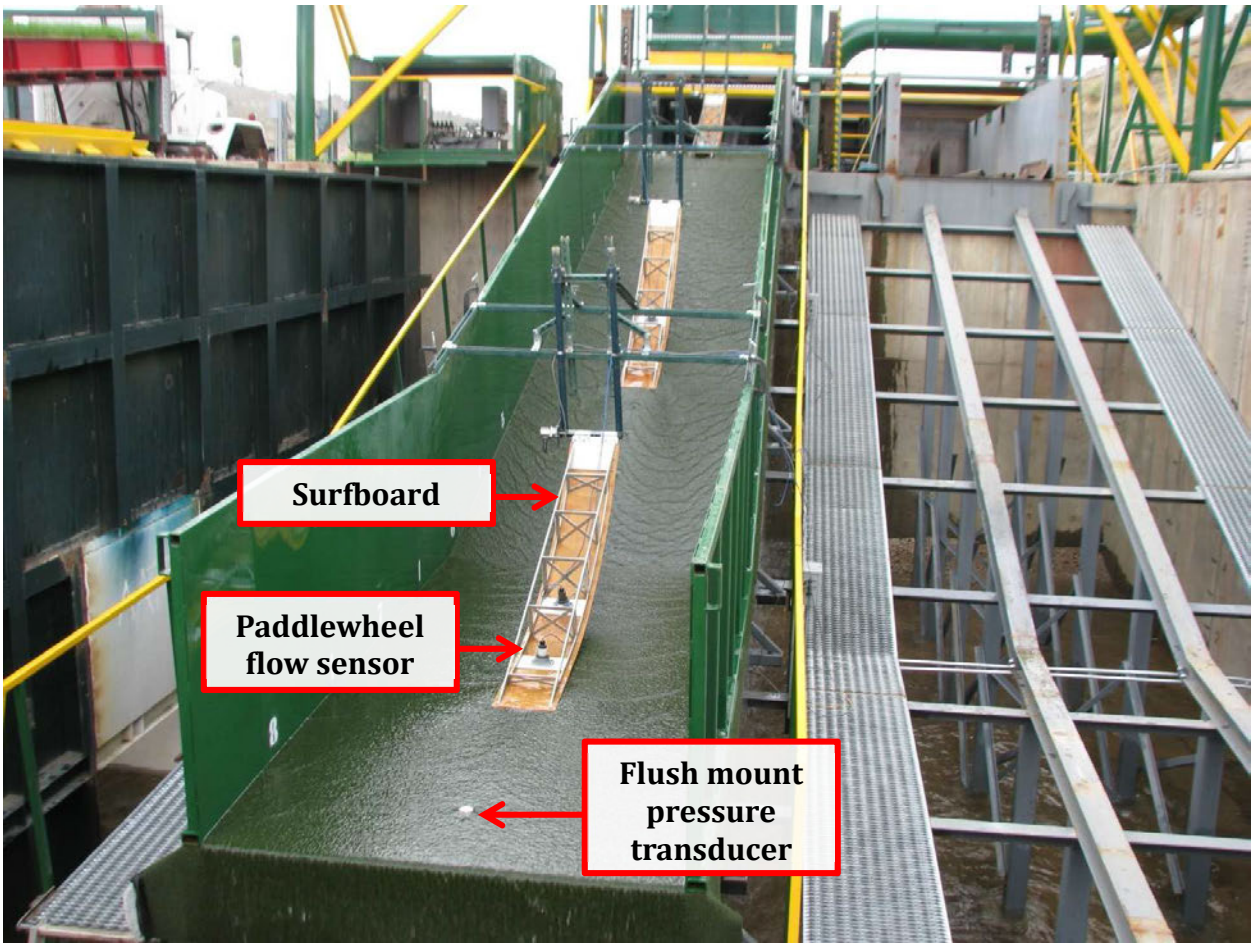

Figure 3-3. CSU wave overtopping test facility instrumentation.

Water to operate the Wave Overtopping Test Facility is supplied from Horsetooth Reservoir shown in the aerial photograph of the CSU Engineering Research Center presented in Figure 3-4. Reservoir water is initially supplied through a 36-inch diameter pipe with maximum head pressure of 250 ft (110 psi), and the simulator is fed by smaller diameter pipes (12-inch or 3-inch

diameter depending on the target average wave overtopping discharge). After water passes through the test facility, it flows to College Lake and is used for irrigation.

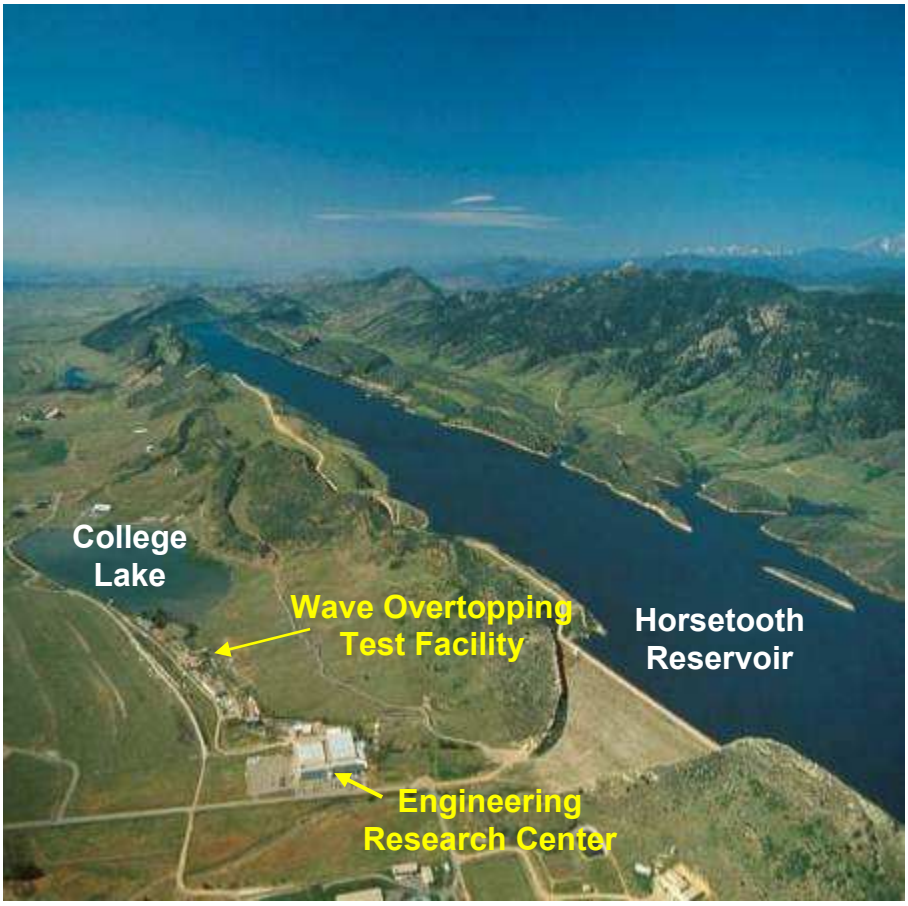

Figure 3-4. Location of wave overtopping test facility.

The CSU wave overtopping simulator has a water volume capacity of approximately 958 ft^3. This simulator has about three times the capacity of the Dutch mobile overtopping simulator (van der Meer 2007a). The simulator can release individual overtopping wave volumes up to 175 ft^3/ft. Depending on the overtopping wave condition being simulated, the Wave Overtopping Test Facility can replicate wave overtopping events having average overtopping discharges in excess of 4.0 ft^3/s per ft.

3.2. Instrumentation

Physical parameters measured to characterize the overtopping waves were volumetric flow rate (q), individual wave volume (V_w), distance from the face of the WOS (x) (crest and slope), surface velocity parallel to the bed (v), pressure (p) and flow thickness perpendicular to the bed (y). Quality, calibrated instrumentation was employed to collect the required data.

3.2.1. Flow measurement

During testing, flow is delivered to the simulator at a constant rate equal to the desired average overtopping rate. The flow rate is set and monitored via an Endress + Hauser® electro-magnetic flowmeter with precision (as determined by Endress + Hauser®) of $\pm$ 0.5% of the measured flow rate. Once the water distribution system reaches an equilibrium state, the constant head of Horsetooth Reservoir creates a constant, virtually unchanging water discharge to the WOS.

3.2.2. Simulator control

A programmable logic controller (PLC), specifically chosen and programmed for the WOS, controls valve operation based on user input wave volumes to be simulated. The PLC sends signals to a hydraulic power unit to open and close the WOS valve. The PLC also measures the rotation of the WOS valve via a rotational digital encoder mounted to the WOS valve axis and transmits a signal to stop opening the valve at the correct rotation allowing for control of the length of time a wave overtops the levee.

Figure 3-5 presents the stainless steel housing for the PLC with the connection cables and internal components. Figure 3-6 presents the hydraulic power unit that moves the WOS valve and the variable speed drive allowing control of WOS valve movement speed.

Figure 3-5. PLC for controlling the WOS.

Figure 3-6. The hydraulic power unit (left) with variable speed drive (right).

User input valve control signals are sent from a local personal computer (pc) to the PLC. A custom user interface on the pc allows user input for wave number in the sequence, wave volume to be simulated, time since beginning of simulation to open the WOS valve, time to close the WOS valve and number of degrees to open the valve. The collection of user input to control the WOS is referred to as a "steering file". The connection between the pc and PLC is an Ethernet CAT 5 cable.

3.2.3. Surfboards

The surfboards (as they are colloquially called) are instruments for measuring flow thickness of overtopping waves as described in van der Meer (2010) and presented in Figure 3-7.

Figure 3-7. Surfboard for measuring flow thickness.

The instrument was designed to hydroplane on the surface of an overtopping wave. The upstream end is hinged to rotate as hydroplaning occurs. The rotation is measured by a Celesco® 8420 potentiometer connected to the hinge which converts rotation to a 4-20 mA signal proportional to the degree of rotation. The logged signal is later converted to a flow thickness using a calibration curve relating the signal to surfboard height above the levee surface.

Surfboards must be constructed using materials and connectors strong enough to withstand the forces of wave impact yet light enough to accurately measure flow thickness. Aluminum frames were manufactured for an acceptable strength to weight ratio. The hydroplane was formed using

thin wood paneling with polyurethane coating and attached using recessed machine screws threaded into the aluminum frame. Three surfboards were constructed and used during testing.

Surfboards are curved to better maintain contact between the surfboard and the water surface. Because the surfboard is curved, high velocity flow can lift the downslope end of the surfboard out of the water along with the downslope paddlewheel. For this reason, there is another paddlewheel mounted in the surfboards. The location of the upslope paddlewheel is such that it is in contact with flow when the downslope paddlewheel is lifted out of the water.

Due to the curvature of the surfboard, the distance from the WOS where flow thickness is measured varies dependent on the flow thickness measured. To determine distance from the WOS corresponding to a given flow thickness, calibration curves were developed for each surfboard installation location similar to the equation for locations one and two

$$y = \frac{27*\left(\text{voltage}_{\text{measured}}\text{-}1.97\right)^{0.83}}{12} \quad (1)$$

$$x = (\text{-}0.41)y^3 + 0.70y^2 \text{-} 1.54y + 12.32 \quad (2)$$

where y equals flow thickness measured in feet and x equals distance in feet downstream from the WOS. All distance equations as a function of flow thickness are presented in Appendix B.

3.2.4. Paddle wheel flow sensor

Flow velocity was measured using Seametric® IP-80 series paddle wheel flow sensors (paddlewheels) mounted through the surfboards. A paddlewheel is presented in Figure 3-8. Two paddlewheels were mounted in each surfboard. The upstream paddlewheel in a surfboard is referred to as paddlewheel one and the downstream paddlewheel in the same surfboard is paddlewheel two. The downstream paddlewheel captured low flow conditions and the upstream

paddlewheel captured high flow conditions when the curvature of the surfboard lifts the low flow paddlewheel out of the flow. The paddlewheels send a pulse signal to a pulse counter which converts pulses to a 4-20 mA output linearly proportional to the pulse rate. The logged signal is later converted to flow velocity using a calibration curve relating pulses, 4-20 mA signal and flow velocity. Paddlewheel data were collected at twenty locations along the levee approximately coinciding with the pressure transducer locations.

Figure 3-8. Paddle wheel flow sensor

3.2.5. Pressure transducers

Overtopping flow thickness was measured using Wika® flush mount IS-21-S pressure transducers mounted up through the levee from the underside. This allowed for mounting as flush as possible with the surface to diminish measurement effects created by flow transitioning from turf to transducer to turf while crossing the transducer. A pressure transducer is presented in Figure 3-9.

Figure 3-9. Pressure transducer

Pressure transducer data were collected at twenty locations on the levee. Two locations were on the horizontal crest, fifteen locations on the 3:1 levee and three locations were located on the 25:1 berm. Distance of each transducer mounting location from the WOS is presented in Table 3-1. Transducers were placed approximately two feet apart in the down slope direction. Pressure transducer output was a 4-20 mA signal proportional to pressure detected by the sensor.

Table 3-1. Pressure transducer mounting locations

	Pressure Transducer Location No.	Distance Downslope from WOS (ft)
WOS		0.00
Horizontal Crest	1	10.81
	2	12.41
Slope Transition		13.09
3:1 Levee Slope	3	13.34
	4	17.58
	5	19.88
	6	21.58
	7	23.58
	8	25.59
	9	27.60
	10	29.59
	11	31.60
	12	34.04
	13	36.16
	14	37.60
	15	39.60
	16	42.10
	17	42.80
Slope Transition		43.58
25:1 Berm Slope	18	45.12
	19	49.58
	20	54.21
End of Simulated Levee		55.75

Locations of other instruments are referenced to a transducer location number when discussed. For example, paddlewheel one in surfboard two at location seven is the upstream paddlewheel mounted in the second surfboard downstream from the WOS and the paddlewheel is over pressure transducer location number seven.

3.2.6. Staff gages

Flow thickness was also measured using staff gages placed at eight locations along the slope and oriented perpendicular to the slope. One staff gage was mounted on the horizontal crest, five staff gages were mounted along the 3:1 levee and two staff gages were mounted on the 25:1 berm. Staff gages were wall mounted and located along the slope to coincide with pressure transducer distances from the WOS. A staff gage is presented in Figure 3-10.

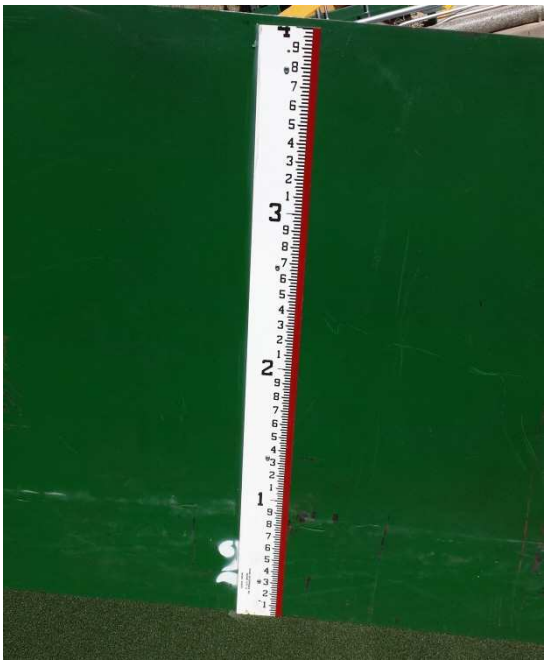

Figure 3-10. Staff gage.

3.2.7. Data collection

Collection of data was accomplished using two methods. The first method was with the electrical instrumentation (surfboard potentiometers, paddle wheel pulse counters and pressure transducers). All electrical instrumentation output a 4-20 mA signal output that was transmitted to a National Instruments® SCB-68 shielded connector block where it was converted to one to five volts. The voltage signal is linearly proportional to the measured process within the measurement range of the instrumentation. The voltage then passed to a National Instruments®

DAQcard-6036E data acquisition card capable of sampling at 200,000 samples per second. The DAQcard was connected to a pc with custom Labview® data logging software capable of recording up to sixteen data channels at a user specified collection rate. The data collection rate was 50 Hz for all electronic instruments.

The second data collection method was visual observation. A team of five to eight people were assembled and each person assigned to a different staff gage. As a wave passed, maximum wave height on the staff gage was noted and recorded. To mitigate observer bias, each person rotated to the next staff gage for the next wave. This was repeated until 27 to 30 observations were collected for each of the selected wave volumes at each staff gage location.

3.2.8. Data collection locations

Electrical instrumentation data collection locations were carefully chosen to best capture wave overtopping simulation flow bulking phenomena. Locations were also chosen to provide sufficient down-slope density of collection points. There were two collection locations on the horizontal crest, fifteen on the 3:1 levee and three on the 25:1 berm for twenty total data collection locations. Spacing was approximately two feet between each location. Location and distance from the WOS of representative collection locations is presented in Figure 3-11. Other locations can be deduced from the pressure transducer number (Xdcr #) and the knowledge the pressure transducers were located approximately 2 ft. apart. Location numbers throughout this document refer to pressure transducer locations (e.g. Location 2 is the location of pressure transducer #2 approximately 13.09 ft downslope of the WOS.) Staff gages were wall mounted at each of the eight pressure transducer locations labeled in Figure 3-11

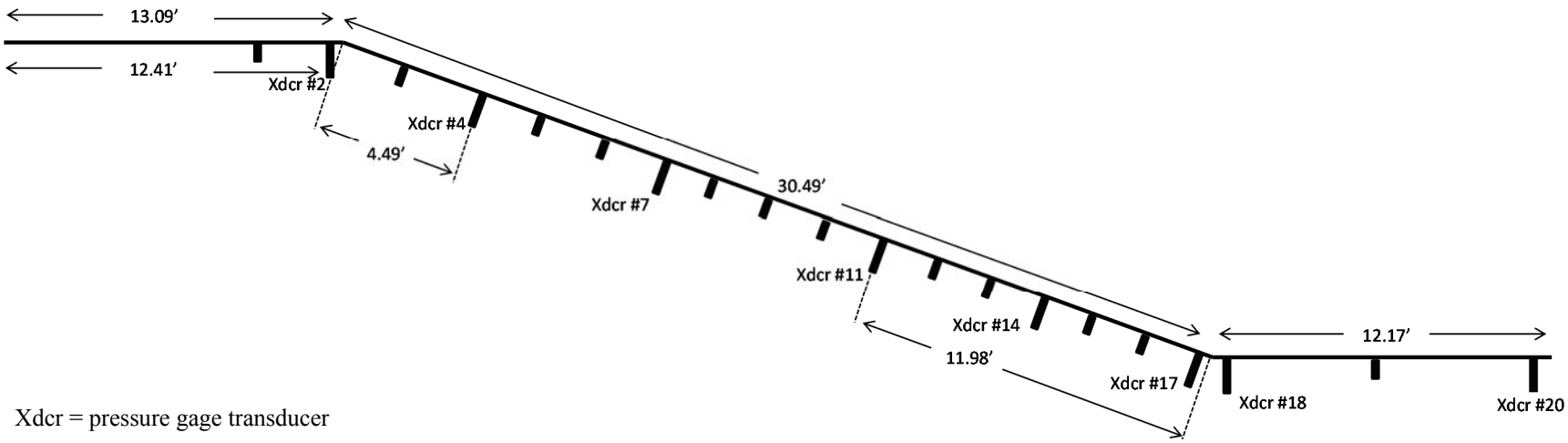

Xdcr = pressure gage transducer
Location 'X' = location of Xdcr 'X'

Figure 3-11. Instrumentation layout (not to scale)

3.2.9. Test program

The test program was developed to characterize the range of wave volumes produced by the WOS at an average overtopping rate of 2.2 cfs/ft. A series of ten recorded tests were conducted in which ninety-six waves presented in Table 3-2 were routed through the WOS. Each test required approximately one hour and ten minutes to complete. At this average overtopping rate, the minimum V_w simulated was 20 ft^3/ft (cf/ft) and the maximum V_w was 175 cf/ft. All volumes of multiple five between the minimum and maximum volumes were simulated. For electrical instrumentation, all volumes were randomized simulated in triplicate for repeatability. Thirty-two unique wave volumes (ninety-six total) were simulated in each of the first seven tests. Simulated wave volumes and order of occurrence is presented in Table 3-2.

Table 3-2. Wave volumes and order of occurrence, tests 1-7

Wave Number	Wave Volume (ft^3/ft)	Wave Number	Wave Volume (ft^3/ft)	Wave Number	Wave Volume (ft^3/ft)	Wave Number	Wave Volume (ft^3/ft)
1	50	**25**	40	**49**	80	**73**	145
2	20	**26**	45	**50**	95	**74**	65
3	45	**27**	145	**51**	100	**75**	150
4	140	**28**	130	**52**	125	**76**	120
5	80	**29**	170	**53**	60	**77**	160
6	155	**30**	170	**54**	25	**78**	45
7	20	**31**	115	**55**	120	**79**	90
8	145	**32**	160	**56**	55	**80**	90
9	140	**33**	75	**57**	110	**81**	105
10	95	**34**	110	**58**	135	**82**	155
11	90	**35**	165	**59**	40	**83**	80
12	75	**36**	155	**60**	125	**84**	130
13	25	**37**	170	**61**	100	**85**	165
14	35	**38**	60	**62**	150	**86**	120
15	30	**39**	165	**63**	40	**87**	110
16	130	**40**	35	**64**	125	**88**	70
17	50	**41**	85	**65**	50	**89**	35
18	175	**42**	115	**66**	115	**90**	85
18	25	**43**	70	**67**	135	**91**	135
20	55	**44**	65	**68**	175	**92**	95
21	75	**45**	160	**69**	105	**93**	85
22	20	**46**	30	**70**	105	**94**	55
23	70	**47**	150	**71**	65	**95**	100
24	30	**48**	175	**72**	140	**96**	60

There were a limited number of data channels available at one time to collect data from instrumentation. For this reason, seven tests were initially conducted. Instrumentation was relocated for each test, as necessary, to ensure velocity, flow thickness and pressure were collected at each location for each wave volume. In addition, a surfboard, paddlewheel and pressure transducer were located on the horizontal crest (Location 1 or 2) during each test for later verification of mass conservation during testing. The inherent assumption in moving instrumentation between tests is wave volumes can be replicated precisely and combining measurements across tests is valid. Maintenance of instrumentation on the crest during every

test allowed for verification that the assumption of replication was valid. Table 3-3 presents overtopping thicknesses for selected wave volumes on the crest for Tests 1-7. The standard deviation values show there is some variability between waves. The low standard error values indicate that mean flow thicknesses are likely to be representative of a larger data set were it to be collected. Time series plots of selected wave thicknesses on the crest are presented in Appendix C.

Table 3-3. Crest flow thickness for select wave volumes, all tests

		Wave Volume (ft^3/ft)						
		20	**45**	**65**	**95**	**125**	**145**	**175**
Test No.	**Wave No.**	**Flow Thickness (ft)**						
1	**1**	0.26	0.40	0.66	0.99	0.94	1.14	1.66
	2	0.27	0.42	0.62	0.91	1.03	1.10	1.45
	3	0.35	0.33	0.60	1.09	0.96	1.12	1.33
2	**1**	0.25	0.39	0.63	0.99	1.02	1.10	1.70
	2	0.38	0.43	0.61	1.00	1.02	0.96	1.45
	3	0.26	0.43	0.59	1.02	0.99	1.06	1.28
3	**1**	0.33	0.40	0.61	1.04	0.94	1.18	1.43
	2	0.25	0.49	0.69	1.03	0.97	1.01	1.44
	3	0.28	0.49	0.63	0.85	1.00	0.99	1.31
4	**1**	0.22	0.49	0.63	0.81	0.90	0.97	1.40
	2	0.36	0.47	0.59	0.87	0.86	0.95	1.17
	3	0.21	0.39	0.62	0.73	0.86	0.97	1.12
5	**1**	0.31	0.55	0.69	0.78	0.94	1.01	1.23
	2	0.23	0.51	0.67	0.87	0.92	1.00	1.18
	3	0.26	0.48	0.66	0.85	0.91	0.93	1.14
6	**1**	0.25	0.40	0.63	0.84	0.87	0.96	1.33
	2	0.28	0.41	0.61	0.97	0.87	1.01	1.16
	3	0.28	0.39	0.59	0.88	0.89	0.94	1.28
7	**1**	0.25	0.40	0.58	0.87	0.83	0.95	1.22
	2	0.23	0.39	0.61	0.79	0.84	0.96	1.14
	3	0.22	0.36	0.61	0.80	0.82	0.95	1.14
Mean		0.27	0.43	0.63	0.90	0.92	1.01	1.31
Standard Deviation		0.05	0.05	0.03	0.10	0.06	0.07	0.16
Standard Error		0.01	0.01	0.01	0.02	0.01	0.02	0.04
Standard Deviation as % of Mean		17	13	5.0	11	7.0	7.2	12

Staff gages required more repetition and manpower due to the nature of collection. For this reason, fewer volumes were replicated and staff gage data collection was accomplished in tests

separate from electronic data collection. Tests 8, 9 and 10 were primarily for staff gage data collection. Pressure transducers were also installed for later comparison to tests one through seven to validate wave profiles appeared equal at equal locations. For staff gage data collection, each wave volume was repeated ten times sequentially before beginning the next higher wave volume. Recording of data occurred as described in Section 3.2.7. A summary of the test program and data collection is presented in Table 3-4.

Table 3-4. Test program

Position	Test Number 1	2	3	4	5	6	7	8	9	10
1	PT, SB, PW	PT, SB	SB	SB	PT, SB	PT, SB	PT, SB	PT		
2	PT, SB, PW	SB, PW	PT, SB, PW	PT, SB, PW	PT, SB, PW	PT, SB, PW	PT, SB, PW	PT, SG	PT, SG	PT, SG
3							PT, SB, PW	PT		
4							PT, SB, PW	SG	PT, SG	SG
5							PT		PT	
6	PT, SB, PW							PT		
7	PT, SB, PW		PT, SB, PW					PT, SG	SG	SG
8		PT, SB, PW	PT, SB, PW					PT		
9		PT, SB, PW		PT, SB, PW				PT		
10				PT, SB, PW	PT, SB, PW				PT	
11					PT, SB, PW	PT, SB, PW		SG	PT, SG	SG
12						PT, SB, PW			PT	
13	PT, SB, PW		PT, SB, PW						PT	
14		PT, SB, PW	PT, SB, PW					SG	SG	PT, SG
15		PT, SB, PW		PT, SB, PW						PT
16				PT, SB, PW						PT
17							PT	SG	SG	PT, SG
18					PT	PT		SG	SG	PT, SG
19					PT	PT, SB, PW	SB,PW			PT
20	PT	PT	PT	PT	PT, SB, PW	PT	PT	PT, SG	PT, SG	PT, SG

(1)PT – pressure transducer
(2)SB – surfboard
(3)PW – paddle wheel sensor
(4)SG – staff gage

4. Data Collection

The data collected during testing included wave volume (V_w), distance downslope from WOS (x), velocity (v), pressure (p), flow thickness by surfboard and flow thickness by staff gage (y). Two means of data collection were employed: electrical and observational. Electrical data consisted of sensor output during ten tests. Observational data were collected during Tests 8-10.

During Tests 1-7, each test was comprised of ninety-six consecutive waves. Thirty-two unique wave volumes were simulated. Each volume was simulated in triplicate, and volumes were multiples of 5 ft^3/ft between 20 and 175 ft^3/ft. Volumes were released from the WOS in random order to more closely simulate levee conditions.

Fourteen sensors were employed during each test including paddlewheel velocity sensors, pressure transducers and surfboards attached to rotational potentiometers. A total of 9,408 unique measurements of wave characteristics were collected electrically between the paddlewheel sensors, pressure transducers and surfboards in Tests 1-7.

Observational data were comprised of staff gage visual observations documented during Tests 8-10. Each test was composed of thirty-two unique wave volumes replicated ten times for a total 320 waves per test. Observations were made at eight locations during each test for a total of 6,708 staff gage observations. Eight pressure transducers were utilized to collect data during the staff gage tests for later comparison to Tests 1-7 pressure transducer data. The complete data set consisted of 16,116 unique observations of wave data values,e.g. V_w and x, v, p, y as a function of time.

4.1. Paddlewheel Flow Sensors

The paddlewheel flow sensors mounted in the surfboards generated a voltage sending a continuous stream of data that was logged to a text file at 50 Hz for the duration of each test. An example portion of plotted voltage data from paddlewheel flow sensor one mounted in surfboard 1 at Location 2 during Test 1 is presented in Figure 4-1. The first five hundred seconds of test one is presented showing voltages resulting from twelve waves ranging in volume from 20 to 155 ft^3/ft.

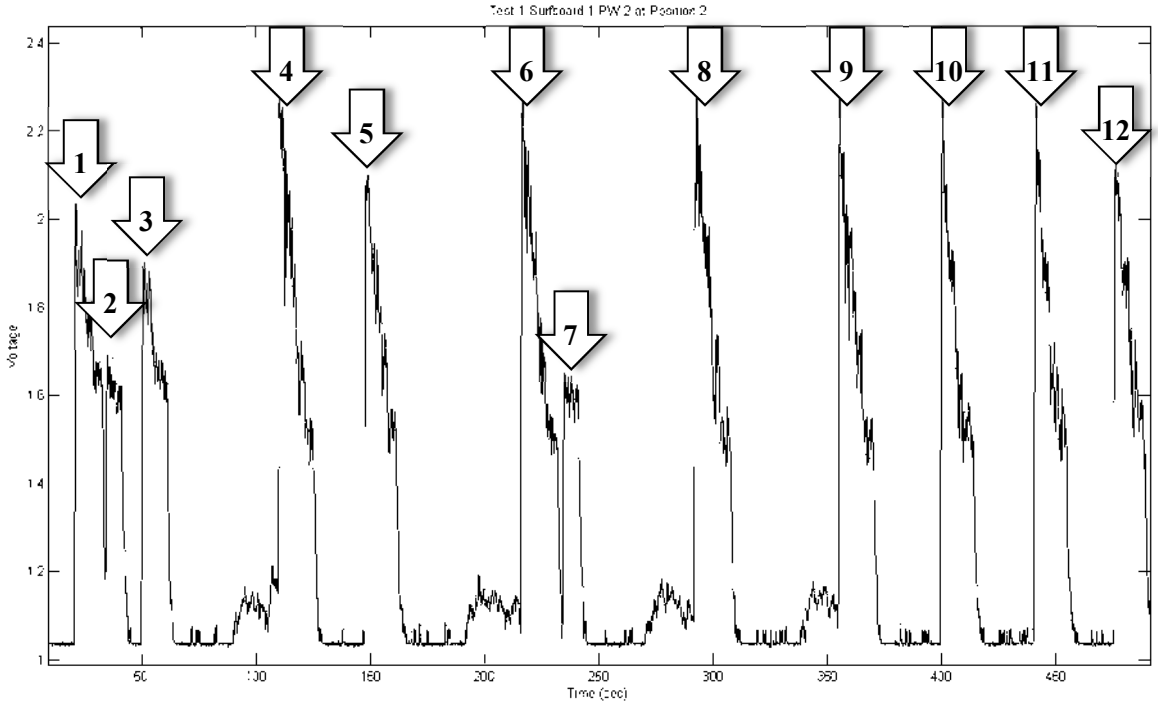

Figure 4-1. Paddlewheel sensor data example.

Voltages were subsequently converted to velocity data using the equation:

$$v = \frac{125 * \left(\text{voltage}_{\text{measured}} - \text{voltage}_{\text{zero}}\right)}{7.29} \tag{3}$$

derived from the calibration curve presented in Figure 4-2 where v equals velocity in feet per second. Multiple paddlewheels were calibrated prior to testing in un-aerated, steady state flow..

Each calibration yielded the same result within tolerances. A $voltage_{zero}$ value was recorded prior to each test.

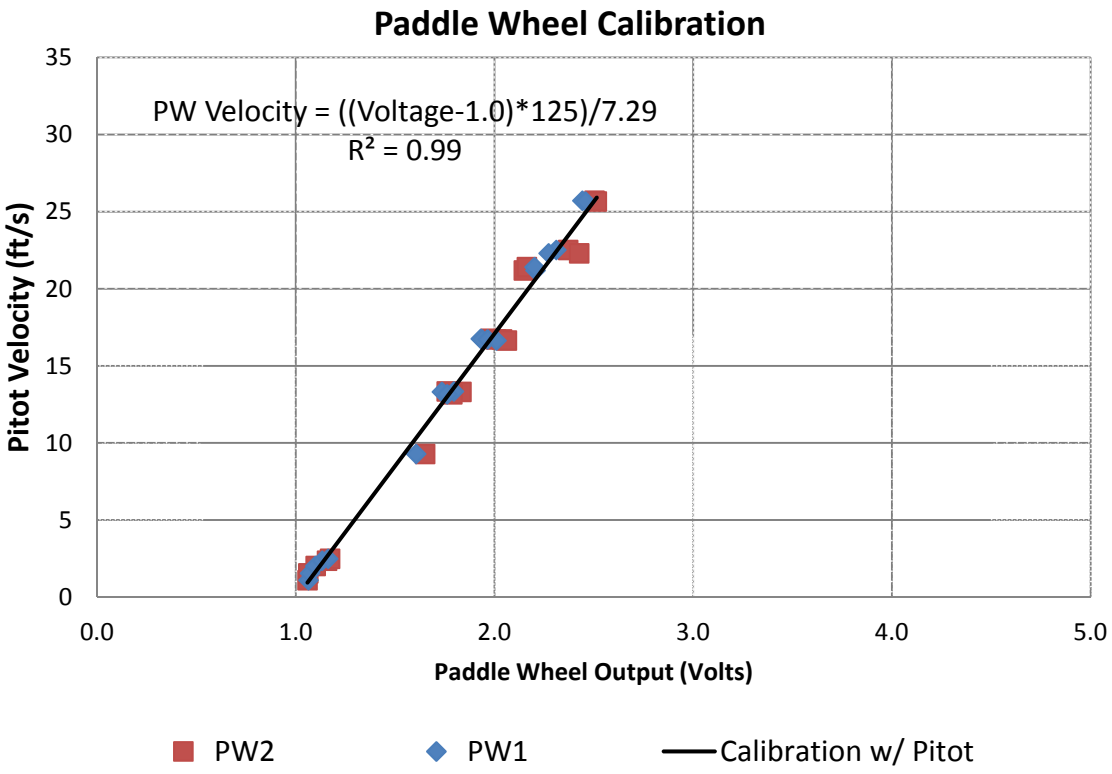

Figure 4-2. Paddlewheel sensor calibration.

Wave data were selected, separated and organized by volume and location to create the working data set. As an example, a 175 ft^3/ft wave velocity profile from the two paddlewheels of surfboard 1 in Test 1 at Location 1 and 2 is presented in Figure 4-3. The measured wave velocity from approximately 674 to 692 seconds during test one has a peak velocity of approximately 25.5 ft/s.

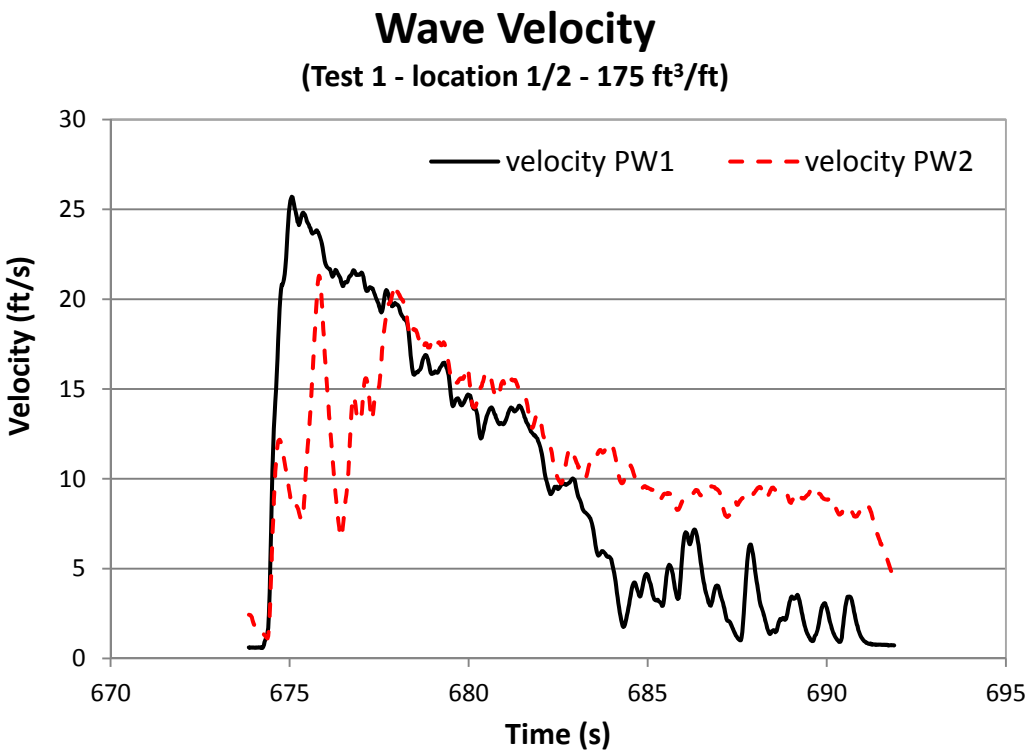

Figure 4-3. Wave velocity profile.

Wave velocity measurements were used along with concurrent flow thickness measurements for mass conservation verification.

4.2. Pressure Transducers

The pressure transducers generated a voltage sending a continuous stream of data that was logged to a text file at 50 Hz for the duration of each test. An example portion of plotted voltage data from pressure transducer 2 during Test 1 is presented in Figure 4-4. The first five hundred seconds of Test 1 is presented showing twelve waves ranging in volume from 20 to 155 ft^3/ft.

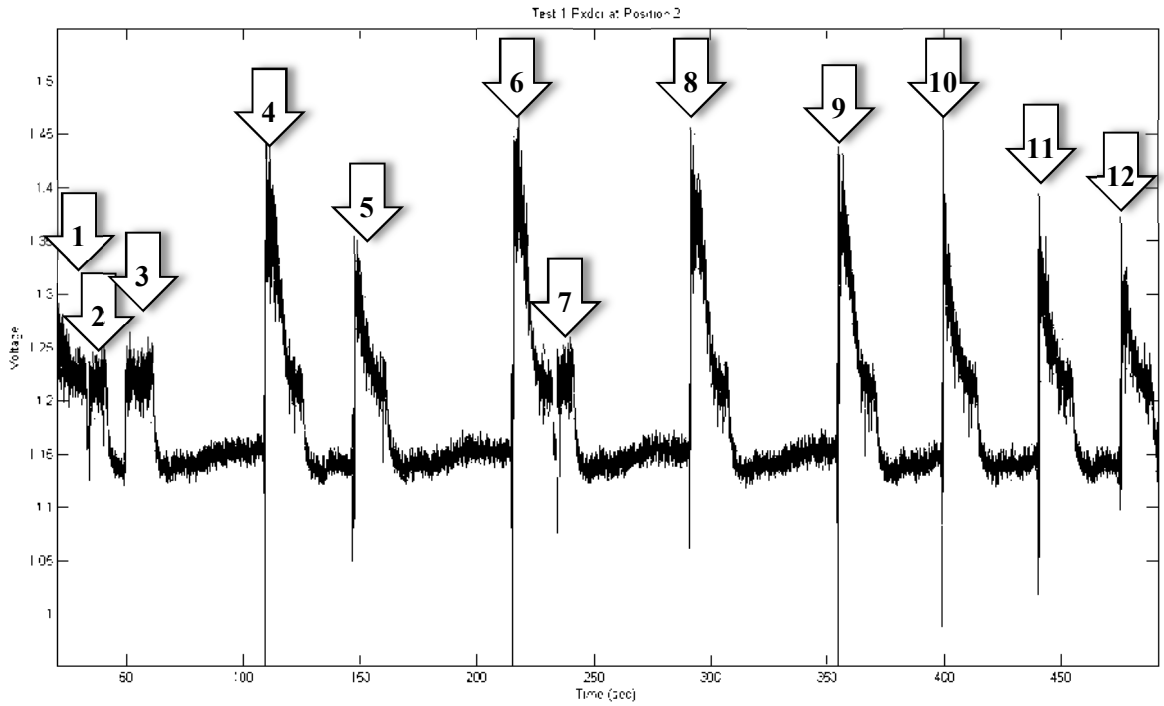

Figure 4-4. Pressure transducer data example.

Voltages were converted to flow thickness data using the equations:

$$p = k*\left(\text{voltage}_{\text{measured}} - \text{voltage}_{\text{zero}}\right) \quad (4)$$

(k = 2.5 or 5.0 depending on the pressure transducer)

$$y = 2.31 * p * \cos\theta \quad (5)$$

where *p* equals pressure in pounds per square inch, *y* equals flow thickness perpendicular to the bed in feet and θ equals slope angle in degrees. A $\text{voltage}_{\text{zero}}$ value was recorded prior to each test.

Pressure transducer data were selected, separated and organized by volume and location to create the working data set. As an example, the measured flow thickness time series of 175 ft^3/ft wave from the pressure transducer at Location 2 during Test 1 is presented in Figure 4-5. Figure 4-5

illustrates the measured wave thickness from approximately 674 to 692 seconds during Test 1 with a peak flow thickness of approximately 2.2 ft.

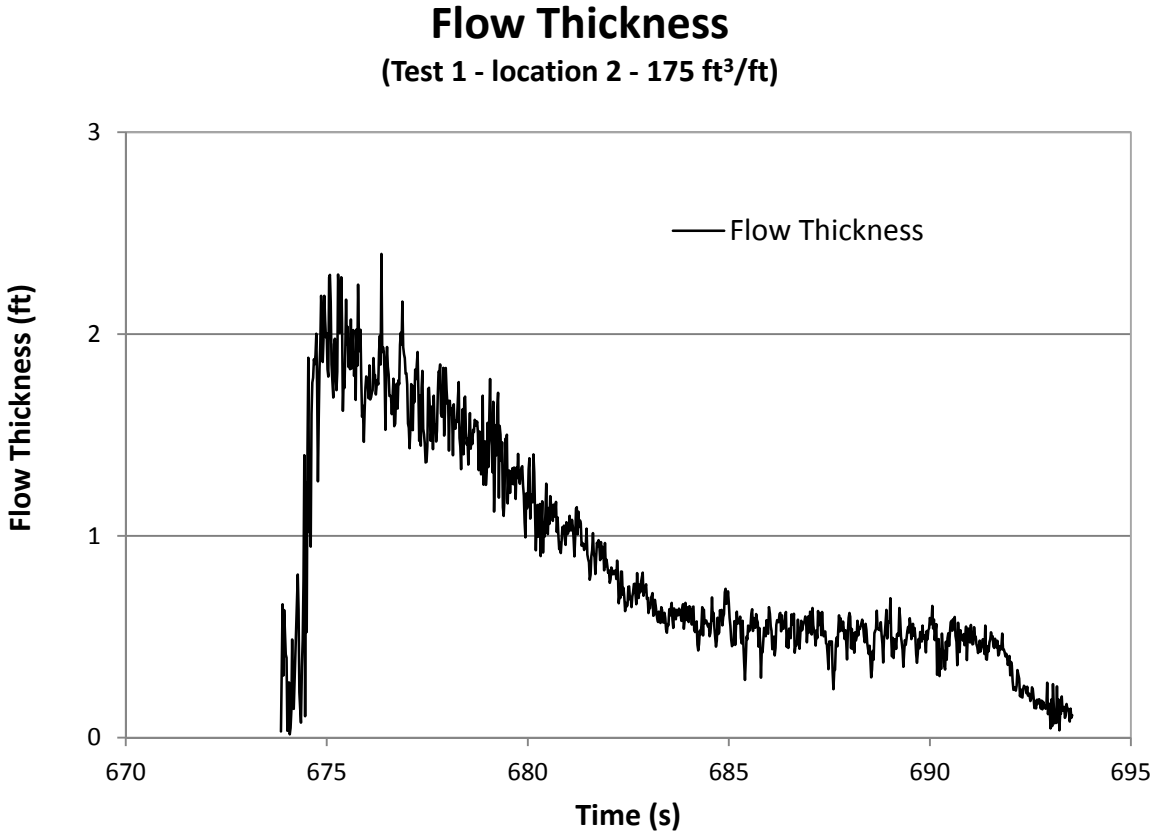

Figure 4-5. Flow thickness by pressure transducer example.

Pressure transducer flow thickness measurements were collected though not used for this analysis. Mass conservation with pressure transducer data was found to be problematic. A possible explanation of this is the great deal of turbulence affecting pressure transducer readings.

4.3. Surfboards

The surfboard rotational potentiometers generated a voltage sending a continuous stream of data that was logged to a text file at 50 Hz for the duration of each test. An example portion of plotted voltage data from surfboard 1 during Test 1 is presented in Figure 4-6. The first five

hundred seconds of Test 1 is presented showing twelve waves ranging in volume from 20 to 155 ft^3/ft.

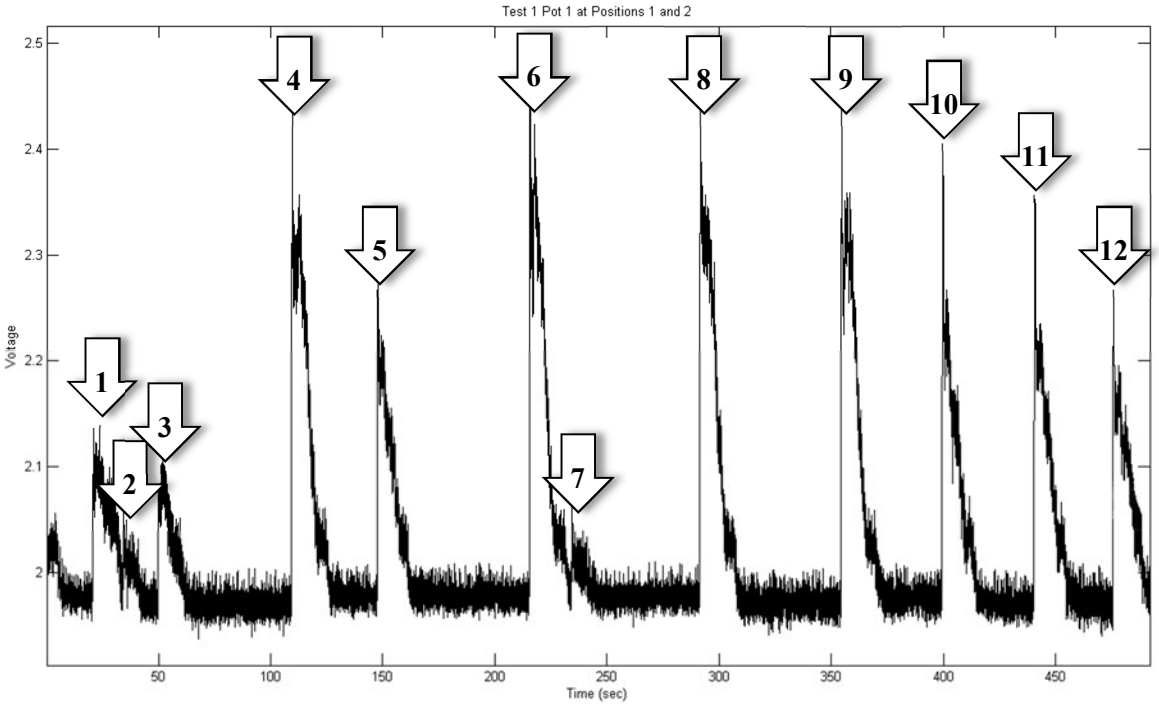

Figure 4-6. Surfboard data example.

Voltages from the rotational potentiometers were converted to flow thickness using the calibrated equations for surfboards 1, 2 and 3:

$$y_{SB1} = 27.0*(voltage_{measured} - voltage_{zero})^{0.83} \quad (6)$$

$$y_{SB2} = 45.1*(voltage_{measured} - voltage_{zero})^{0.87} \quad (7)$$

$$y_{SB3} = 22.3*(voltage_{measured} - voltage_{zero})^{0.83} \quad (8)$$

These relationships were derived from the calibration curves presented in Figure 4-7, Figure 4-8 and Figure 4-9 where y_{sbn} equals flow thickness measured by surfboard 'n' in feet. A $voltage_{zero}$ value was recorded prior to each test.

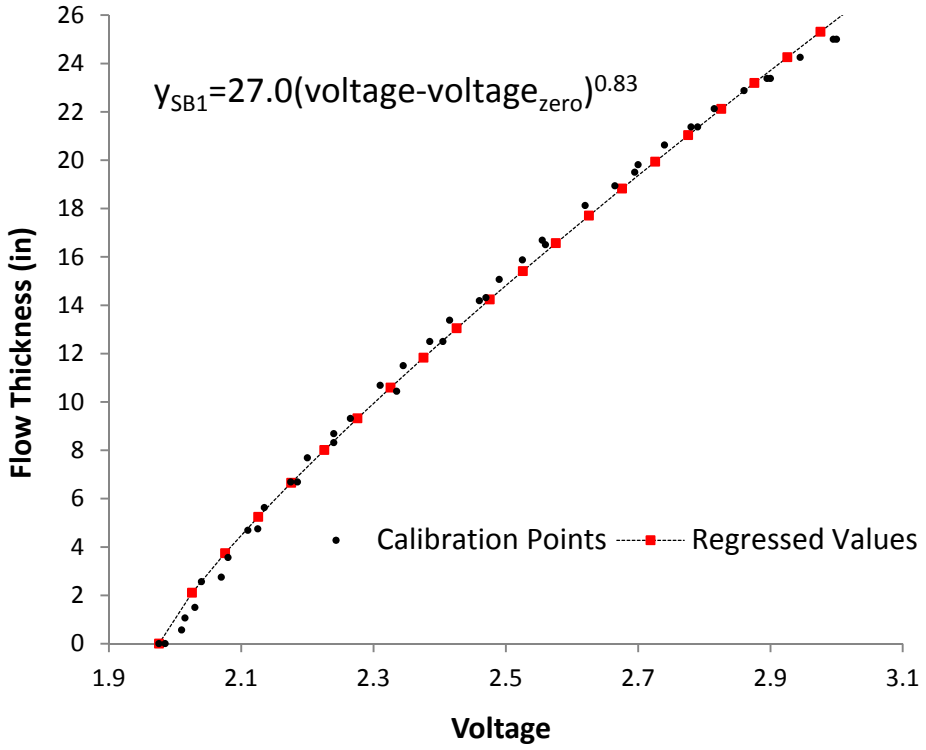

Figure 4-7. Flow thickness calibration curve, surfboard one.

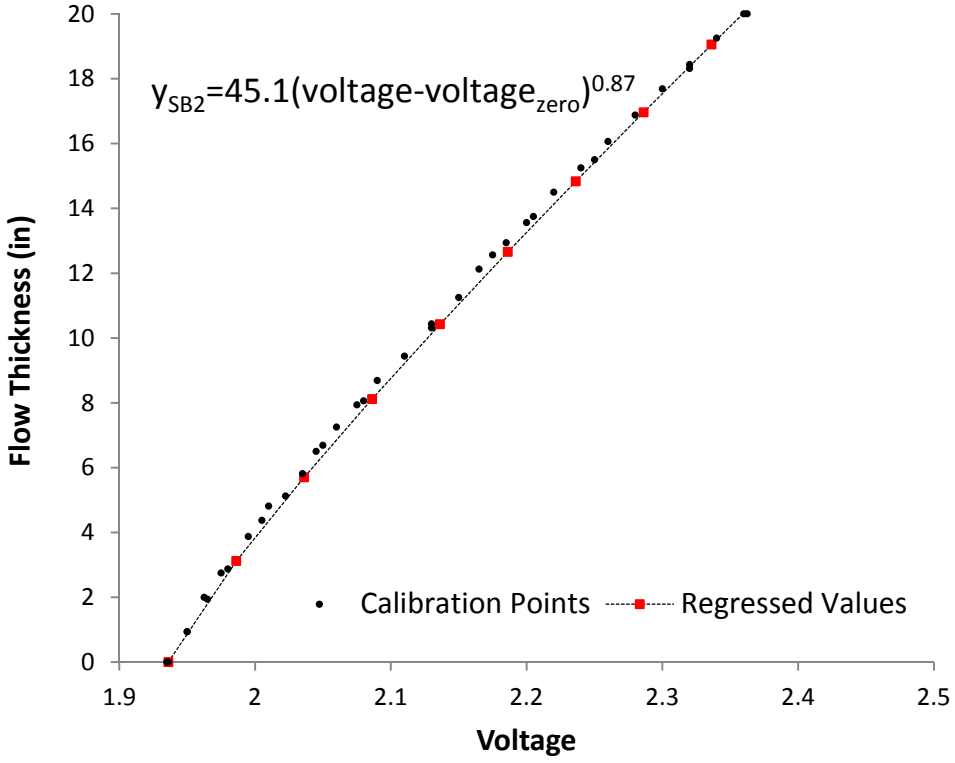

Figure 4-8. Flow thickness calibration curve, surfboard two.

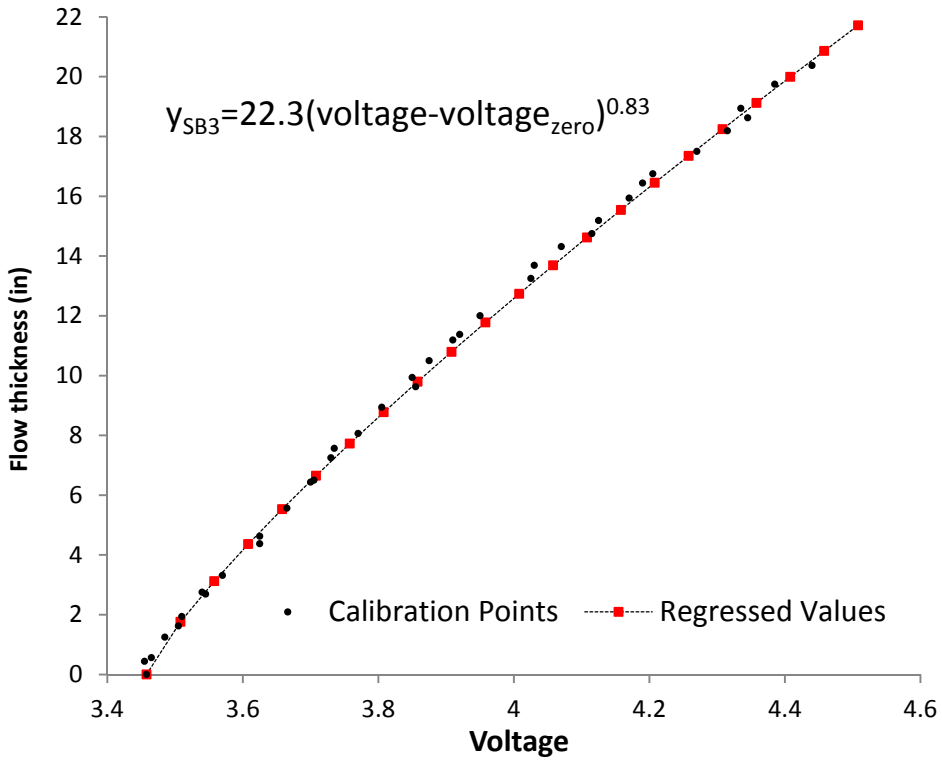

Figure 4-9. Flow thickness calibration curve, surfboard three.

Surfboard data were selected, separated and organized by volume and location to create the working data set. As an example, a 175 ft^3/ft wave flow thickness derived from surfboard measurements at Location 1 during Test 1 is presented in Figure 4-10. The measured flow thickness from approximately 674 to 692 seconds during Test 1 had a peak flow thickness of approximately 1.8 ft.

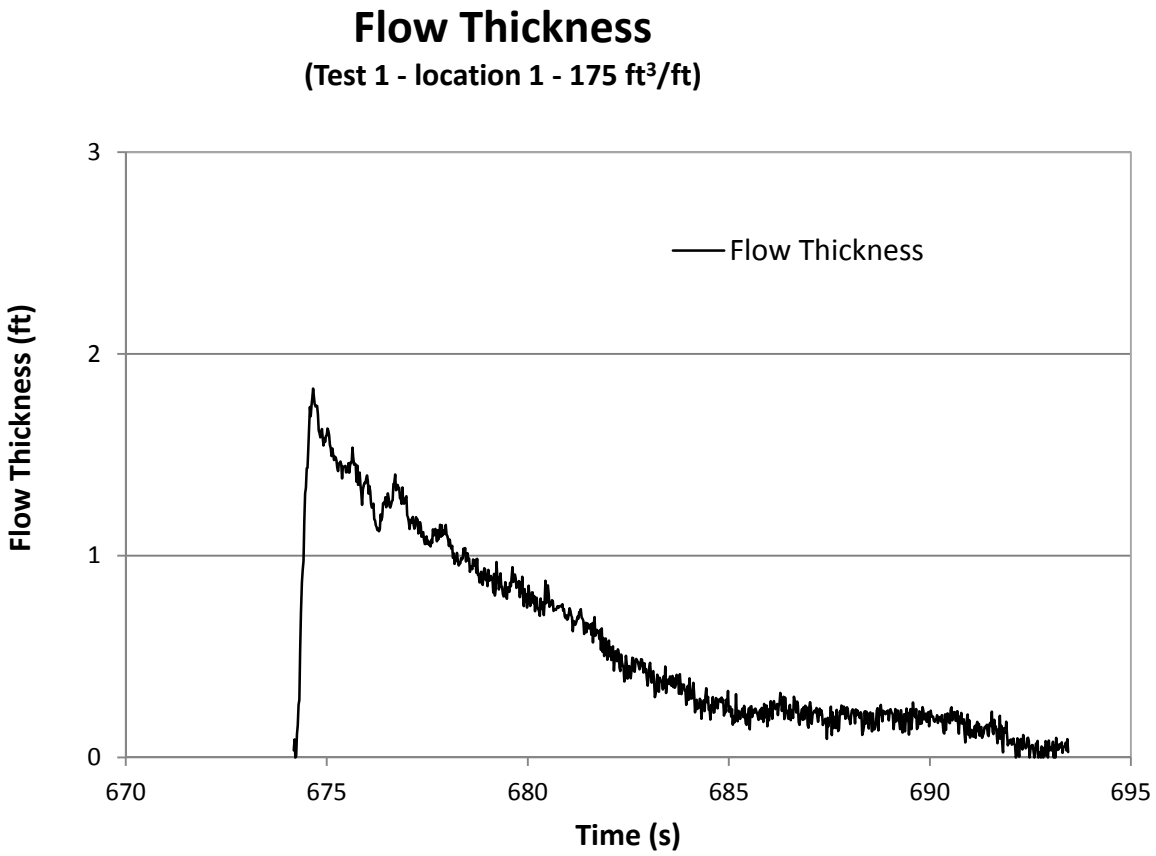

Figure 4-10. Wave thickness by surfboard profile.

Surfboard flow thickness measurements were used for flow thickness determination and mass conservation verification.

4.4. Staff Gages

Collected staff gage data were point values of maximum flow thickness observations made by multiple observers. Thirty-two different wave volumes were each observed for maximum flow thickness from twenty-five to thirty times at eight different locations. An example of wave volume thicknesses for seven wave volumes observed at location two (on the horizontal crest) is presented in Figure 4-11. Plotted for each volume are the thirty observations with the exception of wave volume 20 ft^3/ft which had twenty-five observations. Observed flow thicknesses at

Location 2 for seven wave volumes between 175 and 20 ft^3/ft ranged from approximately 3.5 ft to 0.25 ft., respectively.

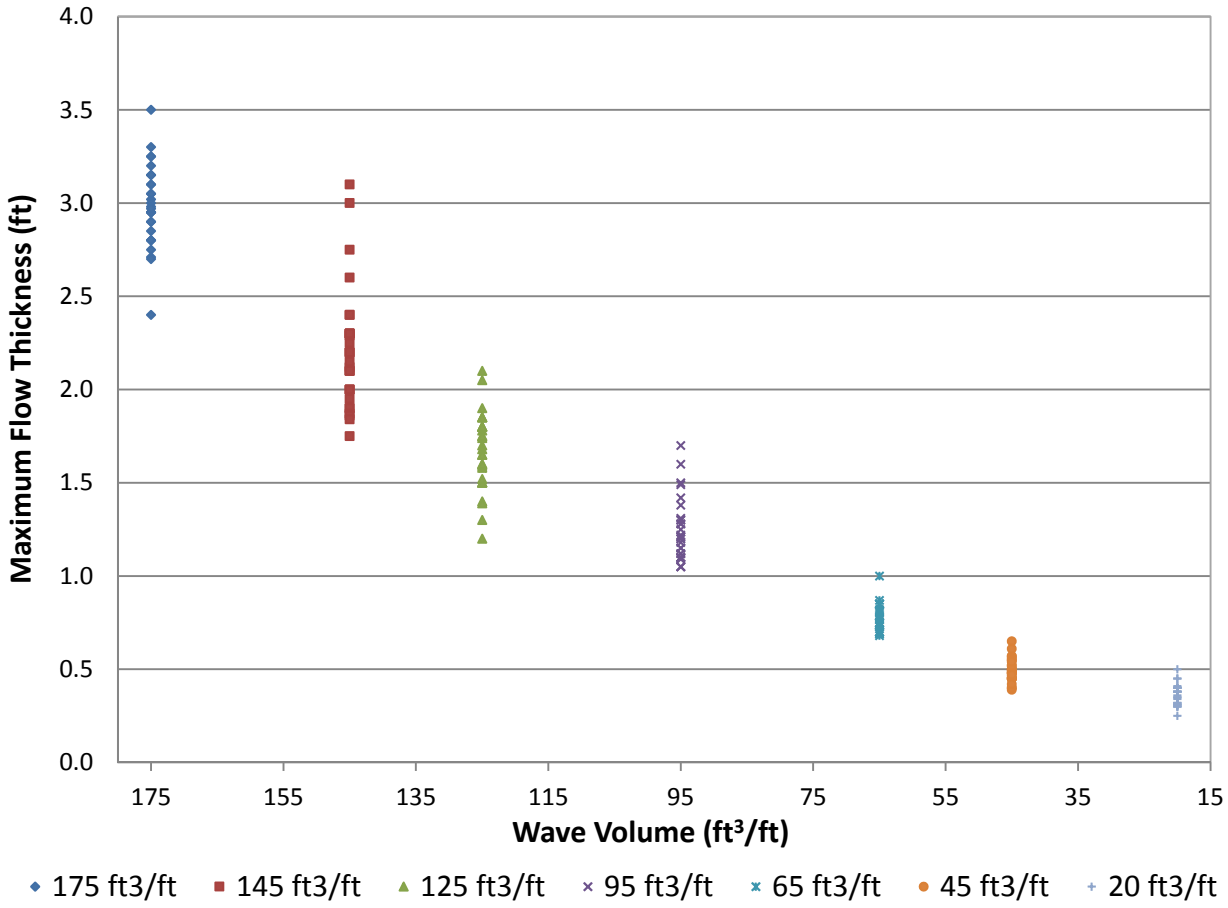

Figure 4-11. Staff gage maximum wave thickness at Location 2 (horizontal crest).

Observed staff gage flow thickness measurements were used for maximum flow thickness determination.

4.5. Test Procedure

Prior to testing, the location of instrumentation for each test was determined to minimize the number of tests while collecting paddlewheel sensor, pressure transducer and surfboard data co-temporally at each location using fourteen data channels. During testing, a procedure was

followed to ensure instrumentation was functioning properly and testing conditions could be replicated. The testing procedure for Tests 1-7 was as follows:

1) Pressure transducers were mounted in the levee slope at pre-determined locations;
2) Surfboards were mounted so paddlewheel velocity meters and flow thickness instruments collected data at installed pressure transducer locations;
3) Data collection cables were attached to instruments;
4) A surfboard calibration curve was determined by raising the surfboard incrementally off the levee surface, fixing the surfboard position, recording the minimum distance between the curved surfboard surface and the levee surface and recording the measured voltage. This was repeated at approximately one inch intervals from zero to twenty-four inches perpendicularly above the levee surface. The collected voltages were later analyzed resulting in the surfboard calibration curves presented in Figure 4-7 through Figure 4-9;
5) All instrumentation was checked to ensure it was functioning and responding to input by exciting the instrument and verifying a change in voltage was measured;
6) Once instrumentation was installed and verified as functioning properly, the wave steering file was loaded in to the WOS computer to produce the wave volumes presented in Table 3-2;
7) The WOS was verified to be functioning and responding to control signals;
8) Ten seconds of data were recorded from each instrument as a "zero" point and checked to verify data collection was occurring;
9) Incoming flow rate was set to 2.2 cfs/ft (13.2 cfs pipe inflow);
10) Data collection began a few seconds prior to beginning a test;
11) Post-test, flow was stopped and data collection was verified and the WOS shut down;
12) Collected data in the form of text files were transferred to CSU servers for later analysis.

Staff gage data were collected in Tests 8-10. The testing procedure for Tests 8-10 was as follows:

1) Pressure transducers were mounted in the levee slope at pre-determined locations;

2) Data collection cables were attached to pressure transducers;
3) All instrumentation was checked to ensure it was functioning and responding to input by exciting the instrument and verifying a change in voltage was measured;
4) Once instrumentation was installed and verified as functioning properly, a wave steering file was loaded in to the WOS computer to produce ten identical wave volumes;
5) The WOS was verified to be functioning and responding to control signals;
6) Ten seconds of electronic data were recorded from each instrument as a "zero" point and checked to verify data collection was occurring;
7) Incoming flow rate was set to 2.2 cfs/ft (13.2 cfs pipe inflow);
8) Six to eight personnel were each assigned to monitor one of eight staff gages mounted to the flume wall;
9) Electronic data collection began a few seconds prior to beginning a test;
10) During testing, observed maximum flow thickness for a wave on a staff gage was recorded by each person. Between waves, personnel rotated to the next staff gage downstream (or to the most upstream gage for the last person downstream) to record the next wave. This was repeated until ten waves of the same volume were simulated. In this manner, eight to ten observations were collected at each staff gage. Personnel rotation was used to help eliminate observational bias;
11) The procedure was repeated for the thirty-two wave volumes;
12) Post-test, flow was stopped, data collection was verified and the WOS shut down;
13) Documented staff gage maximum flow thicknesses were later collated into a working data set. Collected electronic data in the form of text files were transferred to CSU servers for later analysis.

4.6. Data Summary

Data were collected during ten tests. Data consisted of paddlewheel flow sensor, pressure transducer, surfboard and staff gauge observations. Paddlewheel sensor, pressure transducer and surfboard data were converted to velocity and flow thickness values, respectively, using

calibration equations relating sensor voltage output to a measured value. Staff gage observations were recorded directly and compiled into the final data set available for analysis.

5. Analysis, Findings and Discussion

The collected data described in Chapter 4 were reviewed, systematically screened and analyzed for wave thickness trends, including bulking, associated with wave overtopping on the landward side of levees. Data are grouped and displayed based on simulated wave volume, slope distance from the WOS and bulking coefficient. Bulked and un-bulked flow thicknesses are displayed and examined. Simulated wave volumes are examined for mass conservation. Average wave bulking coefficients are quantified for simulated wave volumes at specified slope distances from the WOS. A second order multivariable polynomial regression is used for empirical model development predicting bulking coefficients on the landward side of levees during simulated wave overtopping. The bulking coefficient predictive model residuals are presented. The predictive model is evaluated for engineering conservatism based on the residuals and engineering judgement.

5.1. Analysis Methods

Bulking flow thickness coefficients were determined for each simulated wave volume at each of the data collection locations using un-bulked and bulked maximum flow thicknesses. Un-bulked maximum flow thicknesses were determined using the surfboard continuous data stream described in Section 4.3. It should be noted that the surfboards are the best currently available technology for measuring the un-bulked flow depth during wave overtopping. As with any mechanism designed to "plane", the surfboard's ability to hydro-plane is a function of velocity of flow and *density* of flow. It is likely that there is some level of aeration in the un-bulked overtopping wave thicknesses since a sufficiently high velocity of very low density fluid would cause the surfboards to hydroplane. However, it is the best available method for such

measurements. It is considered acceptable since the additional "un-measured" bulking will only add a level of conservatism in shear stress based design.

Bulked maximum flow thicknesses were determined using the staff gage data described in Section 4.4. A bulking coefficient was determined at each location for each wave volume by normalizing the bulked maximum flow thickness using the un-bulked maximum flow thickness. This collection of bulking coefficients formed the final data set for bulking predictive model development.

For un-bulked maximum flow thickness, surfboard flow thickness values on the 3:1 slope for each wave volume were collected at locations coincident with staff gage locations. Surfboard flow thickness data was analyzed for peak flow thickness. Peak flow thickness was determined using a combination of Mathworks MatLab® and Microsoft Excel® software. Because data collection was a continuous stream of data, Matlab® was used to select each wave beginning and ending time at each location used for analysis. Each wave was analyzed in Excel® for peak flow thickness by calculating a running half second average for the duration of wave overtopping. The highest half second average value was used as the peak flow thickness of the wave at that location. The peak flow thickness values from the three waves of equal volume at equal locations were averaged for the final un-bulked flow thickness data set presented in Table 5-1. Location 17 (42.80 ft. from WOS) was affected by slope geometry and was not included in the final analysis. See Figure 3-11 for downslope locations.

Table 5-1. Surfboard flow thickness, in feet

Wave Volume (ft^3/ft)	Downslope Distance (feet from WOS)				
	12.41	17.58	23.58	31.60	37.60
175	1.48	1.33	1.45	1.27	1.42
170	1.27	1.33	1.43	1.34	1.40
165	1.26	1.30	1.41	1.26	1.37
160	1.11	1.28	1.25	1.34	1.25
155	1.12	1.20	1.27	1.30	1.23
150	1.11	1.20	1.25	1.25	1.14
145	1.12	1.05	1.16	1.18	1.10
140	1.07	1.03	1.22	1.19	1.05
135	1.01	0.99	1.10	1.06	0.93
130	1.02	0.97	1.15	1.09	0.94
125	0.98	0.91	1.05	1.05	0.86
120	1.01	0.95	1.05	1.02	0.87
115	1.00	0.89	1.00	0.98	0.86
110	0.97	0.87	0.95	0.98	0.78
105	1.02	0.85	1.01	0.99	0.77
100	1.00	0.85	0.91	0.90	0.77
95	1.00	0.79	0.95	0.81	0.77
90	0.99	0.75	0.98	0.81	0.71
85	0.93	0.68	0.98	0.78	0.66
80	0.81	0.59	0.84	0.62	0.63
75	0.74	0.52	0.88	0.56	0.64
70	0.72	0.49	0.82	0.55	0.57
65	0.62	0.42	0.73	0.50	0.53
60	0.53	0.41	0.63	0.46	0.49
55	0.52	0.39	0.57	0.42	0.47
50	0.42	0.32	0.45	0.37	0.39
45	0.38	0.29	0.40	0.31	0.35
40	0.34	0.27	0.31	0.22	0.27
35	0.32	0.22	0.29	0.23	0.25
30	0.34	0.22	0.30	0.21	0.26
25	0.29	0.21	0.27	0.20	0.23
20	0.29	0.19	0.26	0.21	0.25

Maximum bulked flow thicknesses were determined from twenty-five to thirty staff gage flow thickness readings recorded for each volume at each location. The staff gage flow thickness values for each wave volume at each location were averaged for the final maximum bulked flow

thickness data set presented in Table 5-2. Average error of staff gage readings from the accepted value was ± 4.9%. Staff gage readings were within ± 4.4% for values greater than 60 ft^3/ft, ± 5.6% for wave volumes 50, 55 and 60 ft^3/ft and ± 6.5% for wave volumes less than 45 ft^3/ft. See Figure 3-11 for downslope locations

Table 5-2. Staff gage flow thickness, in feet

Wave Volume (ft^3/ft)	Downslope Distance (feet from WOS)				
	12.41	17.58	23.58	31.60	37.60
175	2.98	2.89	2.70	1.44	1.40
170	2.86	2.66	2.38	1.45	1.33
165	2.70	2.57	2.13	1.38	1.29
160	2.65	2.26	1.92	1.33	1.23
155	2.32	2.26	1.79	1.27	1.24
150	2.40	1.98	1.77	1.23	1.26
145	2.21	2.07	1.70	1.20	1.16
140	2.09	1.96	1.50	1.17	1.15
135	1.97	1.86	1.48	1.07	1.03
130	1.83	1.78	1.39	1.04	1.05
125	1.67	1.66	1.29	1.04	0.96
120	1.58	1.70	1.23	0.95	0.98
115	1.56	1.66	1.21	0.96	0.92
110	1.34	1.56	1.20	0.90	0.85
105	1.34	1.58	1.14	0.87	0.83
100	1.29	1.51	1.09	0.86	0.83
95	1.24	1.58	1.09	0.82	0.81
90	1.11	1.43	0.97	0.80	0.81
85	1.10	1.31	0.92	0.86	0.81
80	1.05	1.25	0.84	0.71	0.77
75	0.93	1.06	0.79	0.71	0.75
70	0.86	0.95	0.76	0.64	0.67
65	0.77	0.80	0.62	0.56	0.64
60	0.67	0.70	0.56	0.57	0.64
55	0.62	0.69	0.48	0.47	0.54
50	0.56	0.54	0.42	0.50	0.49
45	0.49	0.43	0.37	0.40	0.42
40	0.46	0.38	0.37	0.37	0.40
35	0.42	0.34	0.36	0.33	0.35
30	0.40	0.31	0.32	0.31	0.33
25	0.39	0.29	0.30	0.31	0.32
20	0.36	0.34	0.31	0.26	0.38

5.2. Validity Check

A validity check of mass conservation was performed by computing the mass for each wave volume from collected velocity, flow thickness and collection rate data at the crest location. Conservation of mass is a fundamental principle used to verify the validity of collected data in the form

$$\rho \cdot \forall_{wave} = \rho \cdot \left(\sum_{t=0}^{t_n} V_t \cdot Y_t \cdot \Delta t \right) \tag{9}$$

where ρ = density of water, $\forall_{wave}$ = wave volume in cubic feet per foot of width, t_n = total wave overtopping time, V_t = velocity in feet per second at time t, Y_t = surfboard flow thickness in feet at time t and Δt = time between data samples, in seconds. A spreadsheet was created to differentiate between the two paddlewheel velocities collected at a location and select the highest value. Assuming water in the WOS and that flowing beneath the surfboard have equal densities, the higher flow velocity was multiplied by surfboard flow thickness measured at the same moment and by the time step between data collection times (0.02 sec.) for the length of each individual wave overtopping time. This yielded incremental wave overtopping discharges for a period of 0.02 seconds. All incremental discharges were summed to obtain total overtopping wave volume and the calculated sum was compared to expected wave volumes (programmed into the WOS steering file) on the horizontal crest. Unexplainable discrepancies between the anticipated volume and the calculated volume could indicate instrumentation issues, calibration issues with the WOS or differences in fluid density between the WOS and surfboard measurements. Results are presented in Table 5-3.

Table 5-3. Wave volume by mass conservation

Simulated Wave Volume (ft^3/ft)	Mass Conservation Wave Volume			Average Percent Difference vs. Anticipated Volume
	Wave #1	Wave #2	Wave #3	
175	175.8	167.4	167.0	-2.8
170	158.4	154.9	161.6	-6.9
165	155.8	156.1	159.7	-4.7
160	154.0	147.5	149.6	-6.0
155	147.8	143.2	142.1	-6.8
150	142.2	137.5	139.9	-6.8
145	138.7	138.3	135.2	-5.2
140	137.9	132.2	133.4	-3.9
135	133.3	133.6	129.0	-2.2
130	127.2	121.7	126.8	-3.7
125	124.5	131.3	128.1	2.4
120	127.2	118.7	116.3	0.6
115	112.0	115.4	117.3	-0.1
110	108.9	113.6	111.6	1.2
105	106.8	105.8	105.5	1.0
100	102.2	108.8	105.3	5.4
95	93.2	97.6	98.7	1.6
90	92.3	97.3	93.4	4.9
85	90.7	97.0	85.2	7.0
80	83.0	83.6	83.3	4.1
75	76.9	71.5	79.9	1.4
70	68.0	68.9	71.9	-0.6
65	66.4	59.0	57.9	-6.0
60	52.2	53.4	51.2	-12.9
55	55.7	45.6	45.0	-11.3
50	51.5	43.8	35.6	-12.8
45	35.4	39.0	28.4	-23.8
40	34.6	22.1	23.5	-33.2
35	24.7	20.0	19.7	-38.7
30	21.8	22.9	16.4	-32.1
25	14.2	14.5	13.4	-43.7
20	10.1	10.5	12.7	-44.5

Wave volumes were within $\pm$ 7.0 percent for values greater than 60 ft^3/ft, -11 to 13.0 percent for wave volumes 50, 55 and 60 ft^3/ft and -23 to 45 percent for wave volumes less than 45 ft^3/ft. It is believed the smaller waves had a more significant portion of total wave volume incapable of supporting the surfboard weight. This resulted in greater error for smaller waves. However, acceptable results with higher wave volumes indicate model setup and data collection were functioning properly. Also, flow thickness measurements by the surfboard at the higher wave volumes (which have more bulking) seem to be not greatly affected by flow bulking. For these reasons, all wave volumes were included in the analysis because maximum flow thicknesses should have been unaffected.

5.3. Bulking Predictive Model

Wave flow thicknesses were determined using staff gage and surfboard measurements. Surfboard flow thickness measurements were considered un-bulked maximum flow conditions while staff gage measurements represented bulked maximum flow thickness conditions. For each location and wave volume, the bulking coefficient, B_C, was determined using

$$B_C = \frac{y_{SG}}{y_{SB}} \tag{10}$$

where y_{SG} is the staff gage flow thickness and y_{SB} is the surfboard flow thickness. The bulking coefficient represents the increase to flow thickness as a result of air entrainment at peak flow thickness. Final bulking coefficient values were determined by averaging the three B_C values at each location for each wave volume. Bulking coefficients are presented in Table 5-4.

Table 5-4. Wave bulking coefficients.

Simulated Wave Volume (ft^3/ft)	Downslope Distance (feet from WOS)				
	12.41	17.58	23.58	31.60	37.60
175	2.01	2.17	1.86	1.14	0.99
170	2.25	2.00	1.66	1.08	0.95
165	2.14	1.98	1.52	1.09	0.94
160	2.38	1.76	1.54	0.99	0.98
155	2.07	1.88	1.42	0.98	1.01
150	2.15	1.66	1.42	0.99	1.11
145	1.97	1.97	1.46	1.02	1.05
140	1.95	1.90	1.23	0.98	1.10
135	1.95	1.87	1.35	1.01	1.11
130	1.80	1.84	1.21	0.96	1.11
125	1.71	1.82	1.23	0.99	1.12
120	1.57	1.80	1.17	0.94	1.12
115	1.56	1.86	1.22	0.98	1.08
110	1.38	1.79	1.26	0.92	1.08
105	1.31	1.84	1.13	0.89	1.07
100	1.29	1.79	1.20	0.96	1.09
95	1.24	1.99	1.15	1.00	1.05
90	1.12	1.90	0.99	0.98	1.14
85	1.19	1.92	0.94	1.10	1.22
80	1.30	2.13	1.00	1.14	1.23
75	1.26	2.06	0.90	1.26	1.18
70	1.20	1.95	0.93	1.18	1.17
65	1.24	1.89	0.85	1.11	1.22
60	1.28	1.70	0.90	1.24	1.29
55	1.19	1.76	0.85	1.13	1.16
50	1.34	1.67	0.92	1.37	1.26
45	1.29	1.48	0.91	1.27	1.18
40	1.35	1.42	1.18	1.64	1.49
35	1.32	1.55	1.23	1.42	1.37
30	1.20	1.46	1.07	1.49	1.29
25	1.33	1.37	1.14	1.52	1.35
20	1.25	1.80	1.19	1.22	1.50

Bulking coefficient values less than 1.0 would indicate a flow thickness decrease as a result of aeration. This is not physically possible. Of 160 B_C values, twenty one values are between 1.0 and 0.90 and three values are less than 0.90. To better approach reality, these B_C values were interpreted as measurement error and represented as 1.0 during analysis. The final B_C values used for regression are presented in Table 5-5.

Table 5-5. Final wave bulking coefficients.

Simulated Wave Volume (ft^3/ft)	Downslope Distance (feet from WOS)				
	12.41	17.58	23.58	31.60	37.60
175	2.01	2.17	1.86	1.14	1.00
170	2.25	2.00	1.66	1.08	1.00
165	2.14	1.98	1.52	1.09	1.00
160	2.38	1.76	1.54	1.00	1.00
155	2.07	1.88	1.42	1.00	1.01
150	2.15	1.66	1.42	1.00	1.11
145	1.97	1.97	1.46	1.02	1.05
140	1.95	1.90	1.23	1.00	1.10
135	1.95	1.87	1.35	1.01	1.11
130	1.80	1.84	1.21	1.00	1.11
125	1.71	1.82	1.23	1.00	1.12
120	1.57	1.80	1.17	1.00	1.12
115	1.56	1.86	1.22	1.00	1.08
110	1.38	1.79	1.26	1.00	1.08
105	1.31	1.84	1.13	1.00	1.07
100	1.29	1.79	1.20	1.00	1.09
95	1.24	1.99	1.15	1.00	1.05
90	1.12	1.90	1.00	1.00	1.14
85	1.19	1.92	1.00	1.10	1.22
80	1.30	2.13	1.00	1.14	1.23
75	1.26	2.06	1.00	1.26	1.18
70	1.20	1.95	1.00	1.18	1.17
65	1.24	1.89	1.00	1.11	1.22
60	1.28	1.70	1.00	1.24	1.29
55	1.19	1.76	1.00	1.13	1.16
50	1.34	1.67	1.00	1.37	1.26
45	1.29	1.48	1.00	1.27	1.18
40	1.35	1.42	1.18	1.64	1.49
35	1.32	1.55	1.23	1.42	1.37
30	1.20	1.46	1.07	1.49	1.29
25	1.33	1.37	1.14	1.52	1.35
20	1.25	1.80	1.19	1.22	1.50

Simulated wave volumes, V_w, distance from the WOS, X (in feet) and bulking coefficient values, B_C, were evaluated using the curve fitting tool in Matlab. A second-order polynomial fit resulted using the robust, bi-square method to minimize possible data outlier effects on regression outcome. An empirical bulking coefficient model for the landward side of 3:1 levees during simulated wave overtopping is:

$$B_C = 1.18 + 9.4\text{E-}4V_W - 7.8E\text{-}3X + 1.1E\text{-}5V_W^2 - 7.6E\text{-}5V_W X + 1.1E\text{-}4X^2 \qquad (11)$$

where V_W is wave volume in ft^3/ft and X is slope distance from the WOS in feet. Model coefficient of determination (R^2) is 0.72. The predictive regression curve is presented in Figure 5-1. The predictive curve with upper and lower 95% confidence bounds is presented in Figure 5-2. Figure 5-3 through Figure 5-7 present bulking coefficients by wave volume and location for each wave volume examined on two dimensional plots.

There is a trend of decreasing bulking coefficient with decreasing wave volume and distance from the simulator. However, all influencing factors, such as a measurable "plunging" effect by waves after passing over the crest transition and when bulking caused by surface roughness supersedes bulking created by wave simulation, have not yet been explained in literature. The first phenomena is demonstrated in Figure 5-3 where wave volume 70 ft^3/ft demonstrates a higher bulking coefficient than wave volume 125 ft^3/ft approximately 18 ft from the WOS. The second phenomena is demonstrated in Figure 5-4 where bulking coefficients for large wave volumes are higher than smaller volumes approximately 18 ft from the WOS and subsequently lower than small wave volumes immediately downslope at approximately 24 ft from the WOS. As such, regression equations should be used cautiously.

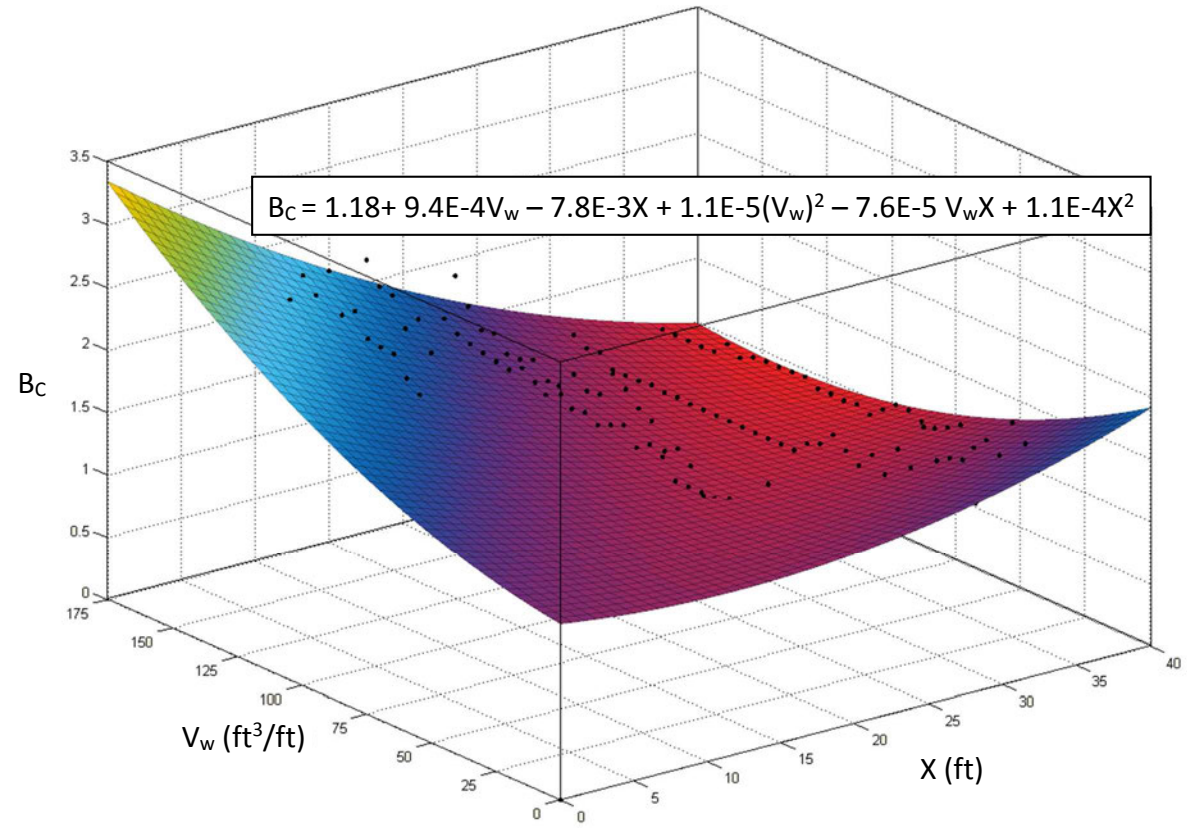

Figure 5-1. Predictive regression curve fit.

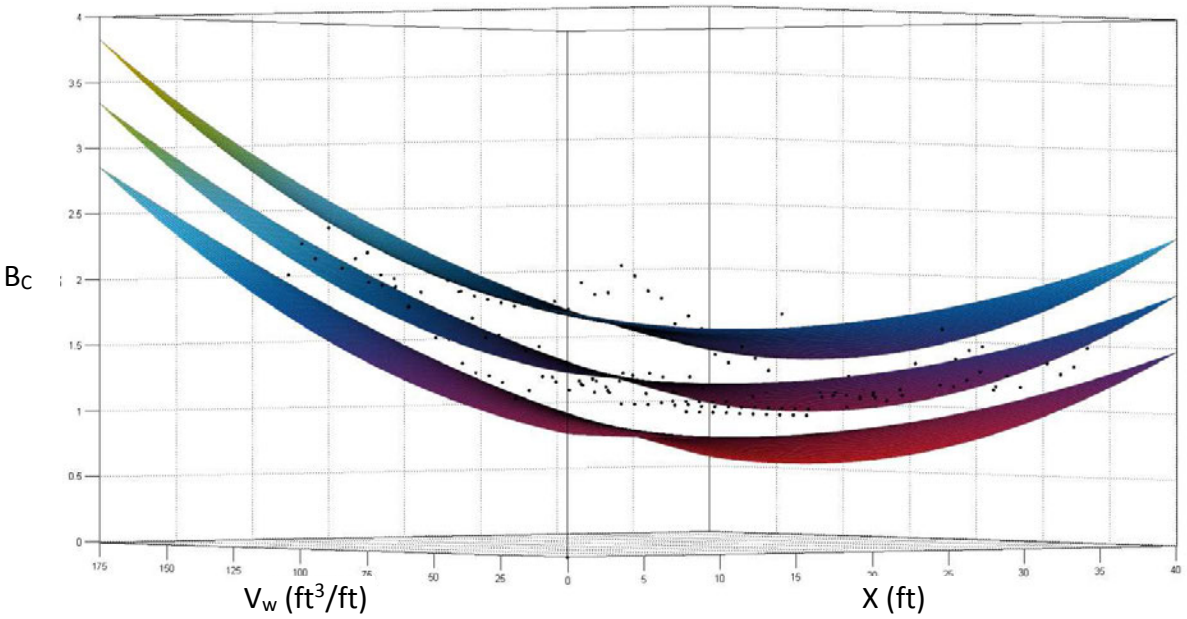

Figure 5-2. Regression curve fit with 95% confidence bounds.

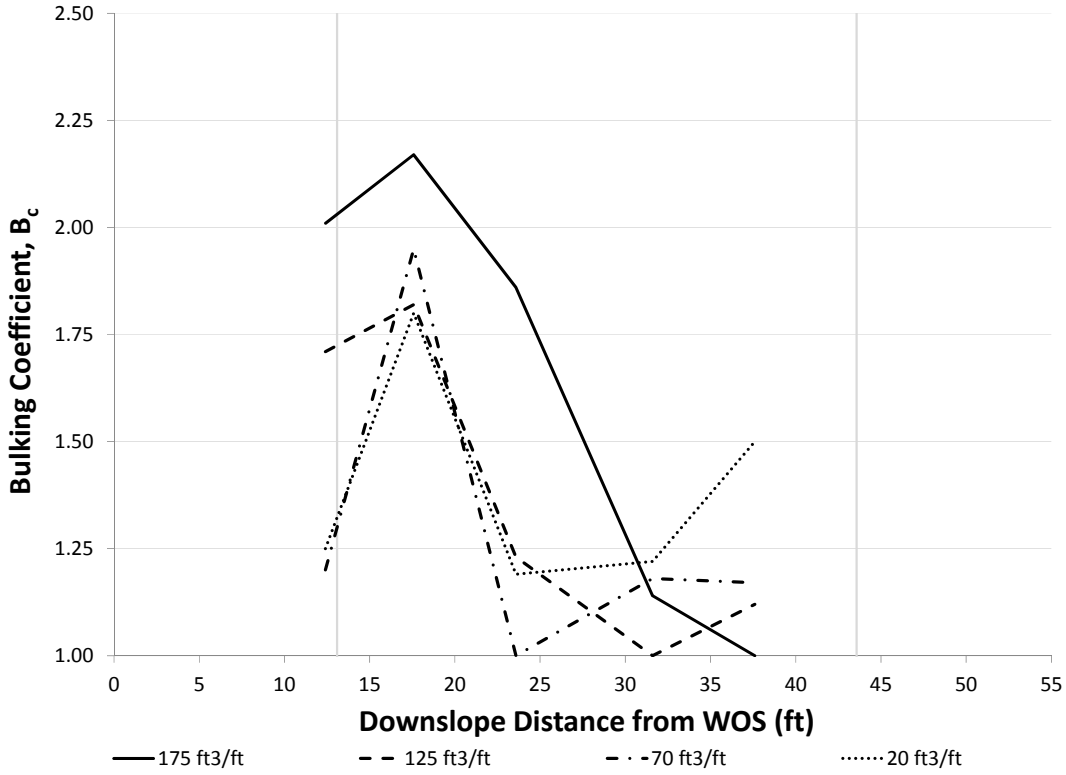

Figure 5-3. Bulking coefficient by wave volume and location, 20 – 175 ft3/ft.

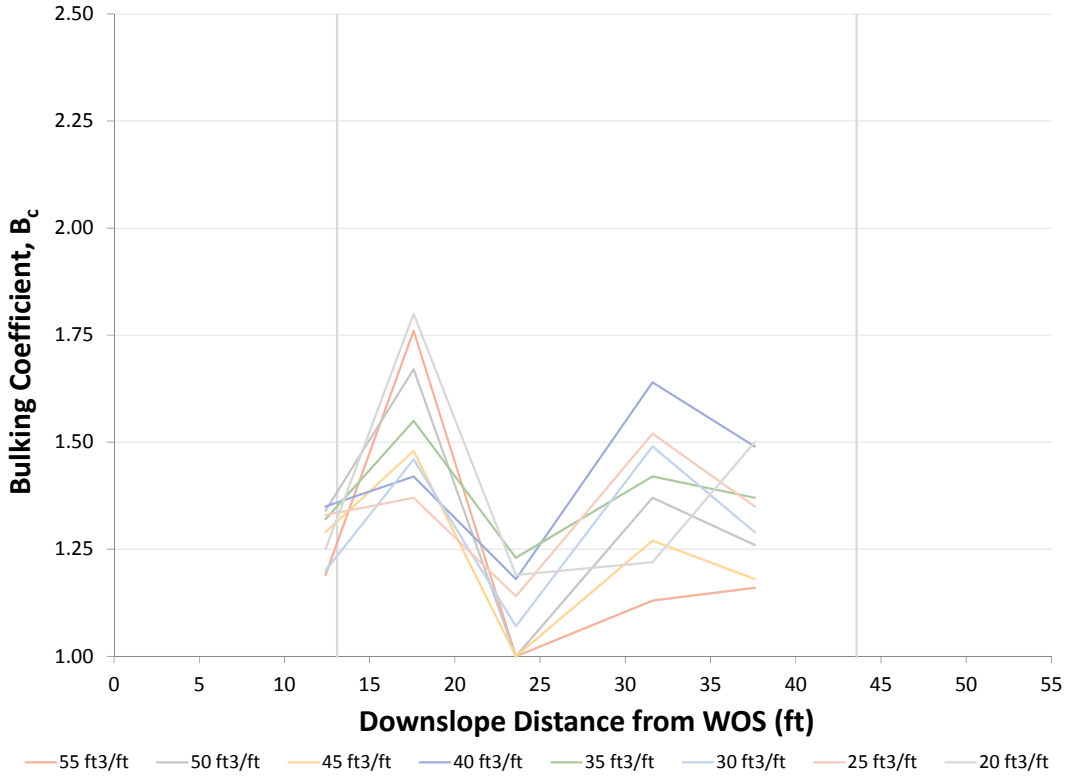

Figure 5-4. Bulking coefficient by wave volume and location, 20 – 55 ft3/ft.

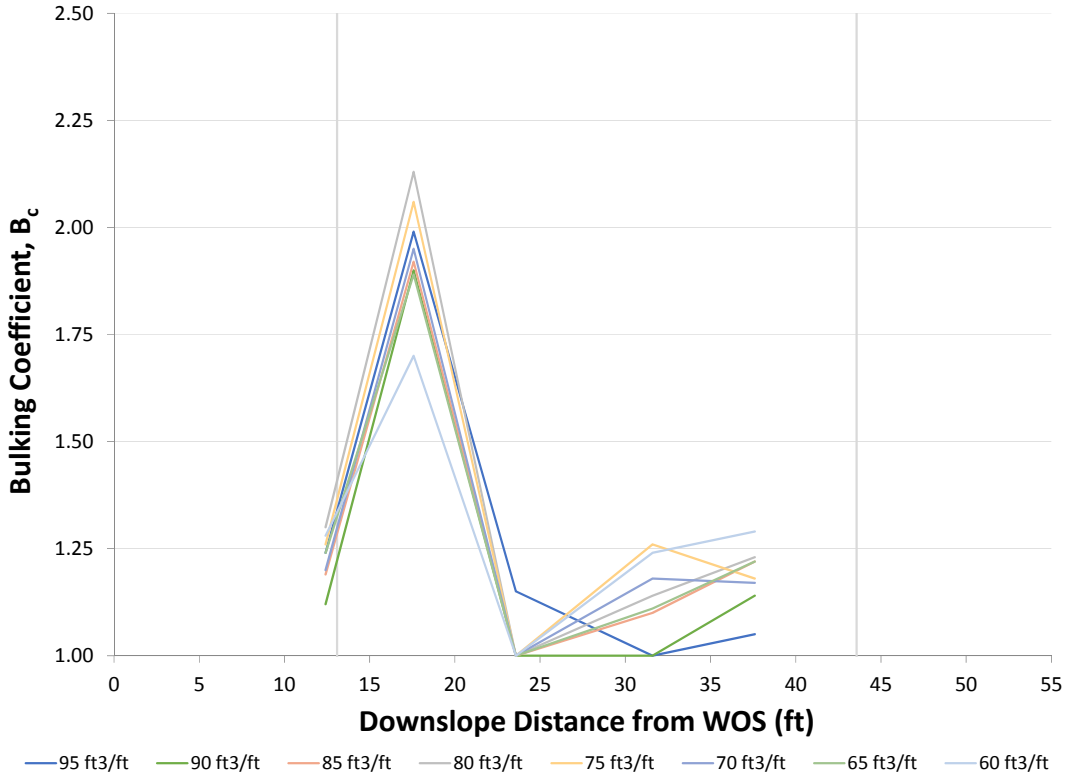

Figure 5-5. Bulking coefficient by wave volume and location, 60 – 95 ft3/ft.

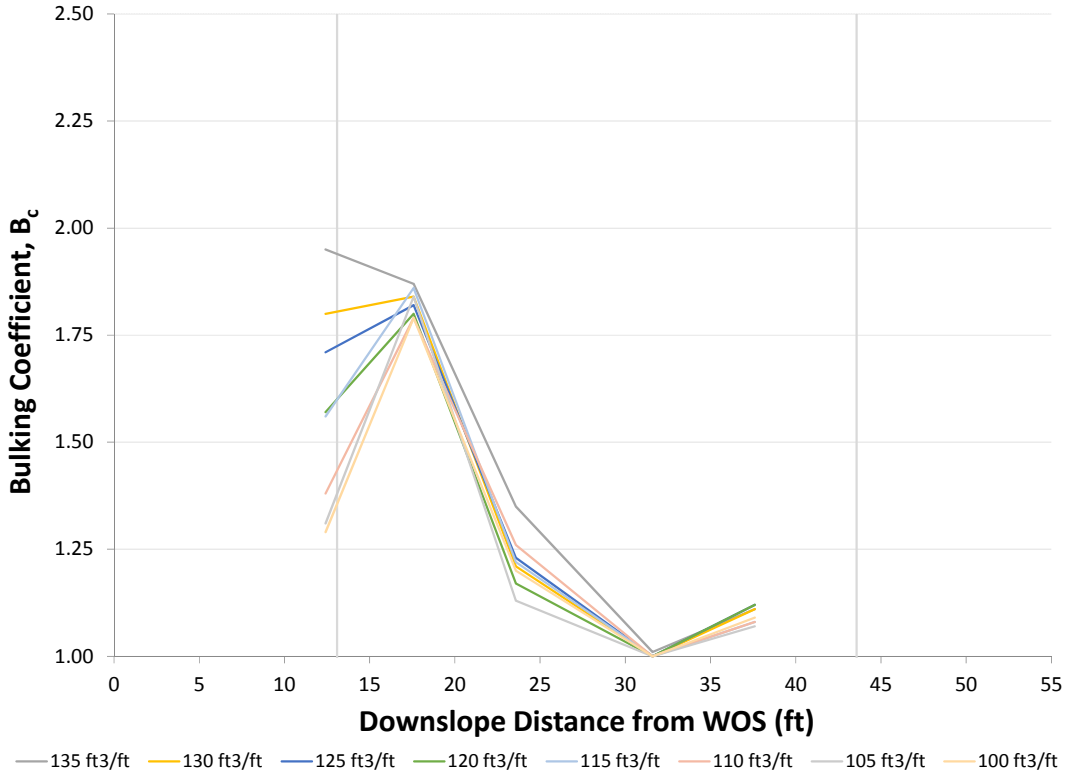

Figure 5-6. Bulking coefficient by wave volume and location, 100 – 135 ft3/ft.

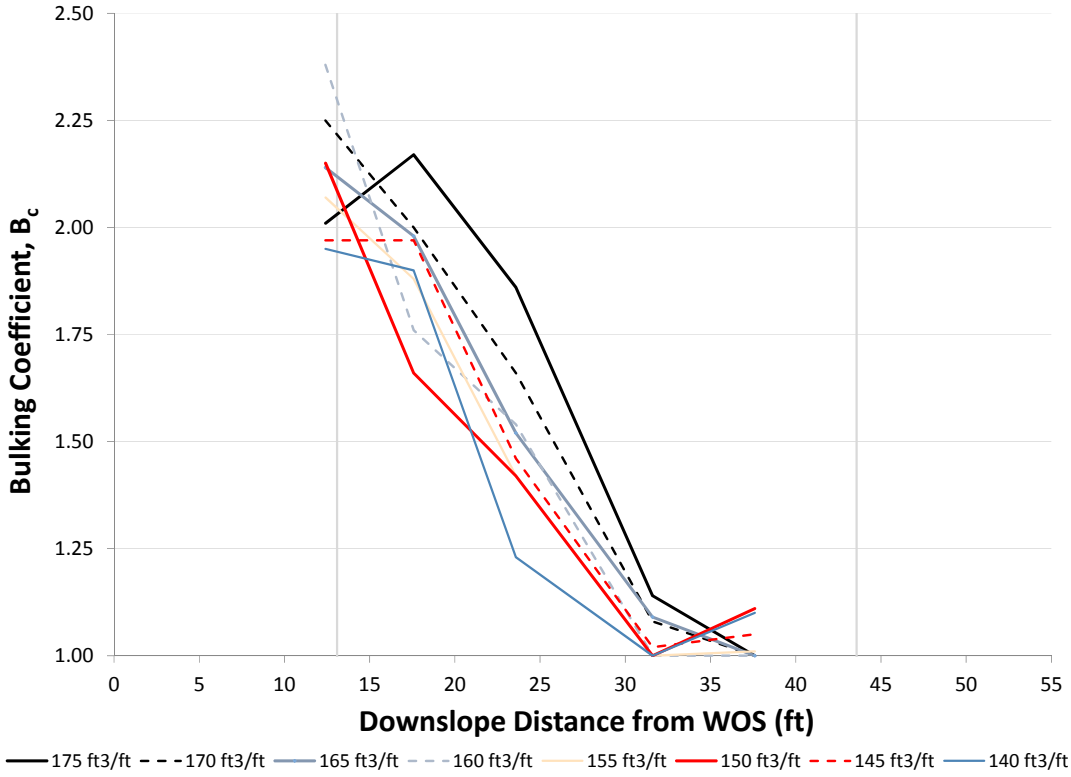

Figure 5-7. Bulking coefficient by wave volume and location, 140 – 175 ft3/ft.

Regression residuals, defined as (Observed – Predicted), are an indicator of model goodness of fit. The closer the residual is to zero, the better the model. Regression residuals are presented in Figure 5-8 and

Table **5-6**. To determine a percent error regression residuals were normalized using observed data. The normalized residuals demonstrate the percent difference between the model and observed condition. The closer the normalized residual is to zero, the better the model. The percent difference between model and observed conditions are presented in Table 5-7.

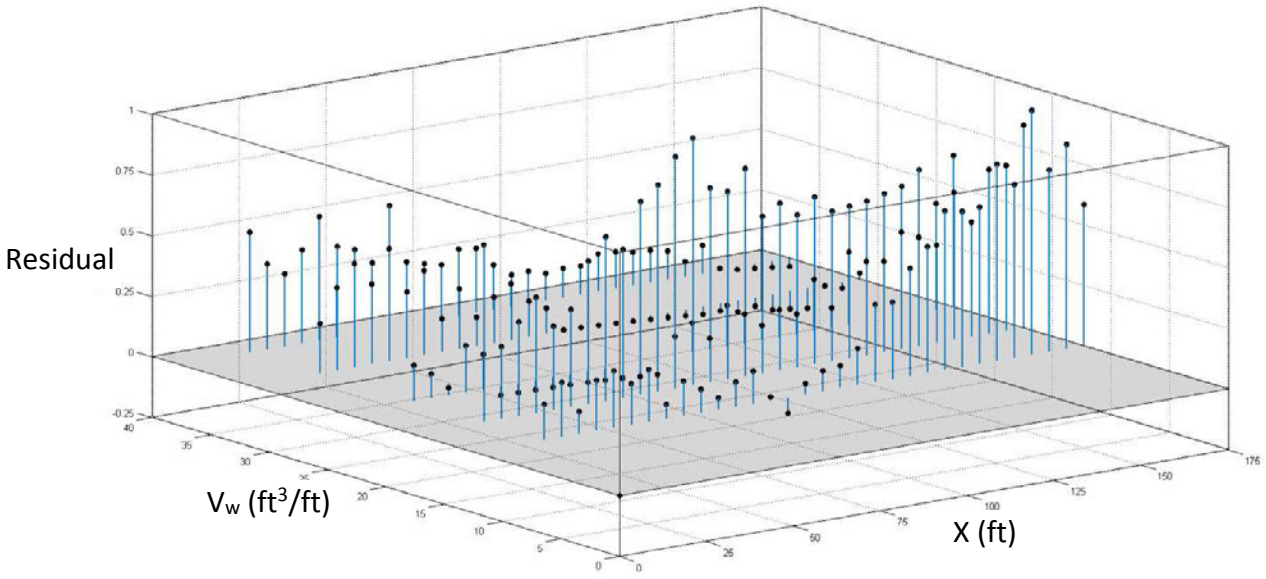

Figure 5-8. Regression residuals.

Table 5-6. Regression residuals (ft).

Simulated Wave Volume (ft^3/ft)	Downslope Distance (feet from WOS)				
	12.41	17.58	23.58	31.60	37.60
175	0.58	0.83	0.62	0.02	-0.04
170	0.84	0.68	0.44	-0.03	-0.03
165	0.75	0.68	0.31	0.00	-0.02
160	1.01	0.47	0.34	-0.08	-0.01
155	0.71	0.61	0.24	-0.07	0.01
150	0.81	0.40	0.25	-0.07	0.11
145	0.65	0.73	0.30	-0.04	0.06
140	0.64	0.67	0.08	-0.05	0.12
135	0.66	0.65	0.21	-0.03	0.13
130	0.52	0.63	0.08	-0.03	0.14
125	0.44	0.63	0.11	-0.03	0.15
120	0.32	0.62	0.06	-0.02	0.15
115	0.32	0.69	0.12	-0.02	0.12
110	0.15	0.63	0.17	-0.01	0.12
105	0.09	0.69	0.05	-0.01	0.11
100	0.08	0.65	0.12	0.00	0.13
95	0.04	0.86	0.08	0.00	0.09
90	-0.07	0.77	-0.07	0.00	0.19
85	0.01	0.80	-0.06	0.11	0.27
80	0.13	1.02	-0.06	0.15	0.27
75	0.10	0.95	-0.05	0.27	0.22
70	0.05	0.85	-0.05	0.19	0.21
65	0.10	0.80	-0.05	0.12	0.26
60	0.14	0.61	-0.04	0.25	0.33
55	0.06	0.67	-0.04	0.14	0.19
50	0.22	0.59	-0.04	0.38	0.29
45	0.17	0.40	-0.04	0.27	0.20
40	0.23	0.34	0.14	0.64	0.51
35	0.21	0.48	0.19	0.42	0.38
30	0.09	0.39	0.03	0.48	0.30
25	0.23	0.30	0.10	0.51	0.35
20	0.15	0.73	0.15	0.20	0.49

Table 5-7. Percent difference between model and observed condition.

Simulated Wave Volume (ft^3/ft)	Downslope Distance (feet from WOS)				
	12.41	17.58	23.58	31.60	37.60
175	-29%	-38%	-33%	-2%	4%
170	-37%	-34%	-26%	2%	3%
165	-35%	-34%	-20%	0%	2%
160	-42%	-27%	-22%	8%	1%
155	-34%	-32%	-17%	8%	-1%
150	-38%	-24%	-18%	7%	-10%
145	-33%	-37%	-21%	4%	-6%
140	-33%	-35%	-7%	5%	-11%
135	-34%	-35%	-16%	3%	-12%
130	-29%	-34%	-7%	4%	-12%
125	-26%	-34%	-9%	3%	-13%
120	-20%	-34%	-5%	2%	-14%
115	-20%	-37%	-10%	2%	-11%
110	-11%	-35%	-13%	1%	-11%
105	-7%	-37%	-4%	1%	-10%
100	-7%	-36%	-10%	0%	-12%
95	-4%	-43%	-7%	0%	-9%
90	6%	-41%	7%	0%	-16%
85	-1%	-42%	6%	-10%	-22%
80	-10%	-48%	6%	-13%	-22%
75	-8%	-46%	6%	-21%	-19%
70	-4%	-44%	5%	-16%	-18%
65	-8%	-42%	5%	-11%	-21%
60	-11%	-36%	5%	-20%	-25%
55	-5%	-38%	5%	-12%	-17%
50	-16%	-35%	4%	-27%	-23%
45	-13%	-27%	4%	-22%	-17%
40	-17%	-24%	-12%	-39%	-34%
35	-16%	-31%	-16%	-29%	-28%
30	-8%	-27%	-3%	-32%	-23%
25	-17%	-22%	-9%	-34%	-26%
20	-12%	-41%	-12%	-17%	-33%

5.4. Bulking Predictive Model Summary

A bulking predictive model for the landward side of 3:1 levees during wave overtopping simulation was developed using bulked and un-bulked flow thicknesses. The predictive model (Equation 11)

$$B_C = 1.18 + 9.4\text{E-}4V_W - 7.8E\text{-}3X + 1.1E\text{-}5V_W^2 - 7.6E\text{-}5V_W X + 1.1E\text{-}4X^2 \quad (11)$$

is based on wave volume (V_W) measured in ft^3/ft and slope distance (X) from the WOS measured in feet. The bulking coefficient, B_C, may be used to predict anticipated increase to flow thickness resulting from flow aeration during wave overtopping simulation. Because simulated flows carried no sediment or debris of any kind, B_C can also be interpreted as mean volumetric aeration, C_e, using the conversion,

$$C_e = 1 - \frac{1}{B_C} \quad (12)$$

Regression residuals were also determined. Residuals indicate the model tends to under predict flow bulking for larger volume waves at the crest and upper slope. Smaller volume waves are under predicted at the crest and toe of the slope. Under prediction occurs for all wave volumes immediately downslope of the crest. Slight over prediction occurs mid-slope for the medium and large waves. Under prediction is conservative for shear stress design and non-conservative for flow thickness design. These results apply strictly to the tested geometry. Application to other geometries is not recommended without prior validation.

5.5. Application

Application of the equation may be used for predicting anticipated bulking coefficients during overtopping simulation or computing bulking coefficients of flow thickness data collected during

overtopping simulation. Using Pullen (2007) and Hughes et al (2012) with the following seaward conditions, wave overtopping volumes to be simulated can be calculated:

- H_s = 8 ft, significant wave height at the toe,
- T_p = 9 sec, peak wave period,
- cot α = 3, seaward facing levee slope angle,
- q = 2.2 ft^3/ft/sec, average overtopping discharge,
- t = 1 hr, test duration

Once wave volumes to be simulated are calculated, corresponding B_C and mean aeration values along the slope can be calculated using Equations 11 and 12. Table 5-8 presents wave volumes to be simulated, Bc and mean aeration 10 ft and 30 ft from the simulator. Ten feet from the WOS is on the horizontal crest approximately 3 ft upstream of the transition to a 3:1 slope. Thirty feet from the WOS is located on the 3:1 slope approximately 13 ft upstream of the transition to the 25:1 berm which is outside the influence on bulking created by the slope transition. Wave volumes less than 20 ft^3/ft would also be in the simulation but are not included as they are outside the range of data used for B_C equation development.

Table 5-8. Bulking coefficients and mean aeration.

Simulated Wave Volume (ft^3/ft)	**B_C** Downslope Distance (feet from WOS)		**mean aeration (%)** Downslope Distance (feet from WOS)		Simulated Wave Volume (ft^3/ft)	**B_C** Downslope Distance (feet from WOS)		**mean aeration (%)** Downslope Distance (feet from WOS)	
	10.0	30.0	10.0	30.0		10.0	30.0	10.0	30.0
157.1	1.41	1.10	29	9	38.0	1.13	1.01	12	1
137.3	1.34	1.06	25	6	37.6	1.13	1.01	12	1
125.8	1.30	1.05	23	4	37.3	1.13	1.01	12	1
117.6	1.28	1.03	22	3	36.9	1.13	1.01	12	1
111.3	1.26	1.03	21	3	36.5	1.13	1.01	12	1
106.2	1.25	1.02	20	2	36.2	1.13	1.01	12	1
101.9	1.24	1.02	19	2	35.8	1.13	1.01	12	1
98.1	1.23	1.02	19	2	35.5	1.13	1.01	12	1
94.8	1.23	1.01	18	1	35.1	1.13	1.01	12	1

Simulated Wave Volume (ft^3/ft)	B_C Downslope Distance (feet from WOS)		mean aeration (%) Downslope Distance (feet from WOS)		Simulated Wave Volume (ft^3/ft)	B_C Downslope Distance (feet from WOS)		mean aeration (%) Downslope Distance (feet from WOS)	
	10.0	30.0	10.0	30.0		10.0	30.0	10.0	30.0
91.9	1.22	1.01	18	1	34.8	1.13	1.01	12	1
89.2	1.21	1.01	18	1	34.5	1.13	1.01	12	1
86.8	1.21	1.01	17	1	34.1	1.13	1.01	12	1
84.6	1.20	1.01	17	1	33.8	1.13	1.01	12	1
82.5	1.20	1.01	17	1	33.5	1.13	1.01	12	1
80.6	1.20	1.00	16	1	33.2	1.13	1.01	12	1
78.8	1.19	1.00	16	1	32.9	1.13	1.01	12	1
77.1	1.19	1.00	16	1	32.6	1.13	1.01	12	1
75.5	1.19	1.00	16	1	32.3	1.13	1.01	12	1
74.0	1.18	1.00	16	0	32.0	1.13	1.01	11	1
72.6	1.18	1.00	15	0	31.7	1.13	1.01	11	1
71.2	1.18	1.00	15	0	31.4	1.13	1.01	11	1
70.0	1.18	1.00	15	0	31.1	1.13	1.01	11	1
68.7	1.17	1.00	15	0	30.8	1.13	1.01	11	1
67.6	1.17	1.00	15	0	30.5	1.13	1.01	11	1
66.4	1.17	1.00	15	0	30.2	1.13	1.01	11	2
65.4	1.17	1.00	15	0	29.9	1.13	1.01	11	2
64.3	1.17	1.00	14	0	29.7	1.13	1.01	11	2
63.3	1.17	1.00	14	0	29.4	1.13	1.01	11	2
62.4	1.16	1.00	14	0	29.1	1.13	1.01	11	2
61.4	1.16	1.00	14	0	28.9	1.12	1.01	11	2
60.5	1.16	1.00	14	0	28.6	1.12	1.01	11	2
59.7	1.16	1.00	14	0	28.3	1.12	1.01	11	2
58.8	1.16	1.00	14	0	28.1	1.12	1.01	11	2
58.0	1.16	1.00	14	0	27.8	1.12	1.01	11	2
57.2	1.16	1.00	14	0	27.6	1.12	1.01	11	2
56.4	1.16	1.00	14	0	27.3	1.12	1.01	11	2
55.7	1.15	1.00	14	0	27.1	1.12	1.01	11	2
54.9	1.15	1.00	13	0	26.8	1.12	1.01	11	2
54.2	1.15	1.00	13	0	26.6	1.12	1.01	11	2
53.5	1.15	1.00	13	0	26.3	1.12	1.01	11	2
52.9	1.15	1.00	13	0	26.1	1.12	1.01	11	2
52.2	1.15	1.00	13	0	25.9	1.12	1.01	11	2

Simulated Wave Volume (ft^3/ft)	B_C Downslope Distance (feet from WOS) 10.0	B_C Downslope Distance (feet from WOS) 30.0	mean aeration (%) Downslope Distance (feet from WOS) 10.0	mean aeration (%) Downslope Distance (feet from WOS) 30.0	Simulated Wave Volume (ft^3/ft)	B_C Downslope Distance (feet from WOS) 10.0	B_C Downslope Distance (feet from WOS) 30.0	mean aeration (%) Downslope Distance (feet from WOS) 10.0	mean aeration (%) Downslope Distance (feet from WOS) 30.0
51.6	1.15	1.00	13	1	25.6	1.12	1.01	11	2
51.0	1.15	1.00	13	1	25.4	1.12	1.02	11	2
50.3	1.15	1.00	13	1	25.2	1.12	1.02	11	2
49.7	1.15	1.00	13	1	24.9	1.12	1.02	11	2
49.2	1.15	1.00	13	1	24.7	1.12	1.02	11	2
48.6	1.15	1.00	13	1	24.5	1.12	1.02	11	2
48.0	1.14	1.00	13	1	24.3	1.12	1.02	11	2
47.5	1.14	1.00	13	1	24.0	1.12	1.02	11	2
46.9	1.14	1.00	13	1	23.8	1.12	1.02	11	2
46.4	1.14	1.00	13	1	23.6	1.12	1.02	11	2
45.9	1.14	1.00	13	1	23.4	1.12	1.02	11	2
45.4	1.14	1.00	13	1	23.2	1.12	1.02	11	2
44.9	1.14	1.00	12	1	23.0	1.12	1.02	11	2
44.4	1.14	1.00	12	1	22.8	1.12	1.02	11	2
43.9	1.14	1.00	12	1	22.5	1.12	1.02	11	2
43.5	1.14	1.00	12	1	22.3	1.12	1.02	11	2
43.0	1.14	1.00	12	1	22.1	1.12	1.02	11	2
42.5	1.14	1.00	12	1	21.9	1.12	1.02	11	2
42.1	1.14	1.01	12	1	21.7	1.12	1.02	11	2
41.7	1.14	1.01	12	1	21.5	1.12	1.02	11	2
41.2	1.14	1.01	12	1	21.3	1.12	1.02	11	2
40.8	1.14	1.01	12	1	21.1	1.12	1.02	11	2
40.4	1.14	1.01	12	1	20.9	1.12	1.02	11	2
40.0	1.14	1.01	12	1	20.8	1.12	1.02	11	2
39.6	1.13	1.01	12	1	20.6	1.12	1.02	11	2
39.2	1.13	1.01	12	1	20.4	1.12	1.02	11	2
38.8	1.13	1.01	12	1	20.2	1.12	1.02	11	2
38.4	1.13	1.01	12	1	20.0	1.12	1.02	11	2

Chanson (1993) demonstrated reduction of the Darcy friction factor, f_D, due to aeration during steady state overtopping. The Darcy friction factor, f_D, is defined as

$$f_D = \frac{8\tau_0}{\rho v^2} \tag{13}$$

The ratio of aerated friction factor to un-aerated friction factor is then

$$\frac{f_{D_{aerated}}}{f_{D_{un\text{-}aerated}}} = \frac{\left(\frac{8\tau_0}{\rho v^2}\right)_{aerated}}{\left(\frac{8\tau_0}{\rho v^2}\right)_{un\text{-}aerated}} \tag{14}$$

Equivalent flows, excepting aeration, have equal velocities and unequal depths. Rearranging terms and canceling,

$$\frac{f_{D_{aerated}}}{f_{D_{un\text{-}aerated}}} = \left(\frac{\tau_{0_{aerated}}}{\tau_{0_{un\text{-}aerated}}}\right)\left(\frac{\rho_{un\text{-}aerated}}{\rho_{aerated}}\right) \tag{15}$$

Applying Chanson (1993) to determine $\frac{f_{D_{aerated}}}{f_{D_{un\text{-}aerated}}}$ and applying Equation 11 and Equation 12 to determine $\left(\frac{\rho_{un\text{-}aerated}}{\rho_{aerated}}\right)$, it is possible to determine $\left(\frac{\tau_{0_{aerated}}}{\tau_{0_{un\text{-}aerated}}}\right)$. The inverse relationship between shear stress and B_C is presented in Figure 5-9.

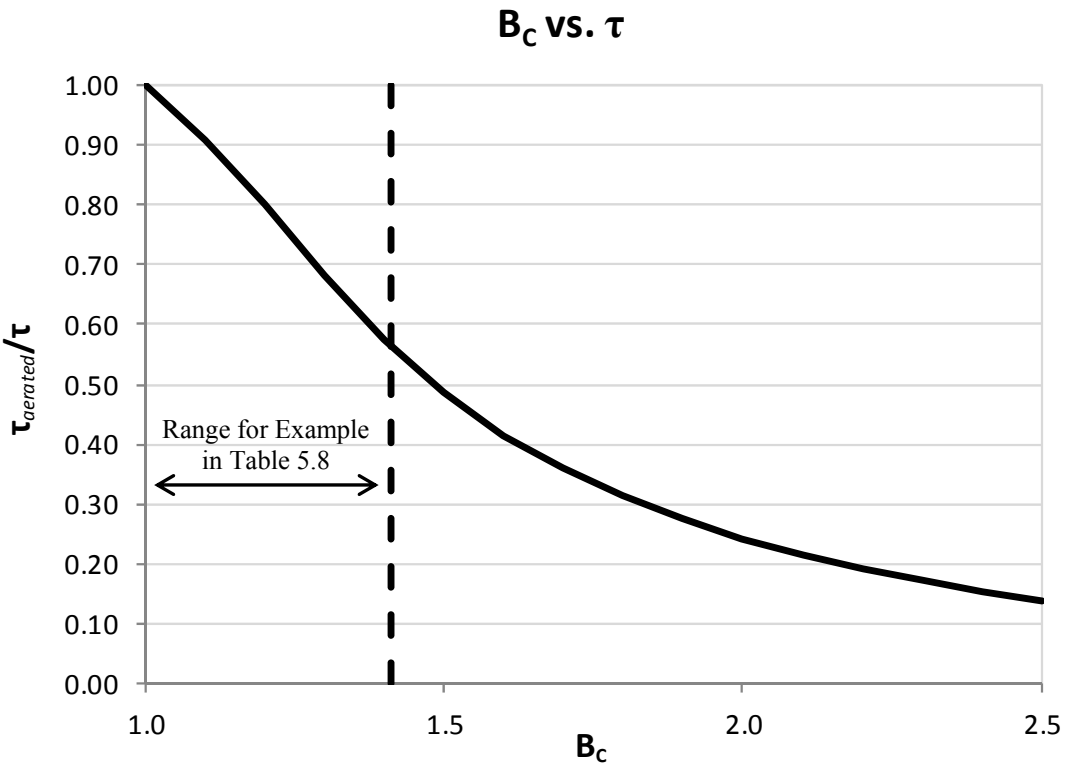

Figure 5-9. B_C vs Shear stress.

Decreasing shear stress with increasing B_C implies a reduction in erosion with increasing B_C.

Dean et al (2010b) investigated methods to determine erosional limits of grass slopes using velocity, shear stress and work based approaches concluding the work based approach is preferable. Hughes (2011a) expanded the results of Dean et al (2010b), applying the results to wave overtopping of levees using cumulative work done by each overtopping wave during a wave overtopping event. The cumulative work is related to an excess wave volume and compared to the volumetric erosional limit of the levee, thus providing a tool to investigate the potential for levee failure during an overtopping event.

The Dean et al (2010b) erosion limit is based on recommended velocity/time limiting values in Hewlett et al (1987). Using the Dean et al (2010b) method, Hughes et al (2011a) confirmed the erosion limit for a good grass cover is

$$\frac{E_W}{K_W \beta_W} = 0.492 \text{ x } 10^6 \frac{m^3}{s^2} \quad (16)$$

E_W is erosion due to excess work, K_W is an unknown coefficient and β_W is a grouping of terms including water mass density and shear stress. Erosion limit values for other grass conditions are provided in Dean et al (2010b), and Hughes et al (2011a) determined the erosion limit for open erosion control mats and filled mats. Hughes (2011a) also derived β_W determining it to be

$$\beta_W = \frac{1}{8} \rho f_D \quad (17)$$

The effect of aeration due to wave bulking on erosion limits can be determined by first combining Equation 16 and Equation 17,

$$\left(\frac{E_W}{K_W \left(\frac{1}{8} \rho f_D \right)} \right) = 0.492 \text{ x } 10^6 \frac{m^3}{s^2} \quad (18)$$

Because the Dean et al. (2010b) and Hughes (2011a) erosional limit values are based on limiting velocity/time curves developed through prototype testing, a deviation from testing conditions should result in an increase/decrease in the erosional limit. Flow bulking during wave overtopping is a deviation. The effect on the erosional limit may be expressed as a multiple of the Dean et al (2010b) erosional equivalence and determined by initially assuming equivalent conditions

$$\left(\frac{E_W}{K_W \left(\frac{1}{8} \rho f_D \right)} \right)_{\text{Hewlett et al}} = \left(\frac{E_W}{K_W \left(\frac{1}{8} \rho f_D \right)} \right)_{\text{bulked}} \quad (19)$$

Canceling like terms and rearranging,

$$\frac{\left(\frac{E_W}{K_W}\right)_{\text{Hewlett et al}}}{\left(\frac{E_W}{K_W}\right)_{\text{bulked}}} = \frac{\rho_{\text{bulked}}}{\rho_{\text{Hewlett et al}}} \frac{f_{D_{\text{bulked}}}}{f_{D_{\text{Hewlett et al}}}} \tag{20}$$

Equation 19 implies changes in flow density or surface roughness from the original testing conditions used for Hewlett et al (1987) may lead to a difference in erosional limit.

Hughes (2011a) uses the Dean et al (2010b) excess work approach and applies it to overtopping wave volumes on levees thus creating an "excess volume" approach to be used for evaluating levee resiliency to wave overtopping events. As overtopping wave volume conditions differ from those used to create the limiting velocity/time curves in Hewlett et al (1987), the wave volume that is "excess" should increase/decrease accordingly. Applying the B_c value determined using Equation 11 and the ratio in Equation 19, and assuming B_C is applicable to the entire wave volume, wave volume excess in Hughes (2011a) can be adjusted accordingly.

From Hughes (2011a), erosional limit for wave overtopping of levees with good grass can be estimated using

$$\left(\frac{E_W}{K_W \beta_W}\right)_{\text{Hewlett et al}} \left(\frac{f_F}{2g\sin\theta}\right) = \left(0.492 \times 10^6 \frac{m^3}{s^2}\right)\left(\frac{f_F}{2\, g \sin\theta}\right) \tag{21}$$

where f_F is the Fanning friction factor (equal to ¼ f_D), g is gravitational acceleration and θ is levee slope. Combining Equation 21 and Equation 20, cancelling and rearranging terms

$$\frac{\left(\frac{E_W}{K_W}\right)_{\text{Hewlett et al}}}{\left(\frac{E_W}{K_W}\right)_{\text{bulked}}} = \frac{\rho_{\text{bulked}}}{\rho_{\text{Hewlett et al}}} \frac{\sin\theta_{\text{bulked}}}{\sin\theta_{\text{Hewlett et al}}} \tag{22}$$

Using Equation 11 and Equation 12, the mean aeration percent for a simulated wave volume can be determined. From mean aeration percent, flow density can be determined by

$$\rho_{bulked} = (\rho_{un\text{-}bulked})(1\text{-}C_e) \quad (23)$$

Mean air concentration during Hewlett et al (1987) testing can be estimated using Chanson (1993)

$$C_e = 0.9 \sin \theta \quad (24)$$

The increase/decrease to be applied to each overtopping wave volume is determined using Equation 22. Following Hughes (2011a), the sum of overtopping wave volumes is then compared to the results of Equation 21 to evaluate levee resiliency.

6. Summary and Conclusions

Prototype scale tests were conducted to determine bulking coefficients for overtopping waves on a landward side levee with 3:1 (horizontal:vertical) slope. Collected data were analyzed to determine a predictive equation for wave bulking during wave overtopping simulation. An empirical model for predicting a bulking coefficient applicable to simulated overtopping wave flow thickness including entrained air was developed for the landward side of a 3:1 levee. Model parameters were wave volume per unit width in ft^3/ft, slope distance from the WOS and a bulking coefficient given as the ratio of bulked thickness divided by un-bulked thickness at maximum flow thickness.

6.1. Research summary and discussion

Levee failure as a result of erosion from wave overtopping was determined to be the major cause of flooding in New Orleans during Hurricane Katrina (Seed et al. 2006, Andersen 2007, Link et al. 2009). Wave overtopping research has documented overtopping wave frequency, velocity and flow thickness, and predictive equations are available for wave overtopping processes (Hughes 2008a, Pullen et al. 2007, Bosman 2007, van der Meer 2006, 2007a, Valk 2009, van Gent 2002b, 2002c, 2003, Schüttrumpf et al. 2001).

Development of a wave overtopping simulator (van der Meer et al. 2006, 2007b, 2008b, 2010, van der Meer 2007) enabled in situ levee testing of wave overtopping conditions. The resiliency to wave overtopping of certain vegetated levees was quantified (van der Meer 2008a) and a larger, stationary wave overtopping simulator was developed (Thornton et al. 2010) to quantify multiple levee armoring methods resiliency to wave overtopping (Thornton et al. 2010, 2011, 2012).

In addition to performance testing, predictive methods for levee resilience have been put forth by van der Meer (2010), Dean et al. (2010b) and Hughes (2011a). Van der Meer et al. (2010) proposed a shear stress based, cumulative hydraulic loading approach reliant on peak overtopping wave velocities and a critical, threshold velocity that is a function of the levee protective cover. Dean et al. (2010b) evaluated three approaches concluding a cumulative excess work approach is the most reasonable of the three evaluated and provides the best results. Hughes (2011a) evaluated Dean et al.'s erosional equivalence method and expanded it to include earthen levee protection during wave overtopping due to severe hurricanes. The expanded erosional equivalence method is a more robust erosional equivalence method for evaluating the ability of landward side levee armoring to resist overtopping waves.

The levee resilience predictive methods do not address or incorporate flow aeration. In light of known effects of flow aeration during steady state overtopping, such as changing friction factors and decreased buoyancy from decreased density (Wood 1983, Chanson 1994b), similar changes to friction factors and buoyancy are likely occurring during wave overtopping. To develop either a deterministic or shear stress based approach to levee resiliency, flow bulking must be quantified.

The development of a wave overtopping simulator (Van der Meer et al. 2006; Van der Meer 2007a; Van der Meer et al. 2008b, Van der Meer et al. 2011) allows for wave overtopping testing under controlled conditions. A wave overtopping simulator is a large container temporarily installed on the crown of a levee or dike and simulates the wave overtopping hydraulics by releasing volumes of water in a manner that duplicates the correct leading edge thicknesses and velocities for a distribution of wave volumes associated with a specific storm condition. The CSU WOS was built as a larger, permanent structure in combination with a levee system for

replicating the landward side of the levee (Van der Meer et al. 2011). This facility provided the means for studying flow bulking on the landward side of a levee under more controlled conditions than realistically feasible in the field.

A series of experiments was conducted in the WOS located at the Engineering Research Center of Colorado State University. Data were collected from the WOS and a downslope, prototype scale, 3:1 levee section. Data included flow velocity from paddlewheel sensors, pressure from pressure transducers, flow thickness from specialized surfboards and flow thickness visually observed from flume wall mounted staff gages.

The collected data were reviewed, systematically screened and analyzed for wave thickness trends, including bulking, associated with wave overtopping on the landward side of levees. Simulated wave volumes were examined for mass conservation with errors of $\pm$ 7.0 percent for values greater than 60 ft^3/ft, -11 to 13.0 percent for wave volumes 50, 55 and 60 ft^3/ft and -23 to 45 percent for wave volumes less than 45 ft^3/ft. Average wave bulking coefficients were quantified for simulated wave volumes at specified slope distances from the WOS. A second-order multivariable polynomial regression was used for empirical model development predicting bulking coefficients on the landward side of levees during simulated wave overtopping. The mathematical model is presented as Equation 11 and has $R^2 = 0.72$. The predictive model was assessed to have engineering conservatism based on the residuals and engineering judgement.

6.2. Conclusions

Important findings resulted from the research that can be used to address the need for design guidance of levee armoring used as protection against failure due to wave overtopping. Meaningful findings from this study are as follows:

- A mathematical model was developed for the quantification of flow bulking during wave overtopping simulation on the landward side of 3:1 levees. The model was developed from prototype scale data of wave overtopping volumes between 20 and 175 ft^3/ft. Conducted research provided the first documented methodology for a predictive tool to quantify flow bulking during simulated wave overtopping. Provided as Equation 11, the flow bulking model is presented as follows:

$$B_C = 1.18 + 9.4\text{E-}4V_W - 7.8E\text{-}3X + 1.1E\text{-}5V_W^2 - 7.6E\text{-}5V_W X + 1.1E\text{-}4X^2 \qquad (11)$$

- The developed method of Equation 11 was tailored to wave volume, slope length and bulking coefficient data from a robust, unique dataset collected from a prototype scale 3:1 levee model. The first-ever-collected bulking coefficient data as a function of wave volume and slope length are provided in Table 5-4.

- The developed method of Equation 11 provided prediction of wave bulking coefficients on the landward side of 3:1 levees during wave overtopping simulation. The method provided an overall R^2 of 0.72 for the range of wave volumes and slope lengths.

- A method for applying Equation 11 to Hughes (2011a) excess overtopping wave volume method is presented assuming B_C is uniform throughout a wave volume.

The equation was developed from a physical model with ranges of altered parameters. Application of the equation outside of the laboratory conditions is not advised.

6.3. Recommendations for further research

The mathematical model developed from this research provides a solid framework for the expansion of predictive models of levee resilience under wave overtopping conditions. Use of

the model in levee resilience predictive relationships could improve the functionality and applicability of the relationships.

The equation was developed from an approximately 30.5 ft. long, 3:1 levee transitioning to a 25:1 berm. Data from a 4:1 levee slope or other commonly built levee slope would supplement results from the present study. Incorporation of data from slope lengths greater than the 30.5 ft slope length used in this study would also be of benefit as levee slopes greater than 30.5 ft. are not uncommon.

The flow bulking coefficient model for simulated wave overtopping on landward side 3:1 levees is based on the average bulking throughout the water column. Developing a method to quantify aeration at specific locations within the water column would provide an improved functionality to levee resilience predictive relationships. Field verification of flow bulking on the landward side during wave overtopping of levees for comparison to simulated wave overtopping conditions would also be of benefit.

The physical environment during wave overtopping conditions is an extremely challenging one to quantify. Overtopping wave velocities can range from 0 to 30+ and back to 0 ft/s during the passage of a single wave in a few seconds. Flow thicknesses can range from 0 to 3+ and back to 0 ft in the same amount of time. Equipment needs to be sturdy enough to withstand multiple, high velocity impacts from waves yet delicate enough react quickly to the fast changing variables. Equipment also needs to accurately measure over the wide range of flow densities, velocities and flow thicknesses that occur in a short time frame. This measurement environment is challenging and is a likely contributor to errors in continuity. Improvements in equipment and/or technology could improve results.

7. References

Andersen, C.F., Battjes, J.A., Daniel, D.E., Edge, B., Espey Jr, W., Gilbert, R.B., Jackson, T.L., Kennedy, D., Mileti, D.S., Mitchell, J.K., Nicholson, P., Pugh, C.A., Tamaro Jr, G. and Traver, R. 2007. "The New Orleans Hurricane Protection System: What Went Wrong and Why" Report by the American Society of Civil engineers Hurricane Katrina External Review Panel. Available at: http://cms.asce.org/uploadedFiles/Publications/ASCE_News/2009/04_April/ERPreport.pdf

Boes, R. M. and Hager, W. H. 1998. "Fiber-optical experimentation in two-phase cascade flow", *Proceedings of the International Roller Compacted Dams Seminar*, K Hansen (editor), U. S. Bureau of Reclamation, Technical Service Center, Denver, Colorado, 13 p.

Bosman, G. 2007. "Velocity and flow depth variations during wave overtopping", Final Report of the Master Thesis, Delft University of Technology, Section of Coastal Engineering, Available from: http://repository.tudelft.nl/search/ir/?q=bosman+Velocity+and+flow+depth+variations+during+wave+overtopping&faculty=&department=&type=&year=

Brunkard, J., Namulanda, G. and Ratard, R. 2008. Hurricane Katrinba Deaths, Louisiana, 2005. Disaster Medicine and Public Health Preparedness. Volume 2, No. 4, pp .215-223.

Chanson, H. 1993. "Self-aerated flows on chutes and spillways"' *Journal of Hydraulic Engineering*, American Society of Civil Engineers, Volume 119, No. 2, 1993, pp. 220-243, Available at: http://espace.library.uq.edu.au/

Chanson, H. 1994b. "Drag reduction in open channel flow by aeration and suspended load", *Journal of Hydraulic Research*, International Association for Hydro-Environment Engineering and Research, Volume 32, No. 1, 1994, pp.87-101, Available at: http://espace.library.uq.edu.au/view/UQ:9388

Chanson, H. 2004a. "Air-water flows in water engineering and hydraulic structures, Basic processes and metrology". *Hydraulics of Dams and River Structures: Proceedings of the International Conference of Dams and River Structures* , Yazdandoost and Attari (editors), Taylor & Francis Group, London, England, 2004, pp. 3-16, Available from: http://espace.library.uq.edu.au/view.php?pid=UQ:9431

Chanson, H. 2004b. "Free-surface aeration in dam break waves: an experimental study", *Hydraulics of Dams and River Structures: Proceedings of the International Conference of Dams and River Structures* , Yazdandoost and Attari (editors), Taylor & Francis Group, London, England, 2004, pp. 25-32, Available from: http://espace.library.uq.edu.au/view/UQ:9264

Chanson, H. 2009. "Turbulent air-water flows in hydraulic structures: Dynamic similarity and scale effects", *Environmental Fluid Mechanics*, Springer Science, June 2008, pp125-142, Available at: http://espace.library.uq.edu.au/eserv/UQ:171996/efm_09a.pdf

Chow, V. T. 1959. Open Channel Hydraulics. McGraw-Hill. New York. 1959.

Dean, R. G.; Rosati, J. D.; Walton, T. L.; and Edge, B. L. 2010b. "Erosional equivalences of levees: Steady and intermittent overtopping", In: Demirbilek (editor), *Ocean Engineering*, Elsevier Ltd., Volume 37, pp 104-113, Available at: http://workhorse.europa.renci.org/~bblanton/OEVol37Issue1/

Ehrenberger, R. 1926. "Wasserbewegung in steilen Rinnen (Schusstennen) mit besonder Berücksichtigung der Selbstbelüftung." Österreichischer Ingeniuer – und Architektverein, No. 15/16 and 17/18, 23 pp. Translated by E.F. Wilsey, U.S. Bureau of Reclamation.

Franco, L., de Gerloni and van der Meer, J.W. 1994. Wave overtopping on vertical and composite breakwaters. Procedures of the 24th International Conference on Coastal engineering. ASCE, New York, pp. 1030-1044.

Hewlett, H. W. M. ; Boorman, L. A.; and Bramler, M. E. 1987, "Design of reinforced grass waterways", Construction Industry Research and Information Association, London, England, Report 116, ProQuest, 116 p., Available at: http://md1.csa.com/partners/viewrecord.php?requester=gs&collection=TRD&recid=200125000630CE&recid=200180003405MT&q=&uid=791574361&setcookie=yes

Hughes, S. A. 2007. "Evaluation of permissible wave overtopping criteria for earthen levees without erosion protection", Engineering Research Center, Colorado State University, Fort Collins, Colorado, 31 p., (unpublished white paper).

Hughes, S. A. 2008a. "Estimation of overtopping flow velocities on earthen levees due to irregular waves," ERDC/CHL CHETN-III-77, January 2008, *Coast and Hydraulics Engineering Technical Note (CHETN)*, U.S. Army Corps of Engineers, Coastal Inlets Research Program (CIRP), Engineer Research and Development Center, Vicksburg, Mississippi , Available at: http://cirp.usace.army.mil/pubs/chetns.html

Hughes, S. A. 2008b. "Levee overtopping design guidance: What we know and what we need", *Proceedings of the Solutions to Coastal Disasters 2008 Conference*, American Society of Civil Engineers, pp 867-880, Available at: http://cedb.asce.org/cgi/WWWdisplay.cgi?162866

Hughes, S. A., and Nadal, N.C. 2009. "Laboratory study of combined wave overtopping and storm surge overflow of a levee." *Coastal Engineering, Elsevier, Vol 56. No.3, pp. 244-259.*:

Hughes, S. A. 2011a. "Adaptation of the Levee Erosional Equivalence Method for the Hurricane Storm Damage Risk Reduction System (HSDRRS)", ERDC/CHL TR-11-3, U.S. Army Corps of Engineers, Coastal & Hydraulics Laboratory, Engineer Research and Development Center, Vicksburg, Mississippi, Available at: http://acwc.sdp.sirsi.net/client/search/asset:asset?t:ac=$N/1000841

Lamb, O. P. and Killen, J. M. 1950. "An electrical method for measuring air concentration in flowing air-water mixtures", St. Anthony Falls Hydraulic Laboratory, University of Minnesota, Minneapolis, Minnesota, 31 p., March 1950, 36 p, Available at: http://purl.umn.edu/107905

Link, L.E., Jaeger, J.J., Stevenson, J., Stroupe, W., Mosher, R.L., Martin, D., Garster, J.K., Zilkoski, D.B., Ebersole, B.A., Westerink, J.J., Resio, D.T., Dean, R.G., Sharp, M.K., Steedman, R.S., Duncan, J.M., Moentenich, B.L., Howard, B., Harris, J., Fitzgerald, S., Moser, D., Canning, P., Foster, J. and Muller, B. 2009. "Performance Evaluation of the New Orleans and Southeast Louisiana Hurricane Protection System", United sates Army corps of Engineers. Available at: http://biotech.law.lsu.edu/katrina/ipet/ipet.html.

Lorke, S., Brüning, A., Bornschein, A., Gilli, S., Krüger, N., Schüttrumpf, H., Pohl, R., Spano, M., and Werk, S. 2009. "Influence of wind and current on wave run-up and wave overtopping," Hydralab – FlowDike, Report 2009, 100pp.

Lorke, S., Brüning, A., Van der Meer, J., Schüttrumpf, H., Bornschein, A., Gilli, S., Pohl, R., Spano, M., Řiha, J., Werk, S., and Schlütter, F. 2010. "On the effect of current on wave run-up and wave overtopping," Proceedings of the 32nd International Conference Coastal Engineering, Shanghai, China, American Society of Civil Engineers. New York. Available at: https://journals.tdl.org/icce/index.php/icce/article/download/1388/pdf_366.

Pullen, T.; Allsop, N. W. H.; Bruce, T.; Kortenhaus, A; Schüttrumpf, H.; van der Meer, J. W. 2007. "EurOtop: Wave overtopping of sea defences and related structures: Assessment Manual", Available at: http://www.overtopping-manual.com

Richardson, E.V., Simons, D.B. and Lagasse, P.F. 2001. "River Engineering for Highway Encroachments." Hydraulic Design Series Number 6. Federal Highway Administration, National Highway Institute. Arlington, VA.

Schüttrumpf, H.; Möller, J.; Oumeraci, H.; Grüne, J.; Weissmann, R. 2001. "Effects of natural sea states on wave overtopping of seadikes", *Proceedings of the 4th International Symposium - Waves,* American Society of Civil Engineers, Volume 2 pp 1565-1574, Available at: http://cedb.asce.org/cgi/WWWdisplay.cgi?130789

Schüttrumpf, H.; Möller, J.; and Oumeraci, H. 2002. "Overtopping flow parameters on the inner slope of seadikes", *Proceedings of the 28th International Conference - Coastal Engineering,* World Scientific, Volume 2, pp 2116-2127, Available at: http://eproceedings.worldscinet.com/9789812791306/9789812791306_0178.html

Schüttrumpf, H. and van Gent, M. R. 2003. "Wave overtopping at seadikes", *Proceedings of Coastal Structures '03*, American Society of Civil Engineers, pp 431-443, Available at: http://ascelibrary.org/proceedings/resource/2/ascecp/147/40733/36_1?isAuthorized=no

Schüttrumpf, H. and Oumeraci, H. 2005. "Layer thicknesses and velocities of wave overtopping flow at seadikes", *Coastal Engineering*, Elsevier, Volume 52, pp 473-495, Available at: http://www.sciencedirect.com/science/article/pii/S0378383905000232

Seed, R.B., R. G. Bea, R. I. Abdelmalak, A. G. Athanasopoulos, G. P. Boutwell, J. D. Bray, J.-L. Briaud, C. Cheung, D. Cobos-Roa, J. Cohen-Waeber, B. D. Collins, L. Ehrensing, D. Farber, M. Hanemann, L. F. Harder, K. S. Inkabi, A. M. Kammerer, D. Karadeniz, R.E. Kayen, R. E. S. Moss, J. Nicks, S. Nimmala, J. M. Pestana, J. Porter, K. Rhee, M. F. Riemer, K. Roberts, J. D. Rogers, R. Storesund, A. V. Govindasamy, X. Vera-Grunauer, J. E. Wartman, C. M. Watkins, E. Wenk Jr., and S. C. Yim. 2006. "Investigation of the performance of the New Orleans flood protection systems in Hurricane Katrina on August 29, 2005". Final Report, July 31, 2006. Available at: http://www.ce.berkeley.edu/projects/neworleans/report/intro&summary.pdf

Thornton, C. I.; Scholl, B. N.; and Abt, S. R. 2010. "Wave overtopping simulator testing of proposed levee armoring materials", Engineering Research Center, Colorado State University, Fort Collins, Colorado.

Thornton, C. I.; van der Meer, J.W.; Scholl, B. N.; Hughes, S. A.; and Abt, S. R. 2011. "Testing levee slope resiliency at the Colorado State University wave overtopping test facility", Engineering Research Center, Colorado State University, Fort Collins, Colorado, 12 p., Available at: http://www.vandermeerconsulting.nl/downloads/stability_a/2011_thornton_slope_resiliency.pdf

Thornton, C. I.; Scholl, B. N.; Hughes, S. A.; and Abt, S. R. 2012. "Full-scale testing of levee resiliency during wave overtopping", *Proceedings of United States Society on Dams Conference 2012*, New Orleans, (in press).

Valk, A. 2009. "Wave overtopping - Impact of water jets on grassed inner slope transitions", Final Report of the Master Thesis, Delft University of Technology, Section of Coastal Engineering, Available from: http://repository.tudelft.nl/search/ir/?q=valk+Wave+overtopping+-+Impact+of+water+jets+on+grassed+inner+slope+transitions&faculty=&department=&type=&year=

Van der Meer, J. W. and Janssen, W. 1995. "Wave run-up and wave overtopping at dikes", In: Kabayashi and Demirbilek (Eds.), *Wave Forces on Inclined and Vertical Wall Structures,* American Society of Civil Engineers, 27 p, Available at: http://repository.tudelft.nl/view/hydro/uuid%3Ad3cb82f1-8e0b-4d85-ae06-542651472f49/

Van der Meer, J.W. 2002. Wave run-up and wave overtopping at dikes. Technical Advisory Committee on Flood Defence (TAW). Delft, Netherlands.

Van der Meer, J. W.; Steendam, G. J.; and Regeling, E. 2006. "The wave overtopping simulator", *Proceedings of the 30th International Conference - Coastal Engineering,* American Society of Civil Engineers, Volume 5 pp 4654-4666, Available at: http://www.vandermeerconsulting.nl/downloads/stability_a/2006_vandermeer_snijders.pdf

Van der Meer, J. W. 2007a. "Design, construction, calibration and use of the wave overtopping simulator", Report version 3.3 of Project 04i03 for ComCoast and Rijkswaterstatt, September, 2007,112 p., Available at: http://repository.tudelft.nl/search/ir/?q=Design%2C%20construction%2C%20calibration%20and%20use%20of%20the%20wave%20overtopping%20simulator

Van der Meer, J. W.; Bernardini, P.; Steendam, G. J.; Akkerman, G. J.; and Hoffmans, G. 2007b. "The wave overtopping simulator in action", *Proceedings of the 5th Coastal Structures International Conference,* World Scientific, pp 645-656, Available at: http://eproceedings.worldscinet.com/9789814282024/9789814282024_0057.html

Van der Meer, J. W. 2008a. "Erosion strength of inner slopes of dikes against wave overtopping - Preliminary conclusions after two years of testing with the Wave Overtopping Simulator", Interim Report to ComCoast, Rijkswaterstaat, and Projectbureau Zeeweringen , August 2008, 21 p., Available at: http://www.vandermeerconsulting.nl/downloads/summary_report_overtopping_tests_v11.pdf

Van der Meer, J. W.; Steendam, G. J.; de Raat, G.; and Bernardini, P. 2008b. "Further developments on the wave overtopping simulator", *Proceedings of the 31st International Conference - Coastal Engineering,* American Society of Civil Engineers, Volume 4 pp 2957-2969, Available at: http://www.vandermeerconsulting.eu/downloads/stability_a/2008_vandermeer_steendam.pdf

Van der Meer, J. W.; Hardeman, B.; Steendam, G. J.; Schüttrumpf, H.; and Verheij, H. 2010. "Flow depths and velocities at crest and landward slope of a dike, in theory and with wave overtopping simulator", *Proceedings of the 32nd International Conference - Coastal Engineering,* American Society of Civil Engineers, Available at: http://journals.tdl.org/ICCE/article/view/1239

Van der Meer, J. W.; Thornton, C. and Hughes, S. 2011. "Design and operation of the U.S. Wave Overtopping Simulator", *Proceedings of the 6th International Conference - Coastal Structures,* American Society of Civil Engineers, Available at: http://www.vandermeerconsulting.nl/downloads/stability_a/2011_vandermeer_design_operation.pdf

Van Gent, M. R. A. 2002b. "Wave overtopping events at dikes", *Proceedings of the 28th International Conference - Coastal Engineering,* World Scientific, Volume 2, pp 2203-2215, http://eproceedings.worldscinet.com/9789812791306/9789812791306_0185.html

Van Gent, M. R. A. 2002c. "Low Exceedance Wave Overtopping Events." Delft Project Identification: DC030202/H3802.

Wood, I. R**.** 1983."Uniform region of self-aerated flow", Journal of Hydraulic Engineering, American Society of Civil Engineers, Volume 109, No. 3, 1983, pp 447-461.

7.1. Additional References

Afshar, N. R.; Asawa, G. L.; and Ranga Raju, K. G.1994. "Air concentration distribution in self-aerated flow", *Journal of Hydraulic Research*, International Association for Hydro-Environment Engineering and Research, Volume 32, No. 4, 1994, pp. 623-631, Available from: http://espace.library.uq.edu.au/view.php?pid=UQ:9099

Ahrens, J. P.; Heimbaugh, M. S.; and Davidson, D. D. 1986. "Irregular wave overtopping of seawall/revetment configurations," Roughans Point, Massachusetts", Technical Report CERC-86-7, U.S. Army Waterways Experiment Station, Vicksburg, Mississippi, Available at: http://www.stormingmedia.us/authors/Ahrens_John_P_.html

Aivazyan, O. M. 2008. "A new technique for the calculation of aeration development zones and nonaerated zones in turbulent flows on the spillway faces of dams and in prismatic flumes and its field verification", *Water Resources*, Pleiades Publishing, Volume 35, No. 3, May 2008, pp. 305-318, Available at: http://www.springerlink.com/content/0097-8078/35/3/

Akkerman, G. J.; van Gerven, K.; Schaap, K.; and van der Meer, J. W. 2007a. "ComCoast WP3 - Wave overtopping erosion tests at a Groningen sea dike", CUR/RWS, Royal Haskoning, Nijmegen, The Netherlands, 81 p., Available at: http://repository.tudelft.nl/view/ir/uuid%3A5a9665be-ca95-4e6a-80d7-60f0a4221db8/

Akkerman, G. J.; Bernardini, P.; van der Meer, J.W; Verheij, H.; and van Hoven, A. 2007b. "Field Tests on sea defences subject to wave overtopping", *Proceedings of the 5th Coastal Structures International Conference,* World Scientific, pp 657-668, Available at: http://www.vandermeerconsulting.nl/downloads/stability_a/2007_akkerman_vandermeer.pdf

Bird, P. A. D.; Crawford, A. R.; Hewson, P. J.; and Bullock, G. N. 1998. "An instrument for field measurement of wave impact pressures and seawater aeration", *Coastal Engineering*, Elsevier, Volume 35, pp 103-122, Available from: http://www.sciencedirect.com/science/article/pii/S0378383998000209

Briaud, J.- L.; Chen, H.- C.; Govindasamy, A. V.; and Storesund, R. 2008. "Levee erosion by overtopping in New Orleans during the Katrina Hurricane", Journal of Geotechnical and Geoenvironmental Engineering, American Society of Civil Engineers, Volume 134, No. 5, May 2008, pp 618-632, Available at: http://cedb.asce.org/cgi/WWWdisplay.cgi?163840

Bung, D. B. 2011. "Non-intrusive measuring of air-water flow properties in self-aerated stepped spillway flow", *Proceedings of the 34th IAHR World Congress - Balance and Uncertainty (Water in a Changing World)*, June, 2011, International Association for Hydro-Environment Engineering and Research, Brisbane, Australia, pp. 2380-2387, Available from: http://www.mendeley.com/research/nonintrusive-measuring-airwater-flow-properties-selfaerated-stepped-spillway-flow/

Chanson, H**.** 1994a. "Air-water interface area in self-aerated flows," *Water Resources*, Elsevier Science Ltd., Volume 28, No. 4, May 1994, pp. 923-929, Available from: http://espace.library.uq.edu.au/eserv/UQ:9260/ARTI15C.pdf

Chanson, H. 1995. "Air concentration distribution in self-aerated flow - Discussion," *Journal of Hydraulic Research*, International Association for Hydro-Environment Engineering and Research, Volume 33, No. 4, 1995, pp. 586-588, Available from: http://espace.library.uq.edu.au/eserv/UQ:9099/DISC_afs.pdf

Dean, R. G. and van Ledden, M. 2010a. "Accounting for levee overtopping duration: A test with Hurricane Katrina Conditions," *Proceedings of the 32nd International Conference on Coastal Engineering,* Coastal Engineering Research Council, 15 p., Available at: http://journals.tdl.org/ICCE/article/viewArticle/1440

Falvey, H. T. 1980. "Air-water flow in hydraulic structures", *Engineering Monograph No. 1*, United States Department of Interior, Water and Power Resources Service, Engineering and Research Center, Denver Colorado, 155 pp., Available at: http://www.usbr.gov/pmts/hydraulics_lab/pubs/EM/EM41.pdf

Ferrando, A. M. and Rico, J. R. 2002. "On the incipient aerated flow in chutes and spillways", *Journal of Hydraulic Research*, International Association for Hydro-Environment Engineering and Research, Volume 40, No. 1, 1994, pp. 95-97.

Frizell, K. H.; Ehler, D. G.; and Mefford, B. W. 1994. "Developing air concentration and velocity probes for measuring highly-aerated, high-velocity flow", *Proceedings of the Fundamentals and Advancements in Hydraulic Measurements and Experimentation Symposium*, American Society of Civil Engineers, April, 1994, pp. 268-277, Available at: http://cedb.asce.org/cgi/WWWdisplay.cgi?89297

Hager, W. H. 1991. "Uniform aerated chute flow", *Journal of Hydraulic Engineering,* American Society of Civil Engineers, Volume 117, No. 4, April 1991, pp 528-533, Available at: http://cedb.asce.org/cgi/WWWdisplay.cgi?69722

Chanson, H. 1992. "Closure of uniform aerated chute flow - Discussion", *Journal of Hydraulic Engineering,* American Society of Civil Engineers, Volume 118, No. 6, June 1992, pp 944-946.

Hanson, G. J. and Temple, D. M. 2002. "Performance of bare-earth and vegetated steep channels under long-duration flows", Transactions of the American Society of Agricultural Engineers, Volume 45 (3), pp 695-701, Available at: https://elibrary.asabe.org/toc_journals.asp?volume=45&issue=3&conf=t&orgconf=t2002

Headland, J. 2009. "Towards a unified approach for design of overtopped coastal structures", Proceedings of the Coasts, Marine Structures and Breakwaters 2009 Conference, Institution of Civil Engineers, Scotland, 11 p.

Henderson, F. M. 1966. "Open Channel Flow," MacMillian Publishing Co., New York.

Hoffmans, G.; Akkerman, G. J.; Verheij, H.; van Hoven, A., and van der Meer, J. W. 2008. "The erodibility of grassed inner dike slopes against wave overtopping", *Proceedings of the 31st International Conference - Coastal Engineering, World Scientific*, pp 3224-3236, Available at: http://eproceedings.worldscinet.com/9789814277426/9789814277426_0267.html

Hughes, S. A. and Shaw, J. M. 2011b. "Continuity of instantaneous overtopping discharge with application to stream power concepts", *Journal of Waterway, Port, Coastal, and Ocean Engineering,* American Society of Civil Engineers, Volume 137, No. 1, January/February 2011, pp 12-25, Available at: http://cedb.asce.org/cgi/WWWdisplay.cgi?273508

Hughes, S. A.; Scholl, B. N.; Hughes, S. A.; and Thornton, C. I. 2012. "Wave overtopping hydraulic parameters on protected- side slopes", *Proceedings of United States Society on Dams Conference 2012*, New Orleans.

Hughes, S.A., C.I. Thornton, J.W. van der Meer and B. Scholl. 2012. Improvements in describing wave overtopping processes. ASCE, Proc. ICCE 2012, Santander, Spain.

Lamarre, E. and Melville, W. K. 1992. "Instrumentation for the measurement of void-fraction in breaking waves: Laboratory and field results", IEEE Journal of Oceanic Engineering, Volume 12, N0. 2, April 1992, pp. 204-219, Available at: http://airsea.ucsd.edu/papers/LAMARRE%20E,%20MELVILLE%20WK%20-%20IEEE%20JOURNAL%20OF%20OCEANIC%20ENGINEERING%2017%20%20-%20%201992.pdf

Le, H. T.; van der Meer, J. W.; Schiereck, G. J.; Vu, M. C.; and van der Meer, G. 2010. "Wave overtopping simulator tests in Viet Nam", *Proceedings of the 32nd International Conference - Coastal Engineering*, Coastal Engineering Research Council, 11 p., Available at: http://journals.tdl.org/ICCE/article/viewArticle/1176

Jaeger, J.J., Stevenson, J., Stroupe, W., Mosher, R.L., Martin, D., Garster, J.K., Zilkoski, D.B., Ebersole, B.A., Westerink, J.J., Resio, D.T., Dean, R.G., Sharp, M.K., Steedman, R.S., Duncan, J.M., Moentenich, B.L., Howard, B., Harris, J., Fitzgerald, S., Moser, D., Canning, P., Foster, J. and Muller, B. 2009. "Performance Evaluation of the New Orleans and Southeast Louisiana Hurricane Protection System", United States Army Corps of Engineers. Available at: http://biotech.law.lsu.edu/katrina/ipet/ipet.html.

Matos, J. 1995. "Air concentration distribution in self-aerated flow - Discussion"' *Journal of Hydraulic Research*, International Association for Hydro-Environment Engineering and Research, Volume 33, No. 4, 1995, pp. 589-592.

Matos, J. and Frizell, K. H. 1997. "Air concentration Measurements in Highly Turbulent Aerated flow", *Proceedings of the 27th Congress of the International Association of Hydraulic Research, Environmental and Coastal Hydraulics: Protecting the Aquatic Habitat*, Sam Y. Wang and Torkild Carstens (editors), American Society of Civil Engineers, pp. 149-154, Available at: http://cedb.asce.org/cgi/WWWdisplay.cgi?106897

Möller, J.; Weissmann, R.; Schüttrumpf, H.; Grüne, J.; Oumeraci, H.; Richwein, W.; and Kudella, M. 2002. "Interaction of wave overtopping and clay properties for seadikes", *Proceedings of the 28th International Conference - Coastal Engineering,* Gottfried Wilhelm Leibniz Universität Hannover, 12 p., Available at: http://www.fzk.uni-hannover.de/uploads/tx_tkpublikationen/icce2002_clay_03.pdf

Möller, J.; Kortenhaus, A ; Oumeraci, H.; de Rouck, J.; and Medina, J. R. 2003 "Wave run-up and wave overtopping on a rubble mound breakwater - Comparison of prototype and laboratory investigations", *Proceedings of Coastal Structures 2003*, American Society of Civil Engineers, pp 456-468, Available from: http://cedb.asce.org/cgi/WWWdisplay.cgi?143017

Pan, Y.; Li, L.; Amini, F.; Kuang, C.; and Briaud, J.-L. 2011. "Erosion resistance of HPTRM strengthened levee from combined wave and surge overtopping **,"** *Innovative Levee Strengthening and Testing under Full Scale Overtopping Conditions for the Southeast Regional Research Initiative (SERRI)*, Jackson State University, Department of Civil and Environmental Engineering, September, 2011, Available at: http://www.serri.org/publications/Documents/JSU%20Project%2080009%20-%20Erosion%20Resistance%20of%20HPTRM%20Strengthened%20Levee%20-%2012%20Sep%202011%20(Pan,%20Li,%20Amini,%20Kuang,%20Briaud).pdf

Smith, G.; Seijffert, J. W. W.; and van der Meer, J. W. 1994. "Erosion and overtopping of a grass dike - Large scale model tests", *Proceedings of the 24th International Conference - Coastal Engineering,* American Society of Civil Engineers, pp 2639-2652, Available at: http://cedb.asce.org/cgi/WWWdisplay.cgi?94035

Soulsby, R. L. and Clarke, S. 2005. "Bed shear-stresses under combined waves and currents on smooth and rough beds", Produced within Defra Project FD1905 (EstProc), Estuary Processes Research Project, HR Wallingford, Hydraulics Research Report TR 137, August, 2005, Available at: http://books.hrwallingford.co.uk/acatalog/free_downloads/TR137.pdf

Steendam, G. J.; van der Meer, J. W.; Hardeman, B.; and van Hoven, A. 2010. "Destructive wave overtopping tests on grass covered landward slopes of dikes and transitions to berms", *Proceedings of the 32nd International Conference - Coastal Engineering,* American Society of Civil Engineers, 14 p., Available at: http://journals.tdl.org/ICCE/article/view/1478

Straub, L. G.; Killen, J. M.; and Lamb, O. P. 1954, "Velocity Measurement of Air-Water Mixtures", St. Anthony Falls Hydraulic Laboratory, Technical Paper No. 10 Series A, American Society of Civil Engineers, Transactions ,Volume 119, 1954, pp. 207-219, Available at: http://purl.umn.edu/107928

Suntoyo, and Tanaka, H. 2007. "Comparing different estimation methods of bottom shear stress for waves characterized by horizontal and vertical axes asymmetry", *Proceedings of the 9th International Summer Symposium,* Yokohama National University, Japan, September 2007, Japan Society of Civil Engineers, 4 p., Available at: http://www.its.ac.id/personal/files/pub/831-suntoyo-oe-iss07.pdf

Van Gent, M. R. A. 2002a. "Coastal flooding initiated by wave overtopping at sea defences", *Solutions to Coastal Disasters '02*, American Society of Civil Engineers, pp 223-237, Available at: http://cedb.asce.org/cgi/WWWdisplay.cgi?130431

Van Steeg, P. 2007. "Wave overtopping aspects of the Crest Drainage Dike - A theoretical, numerical, and experimental research", Final Report of the Master Thesis, Delft University of Technology, Section of Hydraulic Engineering, Available from: http://repository.tudelft.nl/search/ir/?q=wave+overtopping+of+the+crest+drainage+dike&faculty=&department=&type=master&year=2007

Wilhelms, S. C. and Gulliver, J. S. 2005a. "Bubbles and waves description of self-aerated spillway flow", *Journal of Hydraulic Research*, International Association for Hydro-Environment Engineering and Research, Volume 43, No. 5, 2005, pp. 522-531, Available at: http://www.mendeley.com/research/bubbles-waves-description-selfaerated-spillway-flow-description-des-coulements-bulles-et-vagues-sur-dversoir-autoar/

Falvey, H. 2007. "Bubbles and waves descriptive of self-aerated spillway flow-Discussion," *Journal of Hydraulic Research*, International Association for Hydro-Environment Engineering and Research, Volume 45, No. 1, 2007, pp. 142-144.

Pfister, M. 2008. "Bubbles and waves descriptive of self-aerated spillway flow-Discussion," *Journal of Hydraulic Research*, International Association for Hydro-Environment Engineering and Research, Volume 46, No. 3, 2008, pp. 420-423.

Wilhelms, S. C.; Gulliver, J. S.; Ling, J. T.; and Ling, R. S. 2005b. "Gas transfer, cavitation, and bulking in self-aerated spillway flow", *Journal of Hydraulic Research*, International Association for Hydro-Environment Engineering and Research, Volume 43, No. 5, 2005, pp. 532-539.

Kramer, K. 2007. "Gas transfer, cavitation, and bulking in self-aerated spillway flow - Discussion", *Journal of Hydraulic Research*, International Association for Hydro-Environment Engineering and Research, Volume 45, No. 4, 2007, pp. 572-575.

Falvey, H. 2007. "Gas transfer, cavitation, and bulking in self-aerated spillway flow - Discussion", *Journal of Hydraulic Research*, International Association for Hydro-Environment Engineering and Research, Volume 45, No. 6, 2007, pp. 859-860.

Wood, L. R. 1995. "Air concentration distribution in self-aerated flow - Discussion", *Journal of Hydraulic Research*, International Association for Hydro-Environment Engineering and Research, Volume 33, No. 4, 1995, pp. 582-585.

Appendix A

Summary of wave runup and overtopping equations

APPLICATION	SOURCE	EQUATION
1.1 - WAVE RUNUP FLOW HEIGHT		
1.1.1 Outer Slope Runup Flow Height		
Wave Runup Flow Height Above SWL - Average exceeded by 2% of incoming waves (deterministic) for irregular waves	Van der Meer and Janssen (1995) Equation 2 Van Steeg (2007) Equation 2-17 Van der Meer (2002) Equations 3a & 3b Pullen (2007) Equation 5.4 Dean et al. (2010b) Equation 21 Hughes (2011a) Equations 36 & 37	Van der Meer and Janssen (1995) Equation 2 valid for the range $0.5 < \xi_{eq} < 4\ or\ 5$. See note 1. $\frac{R_{u2\%}}{H_s} = 1.6\,\gamma_h\,\gamma_f\,\gamma_B\,\xi_{eq}$ with a maximum of $\frac{R_{u2\%}}{H_s} = 3.6\,\gamma_h\,\gamma_f\,\gamma_B$ Van Steeg (2007) Equation 2-17. $\frac{R_{u2\%}}{H_{m0}} = 1.75\,\gamma_b\,\gamma_f\,\gamma_B\,\xi_{S,-1}$ Van der Meer (2002) Equations 3a & 3b, Pullen (2007) Equation 5.4, Dean et al. (2010-2) Equation 21, Hughes (2011a) Equations 36 & 37. See note 2. $\frac{R_{u2\%}}{H_{m0}} = 1.75\,\gamma_b\,\gamma_f\,\gamma_B\,\xi_{m-1,0} \quad where \quad 0.5 \le \gamma_b\,\xi_{m-1,0} < 1.8$ with a maximum of $\frac{R_{u2\%}}{H_{m0}} = 1.00\,\gamma_f\,\gamma_B\left(4.3 - \frac{1.6}{\sqrt{\xi_{m-1,0}}}\right) \quad where \quad 1.8 < \gamma_b\xi_{m-1,0}$ Note 1: Iribarren number for a slope with a berm $\xi_{eq} = \gamma_b\,\xi_{op}$ Note 2: Iribarren criteria provided in Dean et al. (2010b) Equation 21 Note3 : Per Van der Meer (2002) Equations 3a & 3b valid for the range $0.5 < \gamma_b\,\xi_{m-1,0} \le 8\ to\ 10$.

APPLICATION	SOURCE	EQUATION
Wave Runup Height Above SWL - Average exceeded by 2% of incoming waves (probabilistic) for irregular waves	Van der Meer and Janssen (1995) Equation 4 Van der Meer (2002) Equations 5a & 5b Bosman (2007) Equations 2-2 & 2-3 and 6-9 & 6-10 Valk (2009) Equation 2.6 Pullen et al. (2007) Equation 5.3	Van der Meer and Janssen (1995) Equation 4 (see note 1). $\frac{R_{u2\%}}{H_s} = 1.5\,\gamma_h\,\gamma_f\,\gamma_B\,\xi_{eq}$ with a maximum of $\frac{R_{u2\%}}{H_s} = 3.0\,\gamma_h\,\gamma_f\,\gamma_B$ Van der Meer (2002) Equations 5a & 5b, Bosman (2007) Equations 2-2 & 2-3, Valk (2009) Equation 2.6 (upper equation only), Pullen et al. (2007) Equation 5.3 (see note 2 & note 3). $\xi_{m-1.0} = \leq 1.75$ for breaking waves $\frac{R_{u2\%}}{H_{m0}} = 1.65\,\gamma_b\,\gamma_f\,\gamma_B\,\xi_{m-1,0}$ $\xi_{m-1.0} = > 1.75$ for nonbreaking waves $\frac{R_{u2\%}}{H_{m0}} = \gamma_b\,\gamma_f\,\gamma_B\left(4.0 - \frac{1.5}{\sqrt{\xi_{m-1,0}}}\right)$ Bosman (2007) Equations 6-9 & 6-10 $\xi_{op} \leq 1.75$ for breaking waves $\frac{R_{u2\%}}{H_s} = 1.65\,\gamma_f\,\gamma_B\,\xi_{op}$ $\xi_{op} > 1.75$ for nonbreaking waves $\frac{R_{u2\%}}{H_s} = 1.00\,\gamma_f\,\gamma_B\left(4.3 - \frac{1.6}{\sqrt{\xi_{op}}}\right)$ Note 1: Iribarren number for a slope with a berm $\xi_{eq} = \gamma_b\,\xi_{op}$ Note 2: Iribarren number range criteria show in Bosman formula. Note 3: Per Pullen et al. (2007) Equation 5.3 valid for the range $0.5 < \gamma_b\,\xi_{m-1,0} \leq 8\ to\ 10$.

APPLICATION	SOURCE	EQUATION
Wave Runup Flow Height Above SWL - Average exceeded by 2% of incoming waves	Van Gent (2002b) Equation 1 Bosman (2007) Equations 2-15, 2-16 & 2-24 Schüttrumpf and van Gent (2003) Equations 1a &1b	Van Gent (2002b) Equation 1. $\frac{R_{u2\%}}{H_s} = \gamma\, c_0\,(\xi_{S,-1})\ \ for\ \ \xi_{S,-1} \le p$ $\frac{R_{u2\%}}{H_s} = \gamma \left(\frac{c_1 - c_2}{\xi_{S,-1}}\right)\ \ for\ \ \xi_{S,-1} \ge p$ with $p = 0.5\,\frac{c_1}{c_0}$ Bosman (2007) Equations 2-15 & 2-16, and 2-24 (2-24 upper formula only). $\frac{R_{u2\%}}{H_s} = \gamma_f \gamma_\beta\, c_0\,(\xi_{S,-1}) \quad for\ \ \xi_{S,-1} \le p$ $\frac{R_{u2\%}}{H_s} = \gamma_f \gamma_\beta \left(\frac{c_1 - c_2}{\xi_{S,-1}}\right) \quad for\ \ \xi_{S,-1} > p$ with $p = 0.5\,\frac{c_1}{c_0}$ Schüttrumpf and van Gent (2003) Equations 1a &1b $\frac{R_{u,2\%}}{H_s} = c_0\,(\xi_{S,-1})\ \ for\ \ \xi_{S,-1} \le p$ $\frac{R_{u2\%}}{H_s} = c_1 \left(\frac{c_2}{\xi_{S,-1}}\right)\ \ for\ \ \xi_{S,-1} \ge p$ with $p = 0.5\,\frac{c_1}{c_0}$

APPLICATION	SOURCE	EQUATION
1.2 - WAVE RUNUP FLOW DEPTH and WAVE OVERTOPPING FLOW DEPTH		
1.2.1 Outer Slope Wave Runup Flow Depth and Wave Overtopping Flow Depth		
Wave Runup Flow Depth - Maximum exceeded by 2% of incoming waves (z_A) Wave Overtopping Flow Depth - Maximum exceeded by 2% of incoming waves (R_C) Select Runup or Overtopping output by use of z_A or R_C respectively	Schüttrumpf and van Gent (2003) Equation 3 Van der Meer et al. (2006) Equation 3 Van der Meer (2007a) Equation 2.3 Bosman (2007) Equation 2-9 Van der Meer et al. (2010) Equation 3 Hughes (2007) Equation 1 Hughes (2008a) Equation 1	Schüttrumpf and van Gent (2003) Equation 3. $\frac{h_{ZA2\%}}{H_S} = \mathrm{c}^{*}_{\mathrm{Ah2\%}}\left(\frac{R_{u2\%} - z_A}{H_S}\right)$ Van der Meer et al. (2006) Equation 3, van der Meer (2007a) Equation 2.3. $\frac{h_{C02\%}}{H_S} = \mathrm{c}^{*}_{\mathrm{Ah2\%}}\left(\frac{R_{u2\%} - R_C}{H_S}\right)$ Bosman (2007) Equation 2-9. $\frac{h_{C02\%}}{H_s} = c'_{h2\%}\left(\frac{R_{u\%} - R_c}{H_s}\right)$ Van der Meer et al. (2010) Equation 3. $\frac{h_{C02\%}}{H_s} = c_{Ah}\left(\frac{R_{u\%} - R_c}{H_s}\right)$ Hughes (2007) Equation 1, Hughes (2008a) Equation 1. $\frac{h_{C02\%}}{H_s} = c_{Ah2\%}\left(\frac{R_{u\%} - R_c}{H_s}\right)$ Note: equations can be combined by conforming coefficient notation.

APPLICATION	SOURCE	EQUATION
Wave Overtopping Flow Depth - Maximum at outer crest exceeded by 2% of incoming waves	Bosman (2007) Equations 2-17, 2-25, 4-13, & 6-1 Valk (2009) Equation 2.8 Van der Meer (2007a) Equation 10-3	Bosman (2007) Equations 2-17, 2-25, & 4-13. $\frac{h_{C02\%}}{H_s} = c'_{h,2\%}\left(\frac{R_{u2\%} - R_c}{\gamma_f H_s}\right)$ Bosman (2007) Equation 6-1, and Valk (2009) Equation 2.8. $\frac{h_{C02\%}}{H_s} = \frac{0.007}{sin^2\,\alpha}\left(\frac{R_{u2\%} - R_c}{\gamma_f H_s}\right)$ Van der Meer (2007a) Equation 10-3. $\frac{h_{C02\%}}{H_s} = \frac{0.009}{sin^2\,\alpha}\left(\frac{R_{u2\%} - R_c}{H_s}\right)$
1.2.2 - Crest Wave Overtopping Flow Depth		
Wave Overtopping Flow Depth - Maximum at a point on the crest exceeded by 2% of incoming waves	Schüttrumpf et al. (2002) Equation 3 Schüttrumpf and Oumeraci (2005) Equation 14 Pullen et al. (2007) Equation 5.41 Schüttrumpf and van Gent (2003) Equation 5 Van der Meer (2007a) Equation 2.1 Bosman (2007) Equation 2-27 Hughes (2007) Equation 3 Hughes (2008a) Equation 3	Schüttrumpf et al. (2002) Equation 3, Schüttrumpf and Oumeraci (2005) Equation 14, Pullen et al. (2007) Equation 5.41. $\frac{h_{XC}}{h_{C0}} = \frac{c_{2XC}}{c_{2C0}} = exp\left(-c_3\,\frac{x_C}{B_C}\right)$ Schüttrumpf and van Gent (2003) Equation 5, van der Meer (2007a) Equation 2.1. $\frac{h_{XC2\%}}{h_{C02\%}} = \exp\left(-c^*_{Ch}\,\frac{x_C}{B_C}\right)$ Bosman (2007) Equation 2-27. $\frac{h_{XC2\%}}{h_{C02\%}} = \exp\left(-c^{"}_{h2\%}\,\frac{x_C}{B_C}\right)$ Hughes (2007) Equation 3, Hughes (2008a) Equation 3. $\frac{h_{XC2\%}}{h_{C02\%}} = exp\left(-c_3\,\frac{x_C}{B_C}\right)$ Note: a review of coefficients may allow combining these equations.

APPLICATION	SOURCE	EQUATION
Wave Overtopping Flow Depth - Maximum at inner crest exceeded by 2% of incoming waves	Van Gent (2002b) Equation 2 Bosman (2007) Equation 2-19	Van Gent (2002b) Equation 2. $$\frac{h_{B02\%}}{H_s} = c'_h \left(\frac{R_{u2\%} - R_C}{\gamma_{fA} H_s}\right)$$ Bosman (2007) Equation 2-19. $$\frac{h_{B02\%}}{H_s} = c''_{h2\%} \left(\frac{R_{u2\%} - R_C}{\gamma_{fA} H_s}\right)$$
Wave Overtopping Flow Depth - Maximum at inner crest exceeded by 2% of incoming waves Used for crest or inner slope depth depending on point of crest selected	Van Gent (2002b) Equation 8 Bosman (2007) Equation 2-11	Van Gent (2002b) Equation 8. $$\frac{h_{XC2\%}}{H_s} = c'_h \left(\frac{R_{u2\%} - R_c}{\gamma_{fA} H_s}\right) exp\left(- c''_h \frac{x_C}{B_c}\right)$$ Bosman (2007) Equation 2-11. $$\frac{h_{XC2\%}}{H_s} = c'_{h2\%} \left(\frac{R_{u2\%} - R_C}{H_s}\right) exp\left(- c''_{h2\%} \frac{x_C}{B_C}\right)$$ Note: Duplicated for the inner slope.
Wave Overtopping Flow Depth - Maximum at a point on the crest exceeded by 2% of incoming waves	Bosman (2007) Equations 4-15 & 6-4 Van der Meer (2007a) Equation 10.5	Bosman (2007) Equation 4-15. $$\frac{h_{XC2\%}}{h_{C02\%}} = c_{transh} \; exp\left(- c''_{h2\%} \frac{x_C}{\gamma_{fC} L_{m-1,0}}\right)$$ Bosman (2007) Equation 6-4, van der Meer (2007a) Equation 10.5. $$\frac{h_{XC2\%}}{h_{C02\%}} = 0.81 \; exp\left(- 6 \frac{x_C}{\gamma_{fC} L_{m-1,0}}\right)$$

APPLICATION	SOURCE	EQUATION
1.2.3 - Inner Slope Wave Overtopping Flow Depth		
Wave Overtopping Flow Depth - Maximum at inner crest exceeded by 2% of incoming waves Used for crest or inner slope depth depending on point of crest selected	Van Gent (2002b) Equation 8 Bosman (2007) Equation 2-11	Van Gent (2002b) Equation 8. $$\frac{h_{XC2\%}}{H_s} = c'_h \left(\frac{R_{u2\%} - R_c}{\gamma_{fA} H_s}\right) exp\left(- c''_h \frac{x_C}{B_c}\right)$$ Bosman (2007) Equation 2-11. $$\frac{h_{XC2\%}}{H_s} = c'_{h2\%} \left(\frac{R_{u2\%} - R_C}{H_s}\right) exp\left(- c''_{h2\%} \frac{x_C}{B_C}\right)$$ Note: Duplicated for the crest.
Wave Overtopping Flow Depth and Flow Velocity - Maximum (iterative)	Schüttrumpf et al. (2002) Equations 5 & 5+ (unnumbered following Equation 5) Schüttrumpf and Oumeraci (2005) Equations 41, 42, & 43 Bosman (2007) Equations 2-13 & 2-14 and 2-31 Pullen et al. (2007) Equations 5.43 & 5.44	Schüttrumpf et al. (2002) Equations 5 & 5+ (unnumbered following Equation 5); Schüttrumpf and Oumeraci (2005) Equations 41, 42, & 43; Bosman (2007) Equations 2-13 & 2-14 and 2-31; Pullen et al. (2007) Equations 5.43 & 5.44. $$u_{SB} = \frac{u_{B0} + \frac{k_1 h_{SB}}{f} tanh\left(\frac{k_1 t}{2}\right)}{1 + \frac{f u_{B0}}{h_{SB} k_1} tanh\left(\frac{k_1 t}{2}\right)}$$ with $$t \approx - \frac{u_{B0}}{g \sin\beta} + \sqrt{\frac{u_{SB}^2}{g^2 sin^2\beta} + \frac{2 s_B}{g \sin\beta}}$$ and $$k_1 = \sqrt{\frac{2 f g \sin\beta}{h_{SB}}}$$ and $$h_{SB} = \frac{u_{B0} h_{B0}}{u_{SB}}$$
Wave Overtopping Flow Depth - Maximum on Inner Slope	Hughes (2007) Equation 10 Hughes (2008a) Equation 14	Hughes (2007) Equation 10, Hughes (2008a) Equation 14. $$h_{SB2\%} = \left(\frac{h_{B02\%} u_{B02\%}}{u_{SB2\%}}\right)$$

APPLICATION	SOURCE	EQUATION
Wave Overtopping Flow Depth - Maximum at inner crest exceeded by 2% of incoming waves	Van Gent (2002b) Equation 5 Bosman (2007) Equation 2-22	Van Gent (2002b) Equation 5, Bosman (2007) Equation 2-22. $$h_{SB2\%} = (h_{B02\%})(u_{B02\%}) / \left(\frac{K_2}{K_3} + K_4\, exp(-3\, K_2\, K_3^2\, s_B)\right)$$ with $$K_2 = \sqrt[3]{\mathrm{g} \sin\beta} \qquad K_3 = \sqrt[3]{\frac{1}{2}\frac{f}{(h_{B02\%})(u_{B02\%})}} \qquad K_4 = u_{B02\%} - \frac{K_2}{K_3}$$
1.3 - WAVE RUNUP FLOW VELOCITY and WAVE OVERTOPPING FLOW VELOCITY		
1.3.1 - Outer Slope Wave Runup Flow Velocity and Wave Overtopping Flow Velocity		
Wave Runup Flow Velocity - Maximum exceeded by 2% of incoming waves (z_A) Wave Overtopping Flow Velocity - Maximum exceeded by 2% of incoming waves (R_C) Select Runup or Overtopping output by use of z_A or R_C respectively	Schüttrumpf and van Gent (2003) Equation 2 Van der Meer et al. (2006) Equation 2 Van der Meer (2007a) Equation 2.4 Van der Meer et al. (2010) Equation 4 Hughes (2007) Equation 2 Hughes (2008a) Equation 2	Schüttrumpf and van Gent (2003) Equation 2. $$\frac{u_{ZA2\%}}{\sqrt{g\, H_s}} = c_{Au}^{*} \left(\sqrt{\frac{R_{u2\%} - z_A}{H_s}}\right)$$ Van der Meer et al. (2006) Equation 2, van der Meer (2007a) Equation 2.4. $$\frac{u_{C02\%}}{\sqrt{g\, H_s}} = c_{Au}^{*} \left(\sqrt{\frac{R_{u2\%} - R_C}{H_s}}\right)$$ Van der Meer et al. (2010) Equation 4. $$\frac{u_{C02\%}}{\sqrt{g\, H_s}} = c_{Au} \left(\sqrt{\frac{R_{u2\%} - R_C}{H_s}}\right)$$ Hughes (2007) Equation 2, Hughes (2008a) Equation 2. $$\frac{u_{C02\%}}{\sqrt{g\, H_s}} = c_{Au2\%} \left(\sqrt{\frac{R_{u2\%} - R_C}{H_s}}\right)$$ Note: a review of coefficients may allow combining these equations.

APPLICATION	SOURCE	EQUATION
Wave Runup Flow Velocity - Maximum exceeded by 50% of incoming waves Wave Runup Flow Velocity - Maximum exceeded by 2% of incoming waves Select Runup or Overtopping output by use of z_A or R_C respectively	Schüttrumpf and Oumeraci (2005) Equation 12 Bosman (2007) Equation 2-10 Van der Meer (2007a) Equation 10-4	Schüttrumpf and Oumeraci (2005) Equation 12. $\frac{u_{ZA50\%}}{\sqrt{g\,H_S}} = 0.94\sqrt{\frac{(R_{u2\%} - z_A)}{H_S}}$ Bosman (2007) Equation 2-10. $\frac{u_{C02\%}}{\sqrt{gH_s}} = c'_{u2\%}\sqrt{\frac{R_{u2\%} - R_c}{H_s}}$ Van der Meer (2007a) Equation 10-4. $\frac{u_{C02\%}}{\sqrt{gH_s}} = \frac{.30}{sin\,\alpha}\sqrt{\frac{R_{u2\%} - R_c}{H_s}}$
Wave Overtopping Flow Velocity - Maximum at outer crest exceeded by 2% of incoming waves With coefficients to incorporate slope gradient.	Bosman (2007) Equations 2-18, 2-26, 4-14, & 6-2 Valk (2009) Equation 2.9	Bosman (2007) Equations 2-18, 2-26, & 4-14. $\frac{u_{C02\%}}{\sqrt{gH_s}} = c'_{u2\%}\sqrt{\frac{R_{u2\%} - R_c}{\gamma_f H_s}}$ Bosman (2007) Equation 6-2, Valk (2009) Equation 2.9. $\frac{u_{C02\%}}{\sqrt{gH_s}} = \frac{0.25}{\sin\alpha}\sqrt{\frac{R_{u2\%} - R_c}{\gamma_f H_s}}$

APPLICATION	SOURCE	EQUATION
1.3.2 - Crest Wave Overtopping Flow Velocity		
Wave Overtopping Flow Velocity at a point on the Crest - Maximum (coefficient of 1/2)	Schüttrumpf et al. (2002) Equation 4 Schüttrumpf and Oumeraci (2005) Equation 30 Pullen (2007) Equation 5.42 Hughes (2007) Equation 4 Hughes (2008a) Equation 4	Schüttrumpf et al. (2002) Equation 4, Schüttrumpf and Oumeraci (2005) Equation 30, Pullen (2007) Equation 5.42. $u_{XC} = u_{C0}\, exp\left(-\frac{x_C\, f}{2\, h_{XC}}\right)$ Hughes (2007) Equation 4, Hughes (2008a) Equation 4. $u_{XC2\%} = u_{C02\%}\, exp\left(-\frac{x_C\, f_F}{2\, h_{XC2\%}}\right)$
Wave Overtopping Flow Velocity at a point on the Crest - Maximum (without coefficient of 1/2)	Schüttrumpf and van Gent (2003) Equation 4 Van der Meer (2007a) Equations 2.2 & 10.6 Bosman (2007) Equations 2-28, 4-16, & 6-5	Schüttrumpf and van Gent (2003) Equation 4, van der Meer (2007a) Equation 2.2 $\frac{u_{XC2\%}}{u_{C02\%}} = exp\left(-c^{*}_{Cu2\%}\, \frac{x_C\, f}{h_{XC2\%}}\right)$ Bosman (2007) Equation 2-28. $\frac{u_{XC2\%}}{u_{C02\%}} = exp\left(-c^{"}_{u2\%}\, \frac{x_C\, f}{h_{XC2\%}}\right)$ Bosman (2007) Equation 4-16. $\frac{u_{XC2\%}}{u_{C02\%}} = exp\left(-c^{"}_{u2\%}\, \frac{x_C}{\gamma_{fC}\, h_{XC2\%}}\right)$ Bosman (2007) Equation 6-5, van der Meer (2007a) Equation 10.6. $\frac{u_{XC2\%}}{u_{C02\%}} = exp\left(-0.42\, \frac{x_C}{\gamma_{fC}\, h_{XC2\%}}\right)$ Note: a review of coefficients may allow combining these equations.

APPLICATION	SOURCE	EQUATION
Wave Overtopping Flow Velocity - Maximum at inner crest exceeded by 2% of incoming waves	Van Gent (2002b) Equation 3 Bosman (2007) Equation 2-20	Van Gent (2002b) Equation 3. $$\frac{u_{B02\%}}{\sqrt{g\,H_s}} = c'_u\,(\gamma_{fC})^{0.5}\,\left(\frac{R_{u2\%} - R_C}{\gamma_{fA}\,H_s}\right)^{0.5} \;/\; \left(1 + c''_u\,\frac{B_C}{H_s}\right)$$ Bosman (2007) Equation 2-20 $$\frac{u_{B02\%}}{\sqrt{gH_s}} = c'_{u2\%}\,\sqrt{\gamma_{fC}}\,\sqrt{\frac{R_{u2\%} - R_C}{\gamma_{fA}\,H_s}}\Big/\left(1 + c''_{u2\%}\,\frac{B_C}{H_s}\right) \quad valid\ for\ B_C > H_{m0}$$
Wave Overtopping Flow Velocity - Maximum at inner crest exceeded by 2% of incoming waves	Van Gent (2002b) Equation 9 Bosman (2007) Equation 2-12	Van Gent (2002b) Equation 9. $$\frac{u_{XC2\%}}{\sqrt{g\,H_s}} = c'_u\,\left(\frac{R_{u2\%} - R_c}{\gamma_{fA}\,H_s}\right)^{0.5}\,exp\left(-c''_u\,\frac{x_C\,f_c}{h_{XC2\%}}\right)$$ Bosman (2007) Equation 2-12. $$\frac{u_{XC2\%}}{\sqrt{gH_s}} = c''_{u2\%}\,\sqrt{\frac{R_{u2\%} - R_C}{H_s}}\,\,exp\left(-f\,\frac{B_c}{2\,h_{XC2\%}}\right)$$ Note: Duplicated for Inner Slope
Wave Overtopping Flow Velocity decay rate along crest - Maximum	Van der Meer et al. (2010) Equation 7	Van der Meer et al. (2010) Equation 7. $$\frac{h_{XC2\%}}{u_{C02\%}} = exp\left(\frac{x_C}{L_{m-1,0}}\right)$$

APPLICATION	SOURCE	EQUATION
1.3.3 Inner Slope Wave Runup Flow Velocity and Wave Overtopping Flow Velocity		
Wave Overtopping Flow Velocity - Maximum at inner crest exceeded by 2% of incoming waves	Van Gent (2002b) Equation 9 Bosman (2007) Equation 2-12	Van Gent (2002b) Equation 9 $$\frac{u_{XC2\%}}{\sqrt{g\,H_s}} = c'_u \left(\frac{R_{u2\%} - R_c}{\gamma_{fA}\,H_s}\right)^{0.5} exp\left(-c''_u \frac{x_C\,f_c}{h_{XC2\%}}\right)$$ Bosman (2007) Equation 2-12. $$\frac{u_{XC2\%}}{\sqrt{gH_s}} = c''_{u2\%} \sqrt{\frac{R_{u2\%} - R_C}{H_s}} \; exp\left(-f \frac{B_c}{2\,h_{XC2\%}}\right)$$ Note: Duplicated for the crest.
Wave Overtopping Flow Velocity on Inner Slope - Maximum exceeded by 2% of incoming waves	Van Gent (2002b) Equation 6 Schüttrumpf and van Gent (2003) Equation 6 Bosman (2007) Equations 2-23 & 2-29 Hughes (2007) Equations 5, 6, 7, and 8 Hughes (2008a) Equations 9, 10, 11, & 12	Van Gent (2002b) Equation 6, Schüttrumpf and van Gent (2003) Equation 6; Bosman (2007) Equations 2-23 & 2-29; Hughes (2007) Equations 5, 6, 7, and 8; Hughes (2008a) Equations 9, 10, 11, & 12. $$u_{SB2\%} = \frac{K_2}{K_3} + K_4 \exp(-3\,K_2\,K_3^2\,s_B)$$ with $$K_2 = \sqrt[3]{g\,\sin\beta} \text{ and } K_3 = \sqrt[3]{\frac{1}{2}\frac{f}{(h_{B02\%})(u_{B02\%})}} \text{ and } K_4 = u_{B02\%} - \frac{K_2}{K_3}$$

APPLICATION	SOURCE	EQUATION
Wave Overtopping Flow Velocity - Maximum far down the Inner Slope (S_b approaches infinity)	Schüttrumpf and van Gent (2003) Equation 7 Hughes (2007) Equation 9 Hughes (2008a) Equation 13	Schüttrumpf and van Gent (2003) Equation 7, Hughes (2007) Equation 9, and Hughes (2008a) Equation 13. $$u_{SB2\%} = \frac{K_2}{K_3} = \left[\frac{2g\, h_{B02\%}\, u_{B02\%}\, \sin\beta}{f}\right]^{1/3}$$ with $$K_2 = \sqrt[3]{g\, \sin\beta}$$ and $$K_3 = \sqrt[3]{\frac{1}{2}\frac{f}{(h_{B02\%})(u_{B02\%})}}$$

APPLICATION	SOURCE	EQUATION
1.4 - WAVE OVERTOPPING FLOW DISCHARGE		
1.4.1 - Outer Slope - Wave Overtopping Flow Discharge		
Wave Overtopping Flow Discharge - Average and Crest Freeboard according to van der Meer Wave Overtopping Flow Discharge - Average and Crest Freeboard according to van der Meer - Coefficient A for Equation 2-7 Wave Overtopping Flow Discharge - Average and Crest Freeboard according to van der Meer - Coefficient B for Equation 2-7 Wave Overtopping Flow Discharge - Average (deterministic)	Van der Meer (2002) Equations 21, 22, & 23 Van Steeg (2007) Equations 2-7, 2-8, & 2-9; and 2-10 & 2-11 Pullen et al. (2007) Equation 5.9 Hughes (2011a) Equations 40 & 41	Van der Meer (2002) Equation 21, van Steeg (2007) Equations 2-7, 2-8, & 2-9. $$q = A\, e^{BR_c}$$ $$A = \sqrt{g\, H_{m0}^3}\ \frac{0.067}{\sqrt{\tan\alpha}}\ \xi_{m-1,0}$$ $$B = \frac{-4.3}{H_{m0}}\ \frac{1}{\xi_{m-1.0}\ \gamma_b\ \gamma_f\ \gamma_\beta\ \gamma_v}$$ Van der Meer (2002) Equations 22 & 23, Pullen et al. (2007) Equation 5.9, van Steeg (2007) Equations 2-10 & 2-11, Hughes (2011a) Equations 40 & 41. $$\frac{q}{\sqrt{g\, H_{m0}^3}} = \frac{0.067}{\sqrt{\tan\alpha}}\ \gamma_b\ \xi_{m-1.0}\ e^{-4.3\ \frac{R_c}{H_{m0}\ \gamma_b \gamma_f \gamma_\beta \gamma_v}}$$ with a maximum of $$\frac{q}{\sqrt{g\, H_{m0}^3}} = 0.2\ e^{-2.3\ \frac{R_c}{H_{m0}\ \gamma_f \gamma_\beta}}$$

APPLICATION	SOURCE	EQUATION
Wave Overtopping Flow Discharge - Average (deterministic)	Dean and van Ledden (2010a) Equation 5 Dean et al. (2010b) Equations 26 & 27	Dean and van Ledden (2010a) Equation 5. $$\frac{q_{all}}{\sqrt{gH_{m0}^3}} = 0.067\sqrt{\frac{\tan\alpha}{H_{m0}/L_{m-1,0}}}\, e^{-\frac{4.3\, Z_c \sqrt{H_{m0}/L_{m-1,0}}}{H_{mo}\, \tan\alpha}} \quad for\ \xi_{m-1,0} < 1.8$$ with $$\frac{q_{all}}{\sqrt{gH_{m0}^3}} = 0.2\, e^{-\frac{2.3\, Z_c}{H_{m0}}} \quad for\ \xi_{m-1,0} > 1.8$$ Dean et al. (2010b) Equation 26. for Breaking Waves $\xi_{m-1,0} < 1.8$ $$\frac{q_{TAW}}{\sqrt{gH_{m0}^3}} = 0.067\, \gamma_b \sqrt{\frac{\tan\alpha}{H_{mo}/L_{m-1,0}}}\, e^{-4.3\, F'}$$ with $$F' = \frac{z_c \sqrt{H_{mo}/L_{m-1,0}}}{H_{mo}\, \gamma_b \gamma_f \gamma_\beta\, \tan\alpha}$$ Dean et al. (2010b) Equation 27. for Nonbreaking Waves $\xi_{m-1,0} > 1.8$ $$\frac{q_{TAW}}{\sqrt{gH_{m0}^3}} = 0.2\, e^{-2.3\, F'}$$ with $$F' = \frac{z_c}{H_{mo}\, \gamma_b \gamma_f}$$ Note 1: Dean and van Ledden (2010a) Equation 5 is described as calculating "allowable wave overtopping rates". Dean et al. (2010b) Equations 26 & 27 are described as calculating "total average wave overtopping rates" Note 2: Dean et al. (2010b) Equations 26 & 27 results are described as "determined by Van der Meer (2002) empirical methods" but these equations are not presented in Van der Meer (2002) and the authors do not clarify what is meant by " Van der Meer (2002) empirical methods".

APPLICATION	SOURCE	EQUATION
Wave Overtopping Flow Discharge - Average (deterministic)	Pullen et al. (2007) Equation 5.10	Pullen et al. (2007) Equation 5.10. $$\frac{q}{\sqrt{gH_{m0}^3}} = 0.21 \exp\left(-\frac{R_C}{\gamma_f \gamma_\beta \, H_{m0} \, (0.33 + 0.022) \, \xi_{m-1,0}}\right)$$
Wave Overtopping Flow Discharge - Average (probabilistic)	Van der Meer (2002) Equations 24 & 25. Bosman (2007) Equations 2-5 & 2-6 Pullen et al. (2007) Equation 5.8 Valk (2009) Equations 2.2 & 2.3	Van der Meer (2002) Equations 24 & 25, Bosman (2007) Equations 2-5 & 2-6, Pullen et al. (2007) Equation 5.8, Valk (2009) Equations 2.2 & 2.3. $$\frac{q}{\sqrt{gH_{m0}^3}} = \frac{0.067}{\sqrt{\tan\alpha}} \, \gamma_b \, \xi_{m-1.0} \, exp\left(-4.75 \frac{R_c}{H_{m0}} \frac{1}{\xi_{m-1.0} \, \gamma_b \gamma_f \gamma_\beta \gamma_v}\right)$$ with a maximum of $$\frac{q}{\sqrt{gH_{m0}^3}} = 0.2 \, exp\left(-2.6 \frac{R_c}{H_{m0}} \frac{1}{\gamma_f \gamma_\beta}\right)$$ Note: Bosman (2007) Equation 2-5 uses the coefficient -4.7 rather than the -4.75 used by other papers.
Wave Overtopping Flow Discharge - Average (probabilistic)	Pullen et al. (2007) Equation 5.11	Pullen et al. (2007) Equation 5.11. $$\frac{q}{\sqrt{gH_{m0}^3}} = 10^C \exp\left(-\frac{R_C}{\gamma_f \gamma_\beta \, H_{m0} \, (0.33 + 0.022) \, \xi_{m-1,0}}\right)$$

APPLICATION	SOURCE	EQUATION
Wave Overtopping Flow Discharge - Average for zero freeboard (probabilistic) Can be used for deterministic applications by increasing the average overtopping discharge by one standard deviation.	Pullen et al. (2007) Equation 5.14	Pullen et al. (2007) Equation 5.14. $\xi_{m-1.0} < 2.0$ $$\frac{q}{\sqrt{gH_{m0}^3}} = 0.0537\xi_{m-1.0}$$ $\xi_{m-1.0} \geq 2.0$ $$\frac{q}{\sqrt{gH_{m0}^3}} = \left(0.136 - \frac{0.226}{\xi_{m-1.0}^3}\right)$$ Note: This equation can be used for deterministic design or safety assessment by increasing the average overtopping discharge by about one standard deviation.
Wave Overtopping Flow Discharge exceeded by 2% of incoming waves Schüttrumpf and van Gent (2003) Equation 10 (outer crest) is a modified version of van Gent (2002b) Equation 4	Van Gent (2002b) Equation 4 Schüttrumpf and van Gent (2003) Equation 10	Van Gent (2002b) Equation 4. $$\frac{q_{B02\%}}{\sqrt{g\,H_S^3}} = c_q'\,(\gamma_{fC})^{0.5}\left(\frac{R_{u2\%} - R_C}{\gamma_{fA}\,H_s}\right)^{1.5} \Big/ \left(1 + c_q''\,\frac{B_C}{H_s}\right)$$ Schüttrumpf and van Gent (2003) Equation 10. $$\frac{q_{B02\%}}{\sqrt{gH_S^3}} = c_q'\left(\frac{R_{u2\%} - R_C}{H_s}\right)^{1.5} \Big/ \left(1 + c_q''\frac{B_C}{H_S}\right)$$ Note: Duplicated for inner crest.

APPLICATION	SOURCE	EQUATION
Wave Overtopping Flow Discharge - Average for breaking waves Wave Overtopping Flow Discharge - Average for nonbreaking waves	Schüttrumpf et al. (2001) Equations 4 & 5	Schüttrumpf et al. (2001) Equations 4 & 5. $\xi_{op} = < \xi_{gr}$ for breaking waves $\frac{q}{\sqrt{2\ g\ H_s^3}} = 0.038\ \xi_{op}\ exp\left(-5.5\ \frac{R_c}{R_{u,2\%}}\right)$ $\xi_{op} = \geq \xi_{gr}$ for nonbreaking waves $\frac{q}{\sqrt{2\ g\ H_s^3}} = \left(0.096 - \frac{0.160}{\xi_{op}^3}\right)\ exp\left(-5.5\ \frac{R_c}{R_{u,2\%}}\right)$
1.4.2 - Crest - Wave Overtopping Flow Discharge		
Wave Overtopping Flow Discharge exceeded by 2% of incoming waves See modified version in Schüttrumpf and van Gent (2003) Equation 10 (outer crest)	Van Gent (2002b) Equation 4 Schüttrumpf and van Gent (2003) Equation 10	Van Gent (2002b) Equation 4. $\frac{q_{B02\%}}{\sqrt{g\ H_S^3}} = c_q'\ (\gamma_{fC})^{0.5}\ \left(\frac{R_{u2\%} - R_C}{\gamma_{fA}\ H_s}\right)^{1.5}\ /\ \left(1 + c_q^{"}\ \frac{B_C}{H_s}\right)$ Schüttrumpf and van Gent (2003) Equation 10. $\frac{q_{B02\%}}{\sqrt{gH_S^3}} = c_q'\ \left(\frac{R_{u2\%} - R_C}{H_s}\right)^{1.5} \Big/ \left(1 + c_q^{"}\ \frac{B_C}{H_S}\right)$ Note: Duplicated for outer slope.
1.5 WAVE OVERTOPPING FLOW VOLUME		
1.5.1 - Outer Slope Wave Overtopping Flow Volume		
Wave Overtopping Flow Volume - Maximum in a single wave based on Flow Depth and Flow Velocity variation over time exceeded by 2% of incoming waves	Bosman (2007) Equations 4-27, 5-3, and 6-7	Bosman (2007) Equations 4-27 & 5-3. $\frac{V_{2\%}}{H_s^2} = c_s\ \frac{u_{2\%}}{\sqrt{g\ H_s}}\ \frac{h_{2\%}}{H_s}\ \frac{T_{ovt2\%}}{T_{m-1.0}}$ Bosman (2007) Equation 6-7. $\frac{V_{2\%}}{H_s^2} = 0.40\ \frac{u_{2\%}}{\sqrt{g\ H_s}}\ \frac{h_{2\%}}{H_s}\ \frac{T_{ovt2\%}}{T_{m-1.0}}$

APPLICATION	SOURCE	EQUATION
Wave Overtopping Flow Volume - Maximum in a Single Wave	Smith et al. (1994) Equation 3 Van der Meer and Janssen (1995) Equation 31 Pullen et al. (2007) Equation 5.35 Valk (2009) Equation 2.7 Hughes (2011a) Equation 50	Smith et al. (1994) Equation 3, van der Meer and Janssen (1995) Equation 31, Pullen et al. (2007) Equation 5.35, Valk (2009) Equation 2.7, Hughes (2011a) Equation 50. $V_{max} = a\,[ln(N_{ow})]^{4/3}$ and $a = 0.84\,\frac{T_m\,q}{P_{ov}}$
Wave Overtopping Flow Volume - Maximum per Wave for a given probability of exceedance	Van der Meer and Janssen (1995) Equation 30 Pullen et al. (2007) Equation 5.34 Hughes (2011a) Equation 49	Van der Meer and Janssen (1995) Equation 30, Pullen et al. (2007) Equation 5.34. $V_W = a\,[-\ln(1 - P_{VE})]^{4/3}$ Hughes (2011a) Equation 49. $V_W = a\,[-\ln(P_{VE})]^{4/3}$
Wave Overtopping Flow Volume - Maximum per Wave exceeded by 2% of incoming waves van Gent (2002b) Equation 7 applied to inner slope. Schüttrumpf and van Gent (2003) Equation 11 applied to outer slope	Van Gent (2002b) Equation 7 Schüttrumpf and van Gent (2003) Equation 11	Van Gent (2002b) Equation 7. $\frac{V_{2\%}}{H_s^2} = c_V'\,(\gamma_{fC})^{0.5}\,\left(\frac{R_{u2\%} - R_C}{\gamma_{fA}\,H_s}\right)^2$ Schüttrumpf and van Gent (2003) Equation 11. $\frac{V_{2\%}}{H_s^2} = c_V'\,\left(\frac{R_{u2\%} - R_C}{H_s}\right)^2$ Note: Duplicated for inner slope.

APPLICATION	SOURCE	EQUATION
Wave Overtopping Flow Volume - Maximum as related to Wave Runup Remainder exceeded by 2% of incoming waves	Bosman (2007) Equations 4-30 & 6-8	Bosman (2007) Equations 4-30 & 6-8. $$\frac{V_{2\%}}{H_s^2} = c'_{v,2\%} \left(\frac{R_{u2\%} - R_C}{H_s \gamma_{fC}} \right)^2$$ Note: Bosman (2007) Equation 4-30 not reproduced in the literature review notes.
1.5.2 Inner slope Wave Overtopping Flow Volume		
Wave Overtopping Flow Volume - Maximum per Wave exceeded by 2% of incoming waves van Gent (2002b) Equation 7 applied to inner slope. Schüttrumpf and van Gent (2003) Equation 11 applied to outer slope.	Van Gent (2002b) Equation 7 Schüttrumpf and van Gent (2003) Equation 11	Van Gent (2002b) Equation 7. $$\frac{V_{2\%}}{H_s^2} = c'_V \left(\gamma_{fC}\right)^{0.5} \left(\frac{R_{u2\%} - R_C}{\gamma_{fA} H_s} \right)^2$$ Schüttrumpf and van Gent (2003) Equation 11. $$\frac{V_{2\%}}{H_s^2} = c'_V \left(\frac{R_{u2\%} - R_C}{H_s} \right)^2$$ Note: Duplicated for outer slope.

APPLICATION	SOURCE	EQUATION
1.6 - WAVE OVERTOPPING IRIBARREN NUMBER		
1.6.1 Outer Slope Wave Overtopping Iribarren Number		
Wave Runup Iribarren number for use with Significant Wave Height, Peak Deepwater Wavelength, and Peak Wave Period (#1)	Smith et al. (1994) Equations 2a & 2b and 4& 5 Van der Meer and Janssen (1995) Equations 1, 2, 4, 16, 17, 18, 19, 20, 21, 22, 23, 26 & 27 Schüttrumpf et al. (2001) Equations 2 & 3 and 4 & 5 Bosman (2007) Equations 2-8, 3-6, 3-7, 6-9 & 6-10	Van der Meer and Janssen (1995) Equations 1, 2, 4, 16, 17, 18, 19, 20, 21, 22, 23, 26 & 27; Schüttrumpf et al. (2001) Equation2 & 3 and 4 & 5; Bosman (2007) Equations 2-8, 3-6, 3-7, 6-9 & 6-10. $\xi_{op} = \tan\alpha / \sqrt{H_s/L_{0p}}$ Note: several papers include the Iribarren number subsidiary to a defined equation.
Wave Runup Iribarren number transition point between breaking waves and nonbreaking waves (#1+)	Schüttrumpf et al. (2001) Equations 4 & 5	Schüttrumpf et al. (2001) Equations 4 & 5. $\xi_{op} = < \xi_{gr}$ for breaking waves and $\xi_{op} = \geq \xi_{gr}$ for nonbreaking waves
Wave Runup Iribarren number Equivalent for Slope with Berm (#2)	Van der Meer and Janssen (1995) Equations 2 & 4 and 26 & 27	Van der Meer and Janssen (1995) Equations 2 & 4 and 26 & 27. $\xi_{eq} = \gamma_b \xi_{op}$

APPLICATION	SOURCE	EQUATION
Wave Runup Iribarren number General Term for use with Significant Wave Height and with various Deepwater Wavelengths and Wave Period (#3)	Van Gent (2002a) Equation 1	Van Gent (2002a) Equation 1. $$\xi_x = \tan\alpha/\sqrt{H_s/L_{0x}} = \tan\alpha/\sqrt{2\,\pi\,H_S/g\,T_x^2}$$
Wave Runup Iribarren number General Term for use with Significant Wave Height, Mean Spectral Deepwater Wavelength, and Mean Double or Multiple Wave Period (#4)	Van Gent (2002a) Equation 1 Schüttrumpf and van Gent (2003) Equations 1a & 1b Bosman (2007) Equations 2-15 & 2-16 Van Steeg (2007) Equations 2-1 & 2-2, 2-16 & 2-17	Van Gent (2002a) Equation 1; Schüttrumpf and van Gent (2003) Equations 1a & 1b; Bosman (2007) Equations 2-15 & 2-16; van Steeg (2007) Equations 2-1 & 2-2, 2-16 & 2-17, & 2-24. $$\xi_{S,-1} = \tan\alpha/\sqrt{H_s/L_{m-1,0}}$$ and $$L_{m-1,0} = \frac{g\,T_{m-1,0}^2}{2\,\pi}$$
Wave Runup Iribarren number General Term for use with Significant Wave Height, mean Deepwater Wavelength, and Mean Wave Period (#5)	Schüttrumpf and Oumeraci. (2005) Equation 10 Bosman (2007) Equation 3-8	Schüttrumpf and Oumeraci. (2005) Equation 10, Bosman (2007) Equation 3-8. $$\xi_d = \tan\alpha/\sqrt{H_s/L_{0m}} = \tan\alpha/\sqrt{2\,\pi\,H_S/g\,T_m^2}$$ [-]

APPLICATION	SOURCE	EQUATION
Wave Runup Iribarren number General Term for use with Significant Wave Height based on the Spectrum, Peak Deepwater Wavelength, and Peak Wave Period (#6)	Hughes (2007) Equations 14, 15, & 16	Hughes (2007) Equations 14, 15, & 16. $$\xi_{mp} = \frac{\tan\alpha}{\sqrt{H_{m0}/L_{0p}}} = \tan\alpha \Big/ \sqrt{2\,\pi\,H_{m0}/g\,T_p^2}$$
Wave Runup Iribarren number General Term for use with Spectral Mean Wave Height based on the Spectrum, Spectral Mean Deepwater Wavelength, and Spectral Mean Wave Period (#7)	Van Steeg (2007) Equations 2-8 & 2-9 and 2-10 & 2-11 Bosman (2007) Equations 2-2, 2-3, 2-5 & 2-6 Pullen et al. (2007) Equations 5.3, 5.4, 5.8, 5.9, 5.10, 5.11, 5.14, & 5.16 Valk (2009) Equations 2.2 & 2.3, 2.5 & 2.6 Dean and van Ledden (2010a Equations 5 & 6 Dean et al. (2010b) Equation 21 Hughes (2011a) Equations 36 & 37, 38 & 39, 40 & 41, and 42 & 43	Van Steeg (2007) Equations 2-8 & 2-9 and 2-10 & 2-11; Bosman (2007) Equations 2-2, 2-3, 2-5 & 2-6; Pullen et al. (2007) Equations 5.3, 5.4, 5.8, 5.9, 5.10, 5.11, 5.14, & 5.16; Valk (2009) Equations 2.2 & 2.3, 2.5 & 2.6; Dean and van Ledden (2010a Equations 5 & 6; Dean et al. (2010b) Equation 21; Hughes (2011a) Equations 36 & 37, 38 & 39, 40 & 41, and 42 & 43. $$\xi_{m-1,0} = \tan\alpha/\sqrt{H_{m0}/L_{m-1,0}} = \tan\alpha/\sqrt{2\,\pi\,H_{m0}/g\,T_{m-1,0}^2}$$ [-] and $$L_{m-1,0} = \frac{g\,T_{m-1,0}^2}{2\,\pi}$$

APPLICATION	SOURCE	EQUATION
1.7 - PROBABILITY		
1.7.1 - Outer Slope Probability		
Probability of Wave Overtopping Probability of Wave Overtopping - Coefficient c for Smith et al. (1994) Equation 4	Smith et al. (1994) Equations 4 & 5 Van der Meer and Janssen (1995) Equations 26 & 27	Smith et al. (1994) Equation 4, van der Meer and Janssen (1995) Equation 26. $P_{ow} = \exp\left[- \left(\frac{R_c/H_s}{c} \right)^2 \right]$ Smith et al. (1994) Equation 5 $c = 0.81\, \gamma_f\, \xi_{op}$ with a maximum of $c = 1.62\, \gamma_f$ Van der Meer and Janssen (1995) Equation 27. $c = 0.81\, \gamma_h \gamma_f \gamma_{B\, \xi_{eq}}$ with a maximum of $c = 1.62\, \gamma_h \gamma_f \gamma_B$
Probability of Wave Overtopping Volume per Wave being less than or equal to a given Wave Volume Discrepancy between papers on dimensions for parameter a.	Van der Meer and Janssen (1995) Equations 24 & 25 Pullen et al. (2007) Equations 5.32 & 5.33 Van Steeg (2007) Equations 2-14 & 2-15 Valk (2009) Equation 2.4 Van der Meer et al. (2010) Equations 1 & 2 Hughes (2011a) Equations 44, 46, & 48	Van der Meer and Janssen (1995) Equations 24 & 25, Pullen et al. (2007) Equations 5.32 & 5.33, van Steeg (2007) Equations 2-14 & 2-15, Valk (2009) Equation 2.4, van der Meer et al. (2010) Equation 1 (with Equation 2 below), Hughes (2011a) Equation 44 (with Equation 46 below). $P_V = P(V \leq V_W) = 1 - \exp\left[- \left(\frac{V_W}{a} \right)^{0.75} \right]$ and $a = 0.84\, \frac{T_m\, q}{P_{ow}}$ Van der Meer et al. (2010) Equation 2, Hughes (2011a) Equation 46. $a = 0.84\, T_m\, \frac{q}{P_{ow}} = 0.84\, T_m\, \frac{q\, N_w}{N_{ow}} = 0.84\, \frac{q\, t}{N_{ow}}$ Hughes (2011a) Equation 48. $P_{ow} = \frac{N_{ow}}{N_w}$ and $N_W = \frac{t_E}{T_m}$

APPLICATION	SOURCE	EQUATION
Probability of Wave Overtopping Volume per Wave being greater than or equal to a given Wave Volume Discrepancy between papers on dimensions for parameter a.	Van der Meer et al. (2006) Equation 1 Bosman (2007) Equations 2-7 & 5-1 Hughes (2011a) Equations 45, 46, & 48	Van der Meer et al. (2006) Equation 1, Bosman (2007) Equations 2-7 & 5-1, Hughes (2011a) Equation 45 (with Equation 46 below). $P_{VE} = P(V \geq V_W) = \exp\left[-\left(\frac{V_W}{a}\right)^{0.75}\right]$ and $a = 0.84\,\frac{T_m\,q}{P_{ow}}$ Hughes (2011a) Equation 46. $a = 0.84\,T_m\left(\frac{q}{P_{ow}}\right) = 0.84\,T_m\left(\frac{q\,N_w}{N_{ow}}\right) = 0.84\left(\frac{q\,t_E}{N_{ow}}\right)$ Hughes (2011a) Equation 48. $P_{ow} = \frac{N_{ow}}{N_w}$ and $N_W = \frac{t_E}{T_m}$
Probability of Wave Overtopping per Wave	Pullen (2007) Equations 5.36 & 5.37 Van Steeg (2007) Equation 2-16 Valk (2009) Equation 2.5 Hughes (2011a) Equation 47	Pullen (2007) Equations 5.36 & 5.37, van Steeg (2007) Equation 2-16, Valk (2009) Equation 2.5, $P_{ow} = \exp\left[-\left(\sqrt{-\ln 0.02}\,\frac{R_C}{R_{u2\%}}\right)^2\right]$ and $P_{ow} = \frac{N_{ow}}{N_w}$

Appendix B

Flow thickness based surfboard measurement locations.

Test	Location	Flow Thickness Location (ft. from WOS)
1	1-2	$x=-0.41y^3+0.70y^2-1.54y+12.32$
2	1-2	$x=-0.41y^3+0.70y^2-1.54y+12.33$
3	1-2	$x=-0.41y^3+0.70y^2-1.54y+12.34$
4	1-2	$x=-0.41y^3+0.70y^2-1.54y+12.34$
5	1-2	$x=-0.41y^3+0.70y^2-1.54y+12.34$
6	1-2	$x=-0.41y^3+0.70y^2-1.54y+12.34$
7	1-2	$x=-0.41y^3+0.70y^2-1.54y+12.34$
7	3-4	$x=-0.26y^3+0.0024y^2-0.51y+16.79$
1	6-7	$x=-0.26y^3+0.0024y^2-0.51y+23.04$
3	7-8	$x=-0.26y^3+0.0024y^2-0.51y+23.87$
2	8-9	$x=-0.26y^3+0.0024y^2-0.51y+25.88$
4	9-10	$x=-0.26y^3+0.0024y^2-0.51y+29.61$
5	10-11	$x=-0.26y^3+0.0024y^2-0.51y+31.56$
6	11-12	$x=-0.26y^3+0.0024y^2-0.51y+33.87$
1	13	$x=-0.26y^3+0.0024y^2-0.51y+38.08$
3	13-14	$x=-0.26y^3+0.0024y^2-0.51y+37.78$
2	14-15	$x=-0.26y^3+0.0024y^2-0.51y+39.89$
4	15-16	$x=-0.26y^3+0.0024y^2-0.51y+42.06$
6	19	$x=-0.25y^3+0.43y^2-1.32y+49.34$
7	19	$x=-0.25y^3+0.43y^2-1.32y+49.34$
5	20	$x=-0.25y^3+0.43y^2-1.32y+54.07$

Appendix C

Crest surfboard flow thickness time series.

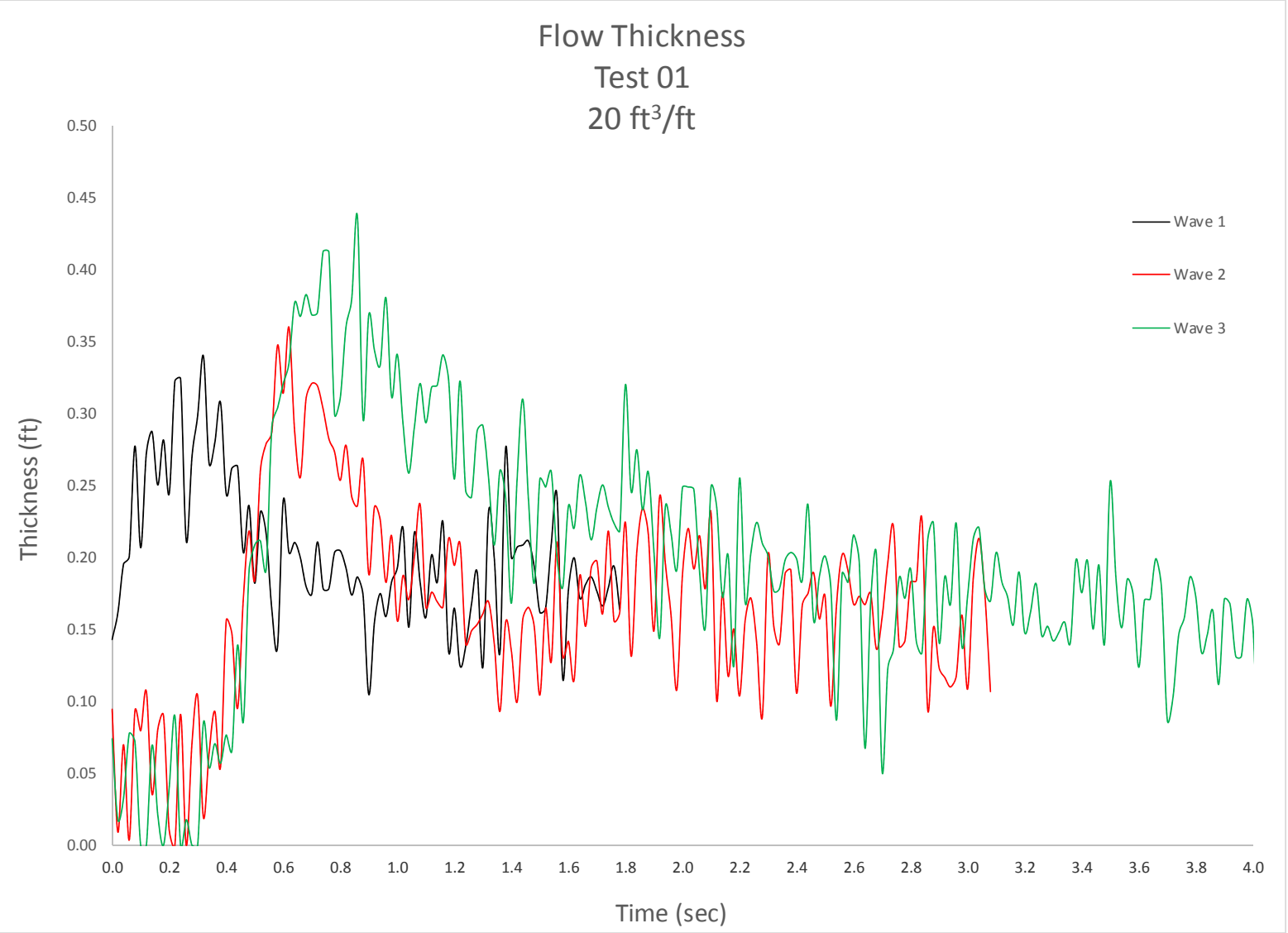

Figure C-1. Crest surfboard flow thickness, 20 ft^3/ft, Test 1.

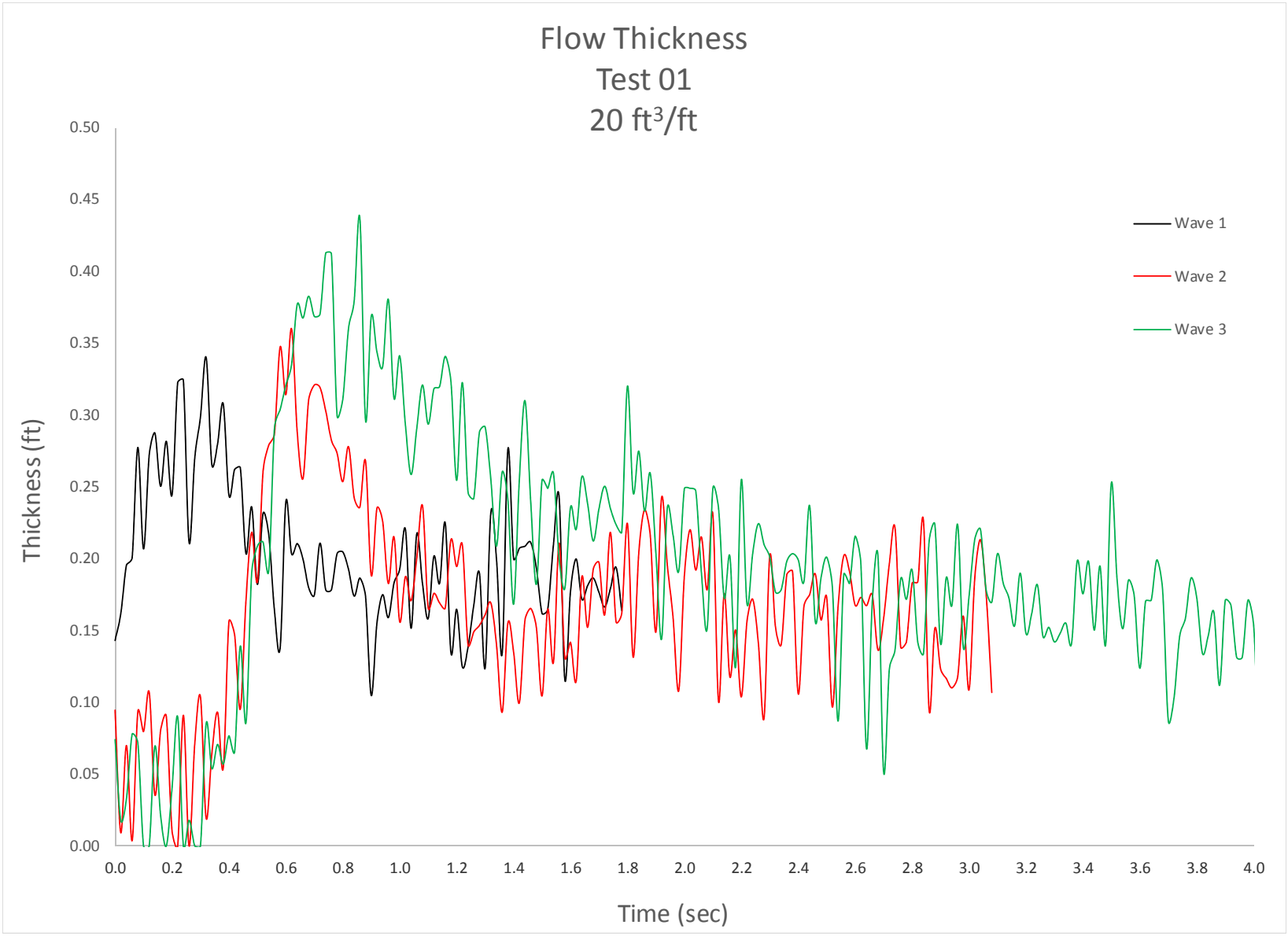

Figure C-2. Crest surfboard flow thickness, 20 ft^3/ft, Test 2.

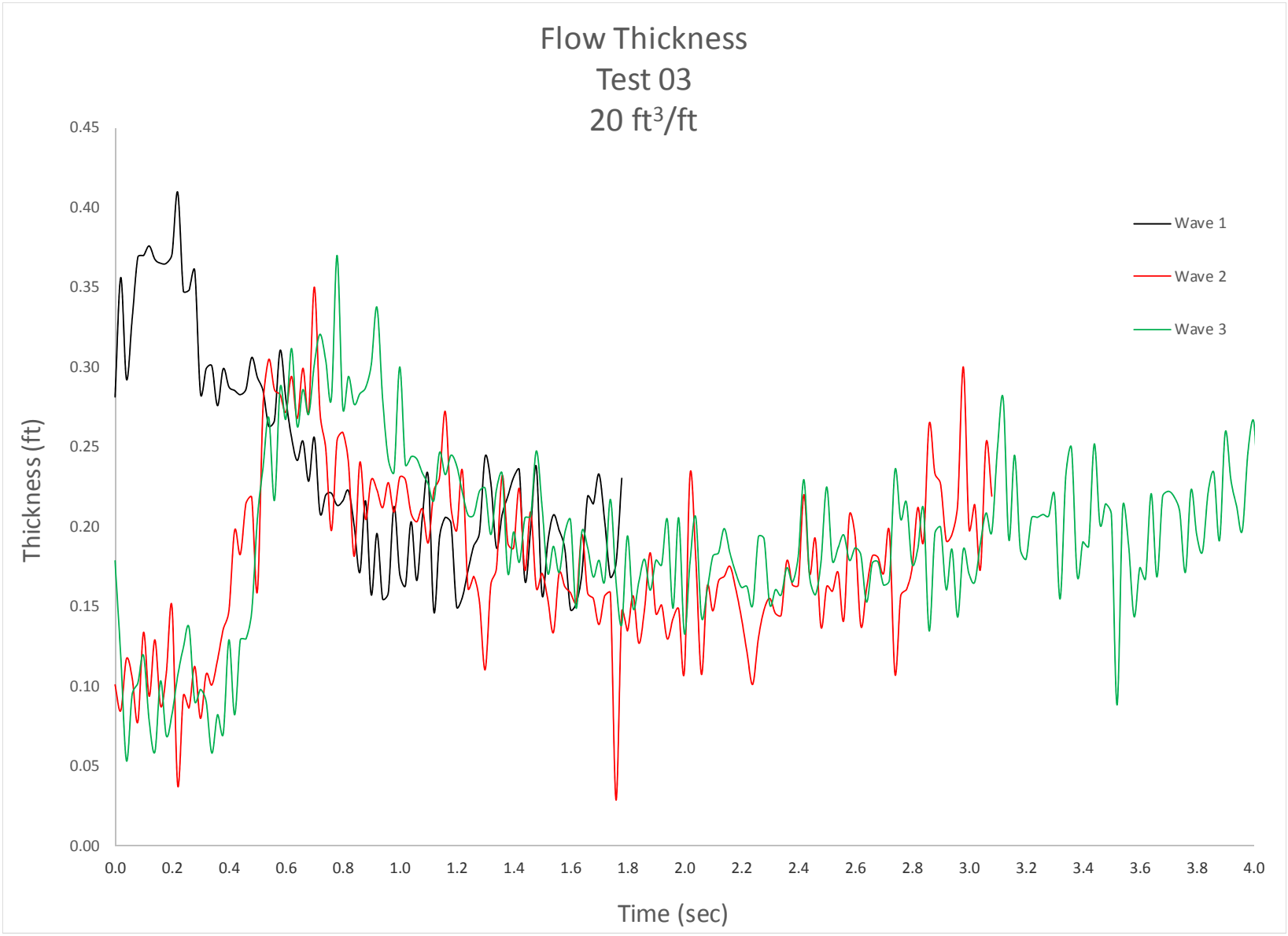

Figure C-3. Crest surfboard flow thickness, 20 ft^3/ft, Test 3.

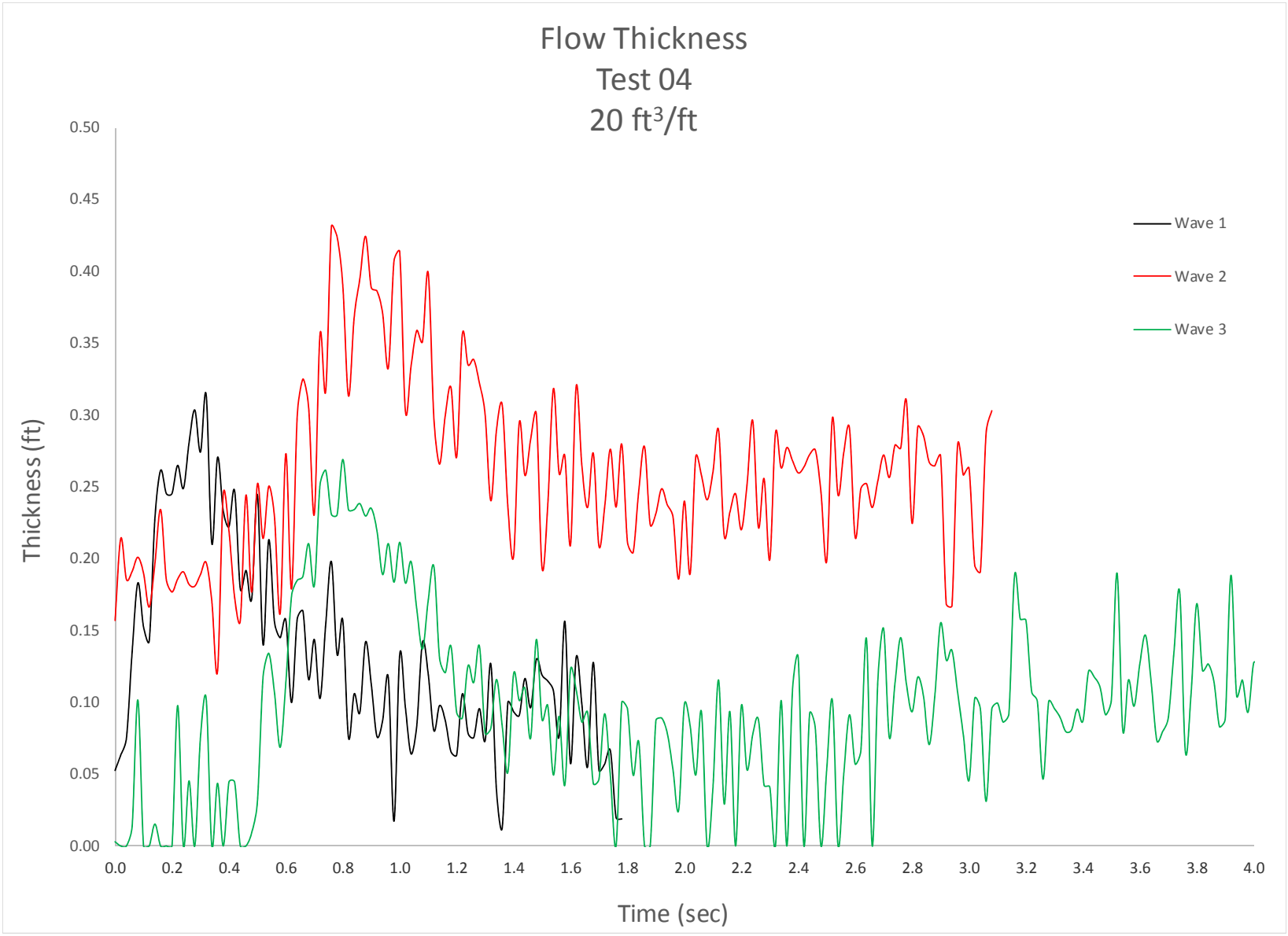

Figure C-4. Crest surfboard flow thickness, 20 ft^3/ft, Test 4.

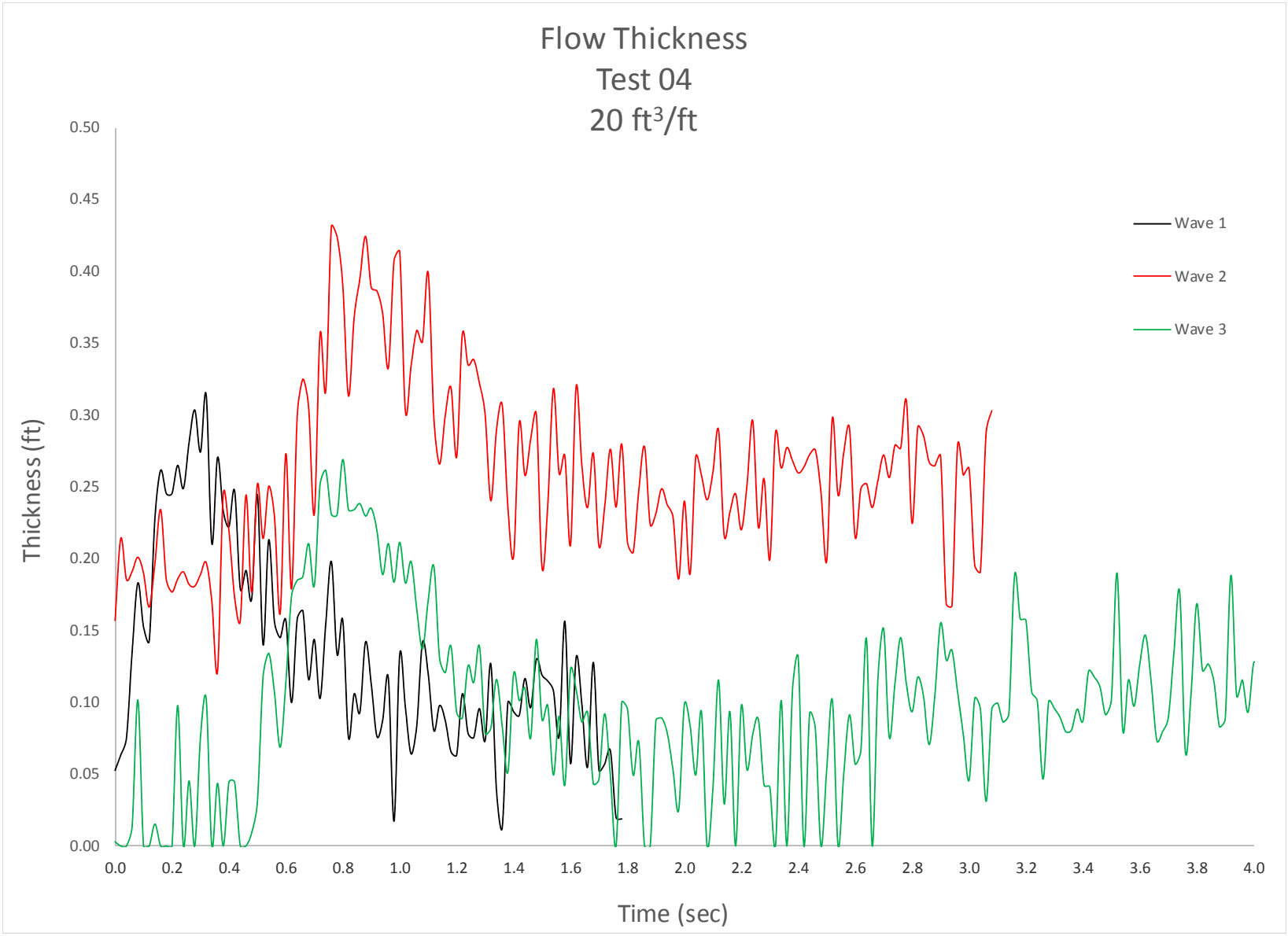

Figure C-5. Crest surfboard flow thickness, 20 ft^3/ft, Test 5.

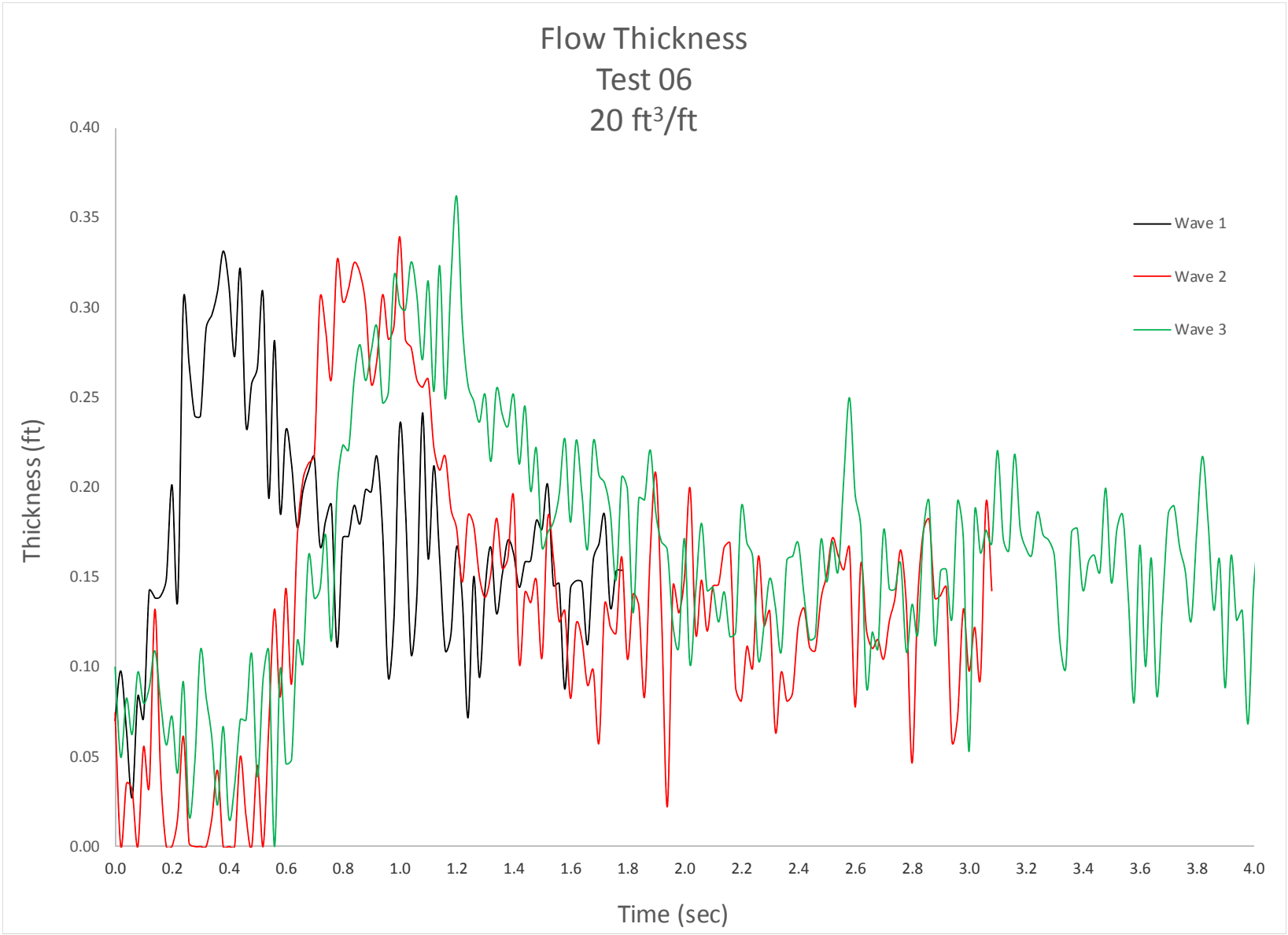

Figure C-6. Crest surfboard flow thickness, 20 ft^3/ft, Test 6.

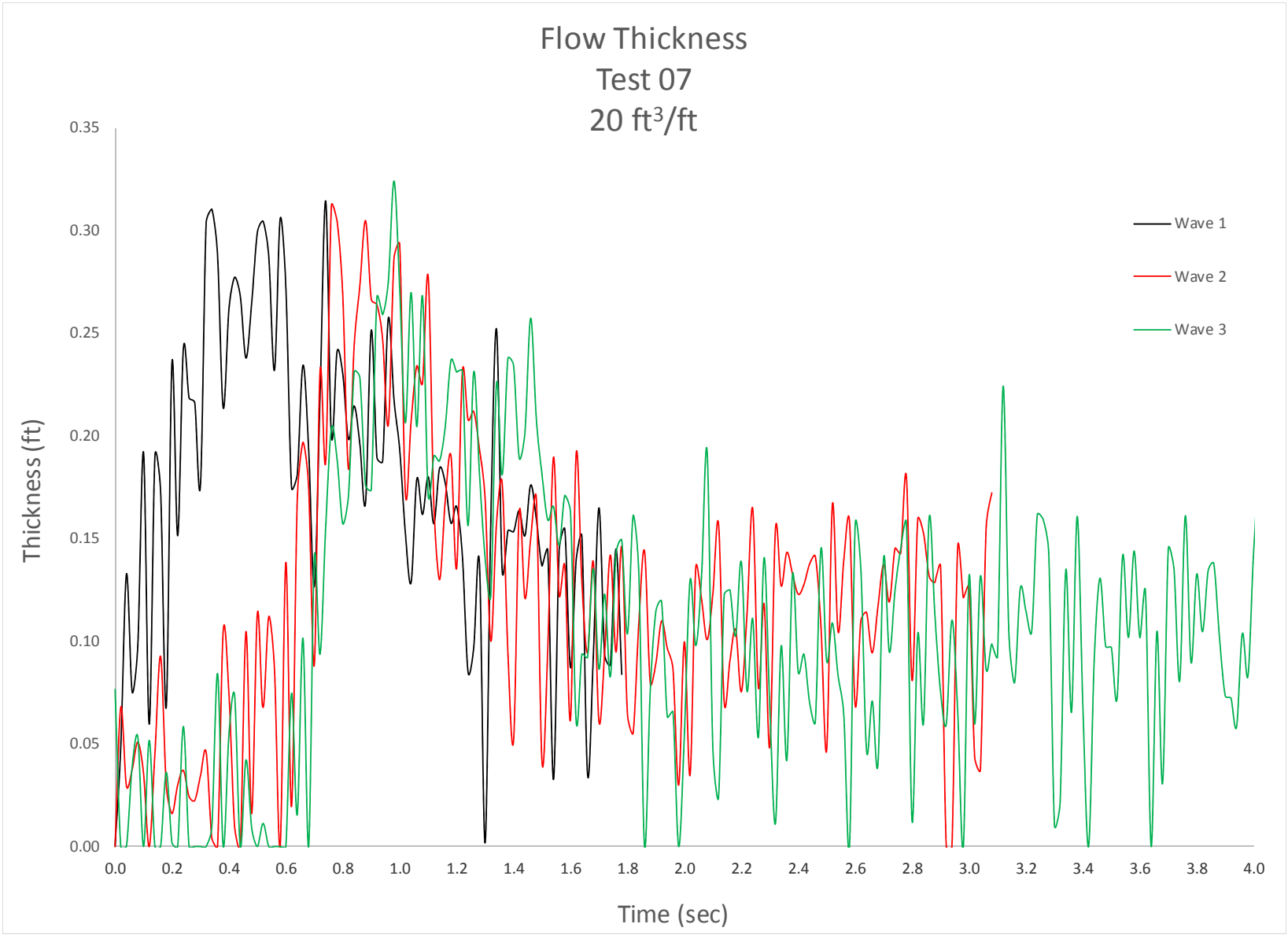

Figure C-7. Crest surfboard flow thickness, 20 ft^3/ft, Test 7.

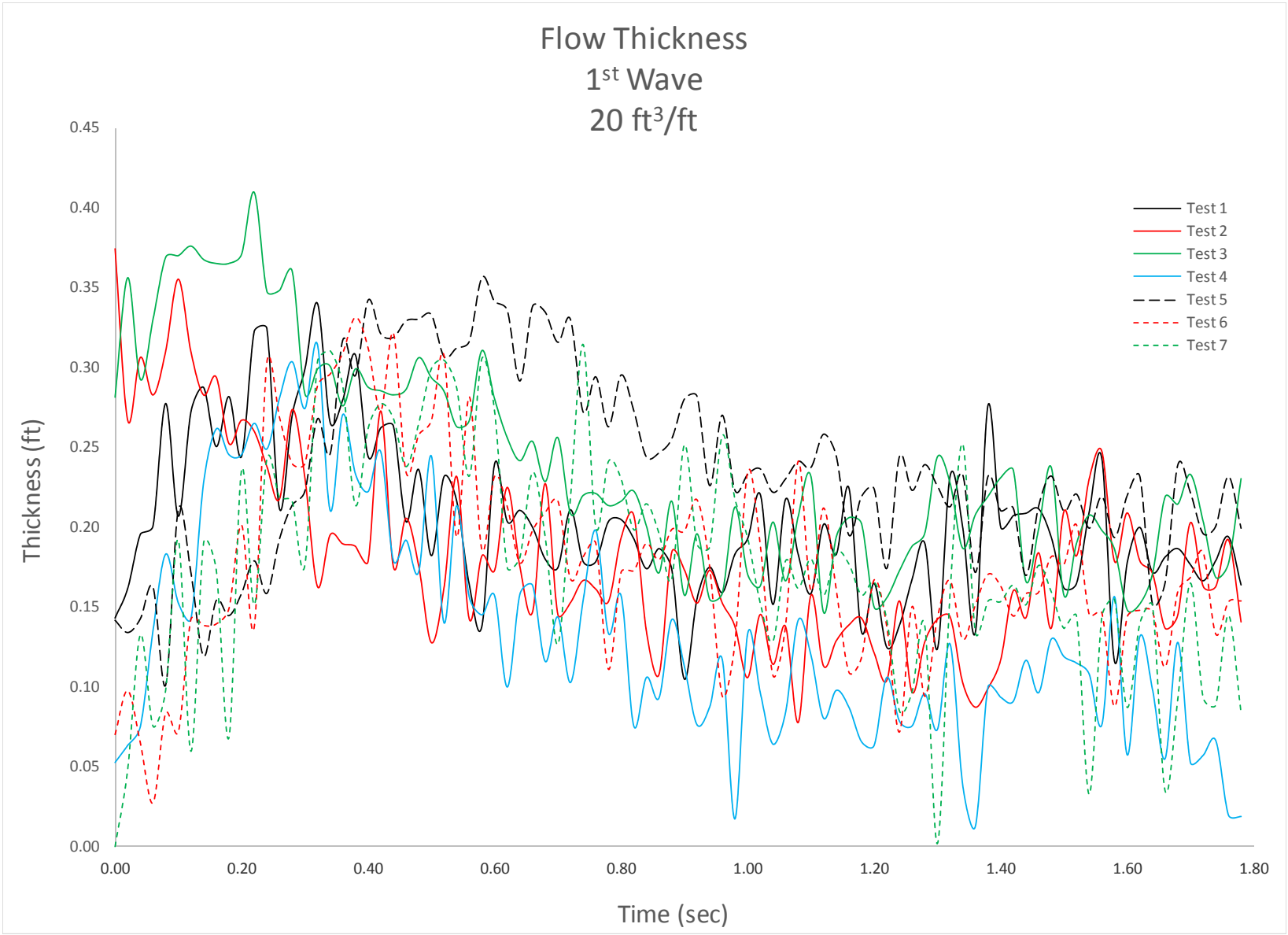

Figure C-8. Crest surfboard flow thickness, 20 ft^3/ft, 1st wave, all tests.

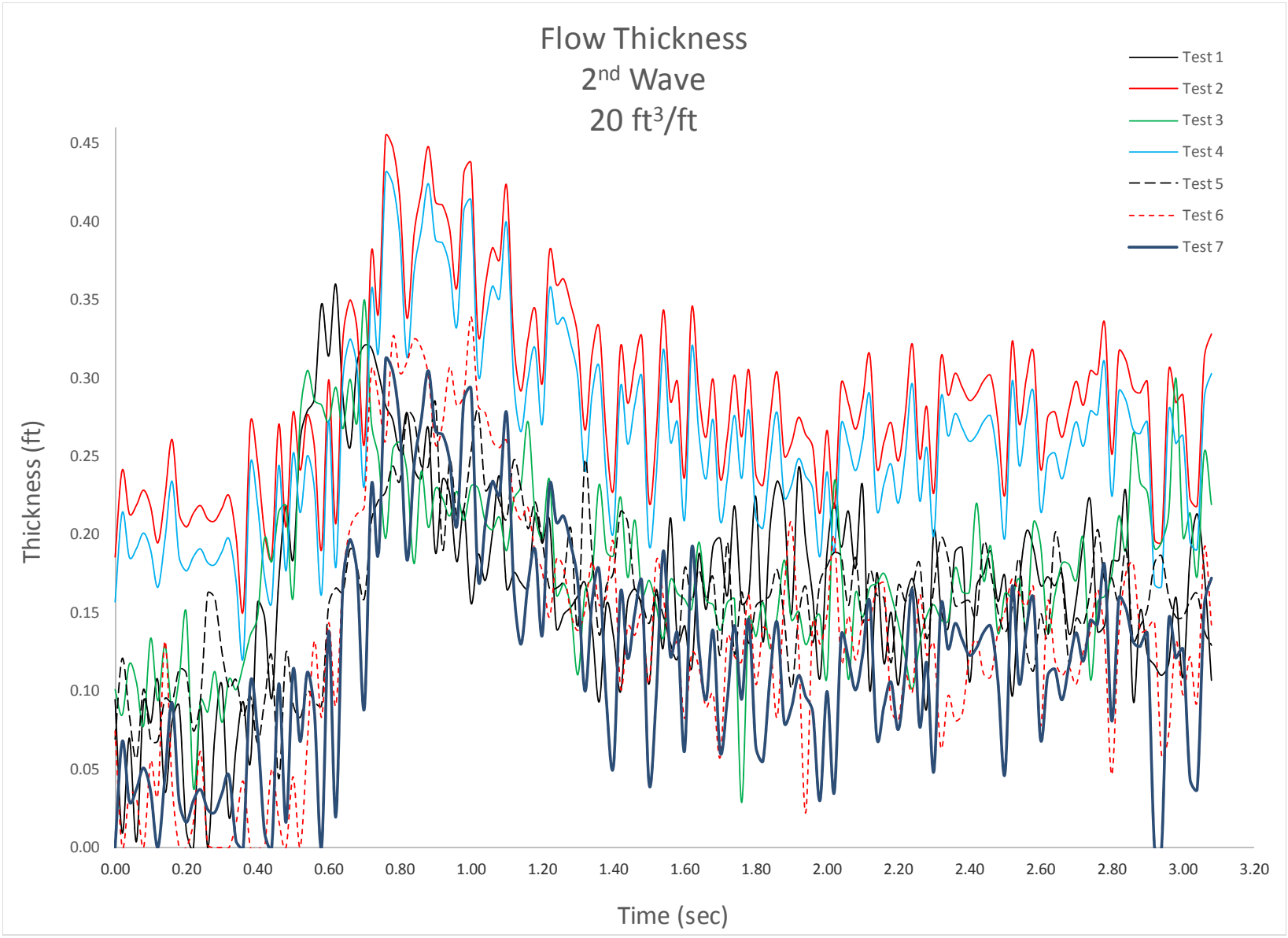

Figure C-9. Crest surfboard flow thickness, 20 ft^3/ft, 2nd wave, all tests.

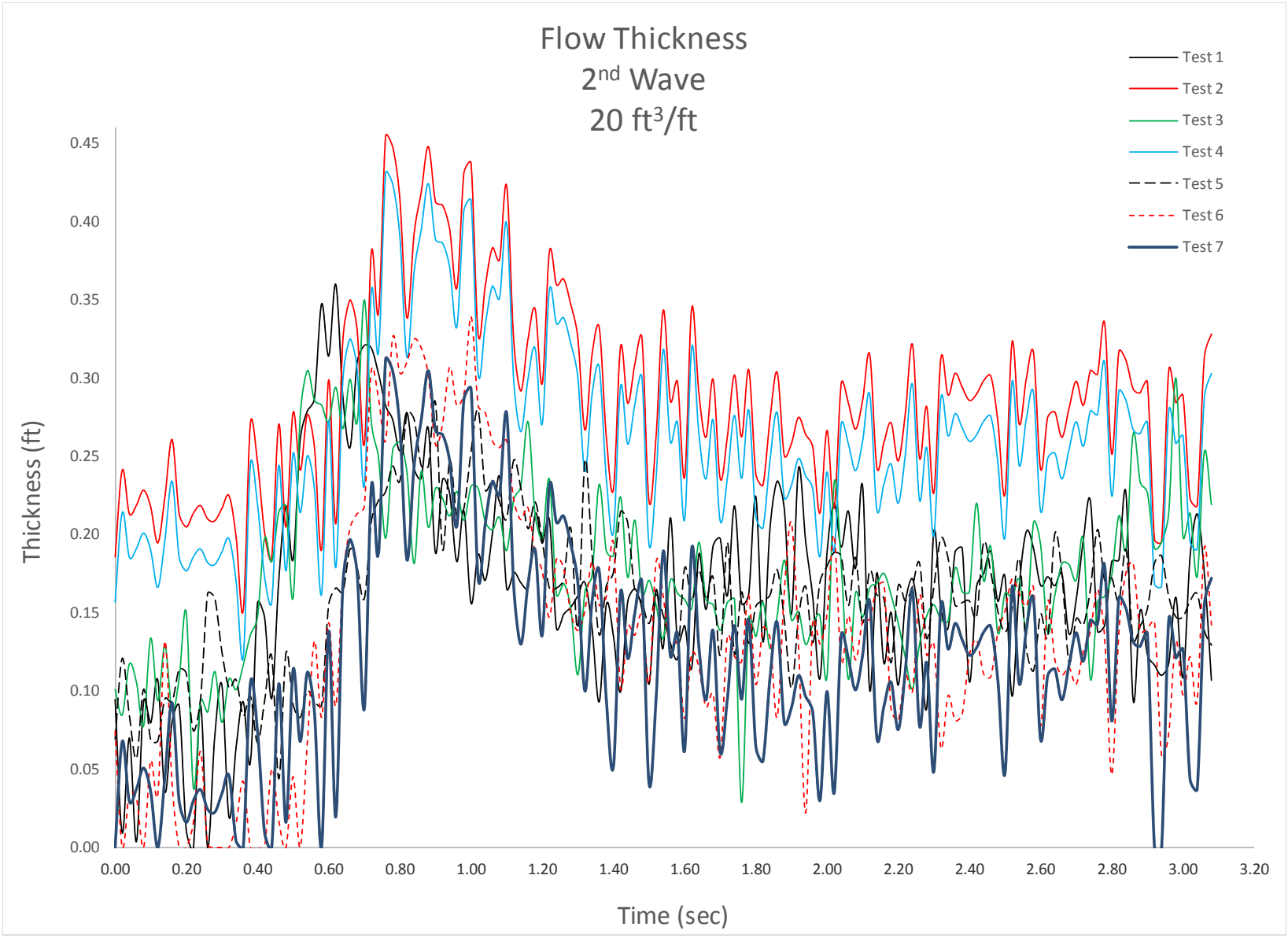

Figure C-10. Crest surfboard flow thickness, 20 ft^3/ft, 3rd wave, all tests.

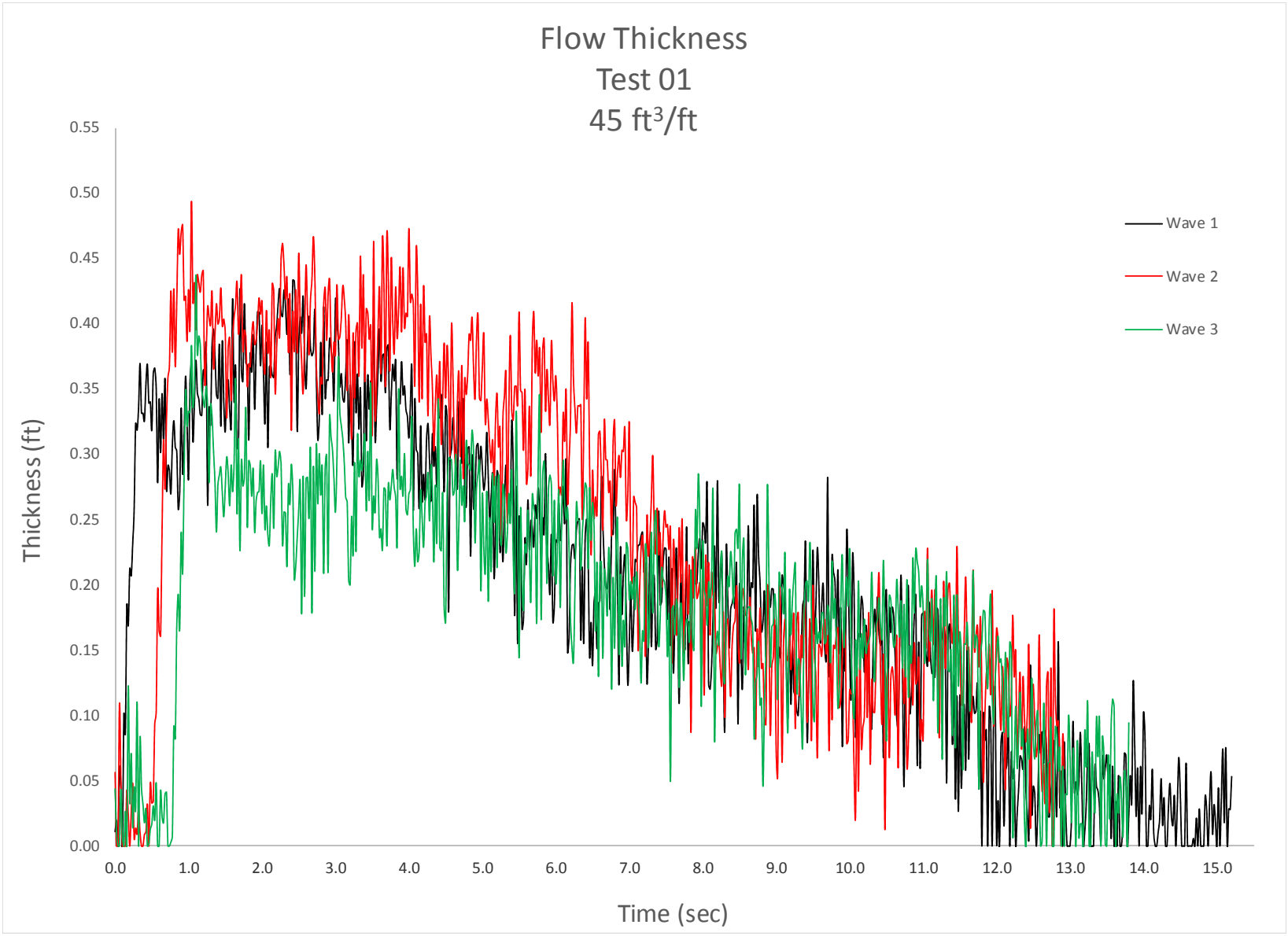

Figure C-11. Crest surfboard flow thickness, 45 ft^3/ft, Test 1.

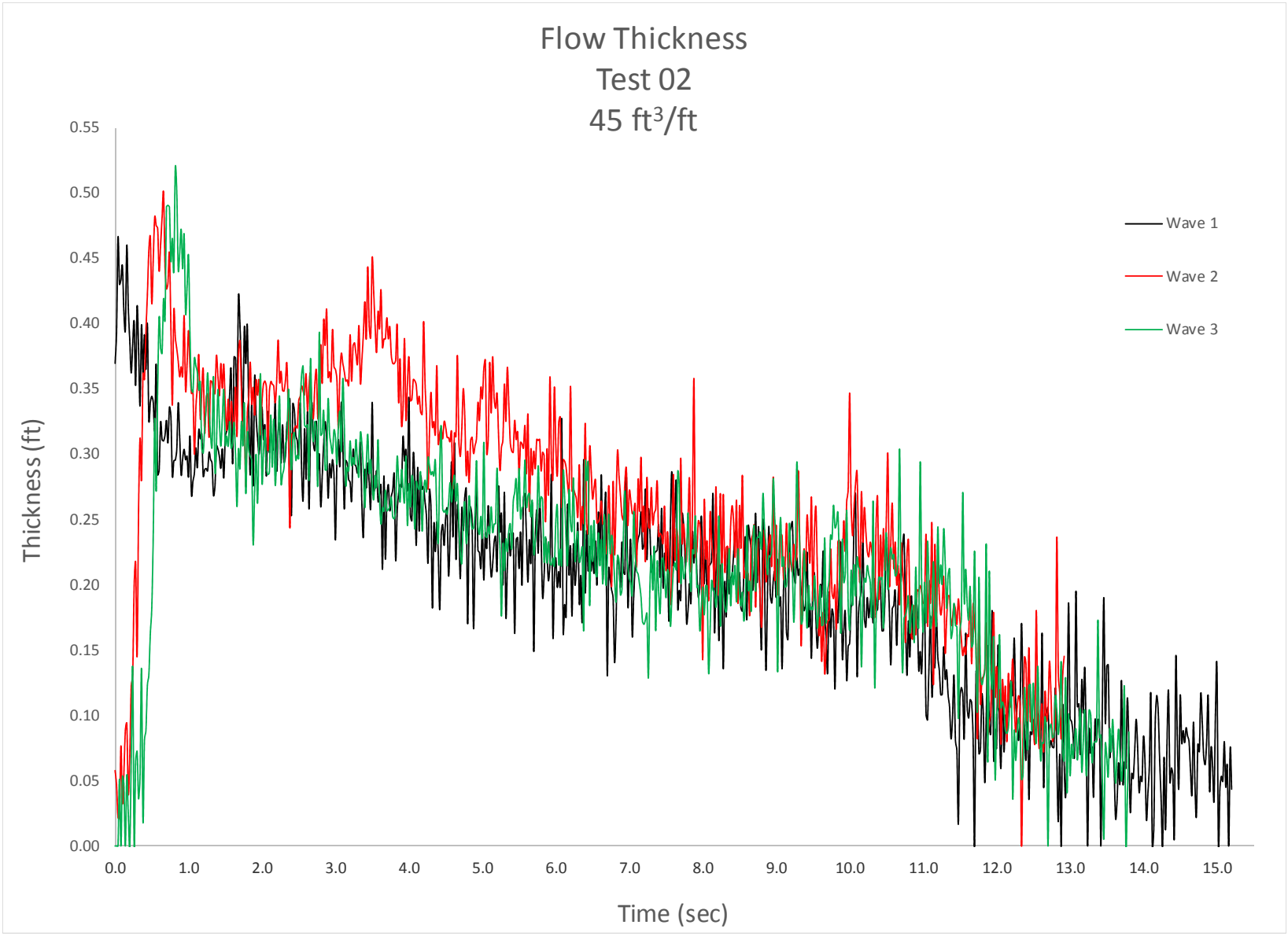

Figure C-12. Crest surfboard flow thickness, 45 ft^3/ft, Test 2.

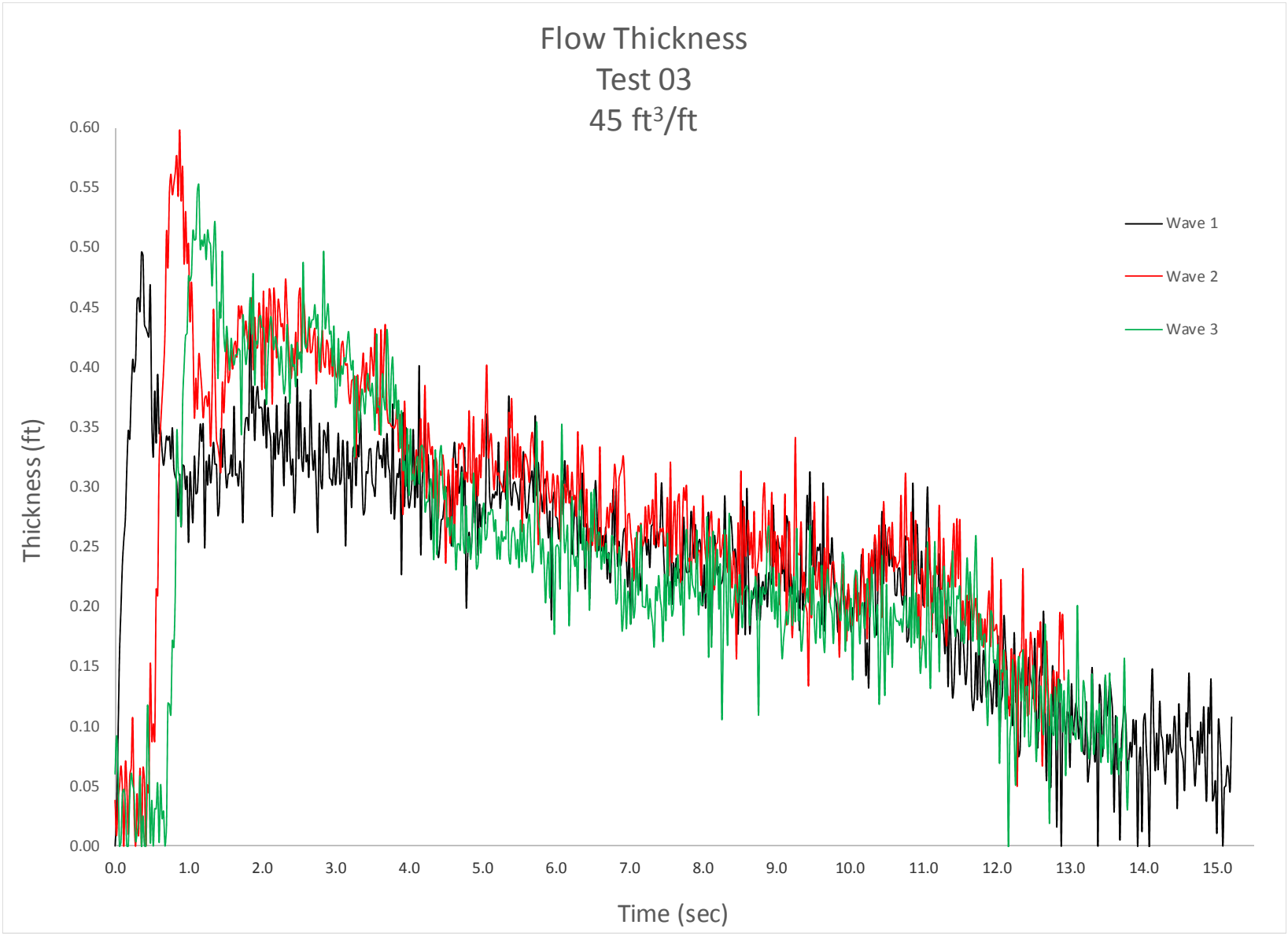

Figure C-13. Crest surfboard flow thickness, 45 ft^3/ft, Test 3.

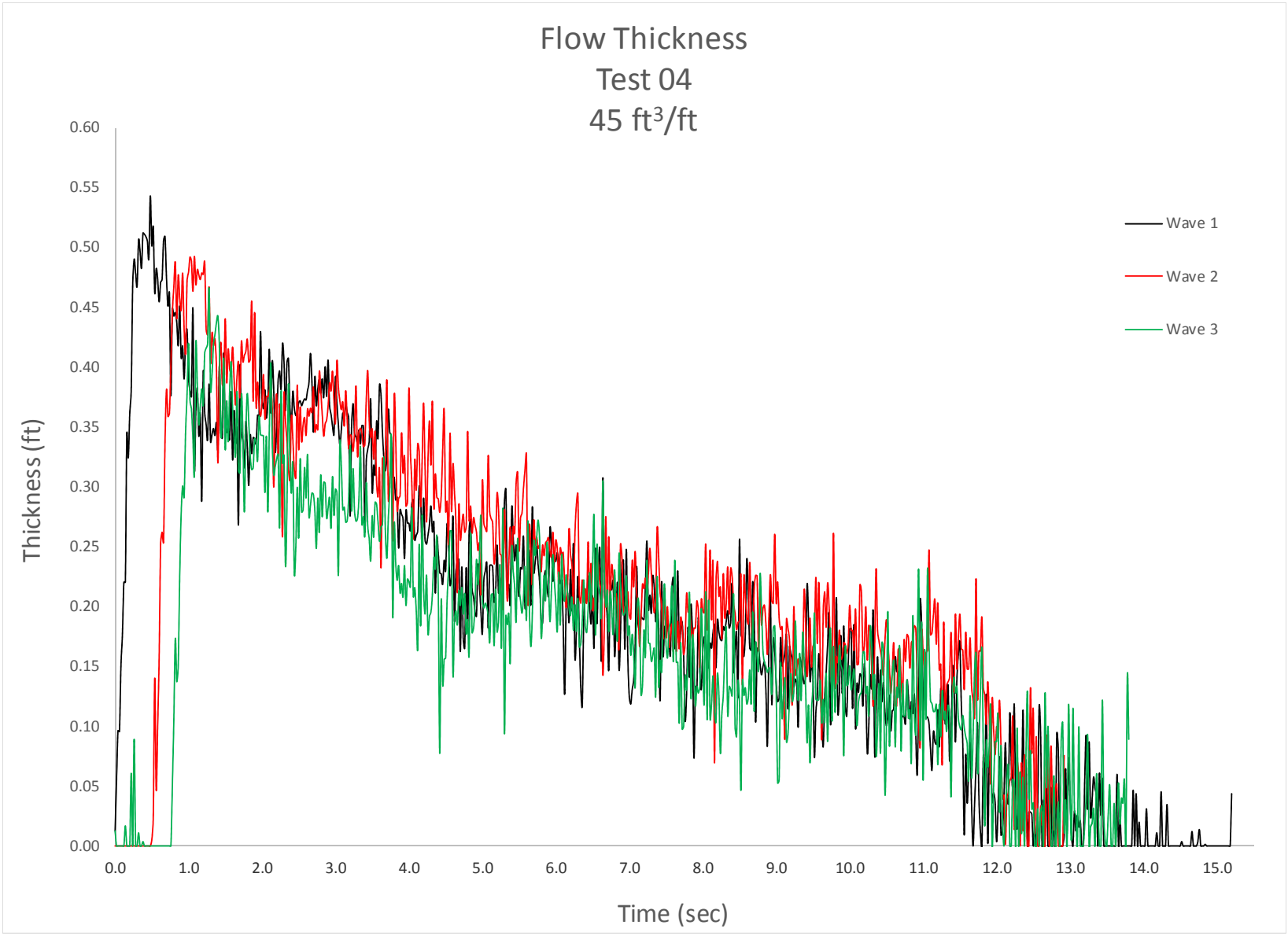

Figure C-14. Crest surfboard flow thickness, 45 ft^3/ft, Test 4.

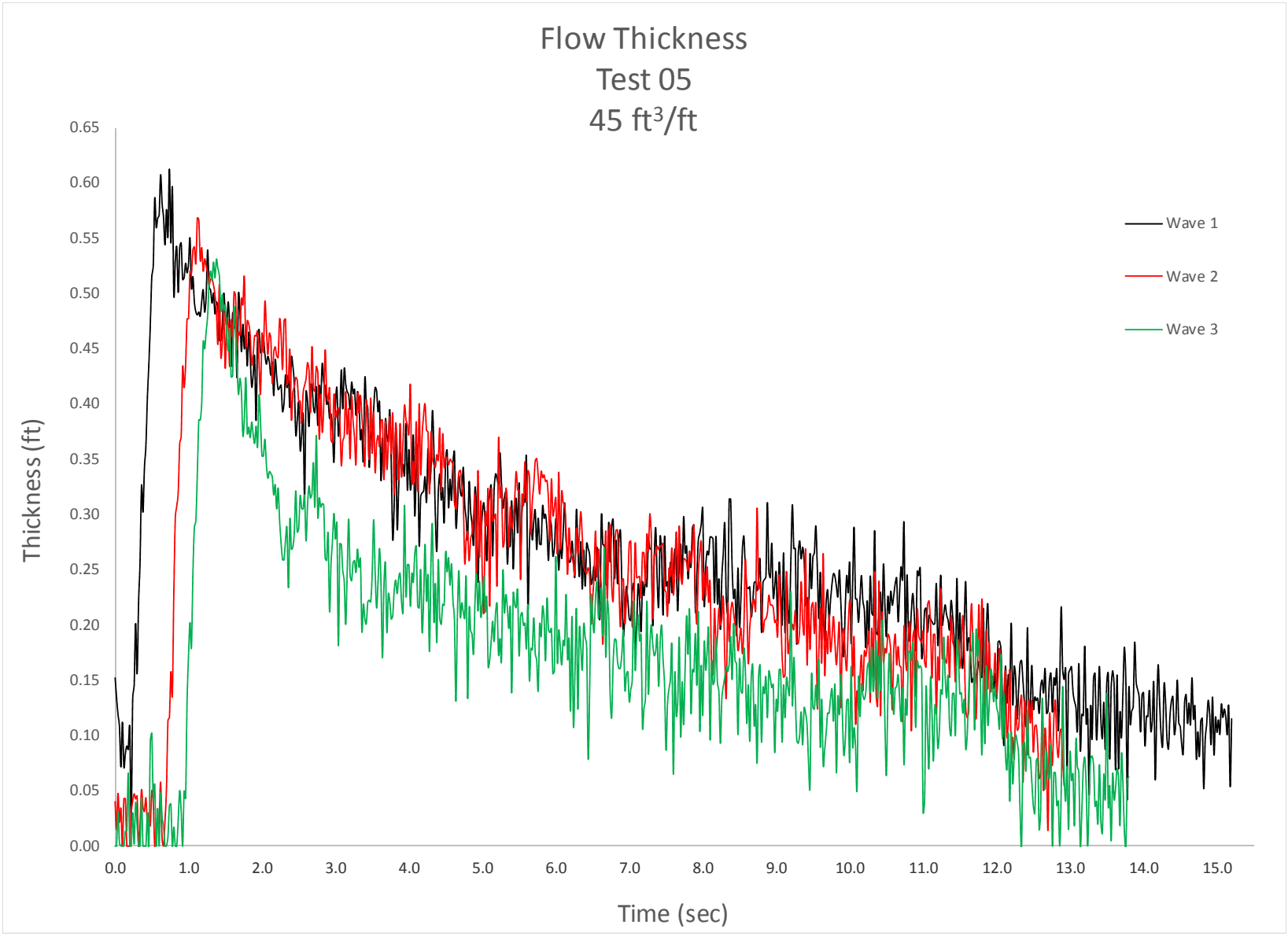

Figure C-15. Crest surfboard flow thickness, 45 ft^3/ft, Test 5.

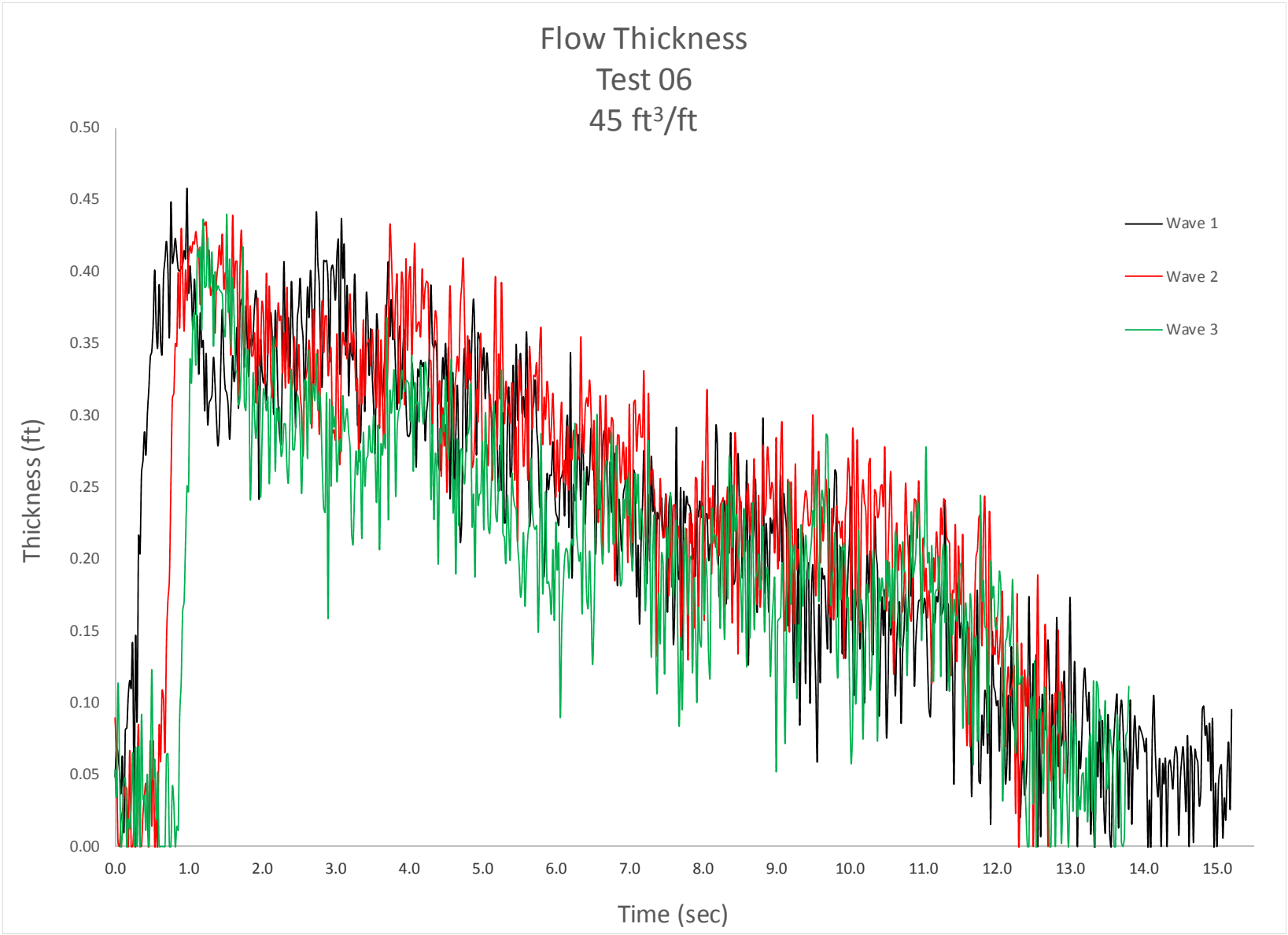

Figure C-16. Crest surfboard flow thickness, 45 ft^3/ft, Test 6.

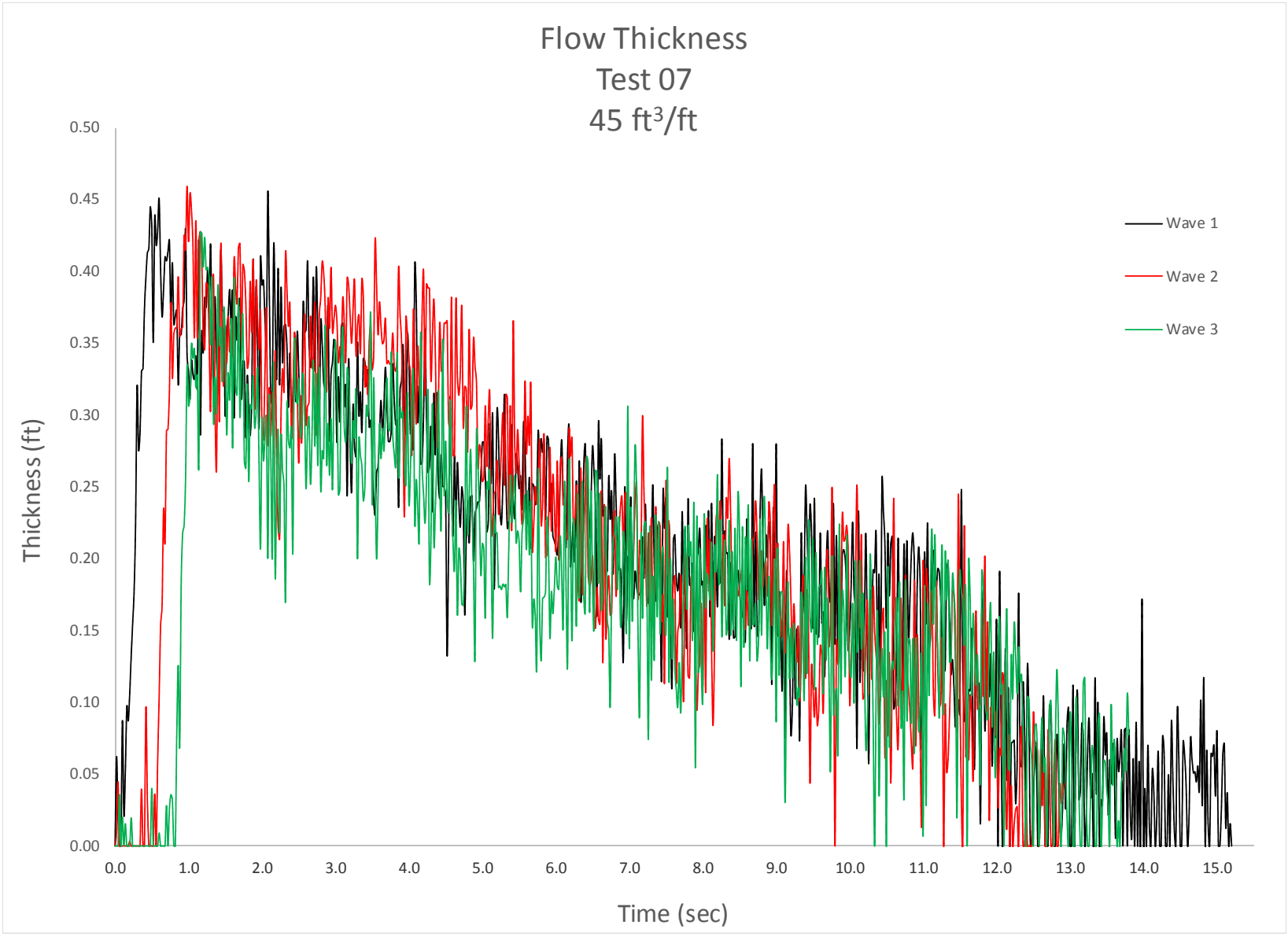

Figure C-17. Crest surfboard flow thickness, 45 ft^3/ft, Test 7.

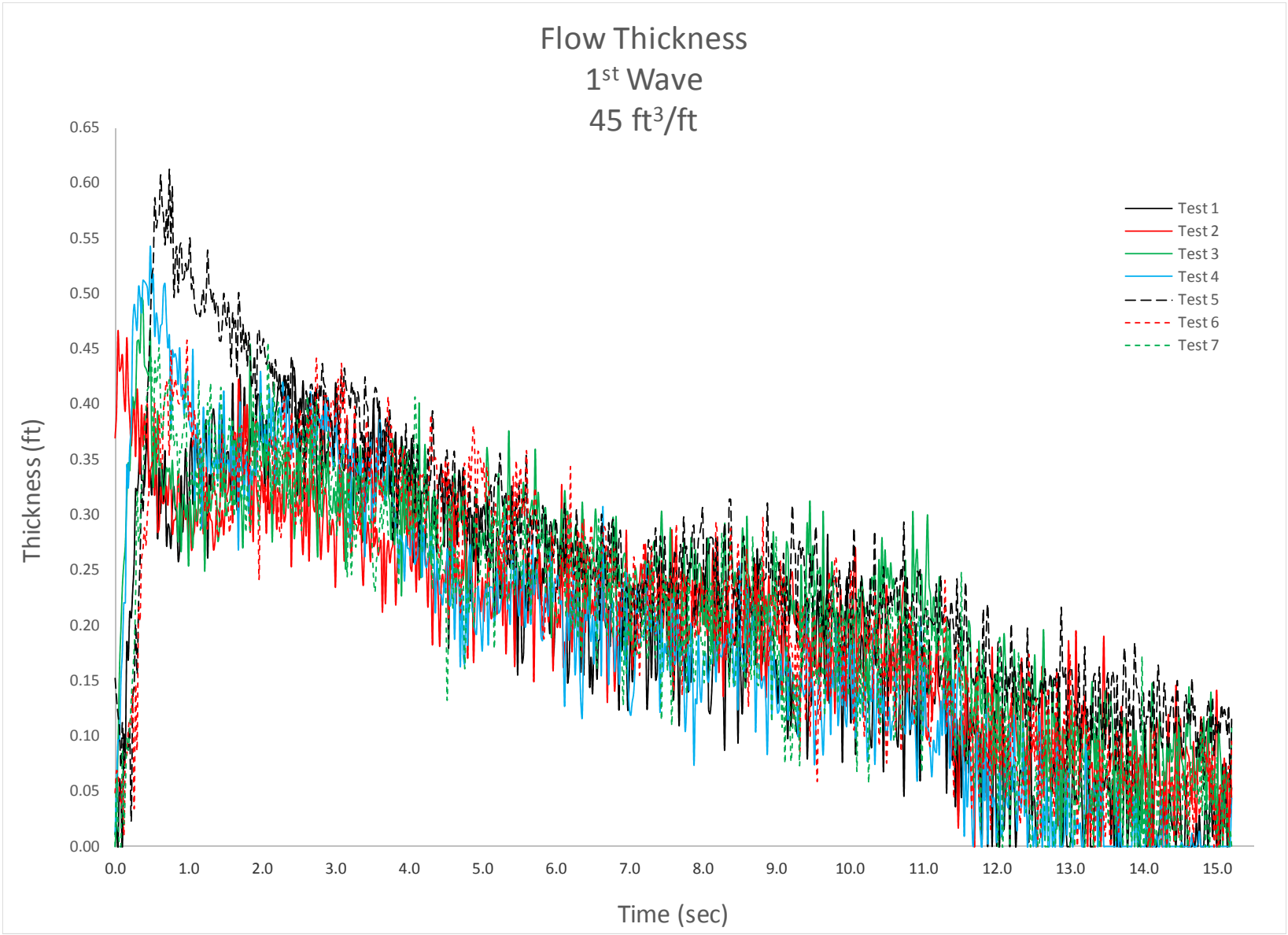

Figure C-18. Crest surfboard flow thickness, 45 ft^3/ft, 1st wave, all tests.

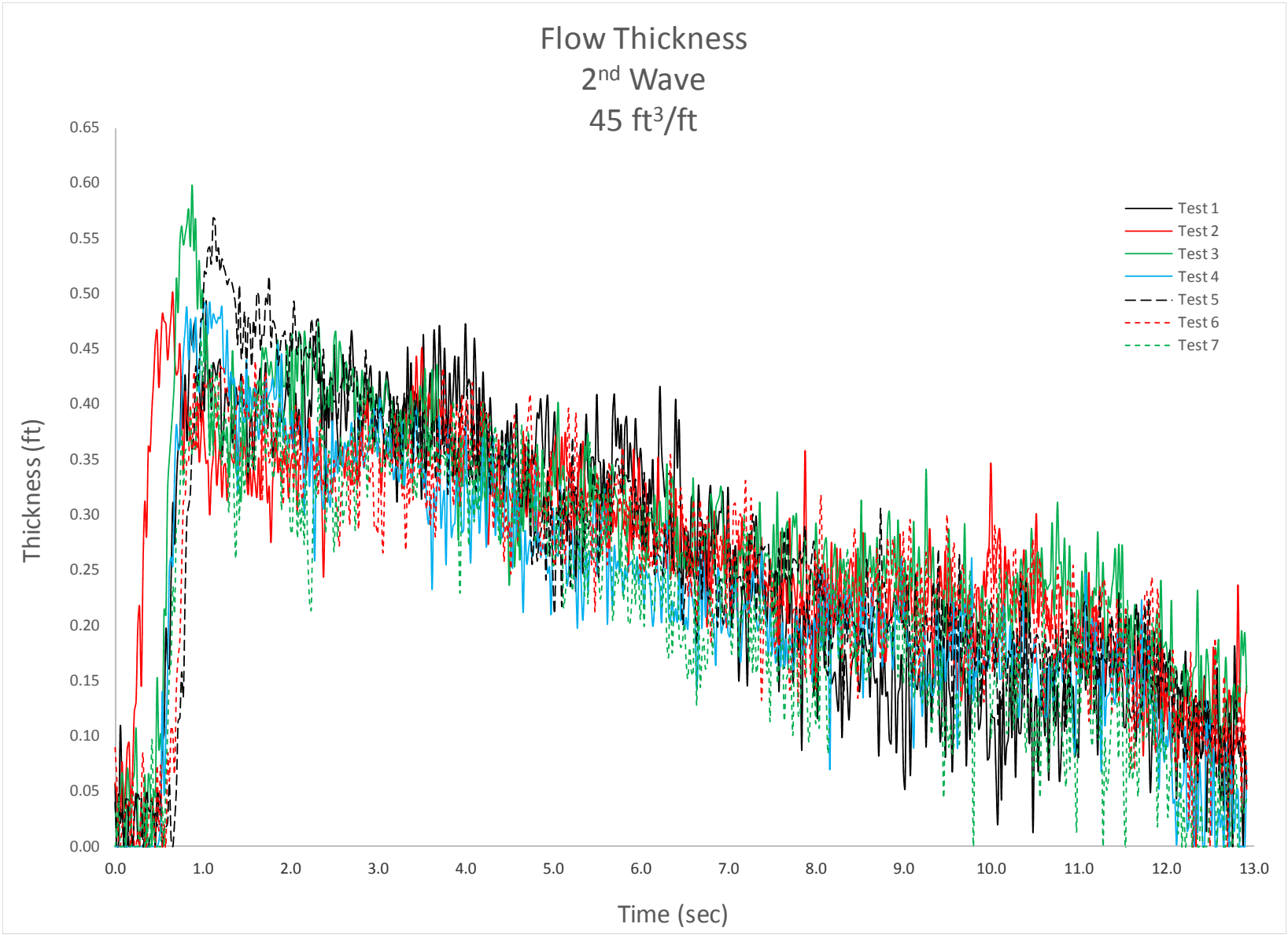

Figure C-19. Crest surfboard flow thickness, 45 ft^3/ft, 2nd wave, all tests.

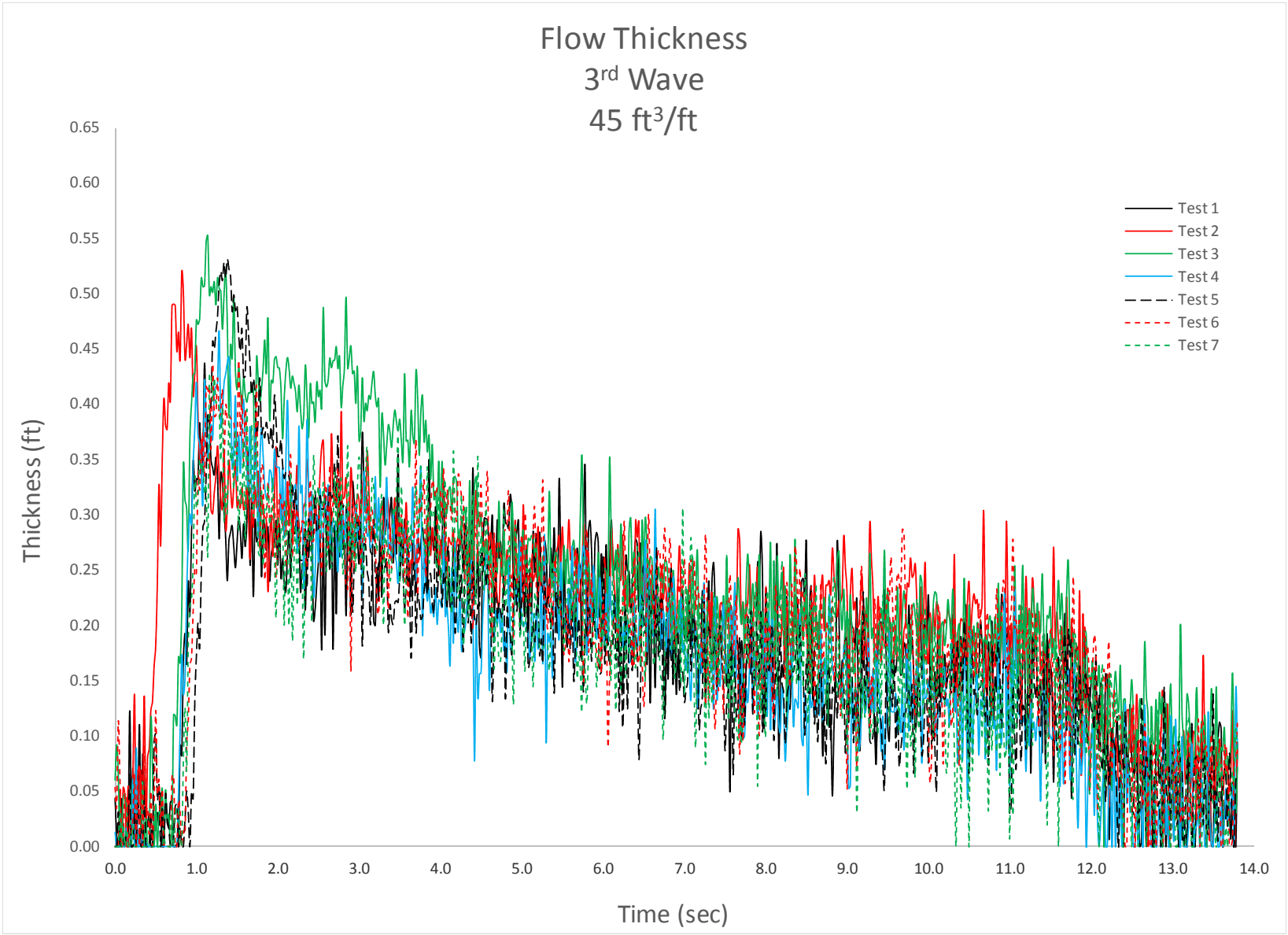

Figure C-20. Crest surfboard flow thickness, 45 ft^3/ft, 3rd wave, all tests.

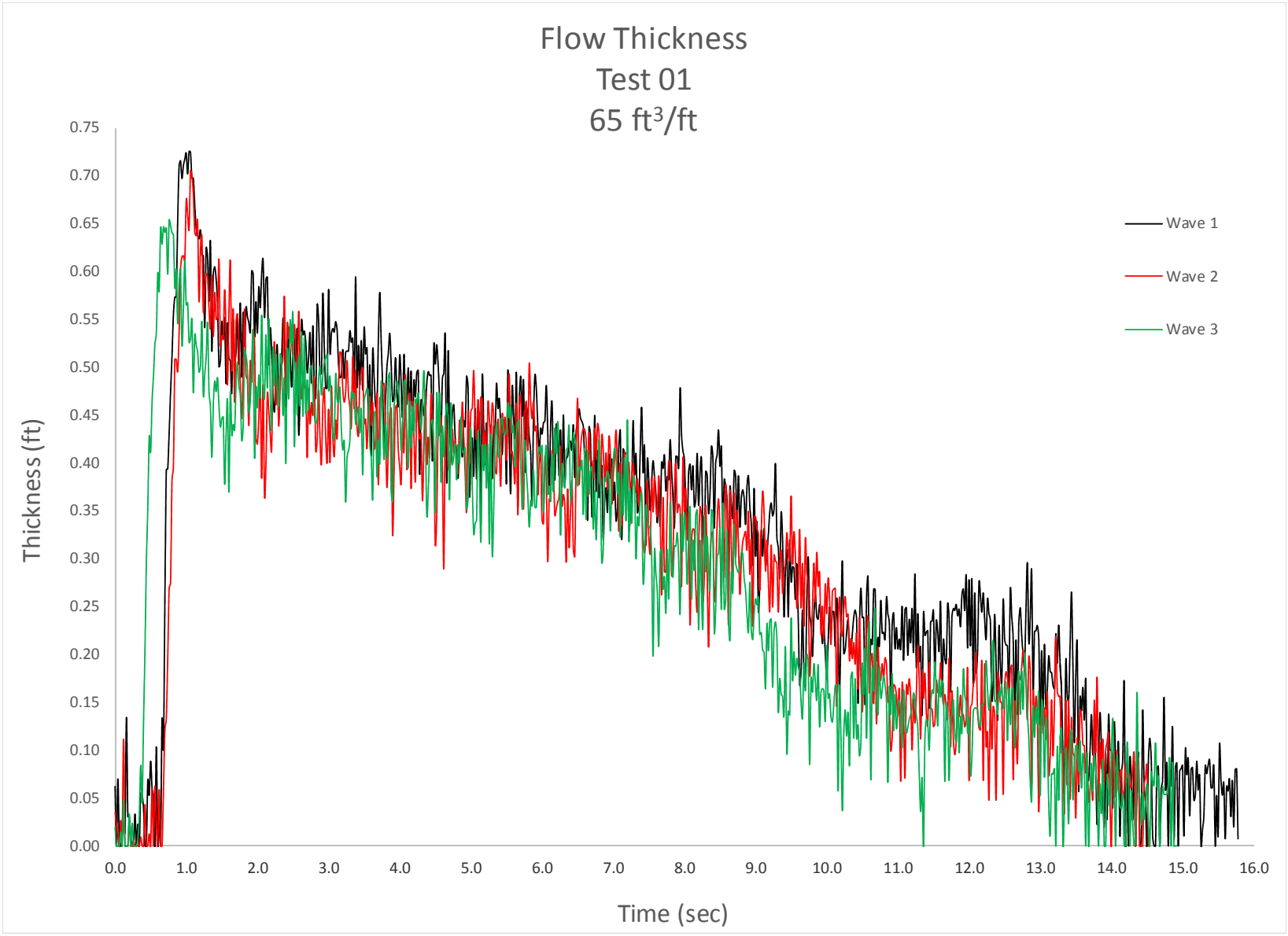

Figure C-21. Crest surfboard flow thickness, 65 ft^3/ft, Test 1.

Figure C-22. Crest surfboard flow thickness, 65 ft^3/ft, Test 2.

Figure C-23. Crest surfboard flow thickness, 65 ft^3/ft, Test 3.

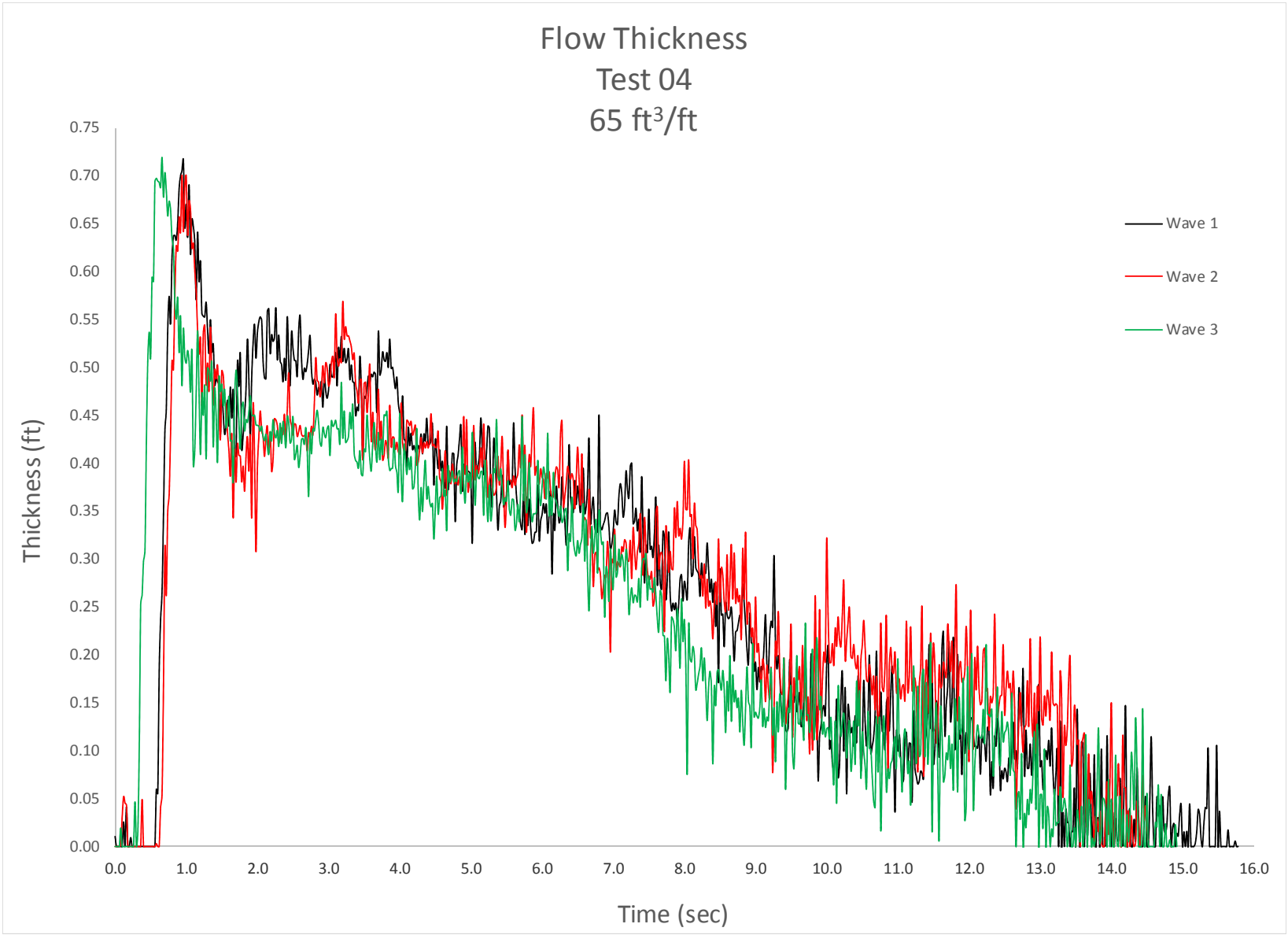

Figure C-24. Crest surfboard flow thickness, 65 ft^3/ft, Test 4.

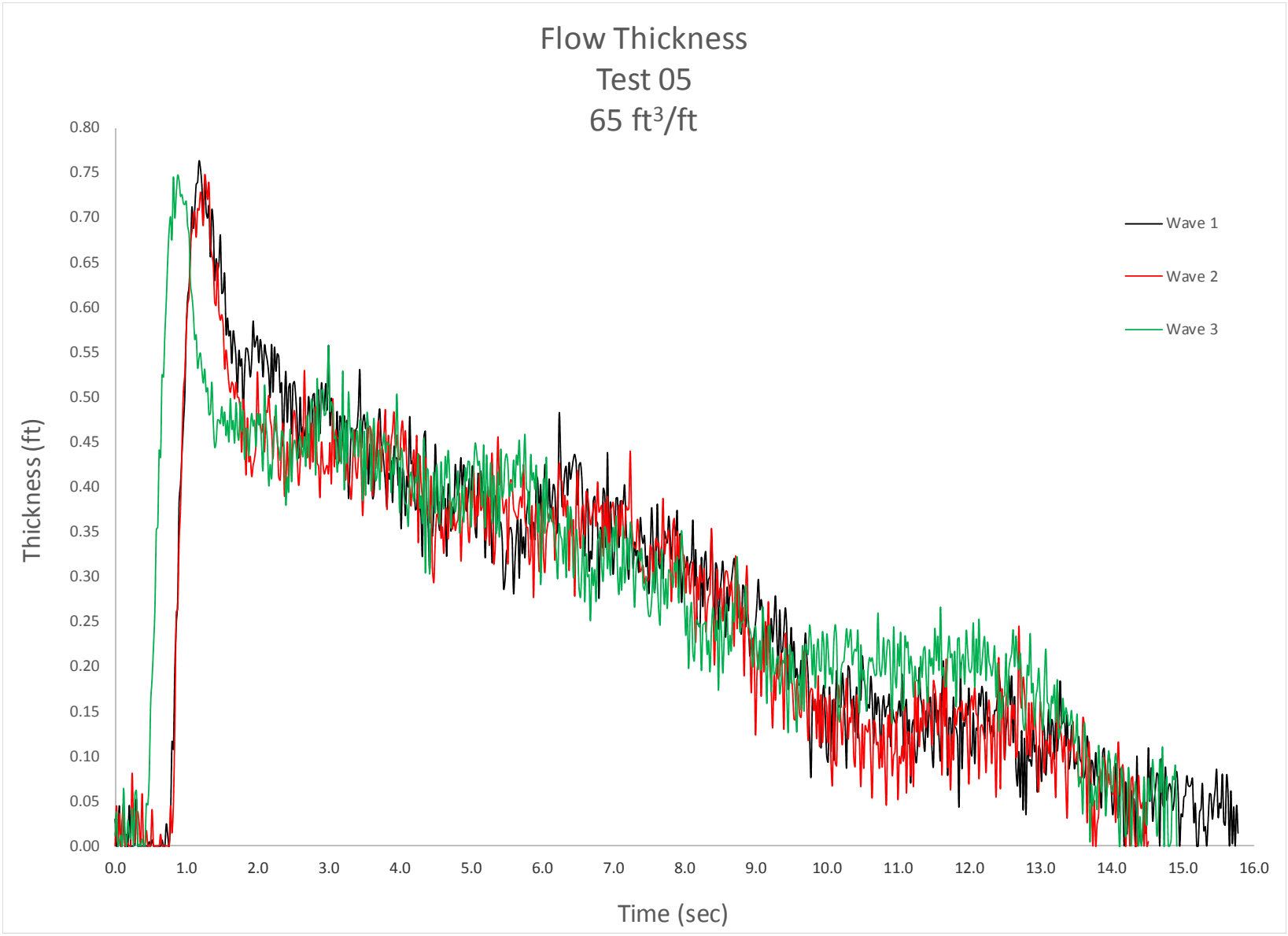

Figure C-25. Crest surfboard flow thickness, 65 ft^3/ft, Test 5.

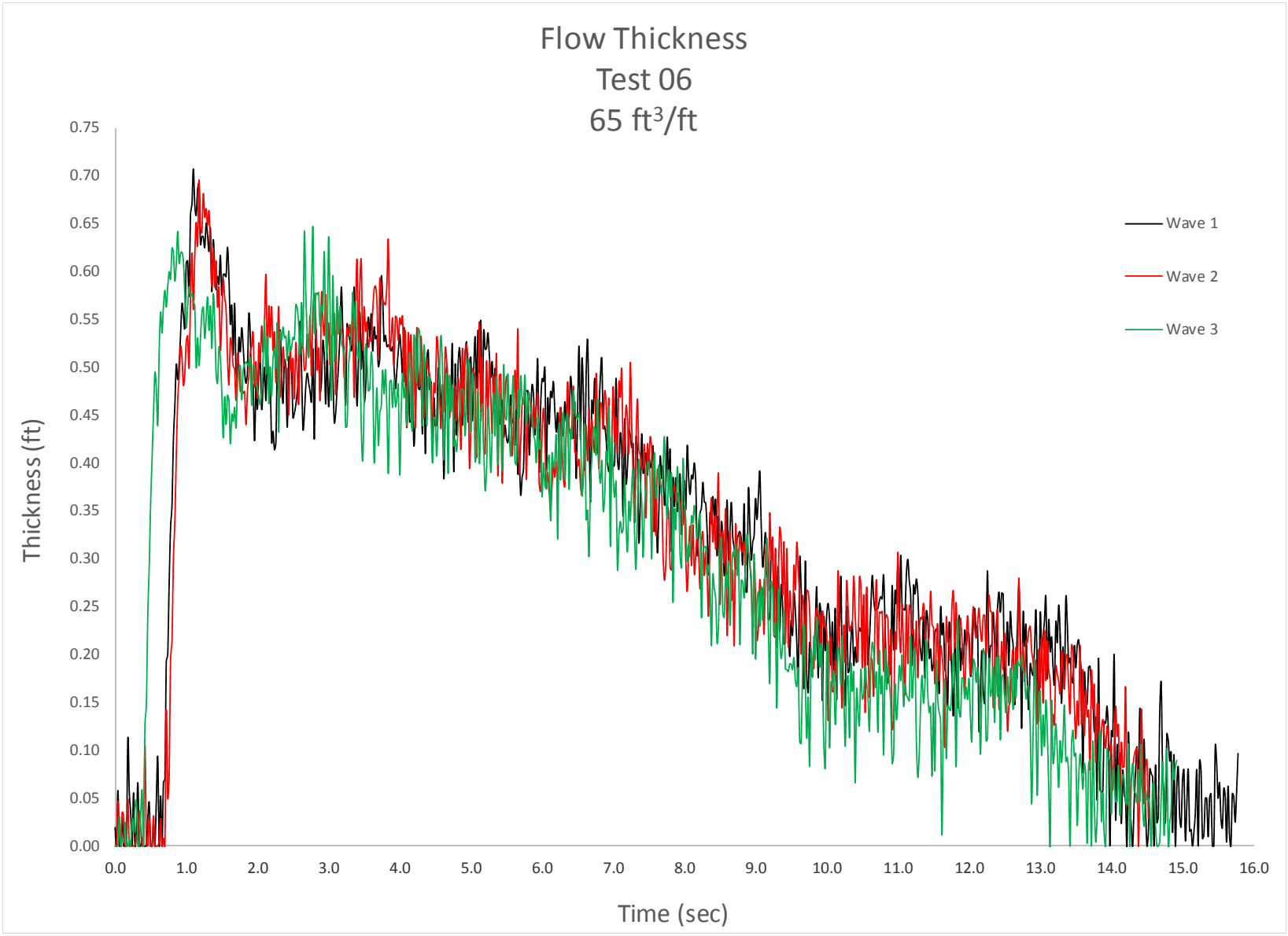

Figure C-26. Crest surfboard flow thickness, 65 ft^3/ft, Test 6.

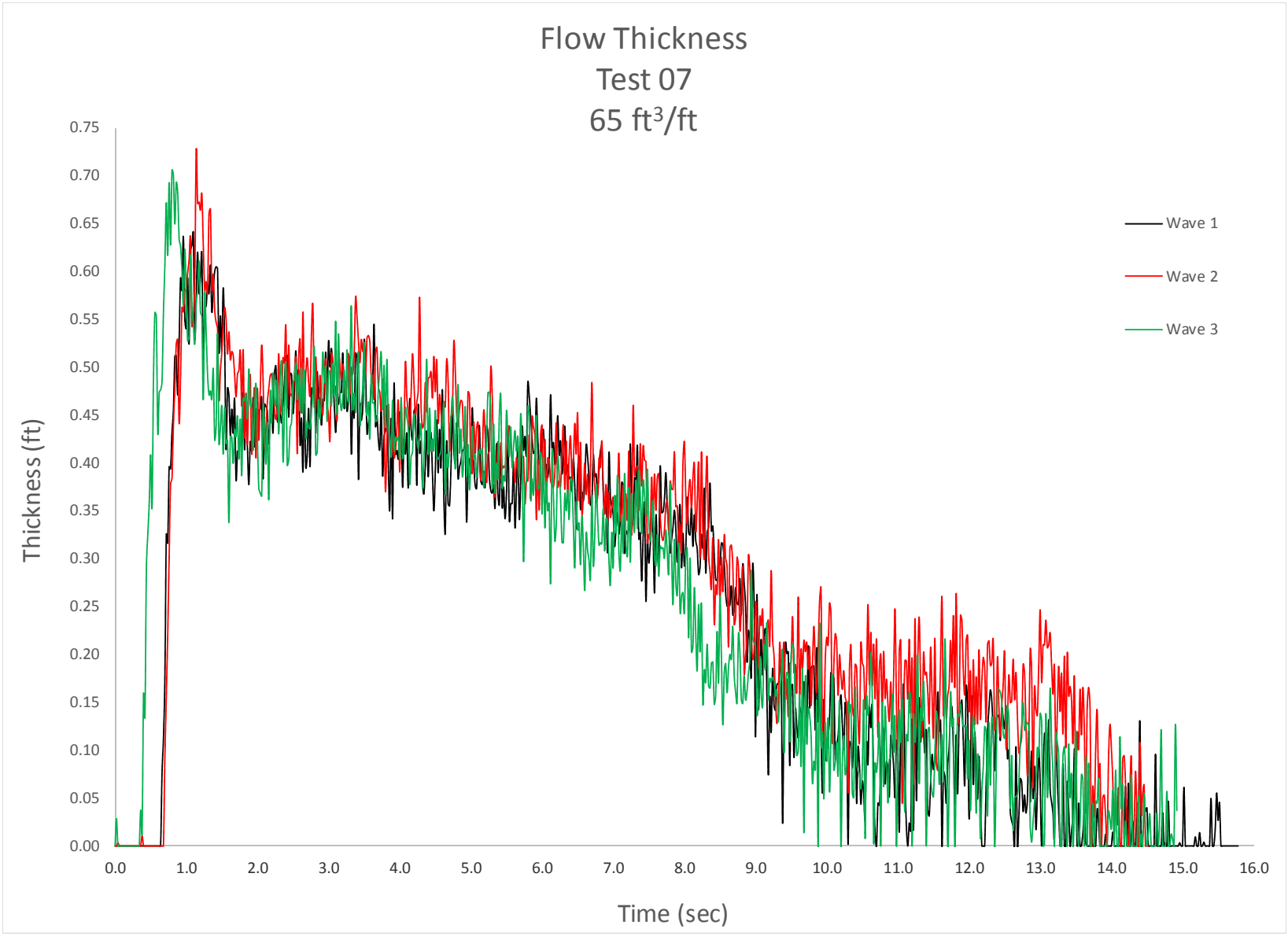

Figure C-27. Crest surfboard flow thickness, 65 ft^3/ft, Test 7.

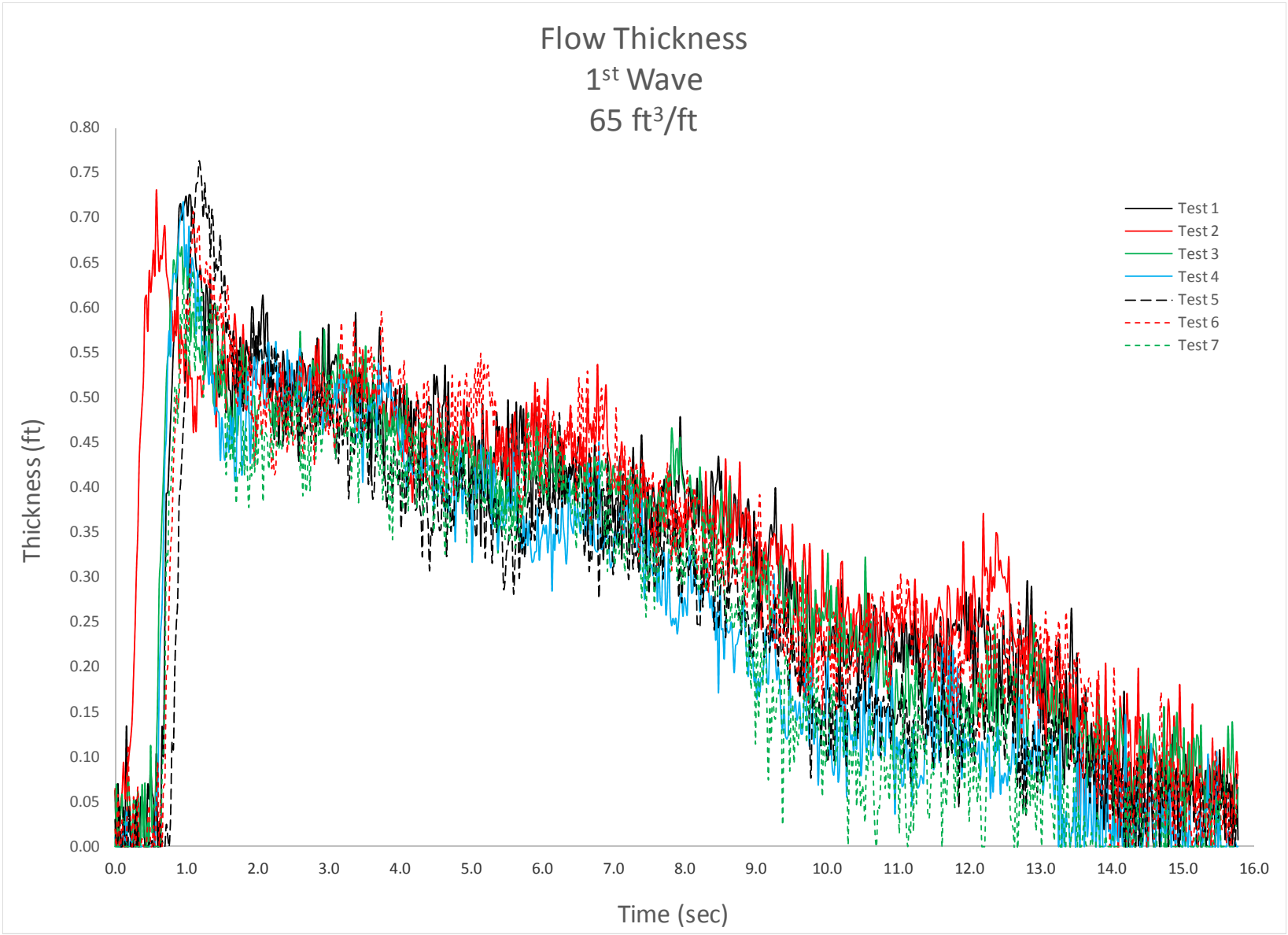

Figure C-28. Crest surfboard flow thickness, 65 ft^3/ft, 1st wave, all tests.

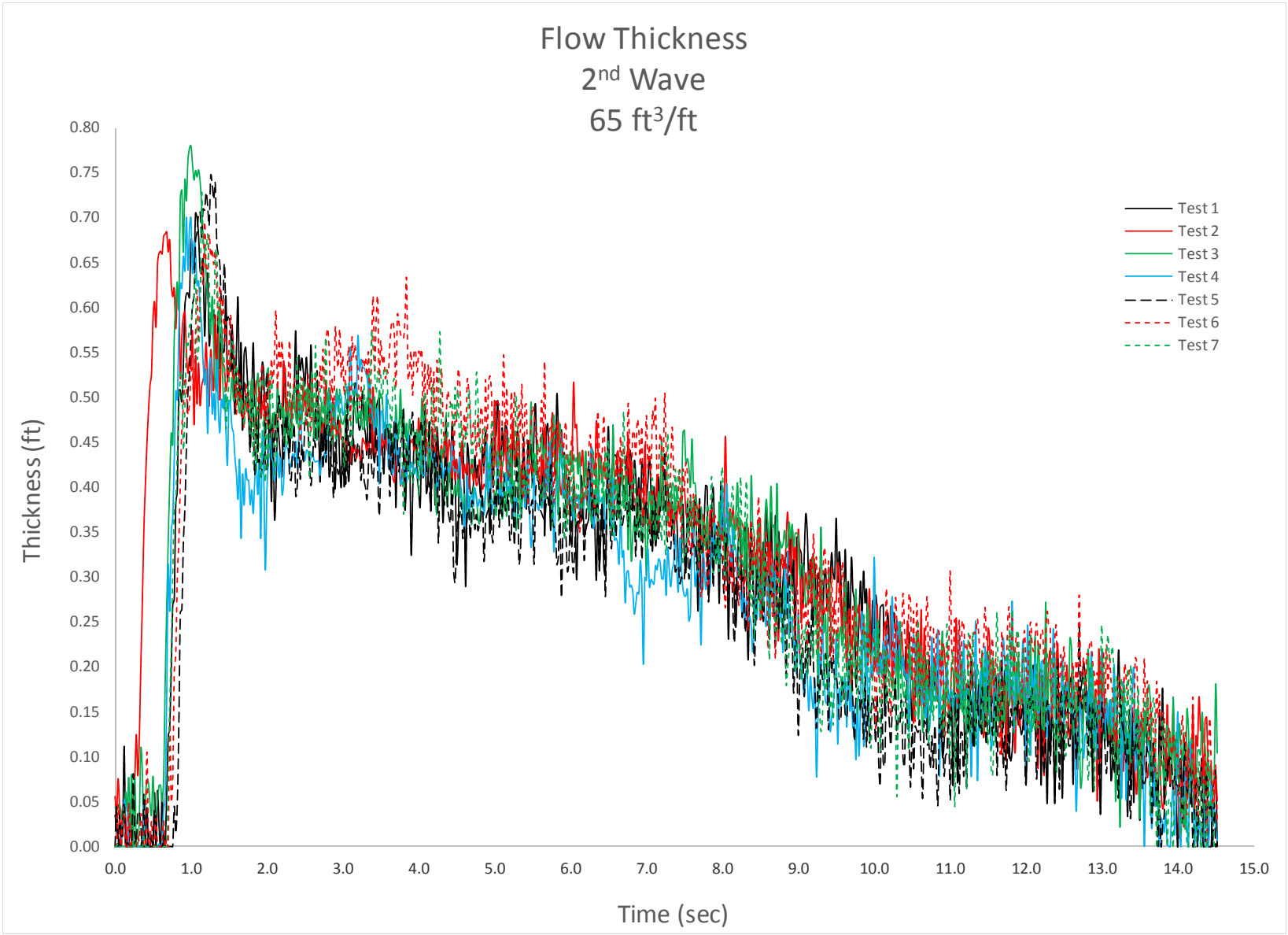

Figure C-29. Crest surfboard flow thickness, 65 ft^3/ft, 2nd wave, all tests.

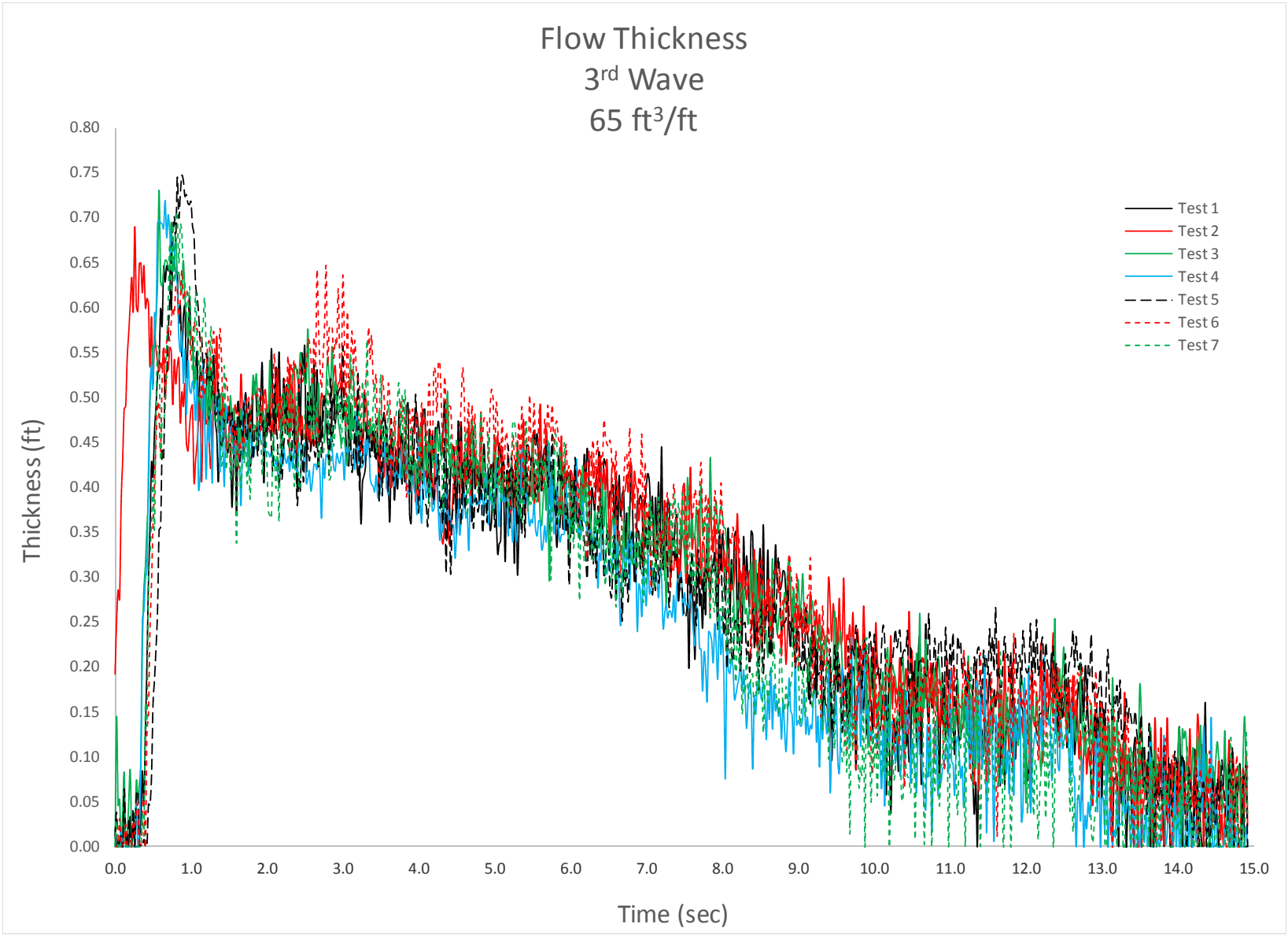

Figure C-30. Crest surfboard flow thickness, 65 ft^3/ft, 3rd wave, all tests.

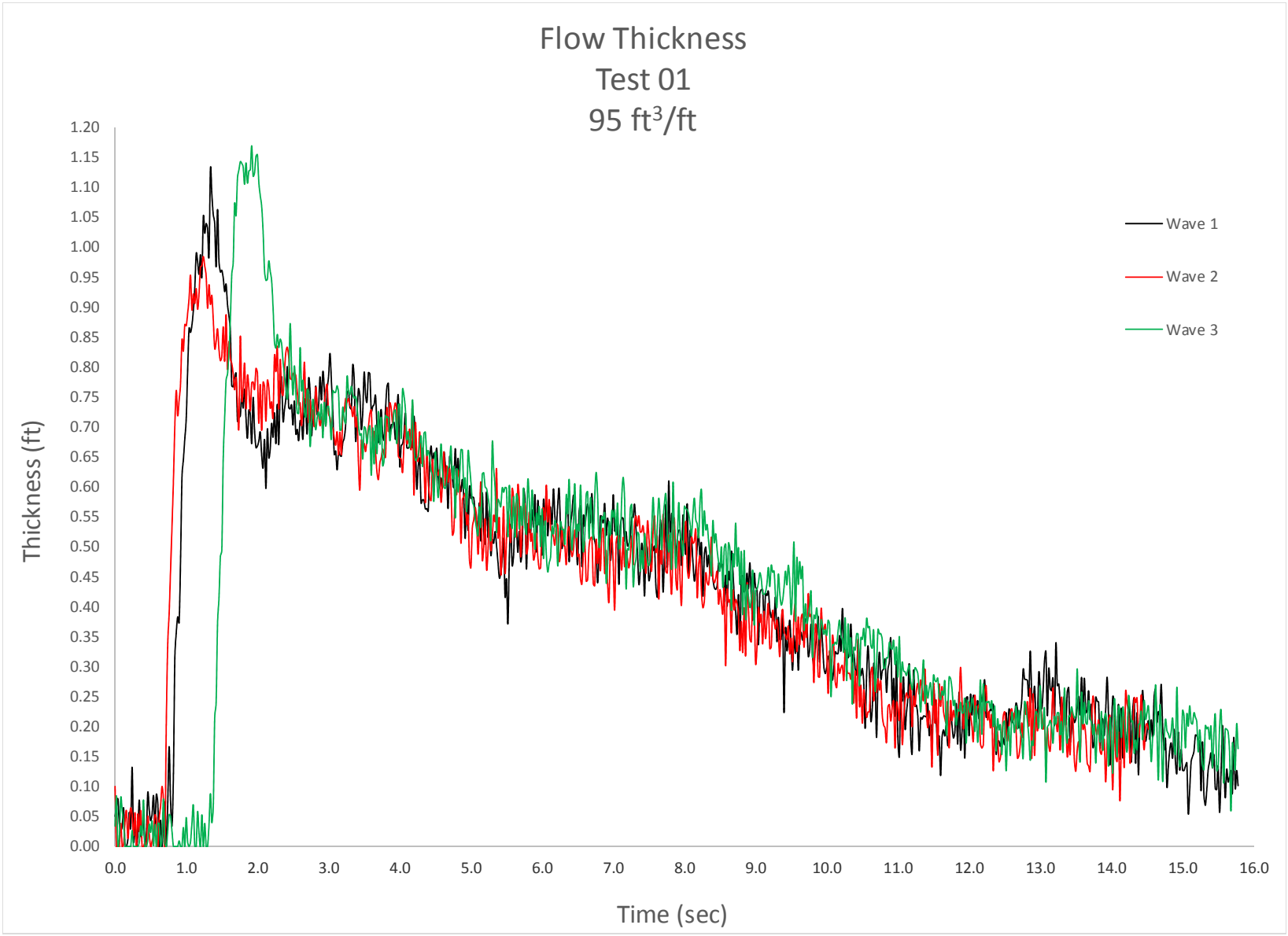

Figure C-31. Crest surfboard flow thickness, 95 ft^3/ft, Test 1.

Figure C-32. Crest surfboard flow thickness, 95 ft^3/ft, Test 2.

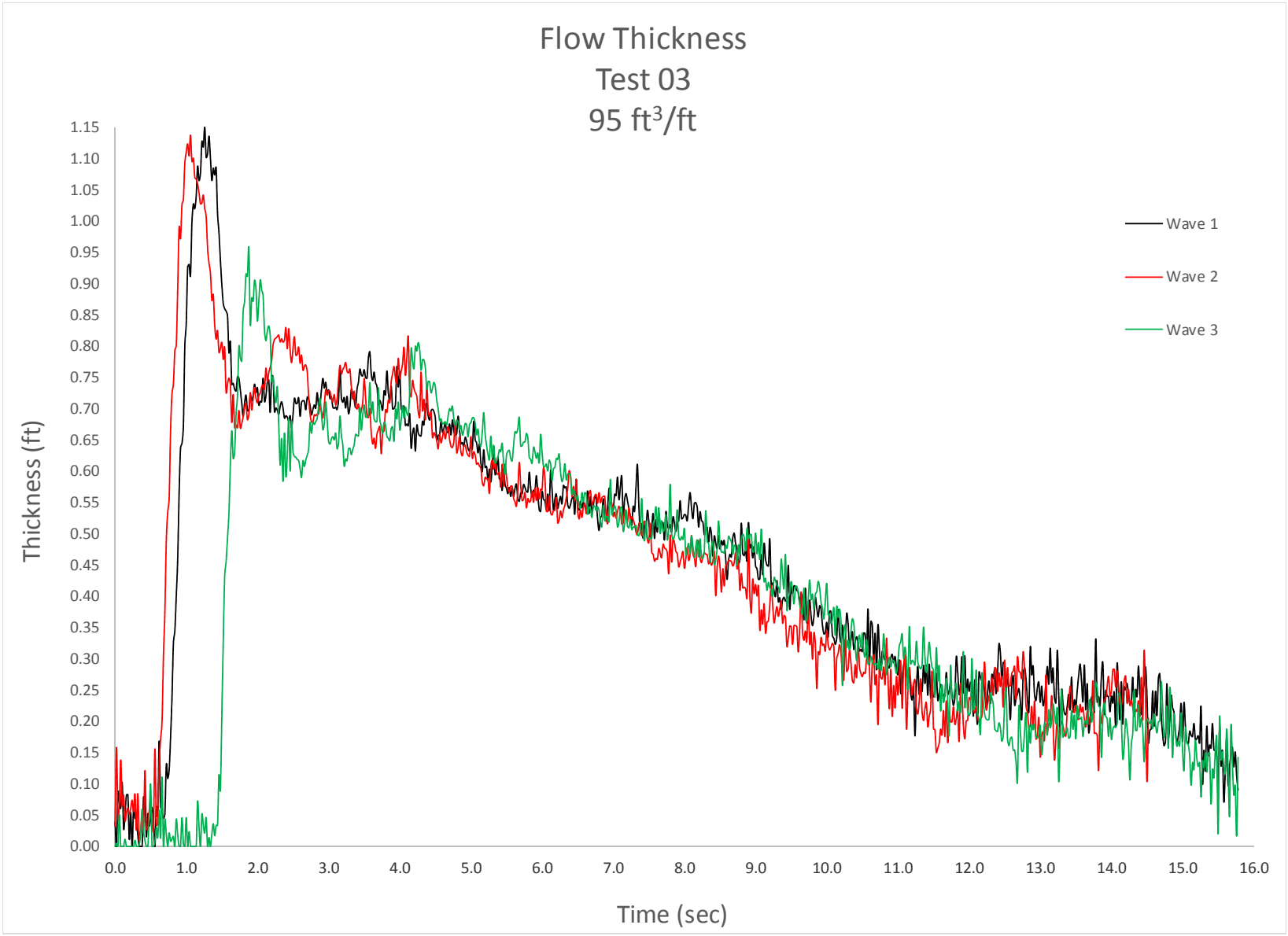

Figure C-33. Crest surfboard flow thickness, 95 ft^3/ft, Test 3.

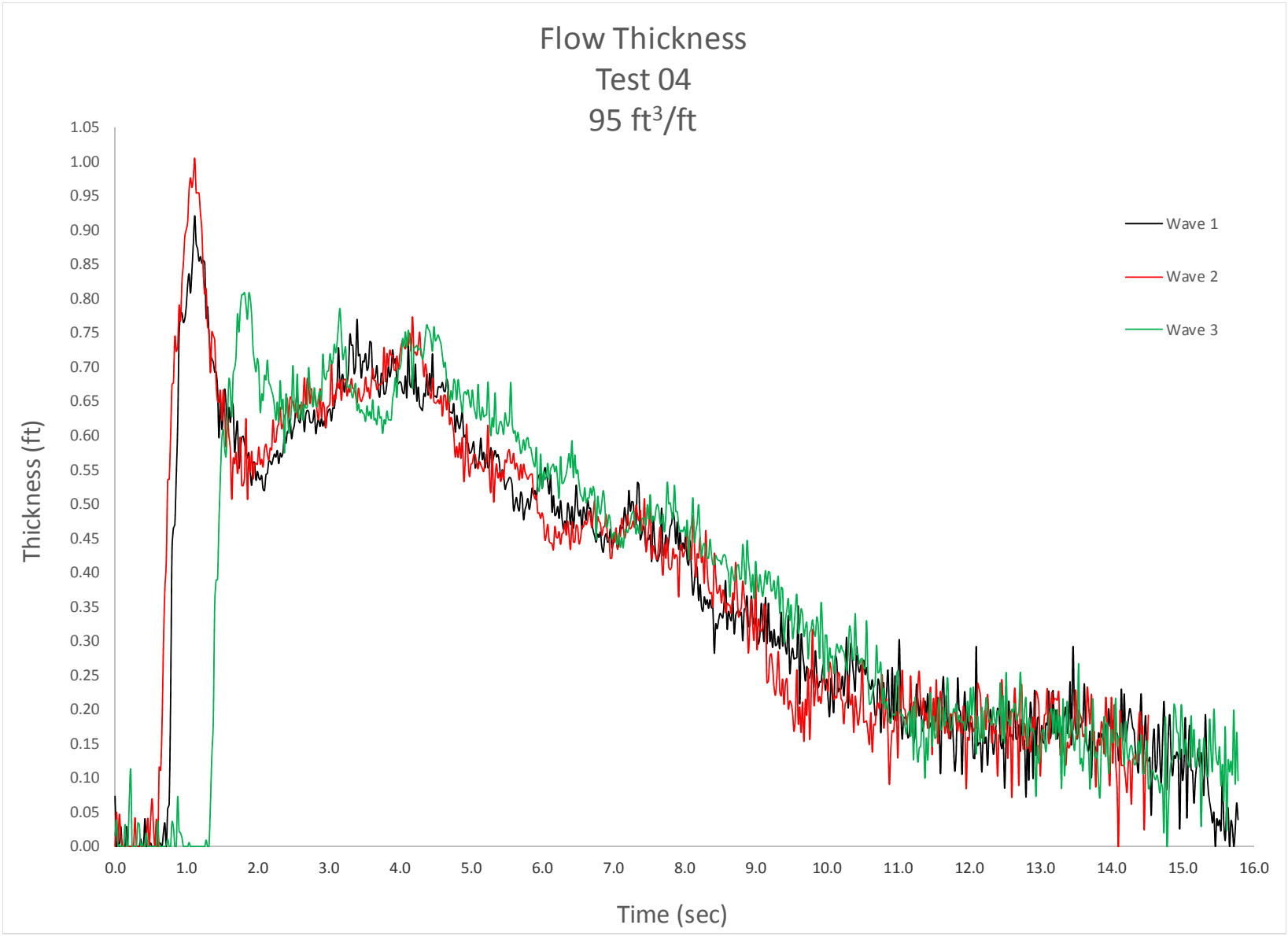

Figure C-34. Crest surfboard flow thickness, 95 ft^3/ft, Test 4.

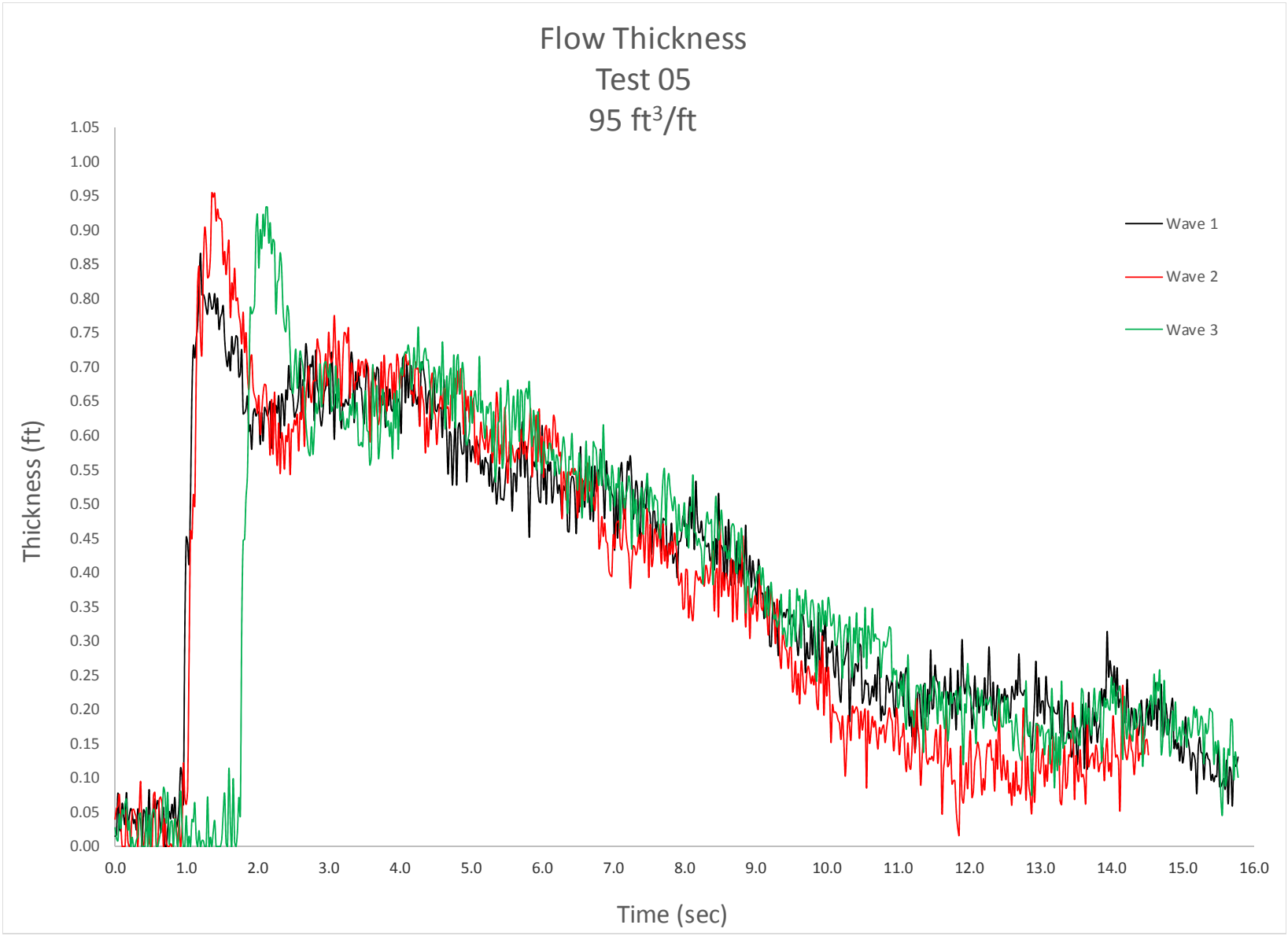

Figure C-35. Crest surfboard flow thickness, 95 ft^3/ft, Test 5.

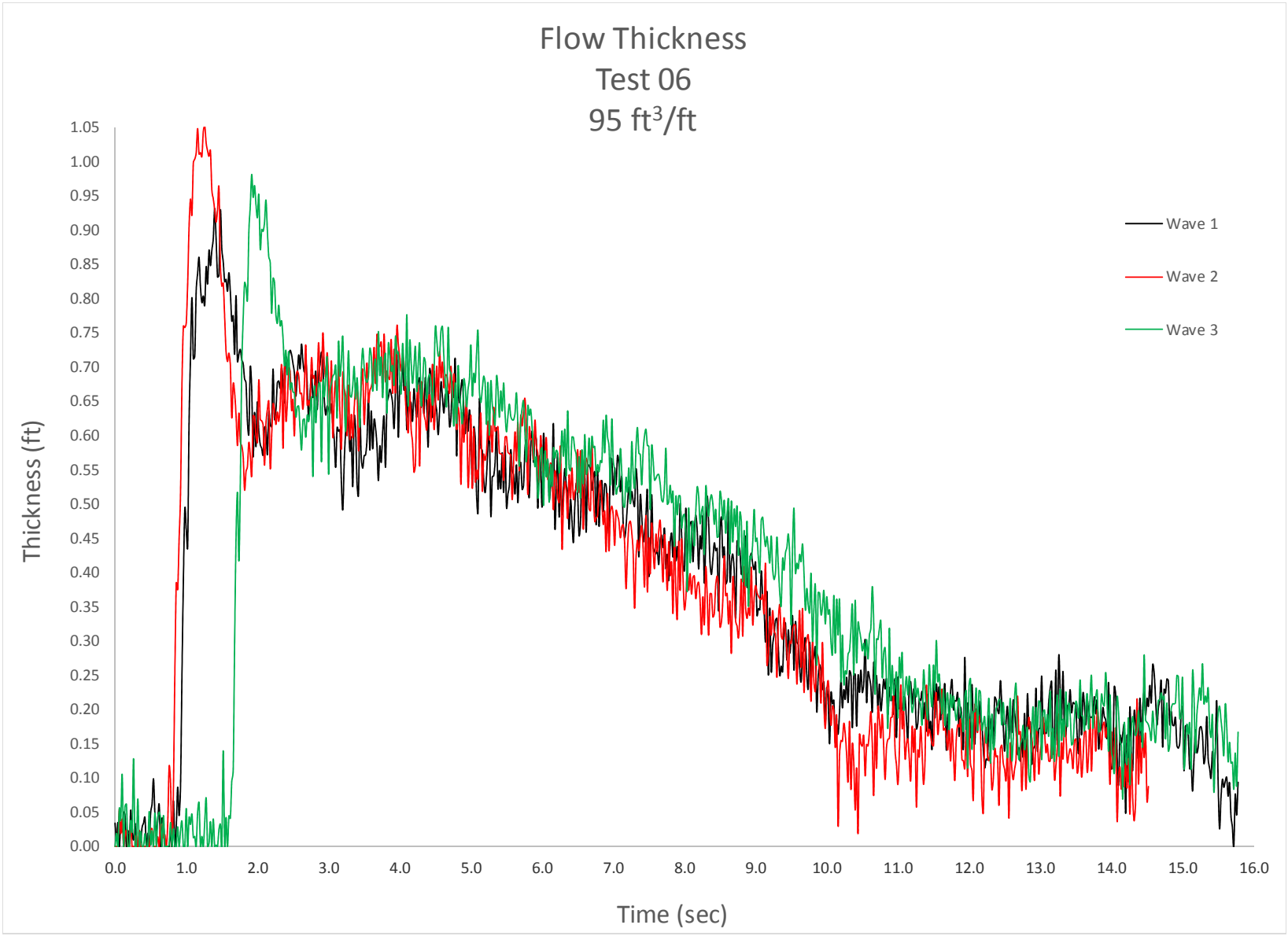

Figure C-36. Crest surfboard flow thickness, 95 ft^3/ft, Test 6.

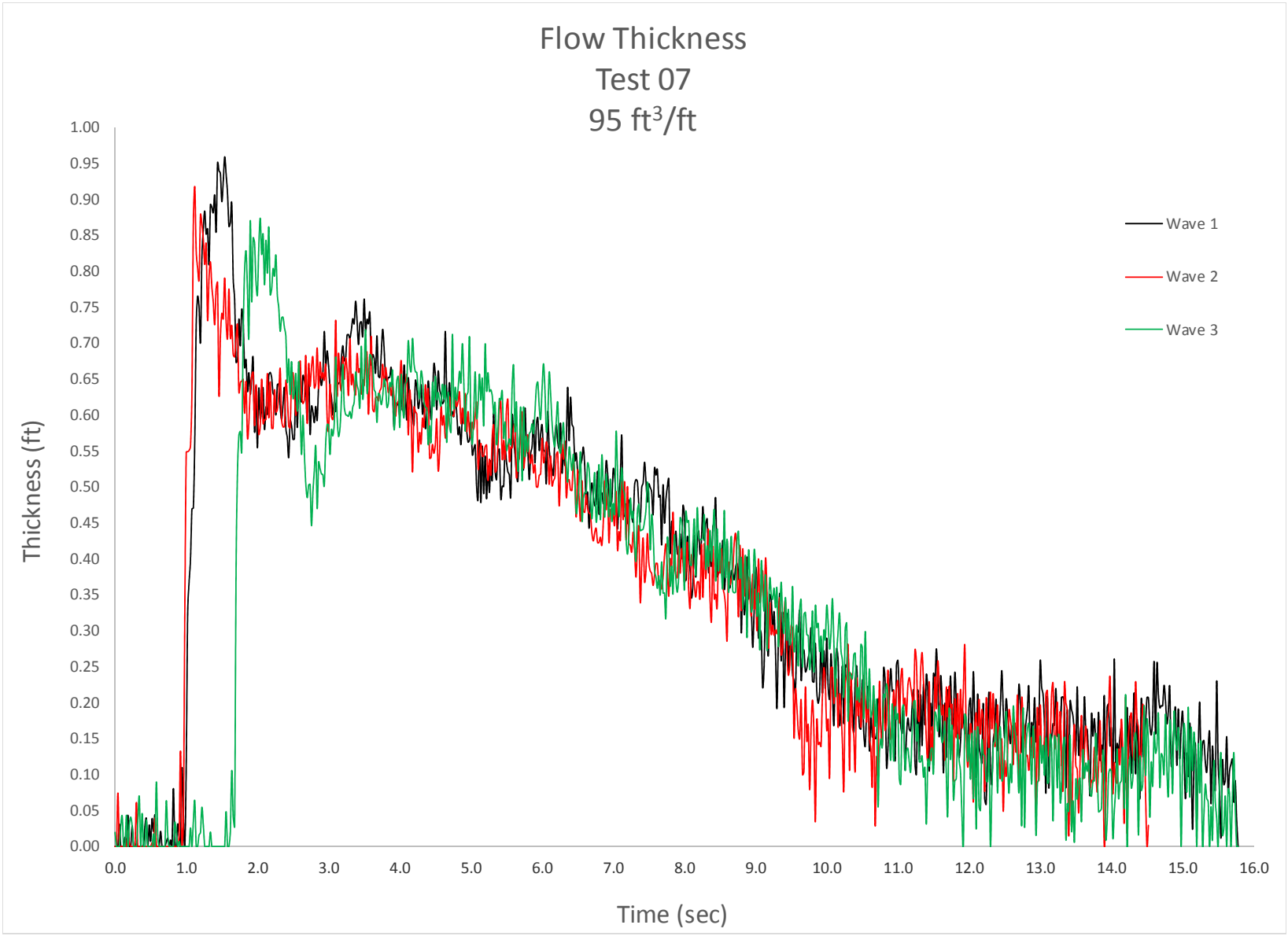

Figure C-37. Crest surfboard flow thickness, 95 ft^3/ft, Test 7.

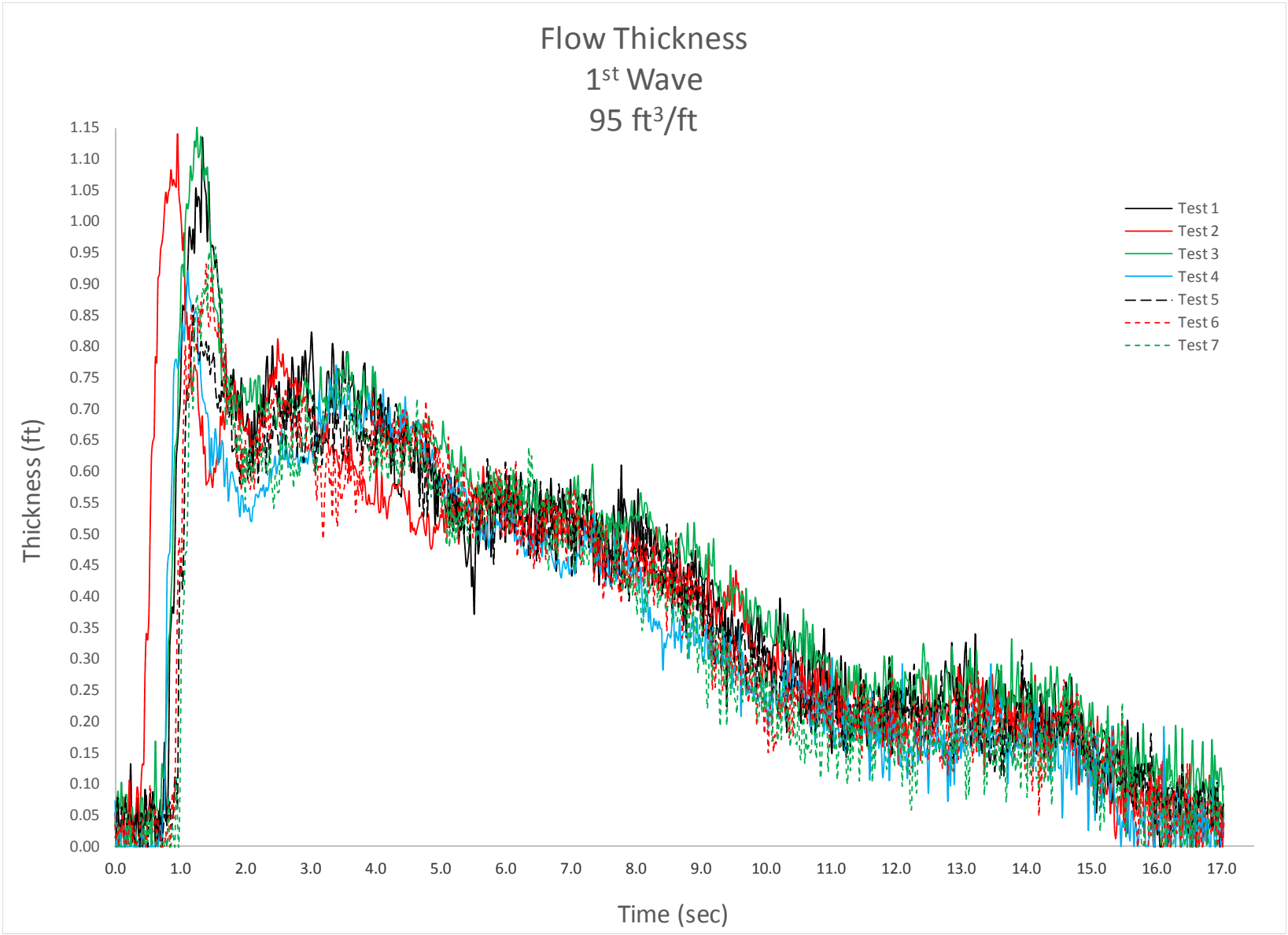

Figure C-38. Crest surfboard flow thickness, 125 ft^3/ft, 1st wave, all tests.

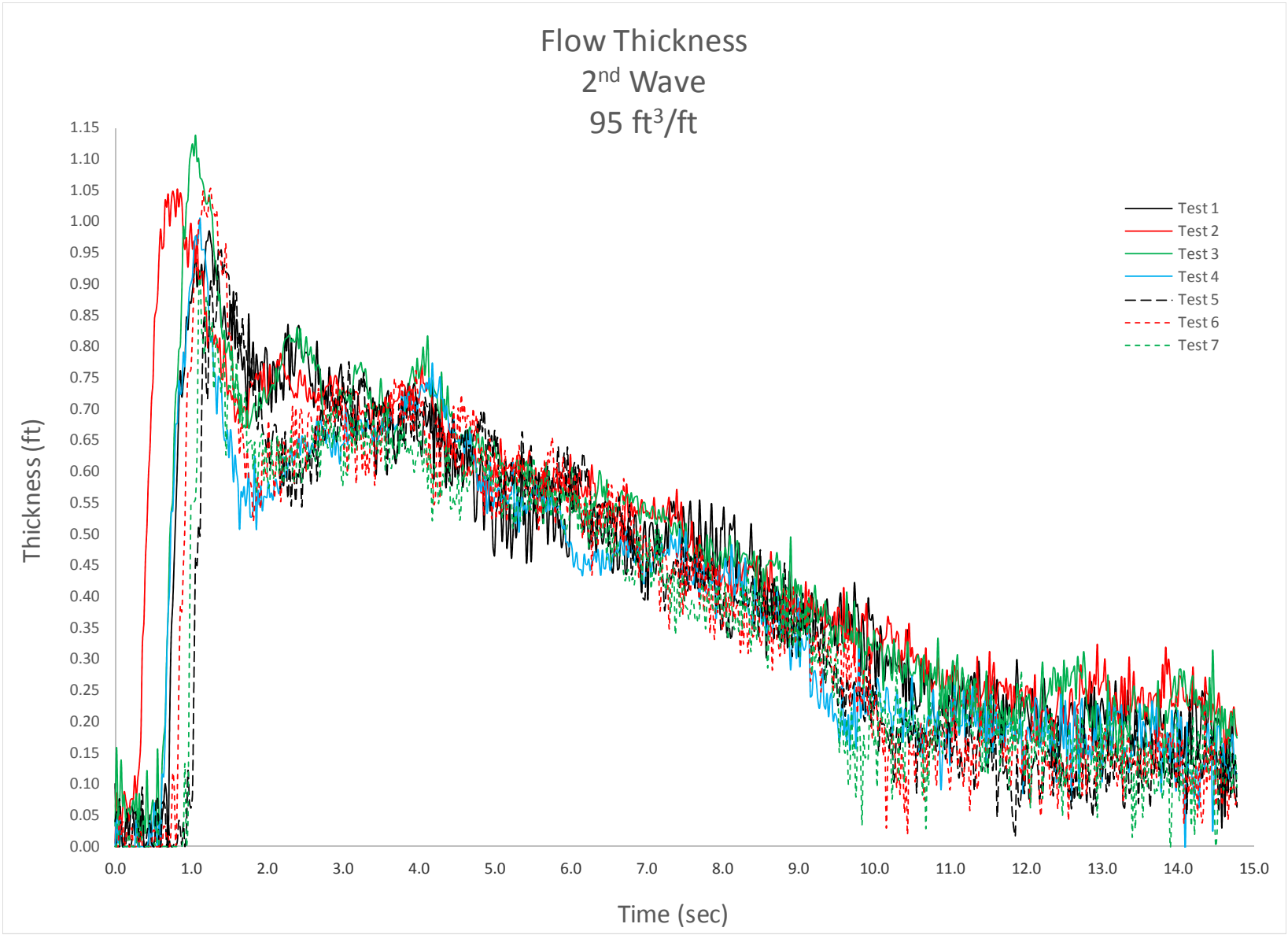

Figure C-39. Crest surfboard flow thickness, 125 ft^3/ft, 2nd wave, all tests.

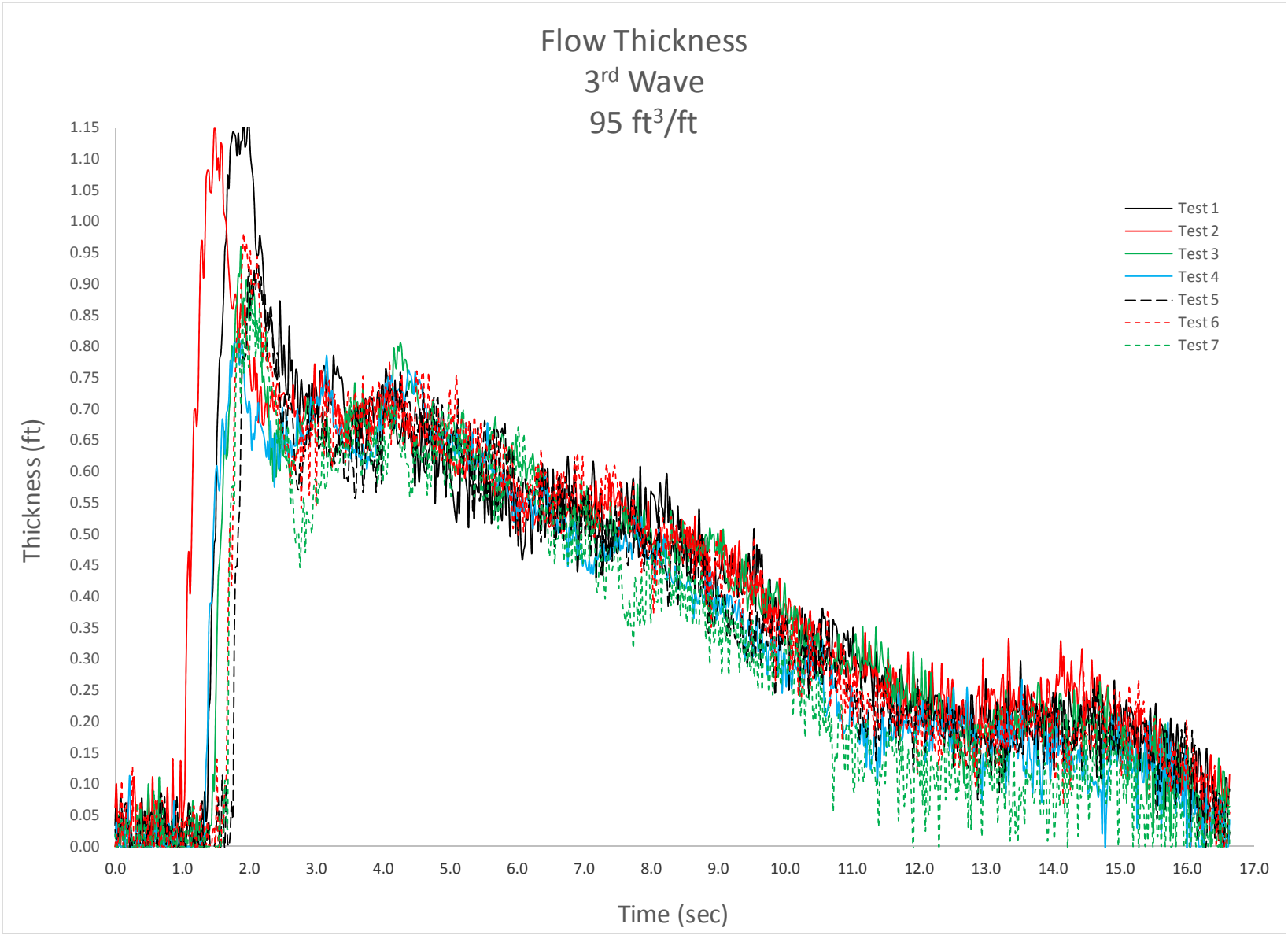

Figure C-40. Crest surfboard flow thickness, 125 ft^3/ft, 3rd wave, all tests.

Figure C-41. Crest surfboard flow thickness, 125 ft^3/ft, Test 1.

Figure C-42. Crest surfboard flow thickness, 125 ft^3/ft, Test 2.

Figure C-43. Crest surfboard flow thickness, 125 ft^3/ft, Test 3.

Figure C-44. Crest surfboard flow thickness, 125 ft^3/ft, Test 4.

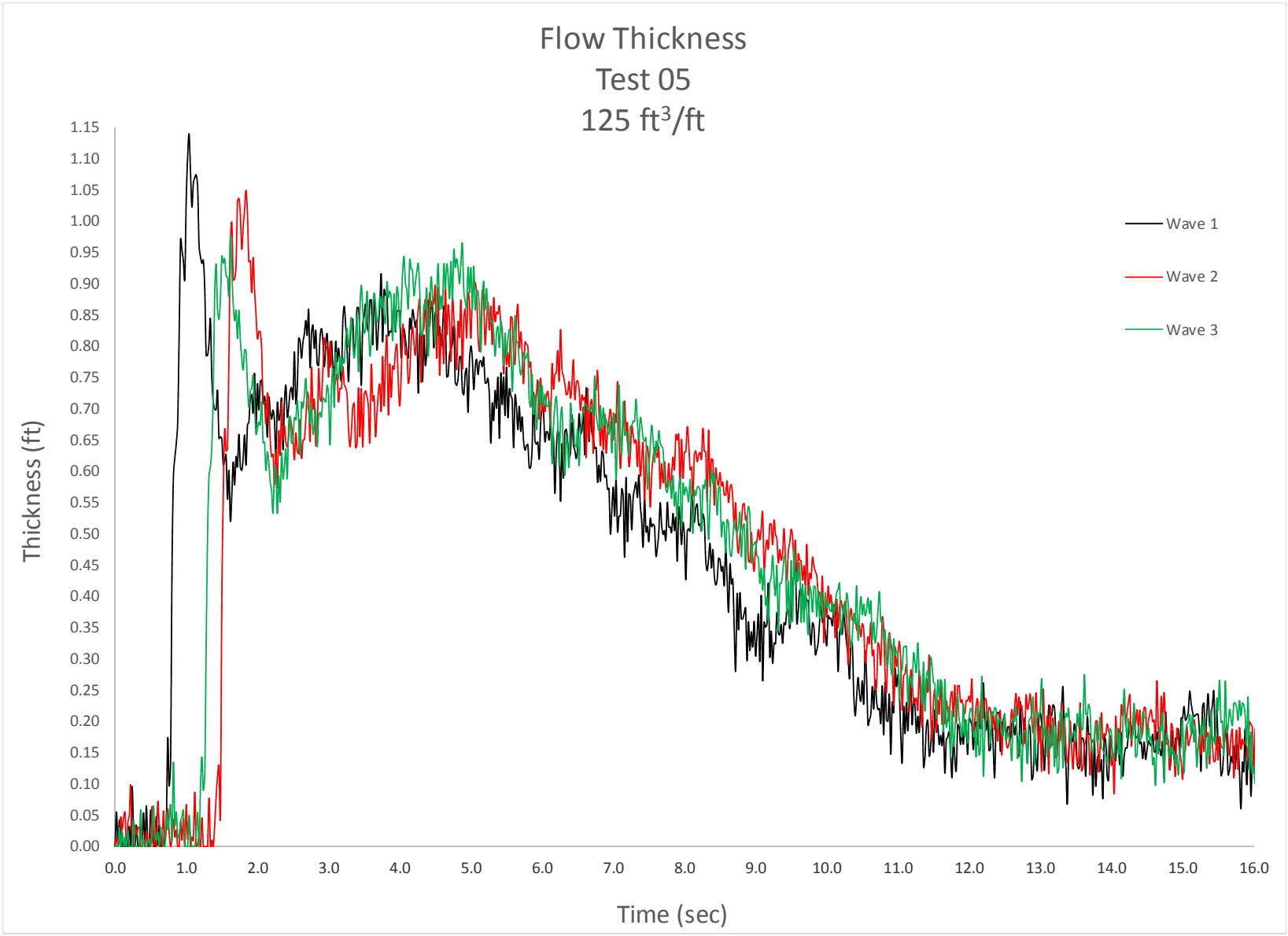

Figure C-45. Crest surfboard flow thickness, 125 ft^3/ft, Test 5.

Figure C-46. Crest surfboard flow thickness, 125 ft^3/ft, Test 6.

Figure C-47. Crest surfboard flow thickness, 125 ft^3/ft, Test 7.

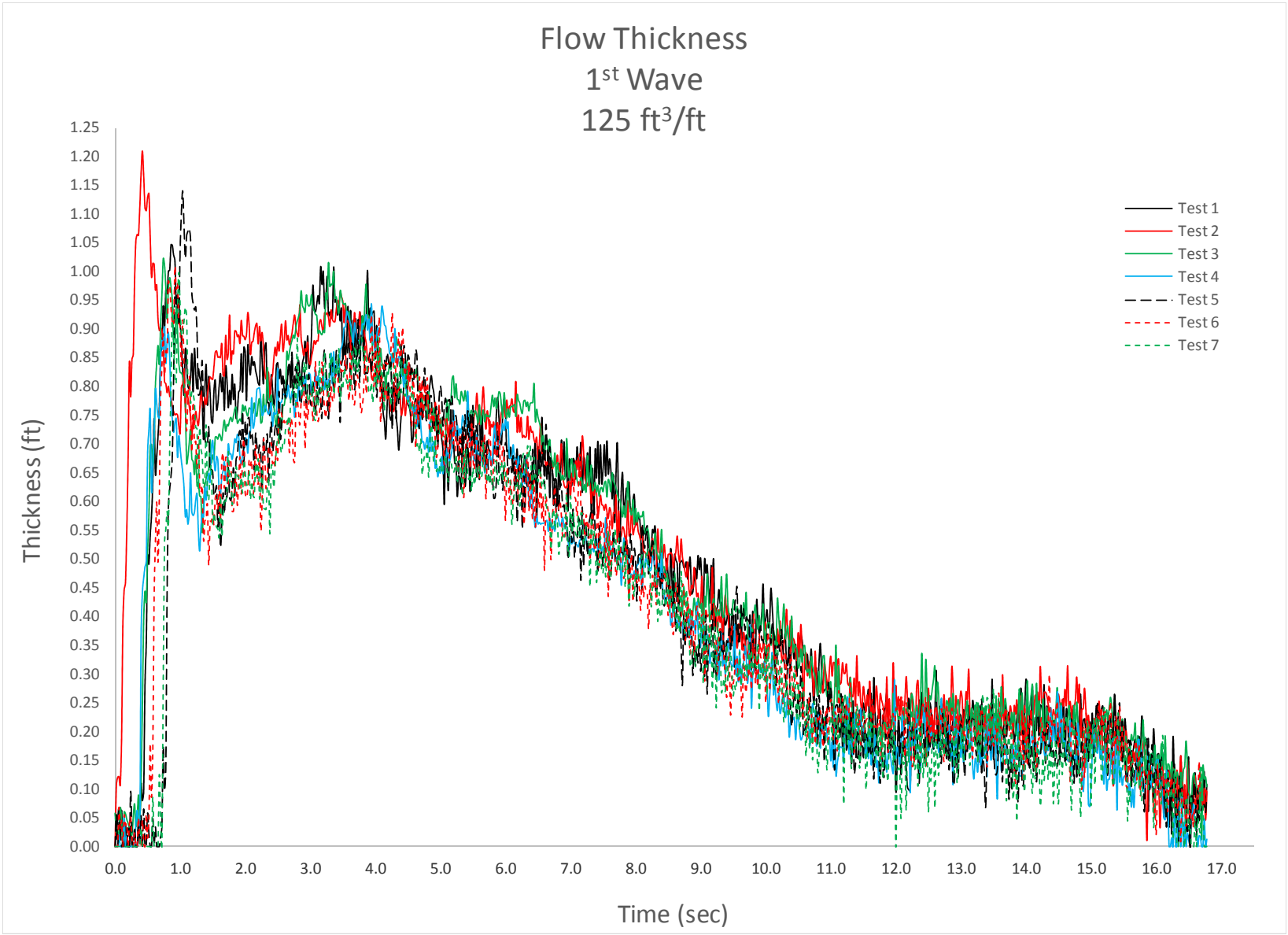

Figure C-48. Crest surfboard flow thickness, 125 ft^3/ft, 1st wave, all tests.

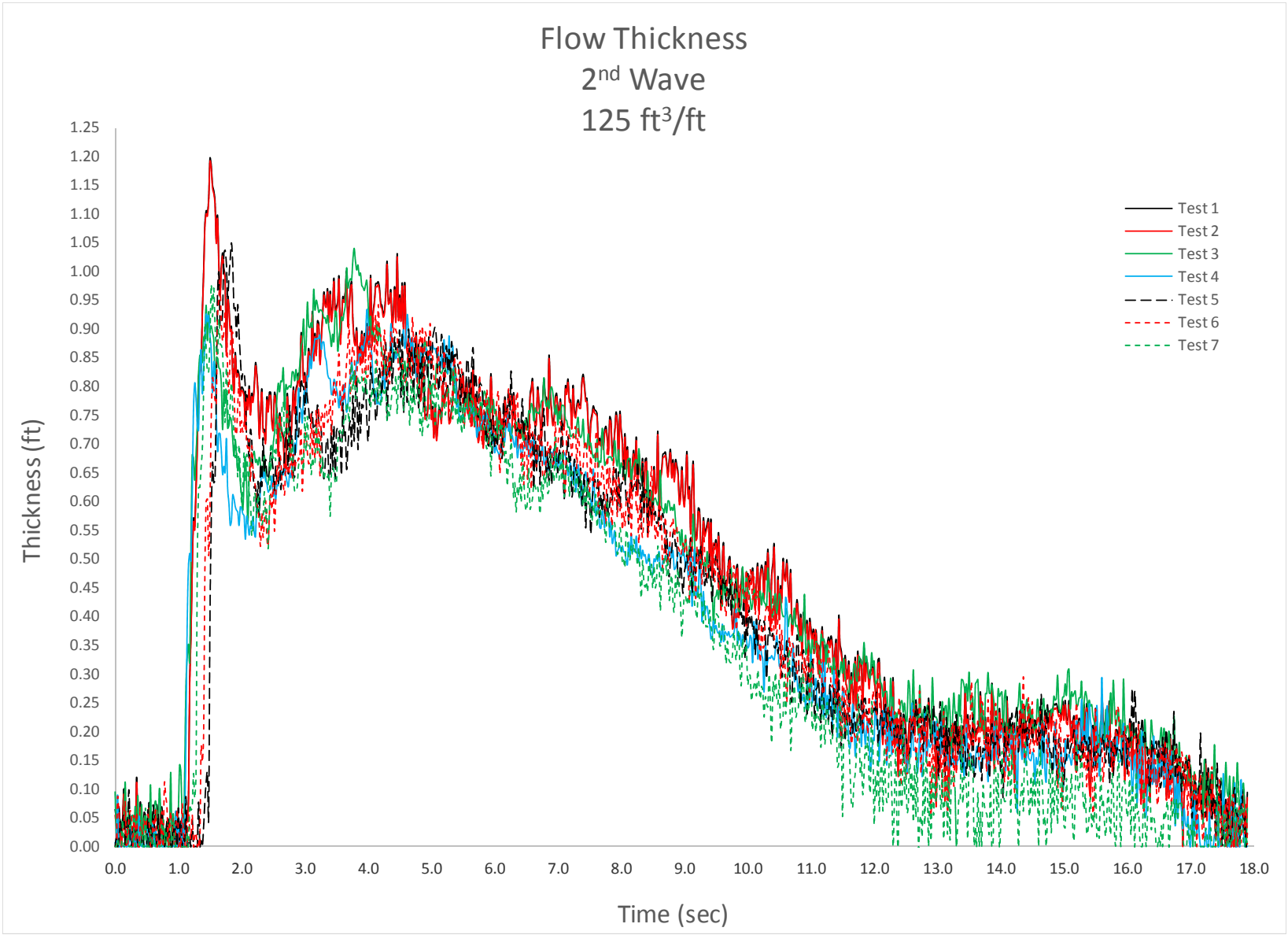

Figure C-49. Crest surfboard flow thickness, 125 ft^3/ft, 2nd wave, all tests.

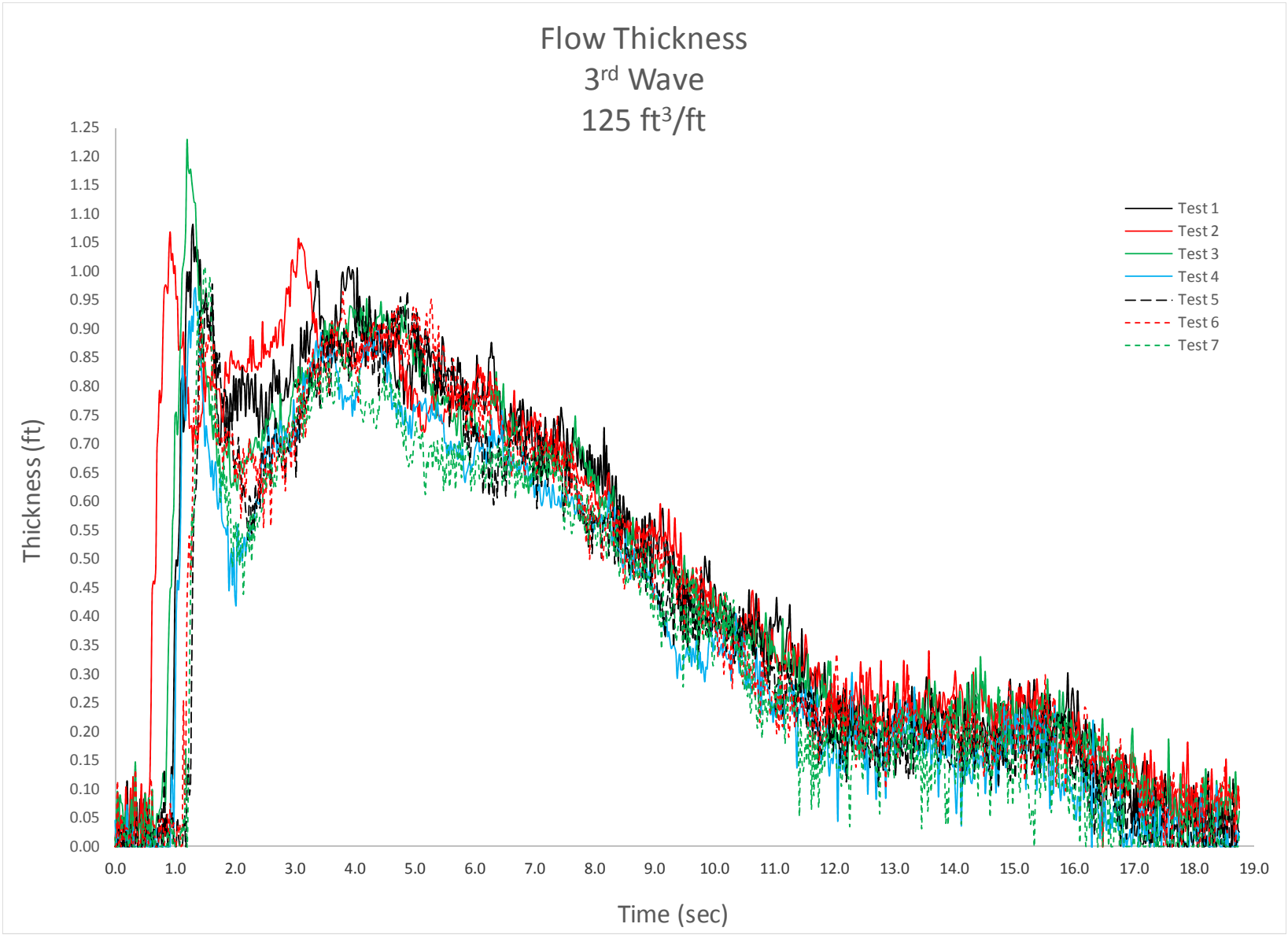

Figure C-50. Crest surfboard flow thickness, 125 ft^3/ft, 3rd wave, all tests.

Figure C-51. Crest surfboard flow thickness, 145 ft^3/ft, Test 1.

Figure C-52. Crest surfboard flow thickness, 145 ft^3/ft, Test 2.

Figure C-53. Crest surfboard flow thickness, 145 ft^3/ft, Test 3.

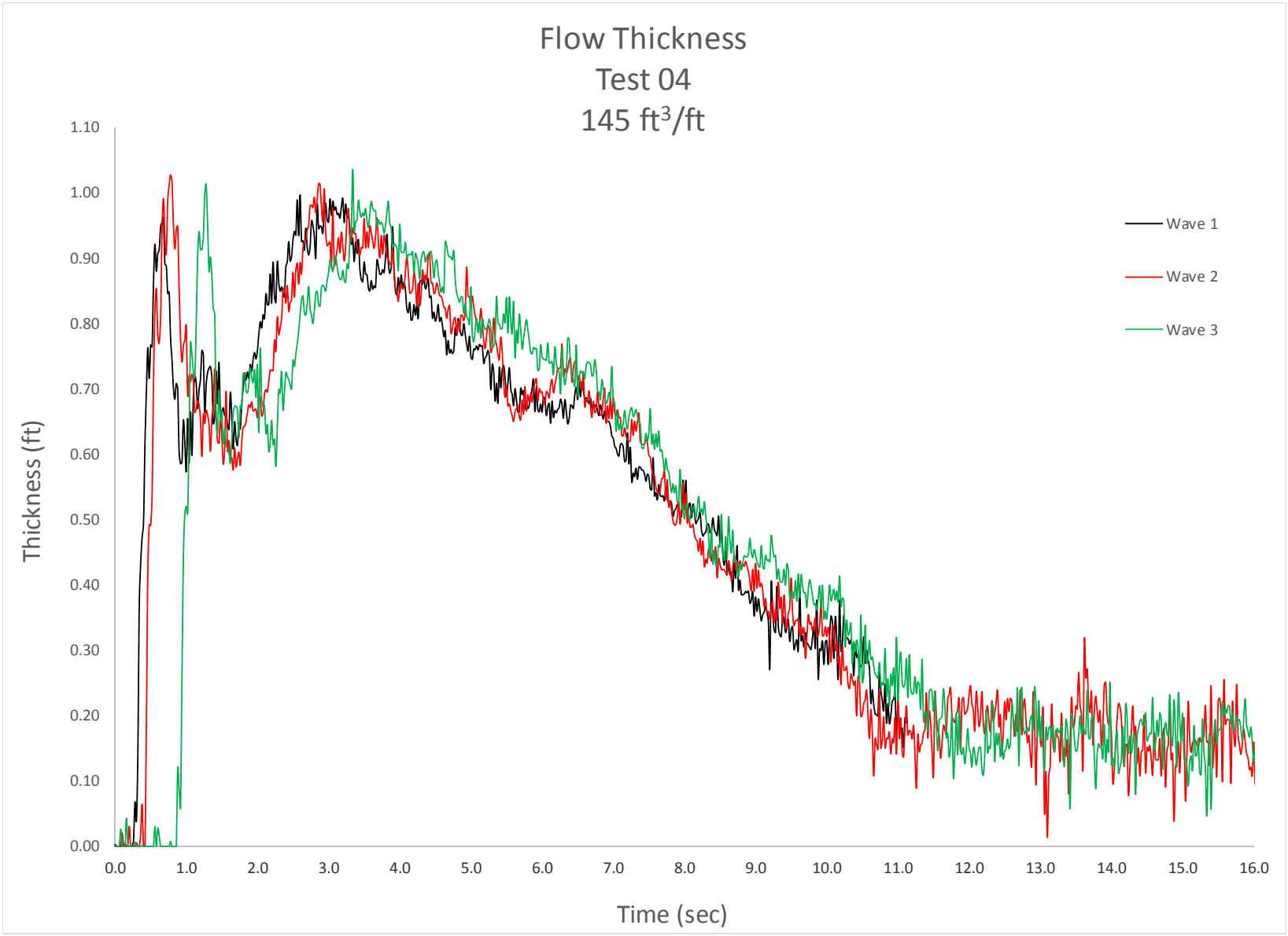

Figure C-54. Crest surfboard flow thickness, 145 ft^3/ft, Test 4.

Figure C-55. Crest surfboard flow thickness, 145 ft^3/ft, Test 5.

Figure C-56. Crest surfboard flow thickness, 145 ft^3/ft, Test 6.

Figure C-57. Crest surfboard flow thickness, 145 ft^3/ft, Test 7.

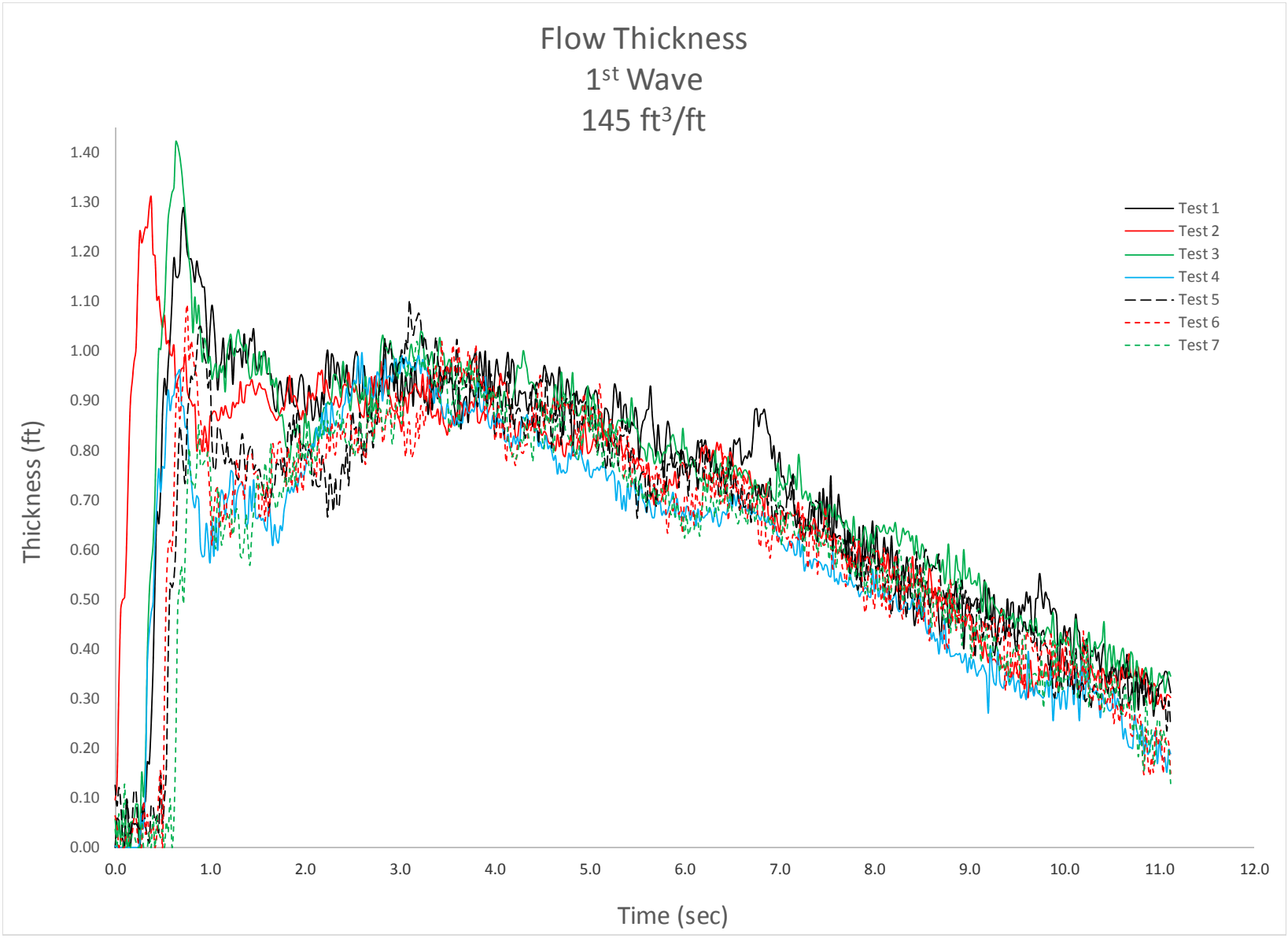

Figure C-58. Crest surfboard flow thickness, 145 ft^3/ft, 1st wave, all tests.

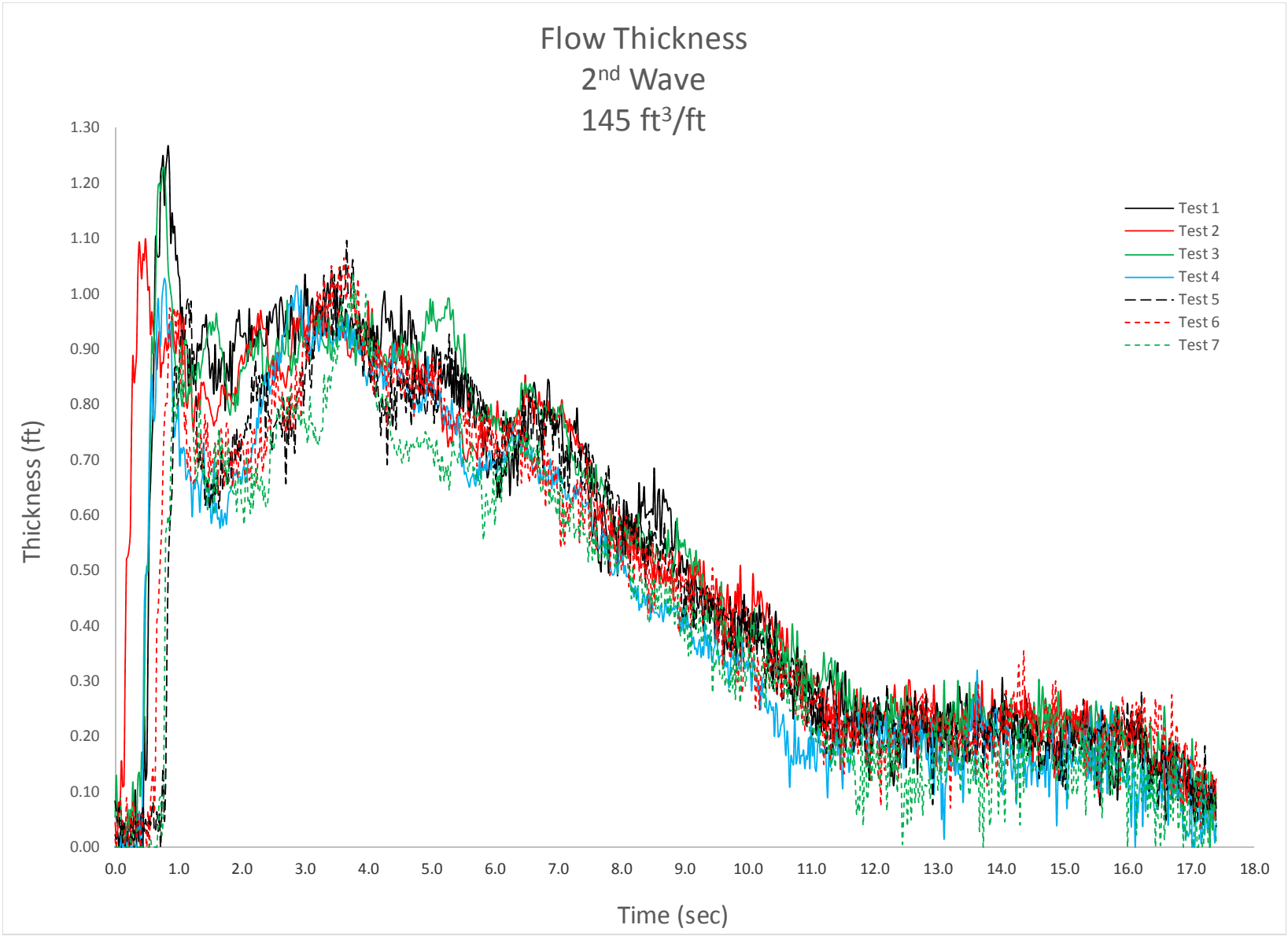

Figure C-59. Crest surfboard flow thickness, 145 ft^3/ft, 2nd wave, all tests.

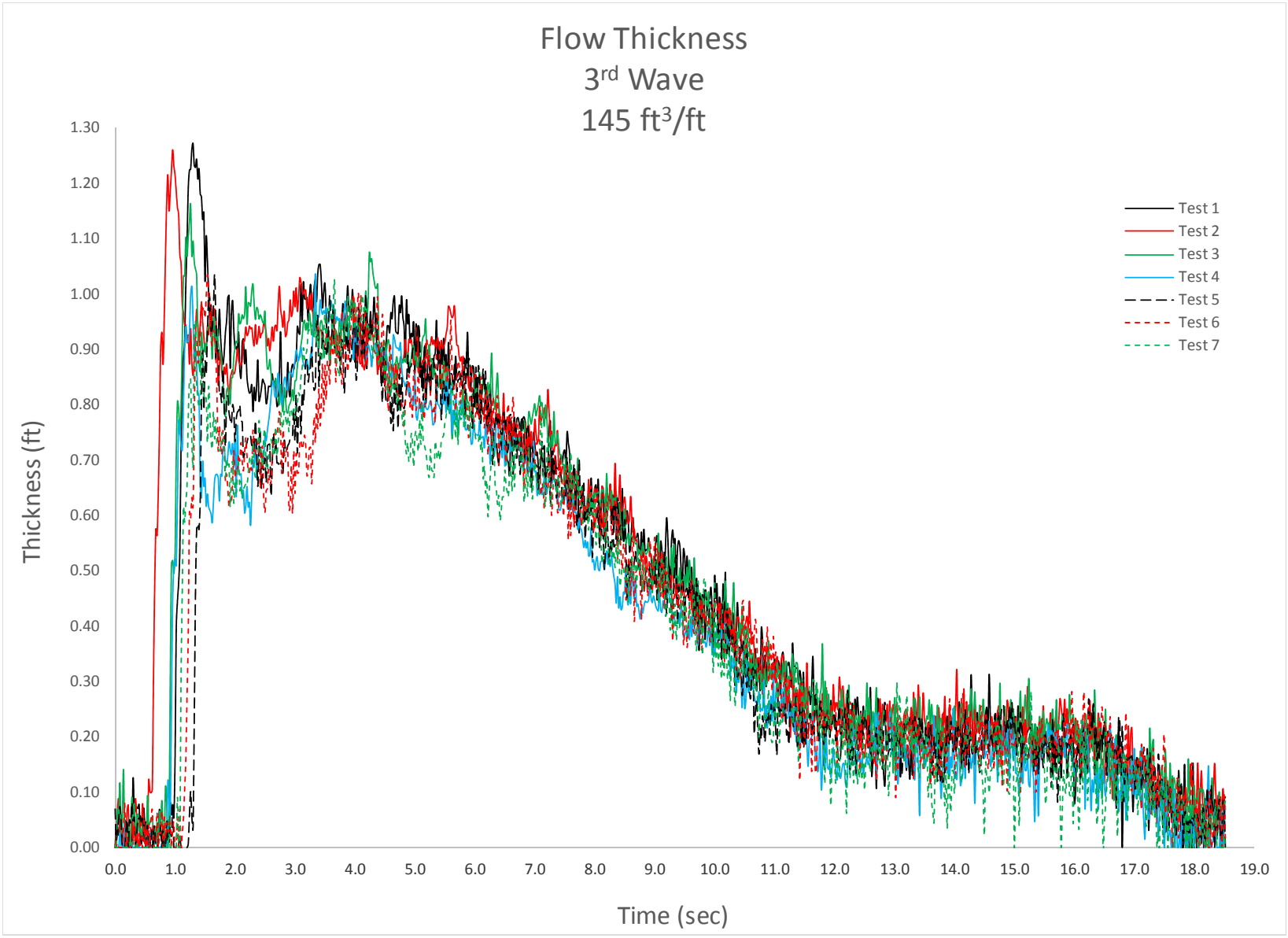

Figure C-60. Crest surfboard flow thickness, 145 ft^3/ft, 3rd wave, all tests.

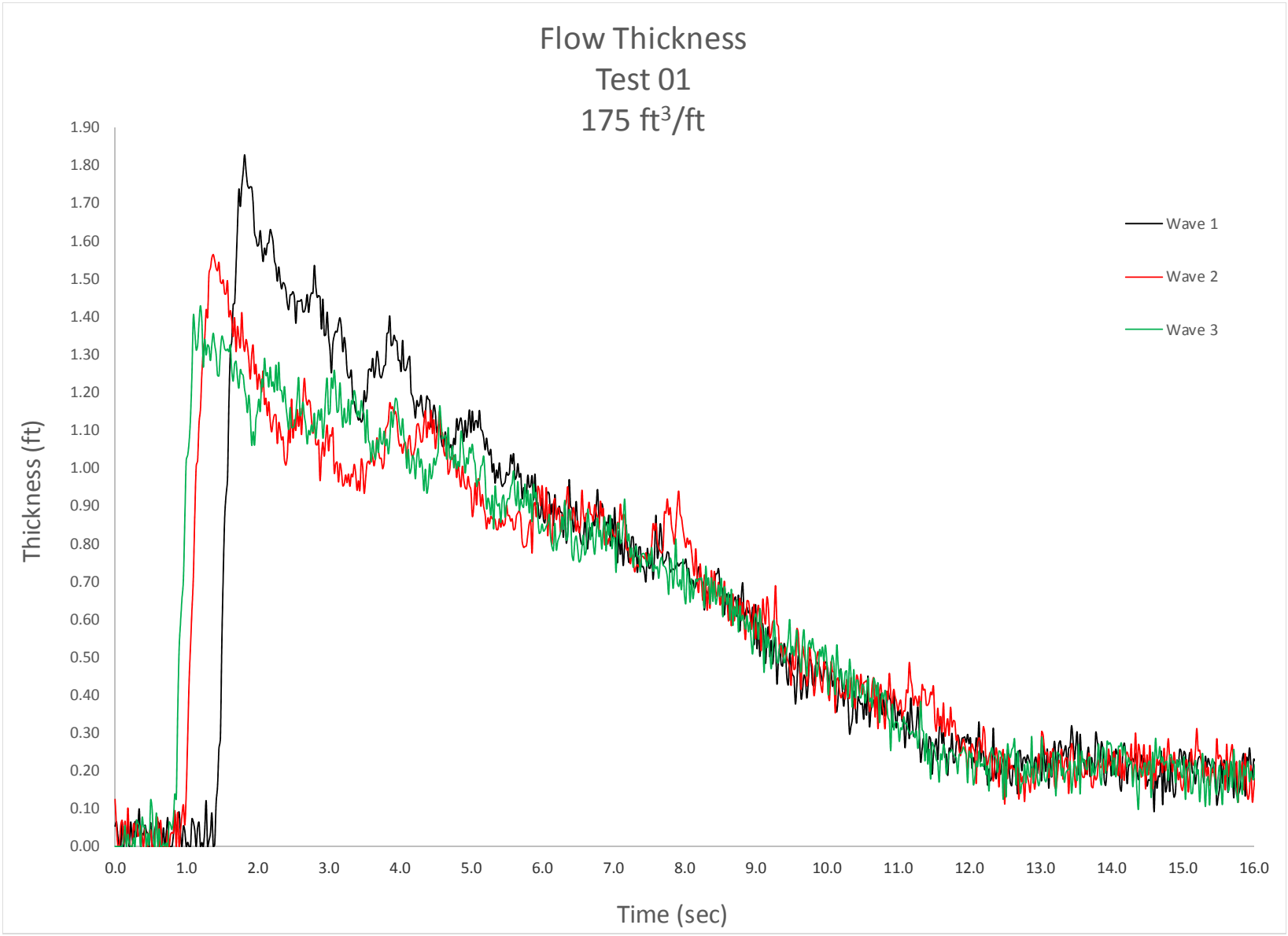

Figure C-61. Crest surfboard flow thickness, 175 ft^3/ft, Test 1.

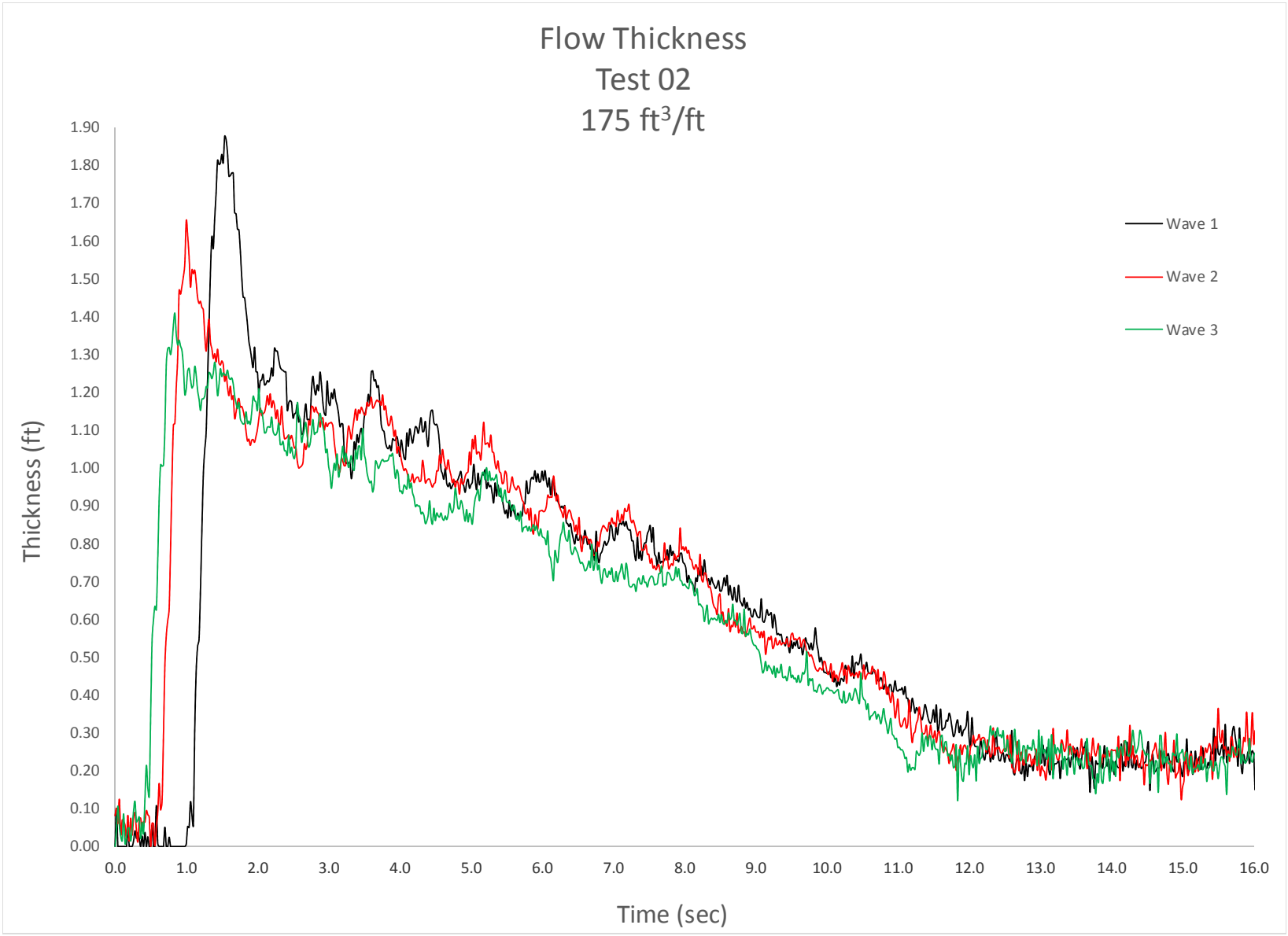

Figure C-62. Crest surfboard flow thickness, 175 ft^3/ft, Test 2.

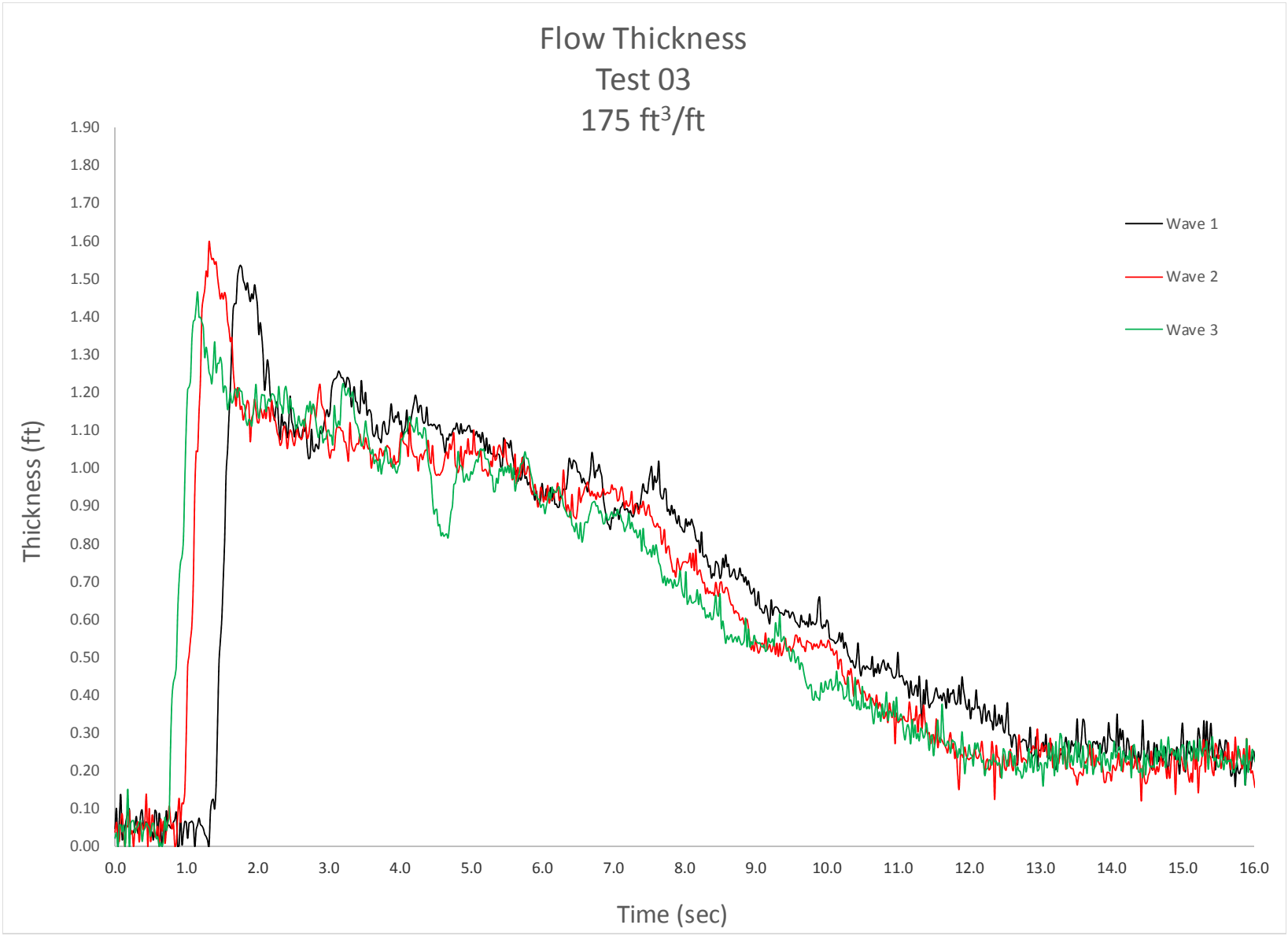

Figure C-63. Crest surfboard flow thickness, 175 ft^3/ft, Test 3.

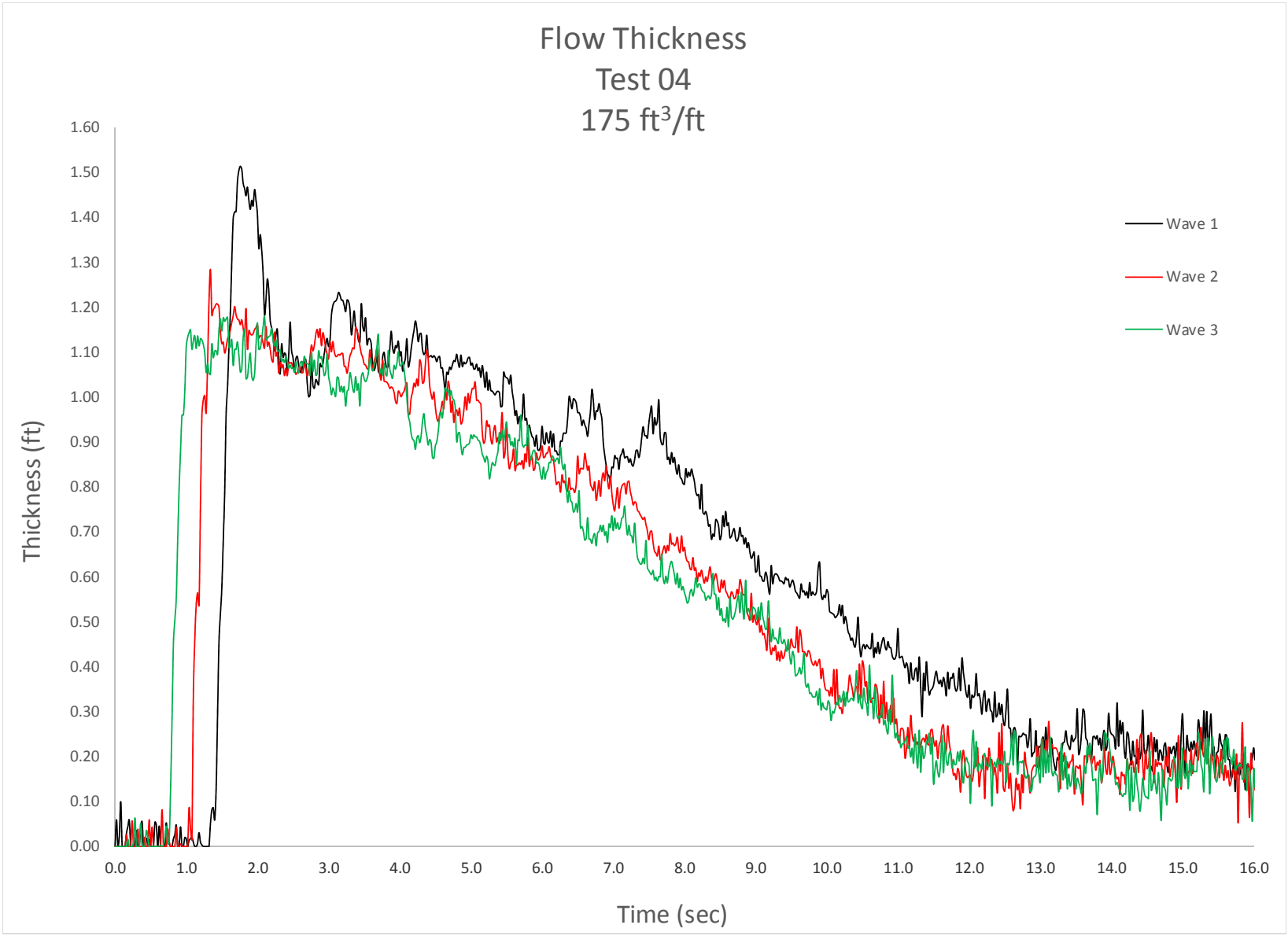

Figure C-64. Crest surfboard flow thickness, 175 ft^3/ft, Test 4.

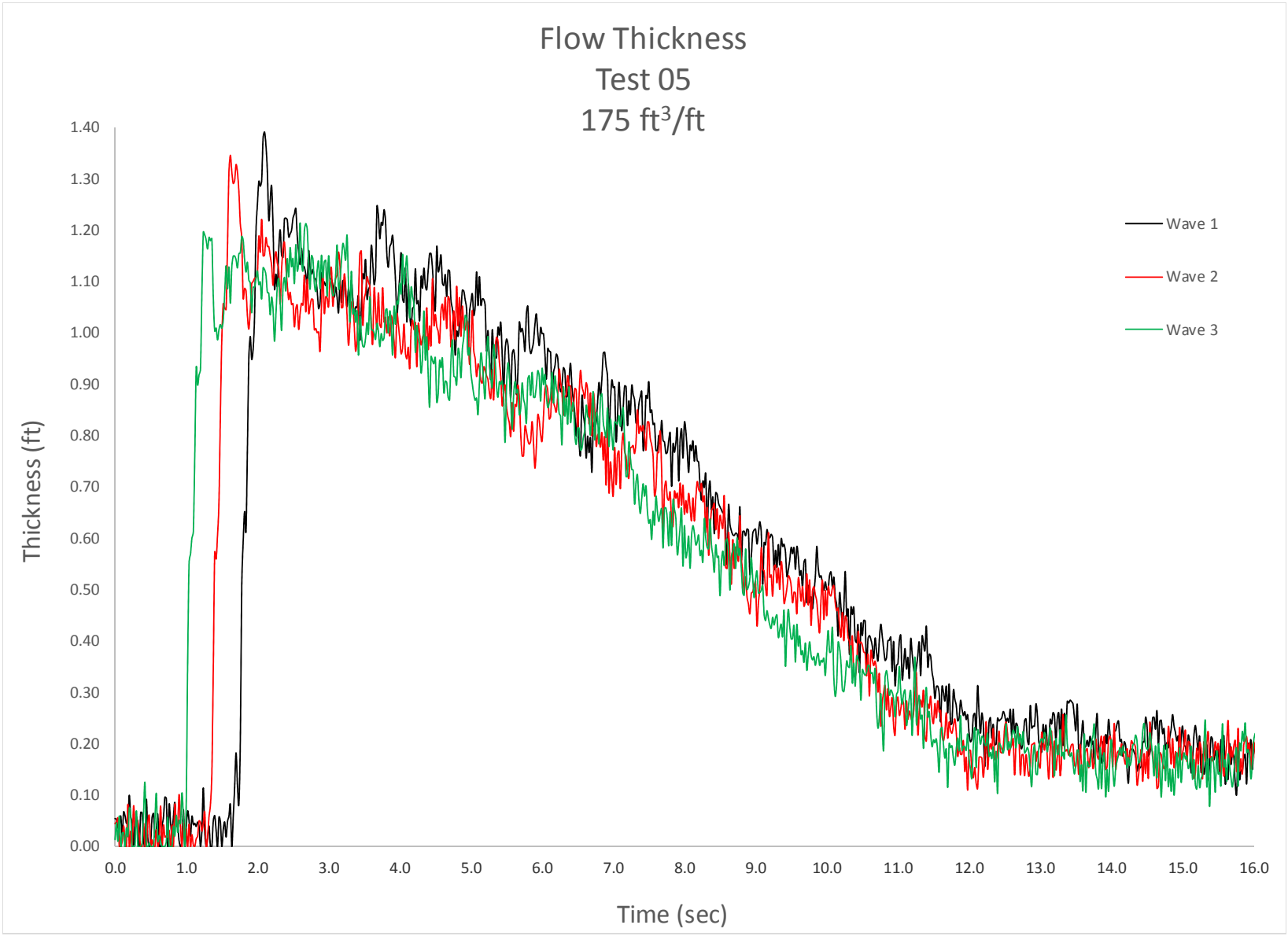

Figure C-65. Crest surfboard flow thickness, 175 ft^3/ft, Test 5.

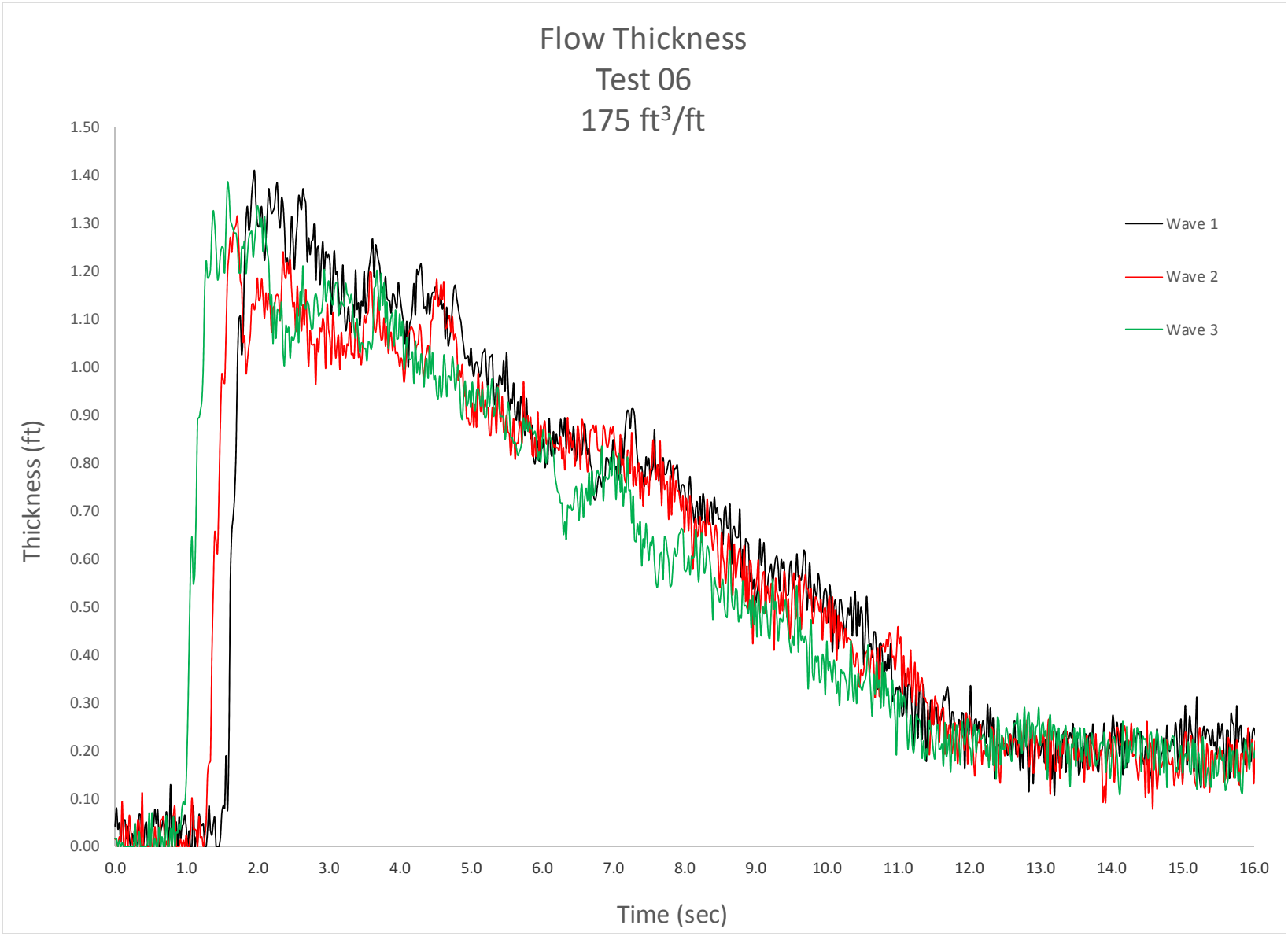

Figure C-66. Crest surfboard flow thickness, 175 ft^3/ft, Test 6.

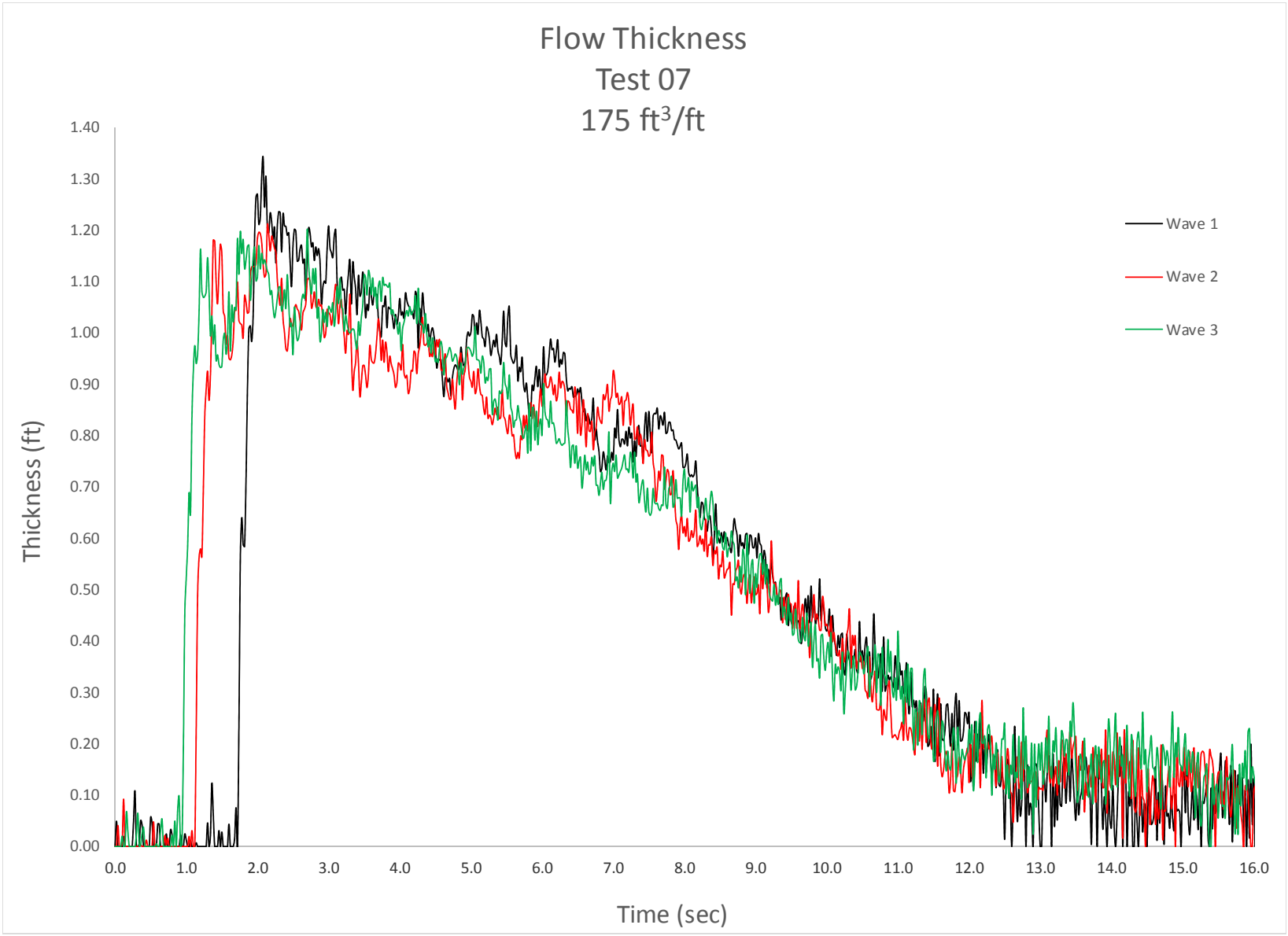

Figure C-67. Crest surfboard flow thickness, 175 ft^3/ft, Test 7.

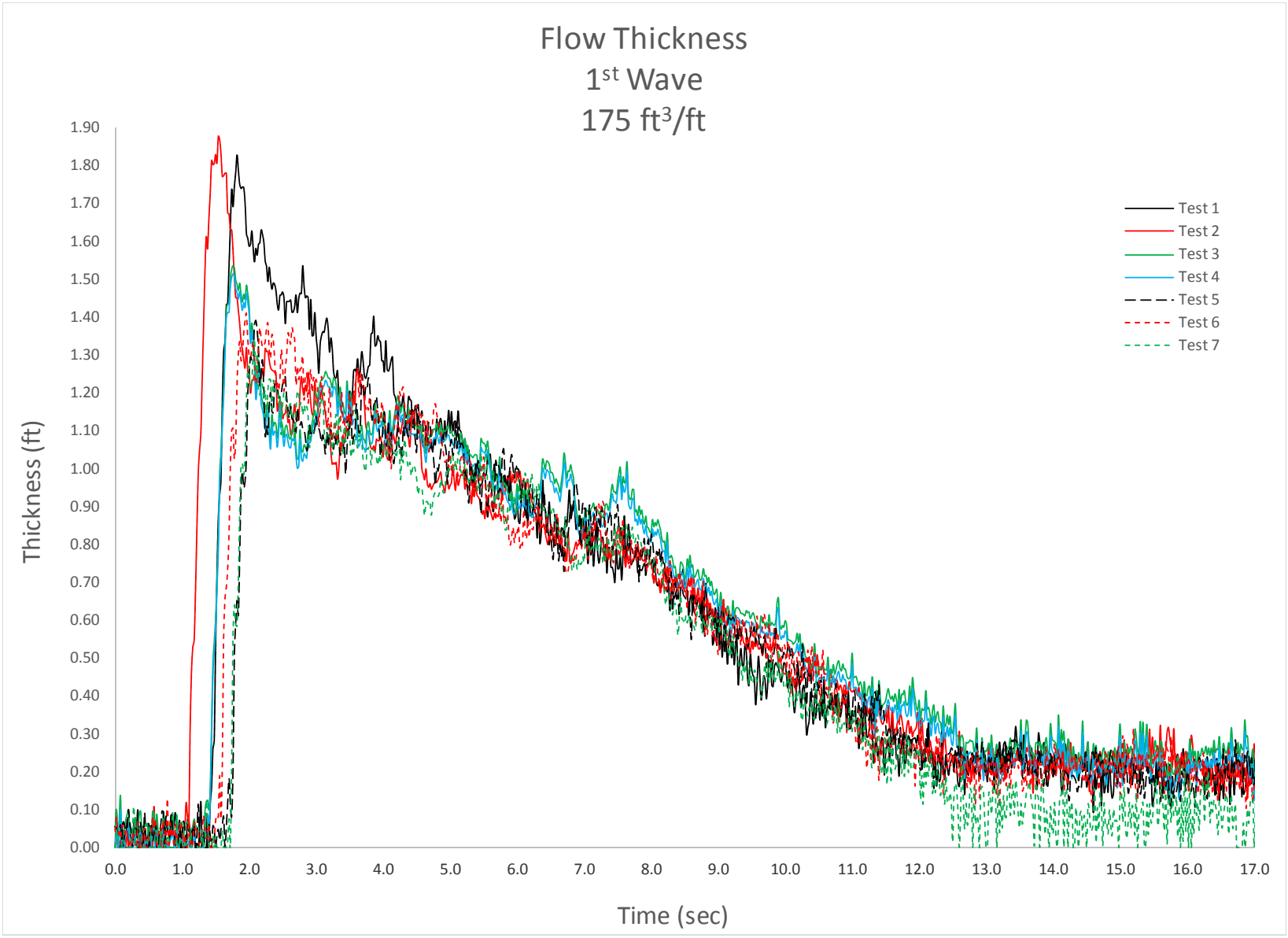

Figure C-68. Crest surfboard flow thickness, 175 ft^3/ft, 1st wave, all tests.

Figure C-69. Crest surfboard flow thickness, 175 ft^3/ft, 2nd wave, all tests.

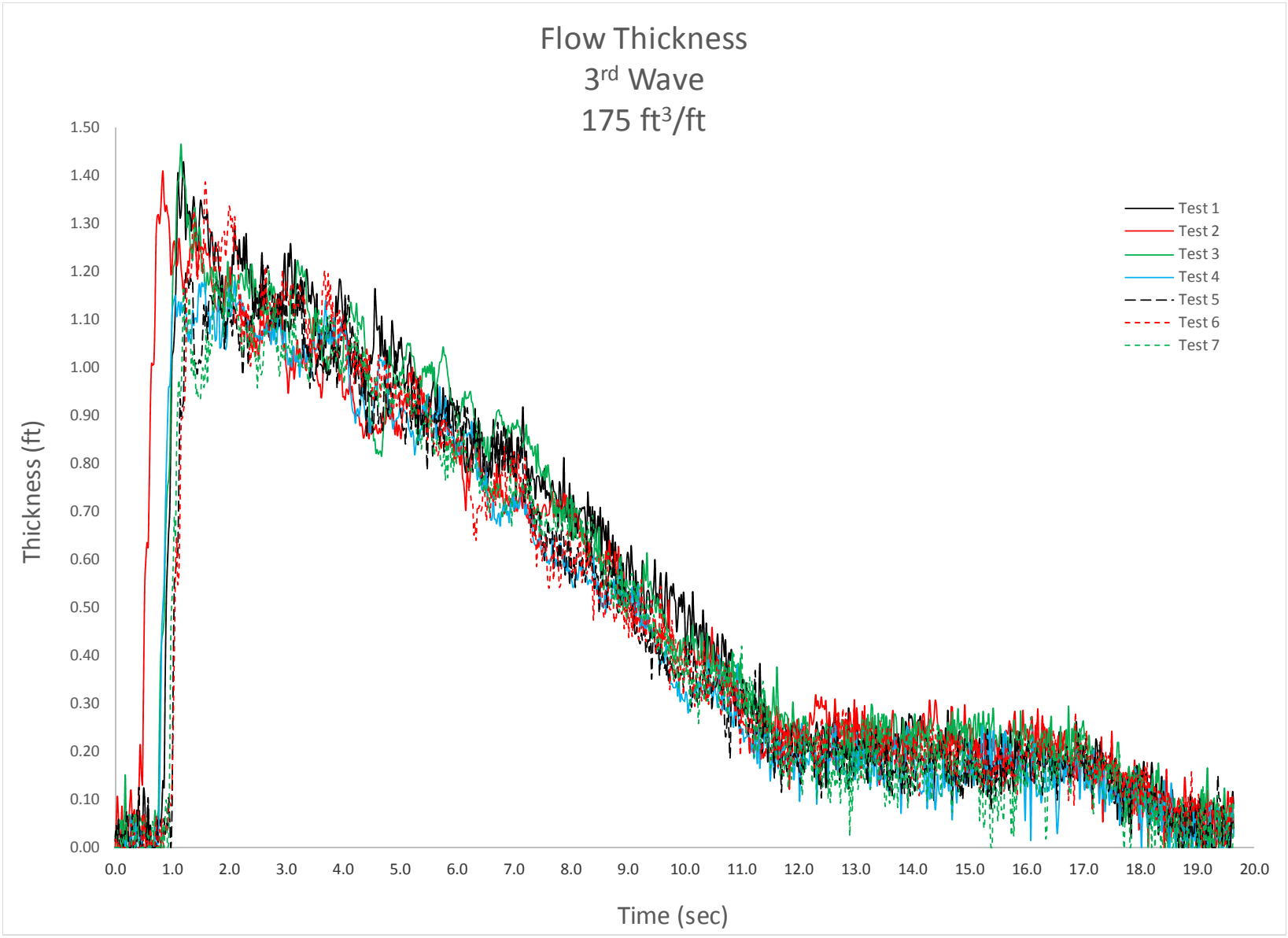

Figure C-70. Crest surfboard flow thickness, 175 ft^3/ft, 3rd wave, all tests.